



**UNIVERSITÀ POLITECNICA DELLE MARCHE**

Department of Life and Environmental Sciences

Doctoral School of Marine Biology and Ecology

---

# **Diversity of sulfur metabolism in microalgae**

**PhD student:**

Daniel Pousa Kurpan Nogueira

**Supervisor:**

Dr. Alessandra Norici

---

XXXIII Cycle

2017-2020



*To all my friends and family that  
I left in Brazil to fulfill this work.  
To my wife that left so much more  
behind, and came with me.*

*“It may never be perfect,  
but still can be great.”*

## **ACKNOWLEDGEMENTS**

My most sincere posthumous acknowledgements to the late Professor Mario Giordano. A good friend, scientist and supervisor.

Thanks to all direct and indirect collaborators. Especially to Professor Peter Kroth, Dr. Carolina Rio Bartulos and Dr. Alexander Schober, from Konstanz University, Germany; and to Professor Charles F. Delwiche and Dr. Charles Goodman from the Molecular Systematics Laboratory of Maryland University, USA.

This work wouldn't be possible without the help, support and contribution of all my past and present lab crew: Professor Alessandra Norici, Dr. Caterina Gerotto, Dr. Alessandra Petrucciani, Aja Trebec and Maria Bruno (this is the present team, there are many important people that were temporarily with me during this work). I thank them all very much.

Due to University's regulation, I couldn't officially designate Dr. Caterina Gerotto as a co-supervisor of this thesis. Here, I would like to acknowledge her huge efforts to help me building this document. A true and highly valued supervisor's work.

The most special acknowledgement is certainly to my wife, who accepted the challenge of living in another country for the sake of a frequently undervalued scientific career. There is not one page of this thesis that doesn't carry her efforts just as much as mine.

## ABSTRACT

Sulfur is a fundamental, yet frequently underestimated, macronutrient resulting on substantially less information about it in literature when compared to other macronutrients. Among photosynthetic organisms, sulfur metabolism is generally assumed to be conserved and most of the available information is limited to vascular plants. The investigation among algae is constrained to very few clades, despite the importance of sulfate – the most available form of sulfur in nature – in seawater. In fact, there is evidence to suggest that sulfate concentration in seawater is one of the most important drivers of phytoplankton composition and may be the responsible for today's dominance of chlorophyll *a + c* microalgae in the phytoplankton – the Sulfate Facilitation Hypothesis (SFH). Facing this scenario, this thesis intends to raise the understanding of the role of sulfur in phytoplankton by implementing a multidisciplinary approach involving various groups of microalgae. First, a broad *in silico* analysis of the cellular localization and phylogenetic relationships of the six core enzymes of sulfate assimilation shows a rather complex origin of the pathway. Data also suggests a relevant role of redox regulation, that appears to function differently among different groups of phototrophs. Then, the function, localization and the *in vivo* redox regulation of one of these enzymes – with a particularly complex phylogeny, named ATPS – was further investigated in the model diatom *Phaeodactylum tricornutum* using novel molecular biology techniques. ATPS seems to be crucial for life and is present in *P. tricornutum* as two non-redundant isoforms that are in different compartments and may function in sulfur partitioning. The recovery of ATPS-knockout mutants by growth medium complementation with alternative sources of sulfur is initially investigated. Finally, using a physiological and biochemical approach, the growth of marine microalgae belonging to various groups was assessed as a function of sulfate concentration in growth medium. The concentration of sulfate that results in growth limitation is strikingly different among microalgae. In fact, chlorophyll *a + c* microalgae can be limited in sulfate concentrations up to 10000-fold higher than the other microalgae, which is highly congruent with the SFH. Interestingly, their responses to sulfate limitation were also different within the red-plastid algae, especially in the iron quota in cells.

## SUMMARY

1. OVERVIEW .....	1
1.1. Objects of study .....	1
1.2. Motivation.....	2
2. GENERAL INTRODUCTION .....	4
2.1. Sulfur in nature .....	4
2.1.1. Oceanic sulfate concentration – Past and present .....	5
2.1.1.1. The relationship between sulfur and phytoplankton .....	6
2.2. Sulfur in living cells.....	8
2.2.1. Sulfur in photosynthetic organisms.....	8
2.2.2. Sulfur metabolism in algae.....	9
2.2.2.1. Sulfate acquisition and transport .....	11
2.2.2.2. Sulfate activation .....	12
2.2.2.3. Primary sulfate assimilatory pathway – Reduction .....	13
2.2.2.4. Secondary sulfate assimilatory pathway – Sulfation.....	15
2.3. Experimental organisms .....	16
2.4. Aim and organization of this thesis .....	18
3. PHYLOGENY OF SULFUR ASSIMILATION ENZYMES.....	19
3.1. Introduction.....	19
3.1.1. ATP Sulfurylase (ATPS).....	20
3.1.2. APS Kinase (APSK) .....	21
3.1.3. APS Reductase (APSR) .....	22
3.1.4. Sulfite Reductase (SiR).....	22
3.1.5. Cysteine Synthase: Serine Acetyl Transferase (SAT) and O-Acetyl Serine- Thyol Lyase (OAS-TL).....	23
3.2. Material and Methods .....	24
3.2.1. Sequence data acquisition .....	24
3.2.2. Sequences targeting predictions.....	25
3.2.3. Sequence alignments and phylogenetic analysis.....	25
3.3. Results and Discussion .....	26
3.3.1. Sequences targeting: sulfate reduction is predicted in chloroplast in algae..	26
3.3.2. Phylogenetic analyses .....	29
3.3.2.1. ATPS phylogenetic analysis reveals functional clusters .....	29
3.3.2.2. APSK and APSR: the fate of APS is differently defined among algal groups .....	33
3.3.2.3. SiR shows a conventional distribution of taxa .....	38
3.3.2.4. Serine Acetyl Transferase.....	41
3.4. Concluding remarks .....	48
3.5. Supplemental material – Chapter 3.....	49
4. CHARACTERIZATION OF ATPS FROM <i>P. TRICORNUTUM</i> .....	55
4.1. Introduction.....	55
4.2. Material and Methods .....	58
4.2.1. Diatom cells culture conditions for GFP fusion and knockouts .....	58
4.2.2. In silico retrieval of putative signal- and transit peptides .....	58
4.2.3. Protein localization.....	58
4.2.3.1. Construction of GFP-fusion vectors.....	58
4.2.3.2. Nuclear bombardment of GFP-fusion vectors.....	59
4.2.3.3. Characterization of GFP mutants by epifluorescence microscopy.....	59
4.2.4. Transcription activator-like effector nucleases (TALEN) mediated gene knockouts .....	60

4.2.4.1. Choosing targeting sequences .....	60
4.2.4.2. Assembly of TALEN plasmids .....	61
4.2.4.3. Nuclear bombardment of TALEN plasmids.....	61
4.2.4.4. Screening transformant colonies .....	61
4.2.5. In vivo redox regulation of ATPS .....	62
4.2.5.1. Culture conditions .....	62
4.2.5.2. Measurement of ATPS activity .....	62
4.3. Results.....	65
4.3.1. ATP Sulfurylases' localization .....	65
4.3.2. ATP Sulfurylase knockouts.....	67
4.3.3. Redox regulation of <i>P.tricornutum</i> ATP Sulfurylase.....	69
4.4. Discussion.....	71
4.4.1. ATP Sulfurylase function and localization in diatoms .....	71
4.4.2. In vivo redox regulation of ATP Sulfurylase .....	72
4.5. Supplemental material – Chapter 4.....	74
5. SULFATE LIMITATION IN MARINE MICROALGAE .....	77
5.1. Introduction.....	77
5.2. Material and Methods .....	80
5.2.1. Culture conditions .....	80
5.2.2. Cell density and volume determination.....	82
5.2.2.1. Bürker hemocytometer .....	82
5.2.2.2. CASY® TT Automatic cell counter.....	83
5.2.3. Determination of specific growth rate.....	83
5.2.4. Extraction and quantification of pigments .....	84
5.2.5. Extraction and quantification of proteins .....	85
5.2.6. Macromolecular pools size – Fourier Transform Infra-Red (FTIR) Spectroscopy .....	86
5.2.6.1. Semi quantification of lipids and carbohydrates .....	87
5.2.7. Elemental composition – Total X-ray Reflection Fluorescence (TXRF) ....	89
5.2.7.1. Quantification of elemental cell quotas.....	89
5.2.8. Elemental composition – Elemental combustion analysis.....	90
5.2.8.1. Sample preparation.....	90
5.2.9. Photosynthetic parameters – Pulse Amplitude Modulated fluorometry .....	91
5.2.9.1. Principles of fluorescence measurements.....	91
5.2.9.2. Fluorescence measurements .....	93
5.2.10. ATP Sulfurylase activity .....	94
5.2.11. Statistical analysis .....	94
5.2.11.1. Univariate analyses.....	94
5.2.11.2. Multivariate analyses.....	94
5.3. Results.....	95
5.3.1. Growth-limiting concentrations of sulfate .....	95
5.3.2. Growth, pigments and sulfate limitation .....	97
5.3.3. Macromolecular pools.....	101
5.3.4. Elemental composition.....	104
5.3.5. Photosynthetic parameters .....	108
5.3.6. ATP Sulfurylase activity .....	113
5.4. Discussion.....	115
5.4.1. Marine algae of different phylogeny are characterized by a different sulfate limiting concentration .....	115
5.4.2. Physiological responses to sulfate limitation .....	118

5.5. Supplemental material – Chapter 5.....	123
6. GROWTH OF <i>P. TRICORNUTUM</i> IN OTHER SOURCES OF SULFUR.....	124
6.1. Introduction.....	124
6.2. Material and Methods .....	125
6.3. Results.....	126
6.3.1. Growth.....	126
6.3.2. Macromolecular pools.....	128
6.3.3. Elemental composition.....	130
6.3.4. Photosynthetic parameters .....	132
6.3.5. ATP Sulfurylase activity .....	134
6.4. Perspectives .....	136
7. Conclusions .....	137
8. Bibliography .....	139

## LIST OF FIGURES

<b>Figure 1:</b> Number of results from the online research of studies correlating each macronutrient with algae and plants.....	2
<b>Figure 2:</b> Sulfur biogeochemical cycle.....	4
<b>Figure 3:</b> Sulfate concentration in seawater and phytoplankton radiation over geological time. ....	7
<b>Figure 4:</b> Main pathways of sulfate metabolism in algae and plants.....	10
<b>Figure 5:</b> Sulfate activation, the reaction catalyzed by ATP Sulfurylase. ....	12
<b>Figure 6:</b> Primary (reductive) sulfate assimilatory pathway, after sulfate activation. ....	14
<b>Figure 7:</b> After sulfate activation, APS can be phosphorylated to PAPS by APS kinase. In fungi and some bacteria, PAPS can be reduced by PAPS reductase and follow the reductive pathway of cysteine synthesis. Or the sulfate in PAPS can be readily incorporated into organic compounds by Sulfotransferases.....	16
<b>Figure 8:</b> General scheme of sulfate assimilation.....	20
<b>Figure 9:</b> Maximum likelihood phylogenetic tree of ATPS with all taxa or collapsed branches. ....	32
<b>Figure 10:</b> Maximum likelihood phylogenetic tree of APSK with all taxa or collapsed branches.....	35
<b>Figure 11:</b> Maximum likelihood phylogenetic tree of APSR with all taxa or collapsed branches.....	38
<b>Figure 12:</b> Maximum likelihood phylogenetic tree of SiR with all taxa or collapsed branches. ....	41
<b>Figure 13:</b> Maximum likelihood phylogenetic tree of SAT with all taxa or collapsed branches. ....	44
<b>Figure 14:</b> Maximum likelihood phylogenetic tree of OAS-TL with all taxa or collapsed branches.....	47
<b>Figure 15:</b> Schematic representation of a TALE, highlighting the amino acid sequence of one tandem repeat module and the RVD within it; RVDs' specificity to each nucleotide; and a pair of TALENs binding the DNA strand. ....	57
<b>Figure 16:</b> Characterization of a non-annotated pre-sequence of ATPS in <i>P. tricornutum</i> (JGI Protein ID 42282) and amino acid sequence with predicted signal-, transit peptides and cut site. ....	65
<b>Figure 17:</b> Confocal photomicrographs showing the localization of the ATPS:GFP fusion expressed in <i>Phaeodactylum tricornutum</i> . ....	66
<b>Figure 18:</b> Photomicrographs showing the KSP:GFP fusion expressed in <i>P. tricornutum</i> . ....	67
<b>Figure 19:</b> Electrophoresis gel of allele specific amplification products from genomic DNA of all colonies resulting from the transformation of <i>P. tricornutum</i> cells with the KSP TALEN plasmids.....	68
<b>Figure 20:</b> ATP Sulfurylase activity of <i>P. tricornutum</i> cell extracts in the absence or presence of the reducing agent DTT <sub>red</sub> . ....	69
<b>Figure 21:</b> ATP Sulfurylase activity of <i>P. tricornutum</i> cell extracts from the same cultures exposed to dark, light, or DCMU in the presence of light for 1, 3, 6 and 24h.....	70

<b>Figure 22:</b> Schematic representation of the suggested sulfate metabolism in diatoms, with emphasis on the partitioning into reduction or sulfation.....	72
<b>Figure 23:</b> Representation and dimensions of a Bürker hemocytometer's grid.....	82
<b>Figure 24:</b> Schematic view of a Michelson's interferometer.....	87
<b>Figure 25:</b> Specific growth rate, final cell yield and average cell volume of <i>Tetraselmis suecica</i> , <i>Porphyridium purpureum</i> , <i>Phaeodactylum tricorutum</i> and <i>Amphidinium carterae</i> as a function of sulfur concentration in AMCONA medium. ....	96
<b>Figure 26:</b> Photoautotrophic batch growth of <i>T. suecica</i> , <i>P. purpureum</i> , <i>P. tricorutum</i> and <i>A. carterae</i> at 20±2°C under irradiance of 100 µmol photons·m <sup>-2</sup> ·s <sup>-1</sup> in S replete and S limited AMCONA medium.....	98
<b>Figure 27:</b> Semi-quantification of macromolecular pools of the four studied microalgae grown in S replete and S limited modified AMCONA medium.....	103
<b>Figure 28:</b> Elemental cell quotas of the four experimental microalgae grown in S replete and S limited modified AMCONA medium at 20±2°C under 100 µmol photons·m <sup>-2</sup> ·s <sup>-1</sup> .....	105
<b>Figure 29:</b> Principal Component Analysis (PCA) of standardized percentage of carbon (C), nitrogen (N), sulfur (S) and phosphorus(P) on the biomass of <i>T. suecica</i> , <i>P. purpureum</i> , <i>P. tricorutum</i> and <i>A. carterae</i> cultivated on S replete and S limited modified AMCONA medium. ....	108
<b>Figure 30:</b> Light curves (LC) of the four studied microalgae grown in S replete and S limited modified AMCONA medium at 20±2°C under irradiance of 100 µmol photons·m <sup>-2</sup> ·s <sup>-1</sup> .....	111
<b>Figure 31:</b> Photosystem II quantum yield (ΦPSII) of the four studied microalgae grown in S replete and S limited modified AMCONA medium at 20±2°C under irradiance of 100 µmol photons·m <sup>-2</sup> ·s <sup>-1</sup> . ....	111
<b>Figure 32:</b> Photochemical quenching (qL) of the four studied microalgae grown in S replete and S limited modified AMCONA medium at 20±2°C under irradiance of 100 µmol photons·m <sup>-2</sup> ·s <sup>-1</sup> .....	112
<b>Figure 33:</b> Non-photochemical quenching (NPQ) of the four studied microalgae grown in S replete and S limited modified AMCONA medium at 20±2°C under irradiance of 100 µmol photons·m <sup>-2</sup> ·s <sup>-1</sup> . ....	112
<b>Figure 34:</b> ATP Sulfurylase activity of the four studied microalgae grown in S replete and S limited modified AMCONA medium at 20±2°C under irradiance of 100 µmol photons·m <sup>-2</sup> ·s <sup>-1</sup> .....	114
<b>Figure 35:</b> Photoautotrophic batch growth of <i>P. tricorutum</i> at 20±2°C illuminated with 100 µmol photons·m <sup>-2</sup> ·s <sup>-1</sup> in AMCONA medium enriched with 25 mmol·L <sup>-1</sup> or 1 µmol·L <sup>-1</sup> Na <sub>2</sub> SO <sub>4</sub> ; Na <sub>2</sub> S; and L-cysteine.....	127
<b>Figure 36:</b> Specific growth rate, final cell yield and average cell volume of <i>P. tricorutum</i> grown at 20±2°C illuminated with 100 µmol photons·m <sup>-2</sup> ·s <sup>-1</sup> in AMCONA medium enriched with 25 mmol·L <sup>-1</sup> or 1 µmol·L <sup>-1</sup> Na <sub>2</sub> SO <sub>4</sub> ; Na <sub>2</sub> S; and L-cysteine.....	128
<b>Figure 37:</b> Proteins, carbohydrates, lipids and chlorophyll pools of <i>P. tricorutum</i> grown at 20±2°C illuminated with 100 µmol photons·m <sup>-2</sup> ·s <sup>-1</sup> in AMCONA medium enriched with 25 mmol·L <sup>-1</sup> or 1 µmol·L <sup>-1</sup> Na <sub>2</sub> SO <sub>4</sub> ; Na <sub>2</sub> S; and L-cysteine.....	129
<b>Figure 38:</b> Elemental cell quotas of <i>P. tricorutum</i> grown in sulfate-replete, Na <sub>2</sub> S, cysteine and sulfate-limited modified AMCONA medium at 20±2°C under 100 µmol photons·m <sup>-2</sup> ·s <sup>-1</sup> .....	130
<b>Figure 39:</b> Elemental ratios of <i>P. tricorutum</i> grown in sulfate-replete, Na <sub>2</sub> S, cysteine and sulfate-limited modified AMCONA medium at 20±2°C under 100 µmol photons·m <sup>-2</sup> ·s <sup>-1</sup> .....	131
<b>Figure 40:</b> Relative electron transport rate as a function of light, and its fitted curve of <i>P. tricorutum</i> grown in sulfate replete, sulfate limited, Na <sub>2</sub> S-, and L-Cysteine- modified AMCONA medium at 20±2°C illuminated with 100 µmol photons·m <sup>-2</sup> ·s <sup>-1</sup> .....	132
<b>Figure 41:</b> Photochemical (qL) and non-photochemical (NPQ) quenching, and photosystem II quantum yield (ΦPSII) of <i>P. tricorutum</i> grown in sulfate replete, sulfate limited, Na <sub>2</sub> S-, and L-cysteine- enriched modified AMCONA medium at 20±2°C under irradiance of 100 µmol photons·m <sup>-2</sup> ·s <sup>-1</sup> .....	134
<b>Figure 42:</b> ATP Sulfurylase activity of <i>P. tricorutum</i> cell extracts cultivated in Na <sub>2</sub> SO <sub>4</sub> -replete; Na <sub>2</sub> S; L-cysteine and Na <sub>2</sub> SO <sub>4</sub> -limited AMCONA medium at 20±2°C under irradiance of 100 µmol photons·m <sup>-2</sup> ·s <sup>-1</sup> . ....	135

## LIST OF TABLES

<b>Table 1:</b> Number of sequences per species and their predicted cellular localization.....	28
<b>Table 2:</b> Cut site, sequences and scores of chosen pairs of TALENs for independent knockout attempts of both tested isoforms of <i>P. tricornutum</i> ATP Sulfurylase. ....	60
<b>Table 3:</b> Recipe of AMCONA medium as used in this study.....	81
<b>Table 4:</b> Reagents used for the determination of total proteins according to Peterson (1977). ....	86
<b>Table 5:</b> FTIR peaks assignment. ....	88
<b>Table 6:</b> Specific growth rate, final cell yield, average cell volume and pigments content of the four studied microalgae grown at 20±2°C under irradiance of 100 µmol photons·m <sup>-2</sup> ·s <sup>-1</sup> .....	100
<b>Table 7:</b> Absolute measured values of proteins per cell, and ratios of macromolecular pools (proteins, lipids and carbohydrates) of S replete and S limited treatments of <i>Tetraselmis suecica</i> , <i>Porphyridium purpureum</i> , <i>Phaeodactylum tricornutum</i> and <i>Amphidinium carterae</i> .....	102
<b>Table 8:</b> Elemental cell quotas and ratios of <i>T. suecica</i> , <i>P. purpureum</i> , <i>P. tricornutum</i> and <i>A. carterae</i> grown in S replete and S limited modified AMCONA medium at 20±2°C under 100 µmol photons·m <sup>-2</sup> ·s <sup>-1</sup> . ....	107
<b>Table 9:</b> Photosynthetic efficiency (F <sub>v</sub> /F <sub>m</sub> ) and rapid light curve's parameters (α, rETR <sub>max</sub> , E <sub>k</sub> ) of the four studied microalgae grown in S replete and S limited modified AMCONA medium at 20±2°C under irradiance of 100 µmol photons·m <sup>-2</sup> ·s <sup>-1</sup> .....	110
<b>Table 10:</b> Approximate growth-limiting concentrations of sulfur and C:S ratios of marine microalgae found in literature. ....	117
<b>Table 11:</b> Comparison between elemental ratios of <i>T. suecica</i> , <i>P. purpureum</i> , <i>P. tricornutum</i> and <i>A. carterae</i> grown in S replete and S limited modified AMCONA medium.....	119
<b>Table 12:</b> Photosynthetic efficiency (F <sub>v</sub> /F <sub>m</sub> ) and rapid light curve's parameters (α, rETR <sub>max</sub> , E <sub>k</sub> ) of <i>P. tricornutum</i> grown in sulfate replete, sulfate limited, Na <sub>2</sub> S, and L-cysteine enriched modified AMCONA medium at 20±2°C under irradiance of 100 µmol photons·m <sup>-2</sup> ·s <sup>-1</sup> .....	133

# 1. OVERVIEW

## 1.1. Objects of study

The denomination “algae” has no taxonomic relevance, covering a highly polyphyletic and heterogeneous group of organisms that perform oxygenic photosynthesis and are not embryophytes (Raven and Giordano 2014). Under this vague denomination, there are eukaryotic, prokaryotic, macro- and microscopic representatives – the last ones are usually called microalgae. Although there are several benthonic and terrestrial species, microalgae are mostly planktonic and, as so, compose the extremely important portion of plankton called phytoplankton (Borowitzka et al. 2016). Due to its cosmopolitan distribution, microalgae exhibit a wide range of morphological and metabolic specializations, that have been thoroughly researched and biotechnologically exploited over the last decades (Borowitzka 2013).

Microalgae are the objects of study of this thesis, and results will be frequently discussed with respect to the evolutive pressures that led to the division of microalgae in its several specialized groups. These groups will be frequently referred to as “green” and “red” – as well as some other pigment-based denominations – according to their plastidial ancestry. In order to thoroughly clarify which specific group of microalgae is represented by each term used, a brief overview of the evolution of photosynthetic organisms is presented below.

Oxygenic photosynthesis appears to have evolved only once, in ancient cyanobacteria, but it subsequently have spread via endosymbiosis to a wide variety of eukaryotic clades (Delwiche 1999). From a schism in early evolution of eukaryotic photosynthesis, two major plastid lineages emerged separated by their origin and pigment composition. The components of each lineage are much closely related by plastid physiology than by the evolutionary history of host cells. One group share the use of chlorophyll *b* as an accessory pigment and is mainly composed by green algae and their descendants, the land plants – here called green lineage or chlorophyll *a + b* microalgae (Raven and Giordano 2014). The second group includes the red algae (rhodophytes), which conserved a set of pigments similar to the cyanobacteria (phycobilisomes), and a wide diversity of algal groups whose plastids – but, again, not the host cells – are evolutionary derived from the rhodophytes via secondary endosymbiosis (Raven and Giordano 2014). These red algae descendants use chlorophyll *c* as accessory pigment –

here called chlorophyll *a + c* microalgae or red lineage algae. Interestingly, successful secondary endosymbiosis occurred almost exclusively within the red lineage. The better “portability” of the red plastid appears to be due to a larger and more efficient set of plastidic genes found in red primary plastids (Falkowski et al. 2004). In fact, the major oceanic phytoplankton taxa present in contemporary oceans possess red secondary plastids.

## 1.2. Motivation

From the wide array of nutrients used for microalgal growth, sulfur (S) is the least studied macronutrient for its impacts on cell physiology and biochemical composition (Mera et al. 2016). In addition to that, the vast majority of available information comes from observations in vascular plants, and those studies conducted on algae are usually limited to very few clades (Giordano and Raven 2014; Figure 1).

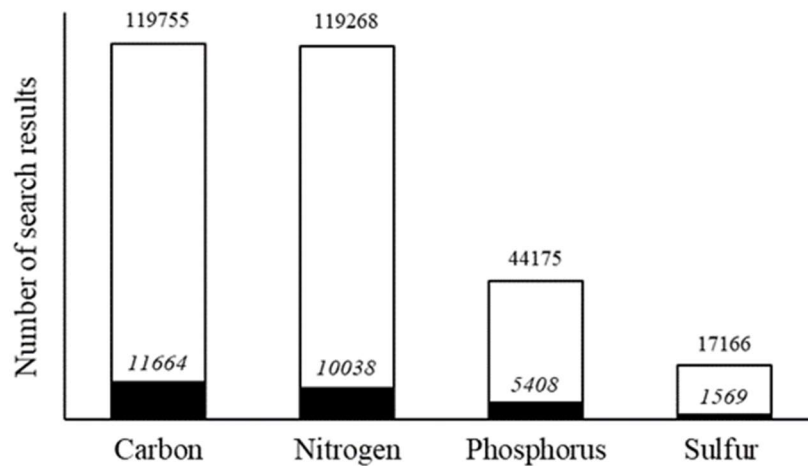


**Figure 1:** Number of results from the online research of studies correlating each macronutrient with algae (black bars) and plants (white bars). Numbers over the bars indicate total query results, and numbers in italic over black bars indicate search results related to algae. Search was performed on August 24<sup>th</sup>, 2020 on Web of Science (Clarivate Analytics) using the topics “*algae AND ‘element’*” and “*plant AND ‘element’*”.

Although the lack of information on sulfur is frequently mentioned in literature, the reasons for this are generally not discussed. Marine phytoplankton – the study object of this thesis – has virtually unlimited availability of sulfur in seawater today and it is not expected to change in the near future (Takahashi et al. 2011). Even anthropogenic S emissions, that once caused imbalance of natural sulfur in soils (Zhao et al. 1998), were

successfully limited by environmental legislation in the end of the 20<sup>th</sup> century and shall no longer impact natural sulfur balance (Giordano et al. 2005b). Hence, when compared to other macronutrients whose availabilities are expected to fluctuate quickly and affect biological communities (e.g.: carbon (Field et al. 1998)), sulfur is a stable nutrient. At least for marine phycologists, this might be the reason why sulfur is less studied than the other nutrients nowadays.

Still, sulfur is an essential nutrient for every living cell and perhaps the most versatile macronutrient for photosynthetic organisms (Hell and Leustek 2005). Recent biochemical experiments conducted on algae showed that, in contrast to what is generally accepted, sulfur reduction and assimilation may differ substantially between algae and higher plants, as well as between different groups of algae (Prioretti et al. 2014, 2016). The evolutive origins of the heterogeneity of sulfur metabolism, as well as its ecological consequences are unclear (Patron et al. 2008). One of the possible effects of it may have been unraveled between the Paleozoic and Mesozoic Eras (about 250 Ma), when a relatively rapid increase of sulfate availability in seawater was followed by a change in phytoplankton composition and abundance (Ratti et al. 2011, Giordano et al. 2018). Apparently, the differences in sulfur metabolism among phytoplanktonic groups was an important – but not the only – factor driving that episode. The mechanistic reasons for that, however, are still obscure (Ratti et al. 2011, Prioretti and Giordano 2016).

Understanding the dynamics of nutrient fluctuations and its impacts in the past may help predicting impacts of nutrient fluctuations in the future. Therefore, it is of utmost importance to clarify how sulfur affect marine phytoplankton. Not only because it is an essential macronutrient, but also because of its unique relationship with photosynthetic organisms.



The only significant non-biological fluxes of sulfur to the atmosphere are the emissions of sulfur dioxide (SO<sub>2</sub>) and hydrogen sulfide (H<sub>2</sub>S) from volcanoes and fumaroles – around 0,4 Tmol·yr<sup>-1</sup>, which is 10-20% of the total S flux (Andreae 1986, Spiro et al. 1992) – and the widely variable, seasonal- and location-dependent anthropogenic emissions, primarily due to fossil fuel combustion (Giordano et al. 2005 and references therein). In land, the breakdown of organosulfur compounds during decomposition of organic matter is probably the most important mechanism for the release of sulfur volatiles – best estimates being around 0,25 Tmol·yr<sup>-1</sup> for total land surface or about 2 mmol·m<sup>-2</sup>·yr<sup>-1</sup> (Charlson et al. 1987). Meanwhile in oceans, the major source of reduced sulfur to the atmosphere – around 2 Tmol·yr<sup>-1</sup>, or about 3 mmol·m<sup>-2</sup>·yr<sup>-1</sup> depending on the region – , most part is released in the form of DMS, a compound largely derived from phytoplankton metabolism (Charlson et al. 1987, Norici et al. 2005, Ayers and Cainey 2007).

Sulfur is, therefore, metabolized in assimilative and dissimilative pathways of various living organisms, cycling through atmospheric, terrestrial and aquatic environments. Oceans, though, play a particularly relevant role in sulfur cycle compared to other ecosystems. This versatile element underwent through notorious mid- and long-term changes in both chemical form and abundance in seawater along the Eras (Giordano et al. 2005b, 2018, Ratti et al. 2011). Such variations are unlikely to have happened in any other environment – land or freshwater – and raise awareness on the rather complex and relevant relationship between sulfur, seawater, and the marine biota to which attention will be addressed next.

### ***2.1.1. Oceanic sulfate concentration – Past and present***

There is solid evidence for the geological history of sulfate concentration in seawater (Ratti et al. 2011 and references therein). In Archean oceans (4-2,5 Gya), sulfate concentration was not higher than 200 μmol·L<sup>-1</sup>. Later, in the Proterozoic Era (2,5 Gya-550 Mya), it increased to about 1 to 5 mmol·L<sup>-1</sup>, reaching transient peaks of around 15 mmol·L<sup>-1</sup> in the Ediacaran oceans (~560 Mya) but declining again into the Cambrian (~540 Mya). During most of the Paleozoic Era (550-250 Mya), sulfate abundance appears to have remained below 10 mmol·L<sup>-1</sup>, at least until the Carboniferous Period (~300 Mya), when it started an unstable increase. Finally, around the boundary between the Paleozoic and Mesozoic Eras (~250 Mya) sulfate concentration in seawater laid in the range of 13

to  $27 \text{ mmol}\cdot\text{L}^{-1}$ , remaining relatively stable ever since (Horita et al. 2002, Gill et al. 2007; Figure 3).

In today's oceans, sulfate is the second most abundant anion after chloride, reaching perhaps the highest concentration ever in seawater ( $\sim 28 \text{ mmol}\cdot\text{L}^{-1}$ ; Ratti et al. 2011, Ueno 2018). The major contributors for oceanic sulfate concentration are weathering of land – mainly pyrite ( $\text{FeS}_2$ ) and gypsum ( $\text{CaSO}_4$ ) – and volcanic and tectonic activity –  $\text{SO}_2$  and  $\text{H}_2\text{S}$  (Andreae 1986). The latter, representing the main sulfur source in hydrothermal vents, where sulfur plays an extremely important ecophysiological role. In these deep oxygen-depleted waters, sulfated compounds are the most relevant oxidation-reduction agents for chemolithotrophic bacteria, the most prominent primary producers (Martin et al. 2008).

#### *2.1.1.1. The relationship between sulfur and phytoplankton*

Changes in oceans' chemistry always have and always will shape the marine biota. This is especially true for phytoplankton, whose growth is primarily supported by seawater chemical state and nutrient availability (Falkowski et al. 2004). In fact, there is a geological coincidence between the increase of oceanic sulfate concentration and the composition of phytoplankton. More specifically, the raise to dominance of microalgae whose plastids contains chlorophyll *a* + *c* (red lineage) occurred simultaneously to the remarkable increase of sulfate concentration in seawater observed in the early Mesozoic Era (Figure 3). It has been suggested that the varying sulfate concentration was one of the most important factors driving this episode (Ratti et al. 2011, 2013), this idea was named the Sulfate Facilitation Hypothesis (SFH). Although recent experiments partially substantiate this hypothesis, showing that red lineage algae were more sensitive to sulfate availability than green lineage and cyanobacteria (Ratti et al. 2011, Prioretti and Giordano 2016), the mechanistic reasons for that difference are still unclear. Furthermore, it has been also showed that the presence of other biological and environmental factors like predators, interspecific competition and other elements availability, may have contributed to the evolutionary history of the modern phytoplanktonic community (Ratti et al. 2011, 2013, Giordano et al. 2018).

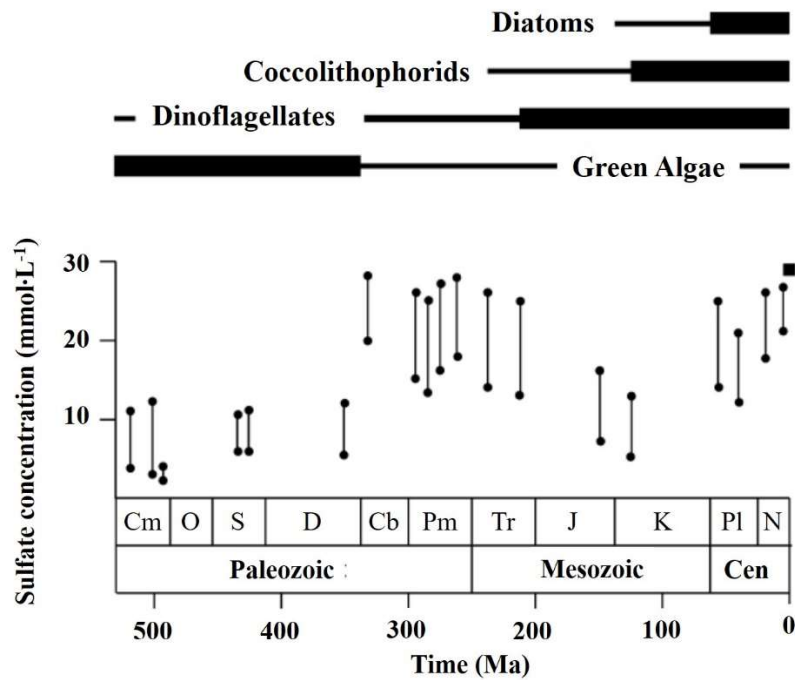


**Figure 3:** Sulfate concentration in seawater and different taxa phytoplankton radiation over geological time. Black circles linked by continuous line represent the range of sulfate concentration in a given period, and the black square shows average concentration of sulfur in today's seawater. Phytoplankton radiation is represented by the thickness of lines presented above (source: Ratti et al. 2011).

There are other remarkable features that serve as example of the relationship between sulfur and marine phytoplankton. For instance, the biosynthesis of dimethylsulfoniopropionate (DMSP), a precursor of DMS produced by phytoplankton. Many marine algae are known to produce high intracellular concentrations of DMSP (100-400 mmol·L<sup>-1</sup>) and it is proposed to serve as osmolyte, cryoprotectant, antioxidant, grazing deterrent and/or storage of carbon and sulfur when nitrogen is limiting, not a rare condition in oceans (Charlson et al. 1987, Sunda et al. 2002, Giordano and Raven 2014). Very little, if any, DMSP is degraded and released as DMS from healthy microalgal cells, such process is commonly associated to grazing or senescence of phytoplankton. The whole pathway from production of DMSP to the release of DMS is best depicted by a network of production, transformation and consumption that involves the entire marine food web (Malin 1997). It is further proposed that DMS release from oceans affects global climate. Charlson et al. (1987) suggested that the DMS produced by plankton would affect climate, and climate would affect phytoplankton growth, thus closing a feedback loop. That idea was named the CLAW hypothesis.

## **2.2. Sulfur in living cells**

Sulfur is a fundamental element for life, not only giving stability to protein structure via disulfide bonds (present in circa 30% of eukaryotic proteins), but also as a constituent of proteogenic amino acids (e.g.: cysteine and methionine), vitamins (e.g.: biotin), coenzymes (e.g.: acetyl coenzyme A) and many other metabolites (Hell and Leustek 2005, Takahashi et al. 2011). In most of these compounds, sulfur is found in a reduced form of organic thiols and sulfides. In contrast, inorganic sulfate is the major form of available sulfur in the environment. Sulfate assimilation is, therefore, essential for the incorporation of reduced sulfur into organic molecules. However, the sulfate assimilation pathway seems to be readily dispensable when the lifestyle of the organism allows (Patron et al. 2008). It is absent in all metazoans, which satisfy their need for reduced sulfur by the ingestion of organic matter from organisms in lower trophic levels. Bacterial and protistan parasites have also adapted their nutrition for metabolites provided by the host and lack a sulfate assimilation pathway (Nozaki et al. 2005). A third group of organisms usually lacking sulfate assimilation are archaea and bacteria using dissimilatory sulfide (or thiosulfate) oxidation or sulfate reduction for respiration and energy conversion (Pérez-Jiménez and Kerkhof 2005). The habitats of such organisms always contain sulfide, therefore, there is no need for sulfate assimilation to sustain cysteine biosynthesis. The enzymes of the dissimilatory pathway, despite catalyzing the same chemical reactions, are either highly divergent or entirely unrelated to those of the sulfate assimilation pathway (Patron et al. 2008).

### ***2.2.1. Sulfur in photosynthetic organisms***

All photosynthetic organisms use sulfate as main sulfur source. Due to its chemical characteristics, sulfate cannot be directly incorporated into organic compounds, and must be converted into sulfide, a more reduced form of sulfur, to be then used for the biosynthesis of a variety of macromolecules (Gonzalez-Ballester and Grossman 2009). The product of the primary (reductive) pathway of sulfate assimilation is the proteinogenic amino acid cysteine, a remarkably versatile molecule. Its chemical reactivity is a consequence of the thiol moiety present in its molecular structure, conferring cysteine the unique ability to perform both nucleophilic and redox-active functions (Jobe et al. 2019). Those will have an important role on protein folding, structure and regulation. Also, cysteine is the precursor of glutathione, a molecule

involved in cell detoxification and responses to oxidative stress; and methionine, another proteinogenic amino acid which, in turn, is used in the biosynthesis of DMSP (Norici et al. 2005).

On the secondary sulfate assimilatory pathway (generally termed sulfation), on the other hand, sulfate is readily transferred from an intermediate metabolite onto various acceptor molecules in its oxidized form by sulfotransferases. This metabolic route can generate a number of sulfated compounds, such as glucosinolates, sulfated peptides and flavonoids, and sulfolipids (Koprivova and Kopriva 2016). The latter being particularly important for marine phytoplankton. Interestingly, it has been shown that, in tomato, the sulfate donor for sulfolipid synthesis is not PAPS but sulfite (Brychkova et al. 2013). At least in plants, sulfolipid synthesis is thus connected with sulfate reduction rather than sulfation pathway and is part of a so-called sulfite network.

### **2.2.2. Sulfur metabolism in algae**

Most of what is known about sulfur metabolism in algae derives from studies carried out on vascular plants and on the model freshwater green alga *Chlamydomonas reinhardtii*. Recent biochemical experiments conducted on other clades of algae, including marine ones, paved the way to a broader view of sulfur metabolism that was elegantly put together by Prioretti et al. (2014) and is summarized on Figure 4. Collectively, the results suggest that this intricate metabolic pathway is not as conserved as once expected amongst photosynthetic organisms, and that more information is necessary, especially within the heterogeneous group of algae.

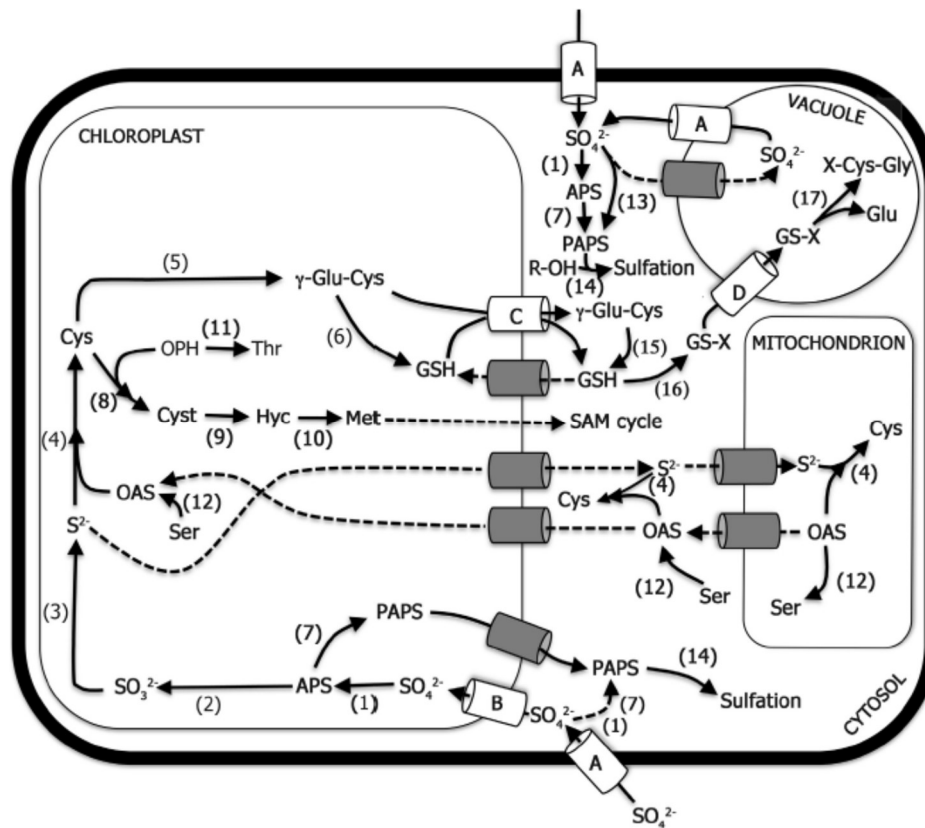


**Figure 4:** Main pathways of sulfate metabolism in algae and plants. The letters identify the type of transporter (if no letter is indicated, no convincing identification of the transporter is available). The numbers indicate the enzymes. Transporters: A =  $\text{nH}^+/\text{SO}_4^{2-}$  (SULTR) or  $\text{nNa}^+/\text{SO}_4^{2-}$  (SLT) co-transporters; B = ABC type transporters or unknown transporter for  $\text{SO}_4^{2-}$  uptake by the chloroplast; C = CLT, thiol transporter (chloroquine resistance transporter-like transporter); D = MRP, multidrug resistance-associated protein. Enzymes: (1) ATP sulfurylase; (2) APS reductase; (3) Sulfite reductase; (4) O-acetylserine (thiol)lyase; (5)  $\gamma$ -glutamylcysteine synthetase; (6) glutathione synthetase; (7) APS kinase; (8) cystathionine  $\gamma$ -synthase; (9) cystathionine  $\beta$ -lyase; (10) methionine synthase; (11) threonine synthase; (12) serine acetyltransferase; (13) fused ATP sulfurylase-APS kinase (present only in some chl *a + c* algae); (14) sulfotransferase; (15) glutathione synthetase; (16) glutathione-S-transferase; (17)  $\gamma$ -glutamyltransferase. Metabolites: Cys, cysteine; Cyst, cystathionine; Glu, glutamate;  $\gamma$ -Glu-Cys,  $\gamma$ -glutamylcysteine; GSH, glutathione; GS-X, glutathione conjugate; Hcy, homocysteine; Met, methionine; OPH, O-phosphohomoserine; APS, adenosine 5'-phosphosulfate; PAPS, 3'-phosphoadenosine 5'-phosphosulfate; R-OH, hydroxylated precursor; SAM, S-adenosylmethionine; Ser, serine; Thr, threonine; X-Cys-Gly, cysteinylglycine conjugate (source: Giordano and Raven 2014).

### 2.2.2.1. Sulfate acquisition and transport

There is no evidence of the direct usage of sulfur-containing organic molecules by photosynthetic organisms. However, in some freshwater systems, a large proportion of sulfur can be contained in these molecules (Giordano et al. 2005b). Many microorganisms, including microalgae, can produce and release enzymes that can cleave inorganic sulfur from organic compounds, making it available for plants and algae (Takahashi et al. 2011). These enzymes are called sulfatases and are classified as aryl- and alkylsulfatases, both producing  $\text{SO}_4^{2-}$  but differing on the residual byproduct: a phenol and an aldehyde, respectively. Eighteen putative arylsulfatases genes (ARS family) were identified in *C. reinhardtii* and they are mostly induced upon sulfate deficiency (Gonzalez-Ballester and Grossman 2009).

Once sulfate is available in the environment, it can be taken into cells via a variety of transporters (Takahashi et al. 2012). The transporters of the SULTR (sulfate transporter) family are integral membrane proteins that perform a  $n\text{H}^+/\text{SO}_4^{2-}$  ( $n \geq 3$ ) and have been identified in all photosynthetic organisms. In *C. reinhardtii*, affinity and activity of SULTR transporters are highly increased under sulfur limitation (Yildiz et al. 1994), and measurements of sulfate uptake – but not directly of SULTR affinity and activity – suggest that this is also true for the marine green alga *Dunaliella salina* (Giordano et al. 2000). In addition to the SULTR family, transporters of the SLT (Sac-1 like transporters) family have been identified in *C. reinhardtii* and in the genome of *Emiliania huxleyi*, albeit the low similarity with the green alga's sequences (Bochenek et al. 2013). These transporters are usually involved in  $\text{Na}^+/\text{SO}_4^{2-}$  co-transport and have been found to increase both expression and protein abundance in the freshwater green alga *C. reinhardtii* exposed to limiting concentrations of sulfate (Pootakham et al. 2010). It is noteworthy that it remains unclear whether the described regulatory mechanisms – for ARS, SULTR and SLT – also exist in other taxa, especially marine algae, since the high sulfate content in oceans apparently makes inducible uptake systems unnecessary (Giordano et al. 2005b).

After sulfate is taken up into the cytoplasm, it is transported into the plastids or, if in excess, stored in the vacuole. Recently, a completely different transport system has been described for the chloroplasts of green algae and some non-vascular plants (Melis and Chen 2005, Takahashi et al. 2012). The ATP-binding cassette (ABC) transporters consist on a transmembrane complex formed by two sulfate permeases heterodimers

(SulP and SulP2), connected to a sulfate-binding protein (Sbp) in the cytosolic side and a ATP-binding protein (Sabc) on the stromal side (Melis and Chen 2005). Since the inner plastidial membrane is derived from the plasma membrane of a cyanobacterium, it is believed that a similar sulfate transport system should present on the plasmalemma of cyanobacteria. However, the evidences for the occurrence of this transport are not strong (Giordano and Raven 2014).

#### 2.2.2.2. Sulfate activation

The standard reduction potential ( $E_0$ , at 25°C, 1 atm, pH 7, in aqueous solution) for the conversion of sulfate to sulfite is -454mV, which is beyond the range of biological reducing agents (Thauer et al. 1977). Sulfate anion is, therefore, biologically inert and thus organisms expend tremendous energy in its adenylation to adenosine 5'-phosphosulfate (APS) catalyzed by the enzyme ATP sulfurylase (ATPS, EC 2.7.7.4) – the reaction is also referred as sulfate activation (Figure 5). In APS, the mixed anhydride bond between phosphate and sulfate has a standard redox potential of about -60 mV, which is compatible with the use of thiols or pyrimidine as electron transporters (Giordano and Raven 2014).

Apparently, one of the major differences between sulfate assimilation of algae and plants resides in sulfate activation. In many algae, this step is susceptible to redox regulation and is believed to be the key regulatory step of the pathway (Prioretti et al. 2014, 2016; more information in the following chapters), whereas in plants and some algae the key regulatory step seems to be the one catalyzed by the enzyme APS reductase (Vauclare et al. 2002).

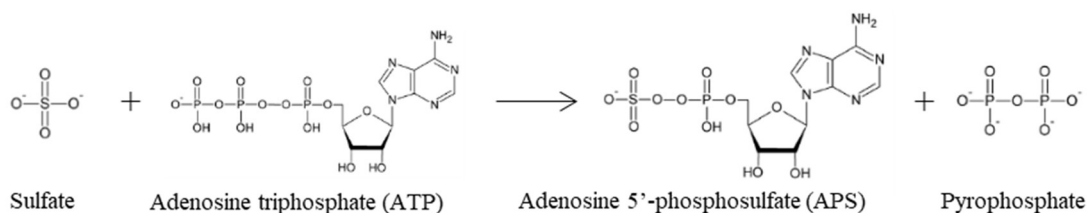


**Figure 5:** Sulfate activation, the reaction catalyzed by ATP Sulfurylase.

APS is the branching point between the primary (reduction) and secondary (sulfation) sulfur assimilation pathways (see Figure 4). After the sulfate activation reaction catalyzed by ATP sulfurylase, APS can finally undergo two destinies: (i) a multi-

step reduction and synthesis of cysteine; or (ii) the incorporation into organic molecules as such.

### 2.2.2.3. Primary sulfate assimilatory pathway – Reduction

In eukaryotic photosynthetic organisms, sulfate reduction occurs primarily in the plastids. The only known exception is *Euglena gracilis*, that reduces  $\text{SO}_4^{2-}$  in the mitochondrion (Hodson et al. 1971). In the reductive pathway (Figure 6), APS is reduced to sulfite ( $\text{SO}_3^{2-}$ ) by APS reductase (APSR, EC 1.8.4.9). Sulfite is then further reduced to sulfide by a nearly constitutive sulfite reductase (SiR, EC 1.8.7.1). Finally, serine acetyl transferase (SAT, EC 2.3.1.30) and O-acetyl serine (thiol) lyase (OAS-TL, EC 2.5.1.47) mediate the incorporation of sulfide into cysteine. The reaction catalyzed by SAT leads to the biosynthesis of O-acetylserine (OAS), using serine and acetyl coenzyme A as substrates. Then, OAS serves as carbon skeleton to which sulfide is attached through the reaction catalyzed by OAS-TL yielding cysteine.

In contrast to plants, very few biochemical data exist on the pathway's localization in algae (see Koprivova et al. 2001, Wirtz et al. 2004 for more information in plants). Although sulfate reduction is believed to be confined in plastids, it is unclear whether sulfate activation and cysteine synthesis can also occur in other cell compartments. *In silico* analyses showed that red algae possess a cytosolic isoform of ATPS besides the chloroplastic one. ATPS activity was also found in the cytosol of *Arabidopsis thaliana*, and it was suggested to be specialized on the sulfation pathway (Koprivova and Kopriva 2016). In *C. reinhardtii*, APSR and SiR were found almost exclusively within the plastids and, furthermore, their distribution suggested that the enzymes may form a multienzyme complex for sulfate reduction (Patron et al. 2008; further discussed in Chapter 4). Assessment of localization of SAT and OAS-TL in algae, in turn, is limited to very rugged *in silico* analyses, due to the huge number of poorly verified sequences, frequently lacking pre-sequences (Bromke et al. 2013).

Further information on phylogenetics, structure and functioning of each enzyme is given in Chapter 3.

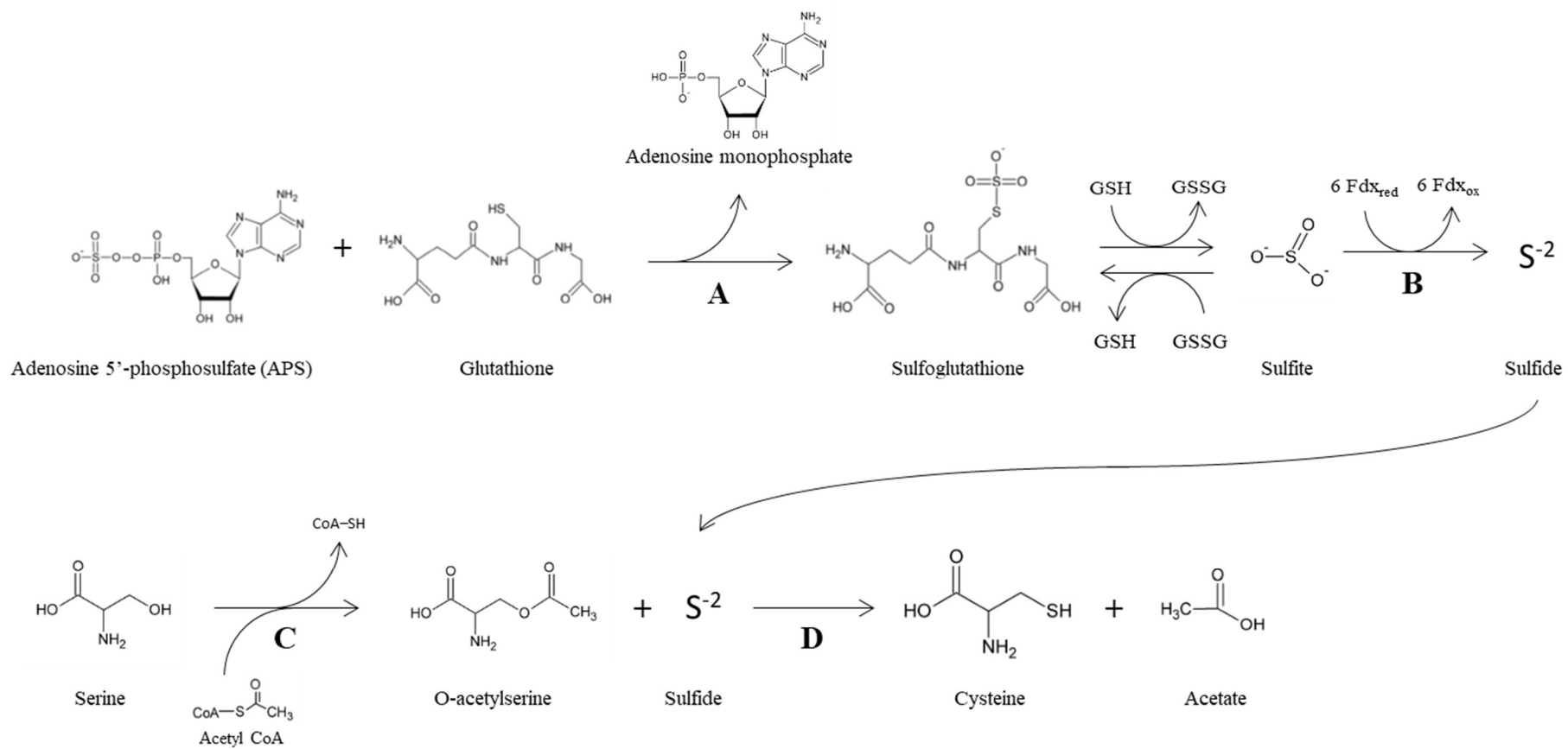


**Figure 6:** Primary (reductive) sulfate assimilatory pathway, after sulfate activation. Figure illustrate the reactions catalyzed by APS reductase (A), Sulfite reductase (B), Serine acetyl transferase (C) and O-acetylserine (thiol) lyase (D).

#### 2.2.2.4. Secondary sulfate assimilatory pathway – Sulfation

Alternatively to the reduction, APS can be phosphorylated to 3'-phosphoadenosine 5'-phosphosulfate (PAPS) by APS kinase (APSK, EC 2.7.1.25), and sulfate from PAPS can then be readily transferred onto various acceptor molecules by sulfotransferases (SOTs; Figure 4). Unlike photosynthetic organisms, fungi and some bacteria with PAPS-dependent sulfate reduction use PAPS as a substrate for sulfite synthesis catalyzed by PAPS reductases (PAPR, EC 1.8.4.8; Patron et al. 2008). Sequences similar to PAPR were found in the genome of marine algae like the diatom *Thalassiosira pseudonana*, but no specific information on the protein is available (Bromke et al. 2013).

In turn, APSK is essential for *Arabidopsis thaliana* (Mugford et al. 2009) and it is likely to be localized both in the cytosol and in the plastids of plants and green algae. In many other algae APSK is often found fused to ATPS, forming a PAPS synthetase complex, likely to be cytosolic and probably increasing catalytic efficiency (Patron et al. 2008). The complex interaction of ATPS, APSK and, sometimes, a pyrophosphatase – like in the case of many Stramenopile algae – was thoroughly assessed by Bradley et al. (2009). Further information on phylogenetics, structure and functioning of APK is given in Chapter 3.

Following the reaction catalyzed by APSK, SOTs transfer the sulfate from PAPS onto hydroxyl groups of diverse metabolites. Due to this substrate diversity, the SOTs form large multigene families in all kingdoms. However, the structures of the proteins are similar, since they are using the same reaction mechanism (Günel et al. 2019). Not much information is available about the biological roles and regulations of SOTs families, even within a single species. The most studied, by far, are those SOTs involved in glucosinolate synthesis in *A. thaliana* (Koprivova and Kopriva 2016). Among algae, as usual, the information is even rarer.

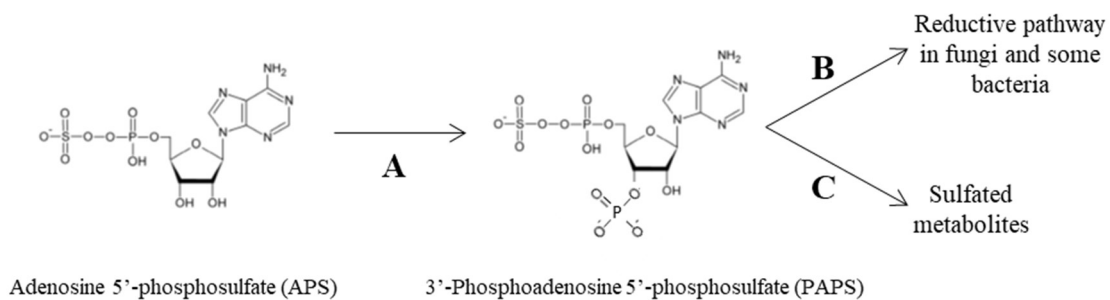


**Figure 7:** After sulfate activation, APS can be phosphorylated to PAPS by APS kinase (A). In fungi and some bacteria, PAPS can be reduced by PAPS reductase (B) and follow the reductive pathway of cysteine synthesis. Or the sulfate in PAPS can be readily incorporated into organic compounds by Sulfotransferases (C).

As a result of the sulfation reactions, the biosynthesis of sulfated polysaccharides and sulfolipids are particularly important for algae (Koprivova and Kopriva 2016). Sulfated polysaccharides are major components of seaweed cell walls (Pomin and Mourão 2008). Some of them – such as agar and carrageenan in red algae; fucans in brown algae; and ulvans in green algae – are commercially exploited due to several desirable properties (see Ngo and Kim 2013 and references therein). Sulfolipids, in turn, are important constituents of the cell membranes, and they seem to compensate the reduction in membrane phospholipids in phosphate-poor environments, not a rare condition in oceans. Hence, its bigger relevance in marine phytoplankton (Van Mooy et al. 2006).

### 2.3. Experimental organisms

The physiological studies presented in this thesis were carried out in four species of marine microalgae belonging to different groups: *Tetraselmis suecica* (Chlorophyta); *Porphyridium purpureum* (Rhodophyta); *Phaeodactylum tricorutum* (Bacillariophyta); and *Amphidinium carterae* (Dinophyta).

#### ***Tetraselmis suecica* (Kylin) Butcher, 1959**

As a representative of the widespread group of green algae, *T. suecica* (Chlorodendrophyceae) harbors a primary green plastid inherited from an ancient cyanobacteria. Its spherical motile cells contain four flagella and are armored with polysaccharide-rich scales synthesized in the Golgi apparatus (Manton and Parke 1965). With around 10 µm in diameter, it is a marine species that can be found in open sea as well as in tidal pools (Hori et al. 1986). *T. suecica* thrives very well when cultured and presents desirable characteristics for biotechnological exploitations, such as aquaculture

and biofuel production (Fábregas et al. 2001, San Pedro et al. 2013). For these reasons, valuable information on *T. suecica*'s cultivation and physiology is vastly available in literature.

### ***Porphyridium purpureum* (Bory) Drew and Ross, 1965**

*P. purpureum* (Porphyridiophyceae) is a red alga, containing red primary plastids and belonging to the phylogenetically diverse Order of Porphyridiales (Yoon et al. 2006). It has been reported that in *Porphyridium* spp. the Golgi apparatus is associated to the mitochondria and the endoplasmatic reticulum, like in the genus *Flintiella* (Scott et al. 1992, Karsten et al. 2003).

This is a ubiquitous species, found in brackish inland salt marshes, limestone areas, terrestrial habitats, on soil with a rich supply of organic matter and, less commonly, in marine environments. Its cells characteristically form red patches (1-3 cm diameter) in the surface where they are thriving, are spherical with 4,5-5,5 µm in diameter and possess a stellate plastid with a naked pyrenoid (Nelson and Ryan 1988).

### ***Phaeodactylum tricornutum* (Bohlin, 1897)**

Diatoms (Bacillariophyceae) are a highly diversified group that can be found in virtually any aquatic environment. They possess secondary plastids derived from red algae, compose the most abundant group of marine phytoplankton and phytobenthos and are believed to account for one-fifth of global primary productivity (Archibald 2009). Their cells are encased by a bi-partite silica coverage called frustule, that can be well preserved in the fossil records allowing relatively precise dating of diatoms' evolution through geological Eras (Kooistra et al. 2007).

*P. tricornutum* is a widespread marine pennate diatom, with 25-35 µm length, whose cells can present three distinct shapes: fusiform, oval and, more rarely, triradiate. The cultivation and physiology of *P. tricornutum* have been extensively studied in the context of exploring its biomass for aquaculture and biotechnology (Chisti 2007, Kurpan Nogueira et al. 2015). Its genome sequencing revealed a 27,4 Mb size and a remarkably high number of genes predicted to have been transferred between bacteria and this diatom (Bowler et al. 2008). Given the availability of its genome sequence as well as the existence of efficient genetic transformation techniques (Apt et al. 1996, De Riso et al. 2009, Serif et al. 2017), *P. tricornutum* has become a model system for genetic manipulation in diatoms.

### ***Amphidinium carterae* (Hulburt, 1957)**

As most dinoflagellates, *A. carterae* (Dinophyceae) hosts a secondary plastid derived from red algae, containing the carotenoid peridinin (Hofmann et al. 1996). This phylum, however, also contains representatives with secondary plastids derived from green algae, and tertiary endosymbiotic plastids (Archibald 2009). Although most dinoflagellates are primary producers, the group harbors a great metabolic diversity, shares many features with parasitic protists and its phylogeny is not fully resolved yet (Butterfield et al. 2013, Bachvaroff et al. 2014).

*A. carterae* is athecate – or “naked” –, lacking the typical polysaccharide cell wall present in armored dinoflagellates, called theca. It has an oval shape, dorsoventrally flattened, 10-20 µm long and 9-13 µm wide, with a crescent-shaped epicone deflected towards the left (Lee et al. 2013). This is a truly cosmopolitan species, being reported in the sediments and water column from the arctic to tropical waters. It has also been found as a symbiont in the jellyfish *Cassiopea xamachana* in the Caribbean Sea (Murray et al. 2004).

## **2.4. Aim and organization of this thesis**

The aim of this thesis was to investigate the diversity of sulfur metabolism within the diverse group of algae. The evolution of sulfur metabolism among algal groups is further investigated in Chapter 3, which consists of a broad *in silico* phylogenetic assessment of the six core enzymes of sulfur reduction and assimilation with emphasis in algae. Chapter 4 focuses on a peculiar enzyme of sulfur metabolism named ATP Sulfurylase, thoroughly assessing the specific function, cellular localization and regulation of this enzyme on the model diatom *Phaeodactylum tricornutum*. Results were then compared to what is known in other algal groups. In Chapter 5, the impacts of growth-limiting concentrations of sulfur on the physiology and biochemical composition of marine microalgae belonging to different clades is thoroughly investigated. Results were discussed as an attempt to address a physiological link between the sensitivity to sulfur limitation and the SFH (see Section 2.1.1.1). Finally, Chapter 6 recalls results from Chapter 4 and investigates the growth of *P. tricornutum* on other sources of sulfur, hypothesizing the complementation of ATP Sulfurylase knock out mutants.

### 3. PHYLOGENY OF SULFUR ASSIMILATION ENZYMES

#### 3.1. Introduction

Sulfate reduction and assimilation is often assumed to be conserved in all photosynthetic organisms. However, the available information is mostly limited to vascular plants, with little information on other clades – mostly at the genomic or, at most, expression level (Hell 2002). The rare studies conducted on algae, or at least considering algal diversity, indicate that there are some rather important differences among taxa and from plants. For instance, Patron et al. (2008) elegantly reviewed the phylogenetic relationship in eukaryotes of the three enzymes involved in sulfate reduction (ATPS; APR and SiR). Bromke et al. (2013), similarly, reviewed the whole sulfate reduction pathway – from transporters to cysteine synthesis – with emphasis on the diatom *Thalassiosira pseudonana*. Both authors observed a remarkable diversity and intriguing features, like the evidence of eukaryote-to-prokaryote gene transfer in ATPS and the retargeting of APSR to the mitochondrion in *Euglena gracilis*. Further, Prioretti et al. (2014) focused on ATPS, the first committed enzyme for sulfate assimilation, and proposed that its diversity mainly consisted in the number and position of cysteine residues and, hence, the susceptibility of redox regulation. This idea was later showed to be true with biochemical *in vitro* assays (Prioretti and Giordano 2016, Prioretti et al. 2016).

Still, the origins and diversity of the sulfate assimilation pathways are obscure; the localization and level of redundancy of the assimilation steps are not clear whatsoever, especially when compared to the knowledge on other macronutrients, such as nitrogen and phosphorus (Giordano and Raven 2014). In this chapter, to obtain an insight into the evolution of the sulfate assimilation pathway in algae and relationships of the differently compartmentalized isoforms, the enzymes' locations were predicted, and phylogenetic analyses were performed in sequences of the six core enzymes involved in sulfate assimilation (Figure 8). As their functional characteristics were introduced in the previous Section, a more thorough structural and physiological description is given in the following paragraphs.

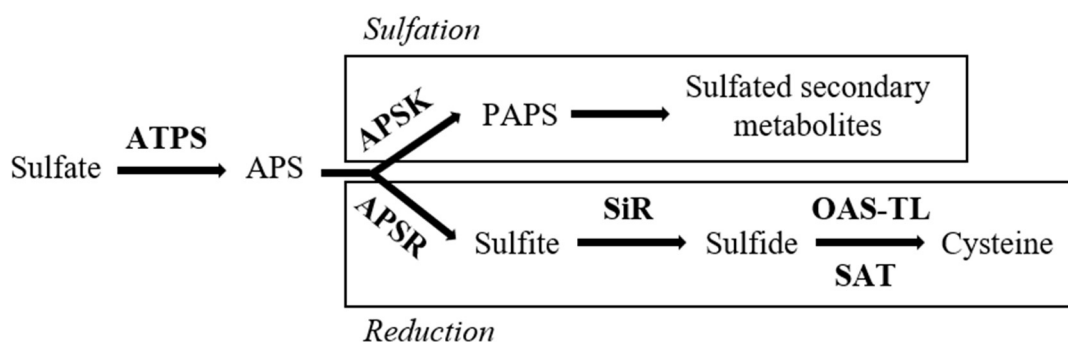


**Figure 8:** General scheme of sulfate assimilation. The six core enzymes are highlighted in bold and represented as the respective acronyms used in text (for the detailed pathway, see Figure 5, Figure 6 and Figure 7).

### 3.1.1. *ATP Sulfurylase (ATPS)*

ATPS is a nucleotidyltransferase that belongs to the superfamily of  $\alpha/\beta$  phosphodiesterases. It catalyzes the non-reductive adenylation of sulfate to adenosine 5'-phosphosulfate (APS) and pyrophosphate (PPi) (Figure 5). It is encoded by a multigene family and its activity can be detected in cytosol and chloroplasts in plants (Bohrer et al. 2015). Although a fair amount of information is available on bacterial and fungal ATPS (Mueller and Shafqat 2013), the same is not true for phototrophic organisms, especially algae.

Bacterial ATPS consists of four heterodimers composed of 35 kDa CysD and 53 kDa CysN subunits (Taguchi et al. 2004, Parey et al. 2013), and plant ATPS forms a homotetramer of 52-54 kDa (Murillo and Leustek 1995). In fungi, ATPS and APS kinase (APSK) are fused into a single 59-64 kDa subunit that assemble into a homohexamer (MacRae et al. 2001). In fact, ATPS is susceptible to a number of gene fusions with APSK and, to a lesser extent, APS reductase (APSR) (Bradley et al. 2009, Prioretti et al. 2014). For instance, in metazoans, a fused, sequentially acting bifunctional enzyme commonly known as PAPS synthetase has a kinase domain at the amino-terminal end of the protein, followed by a sulfurylase domain (Lyle et al. 1994). The exclusive function of this fusion in metazoans is thought to be PAPS synthesis for use in sulfation. In some fungal and bacterial species, a fusion of the sulfurylase and kinase domains is found with a reversed domain order relative to the metazoan gene. In those cases, the kinase domain is highly degenerated, and a range of functions have been attributed to it in different organisms (MacRae and Segel 1997, Hanna et al. 2002, Lalor et al. 2003). Furthermore, a triple

fusion protein containing a kinase, a sulfurylase and a pyrophosphatase domain is found in several organisms within the Stramenopiles lineage. The three domains appear to physically interact and activate more sulfate than the “kinase-sulfurylase” alone (Bradley et al. 2009). Finally, a reductase domain is amino-terminally fused with ATPS in dinoflagellates, but hitherto information about this protein is too superficial to draw general conclusions (Prioretti et al. 2014).

Different modes of regulation have been proposed to algal ATPS, which appear to be subject to redox regulation in oceanic cyanobacteria and eukaryotic algae (except dinoflagellates); but not in freshwater and coastal cyanobacteria and dinoflagellates. Although this idea is sustained by sequence analysis and *in vitro* assays (Prioretti et al. 2014, 2016), the *in vivo* mechanisms that regulate ATPS and how it can be linked to physiological differences within algae groups is unclear (see Chapter 4 for preliminary results on *in vivo* regulation).

### **3.1.2. APS Kinase (APSK)**

APSKs are small phosphotransferases that catalyze the transfer of the  $\gamma$ -phosphate from ATP to the 3'-hydroxyl group of the APS adenine ring to yield PAPS and ADP. Thus, it directs APS to the sulfation pathway in most organisms, apart from fungi and some bacteria, where PAPS is an ordinary intermediate in the sulfate reduction (Figure 7). Bacterial, fungal and plant APSK functions as homodimers of 21-27 kDa subunits, and the kinetic mechanism was thoroughly described in fungi: first, MgATP binds the enzyme, followed by APS; then PAPS leaves the system before MgADP (Satishchandrans and Markham 1989).

The vascular plant *Arabidopsis thaliana* contains four isoforms of APSK, one cytosolic and three plastidic (Mugford et al. 2009). Although knockouts of up to three APSK genes still produces viable plants, the knockout of all the four genes is lethal, showing that APSK is an essential enzyme (Mugford et al. 2010). These experiments also showed specialized function among isoforms. For example, APK2 is the only isoform unable to produce viable pollen when expressed alone (Mugford et al. 2010). There is no information about APSK redundancy and compartmentalization on other photosynthetic organisms.

All APSKs studied so far showed a remarkably high affinity for APS ( $K_m \sim 10^{-6}$  M) and, in addition, that purified from the green freshwater algae *Chlamydomonas*

*reinhardtii* appeared to be regulated by reduced thioredoxin (Schwenn and Schriek 1984). Similarly, structure and sequence analyses observed that is likely that APSK from *A. thaliana* is also redox regulated, suggesting that the redox state of the environment may regulate the partitioning of APS into the primary and secondary sulfate assimilation pathways (Ravilious et al. 2012).

### **3.1.3. APS Reductase (APSR)**

APSR catalyzes the reduction of APS, yielding adenosine-monophosphate, sulfoglutathione and sulfite (Figure 6). It exists as a homodimer in prokaryotes and is fused to thioredoxin in plants and green algae (Kopriva et al. 2007). In plants, it is thought to be the primary regulation point for sulfate assimilation (Leustek 1996, Ravilious et al. 2012). Sequence analysis shows high similarity between APSR from green algae and vascular plants and, in both cases, the enzyme is localized mainly in plastids (Gao et al. 2000, Patron et al. 2008). Despite the lack of information available for other marine algae clades, it appears that APSR activity is higher in DMSP-producing organisms (Gao et al. 2000).

In fungi and some bacteria, the product of APS phosphorylation by APSK, PAPS, can be further directed to reduction by PAPS Reductases (PAPR). PAPRs are similar to bacterial APSRs but, unlike most APSRs, do not bind FeS clusters, an important characteristic that separates organisms that reduce APS or PAPS (Kopriva et al. 2002). However, a variant of APR from early branching streptophyte lineages (bryophytes and lycophodiophytes) has been shown to catalyze APS reduction without the FeS chemistry (Kopriva et al. 2002, 2007), and some enzymes has been shown to be able to catalyze the reduction of both APS and PAPS (Bick et al. 2000).

### **3.1.4. Sulfite Reductase (SiR)**

SiR catalyzes the six-electron reduction of sulfite to sulfide and is functionally and structurally diverse among organisms. Bacterial and fungal SiR utilizes NADPH as an electron donor for its catalysis. Whereas in bacteria SiR is composed by four 66 kDa catalytic hemoprotein subunits and eight 66 kDa flavoprotein subunits, in fungi it is composed by two  $\alpha$  and  $\beta$  subunits of 116 and 167 kDa respectively (Kobayashi and Yoshimoto 1982, Crane et al. 1995). Plant SiR, on the other hand, requires ferredoxin as a physiological electron donor and is a 65 kDa monomeric enzyme containing one

siroheme and a FeS cluster (Nakayama et al. 2000). It was shown that, in *A. thaliana*, SiR is a crucial enzyme, once its downregulation resulted in severe growth impairment (Khan et al. 2010). Since it requires ferredoxin as an electron donor, SiR is believed to exist exclusively within the plastids in plants, and it is supported by sequences analyses and biochemical assays (Nakayama et al. 2000). At least in the freshwater green alga *C. reinhardtii*, SiR was shown to be located only in chloroplasts and there is no strong evidence to think differently about other algae so far. The only known exception is the green alga *Euglena gracilis*, but its SiR sequence is not related to those of other algae (Patron et al. 2008).

Sulfite and nitrite reductases (NiR) are closely related proteins that can reduce the reciprocal substrate, albeit at lower efficiency. Fd-SiR and NADPH-SiR show a low but significant sequence homology with Fd-NiR, where the regions forming the FeS cluster and the siroheme are well conserved (Nakayama et al. 2000). By primary sequence analysis, it is not always possible to conclude if an unknown sequence belongs to SiR or NiR, hindering sequence-based analyses (Patron et al. 2008).

### ***3.1.5. Cysteine Synthase: Serine Acetyl Transferase (SAT) and O-Acetyl Serine-Thiolyase (OAS-TL)***

SAT catalyzes the acetylation of L-serine by acetyl CoA to yield O-acetylserine (OAS). Then, sulfide is incorporated into OAS to produce L-cysteine, in a reaction catalyzed by OAS-TL (Figure 6). These two enzymes are thought to form a complex known as cysteine synthase (Feldman-Salit et al. 2009). The cysteine synthase complex was first described from the pathogenic enterobacterium *Salmonella typhimurium* and consisted on a 309 kDa hetero-oligomeric structure, with 160 kDa SAT homomers and 68 kDa OAS-TL homomers (Kredich 1971). While all SAT activity is associated with the complex, OAS-TL exists also as a free homodimer (Hell 2002). The complex is thought to function similarly in plants and other phototrophs. However, the overall structure is still not completely resolved.

SAT and OAS-TL seems to be required in every cell compartment where protein biosynthesis is carried out, and it was thought to be a consequence of the inability to transport cysteine through the organelles' membranes (Lunn et al. 1990). However, more recent analyses of *A. thaliana* mutants showed that cysteine synthesis can be restricted to a single cell compartment with small effects on growth, suggesting that cysteine – or a

precursor – must be transported inside the cells (Birke et al. 2012). The identity of such transporters remains unknown (Gigolashvili and Kopriva 2014). A number of isoforms have been found in cytosol, plastids and mitochondria of various plants (Lunn et al. 1990, Ruffet et al. 1994). Even if the information on algae is scarce, the model green alga *C. reinhardtii* seems to harbor two isoforms of SAT and four of OAS-TL, a lower number when compared to vascular plants (Ravina et al. 1999, 2002).

In contrast to SATs, OAS-TLs have a higher functional plasticity and may be involved in the synthesis of secondary products in some plants (Murakoshi et al. 1986, Maier 2003). OAS-TLs belong to the pyridoxal phosphate-dependent superfamily (PLP) of  $\beta$ -substituting alanine synthases, sharing a high amino acid homology with enzymes like  $\beta$ -cyanoalanine synthase (CAS). In fact, from the eight functionally transcribed OAS-TL-like proteins in *A. thaliana*, at least one is predicted to act as a CAS *in vivo*, within the mitochondria (Jost et al. 2000, Yamaguchi et al. 2000). Additionally, in prokaryotes such as *S. typhimurium* two OAS-TLs were described, named CysK (OAS-TL A) and CysM (OAS-TL B). Whereas the first is preferentially used in aerobic growth, the latter is more active in anaerobiosis (Filutowicz et al. 1982).

## 3.2. Material and Methods

### 3.2.1. Sequence data acquisition

Amino acid sequences from the six enzymes involved in the core S reduction and assimilation (ATP Sulfurylase, ATPS: EC2.7.7.4; APS Kinase, APSK: EC2.7.1.25; APS Reductase, APSR: EC1.8.4.9; Sulfite Reductase SiR: EC1.8.1.2 / EC1.8.7.1; Serine Acetyl Transferase, SAT: EC2.3.1.30; O-Acetyl Serine Thiol Lyase, OAS-TL: EC2.5.1.47) were manually extracted from the organism menu of the sulfur metabolism pathway (map 00920) of KEGG (Kyoto Encyclopedia of Genes and Genomes) Database (Kanehisa et al. 2020). All algal sequences were extracted, in addition to sequences from arbitrary species from other relevant groups (e.g. plants). Those sequences, belonging to a variety of taxa, were then used as queries on BLAST (Basic Local Alignment Search Tool). The resulting sequences from NCBI (National Center for Biotechnology Information) Database were selected using an arbitrary threshold of 70% identity.

### ***3.2.2. Sequences targeting predictions***

Sequences from photosynthetic eukaryotes retrieved were then evaluated for the presence of signal- and transit peptides with the aid of web application tools. Sequences from plants and green and red algae were assessed using TargetP 1.1 (Emanuelsson et al. 2007), whereas those from red lineage microalgae containing complex plastids were inputted into the heterokont subcellular localization targeting method (HECTAR; Gschloessl et al. 2008).

### ***3.2.3. Sequence alignments and phylogenetic analysis***

Multiple Sequence Alignments (MSA) were generated in MFFT Software (Kato et al. 2018) with a gap opening penalty of 1,53 and maximum of three iterative refinements. Alignments were then visually examined for consistency, and highly divergent regions were masked. Extremely high divergence generally indicates non-essential regions that might allocate huge insertions and/or deletions and overestimate evolutionary changes at the amino acid level. Masking was made with the aid of HMMER (Johnson et al. 2010) fed with a Pfam profile database (El-Gebali et al. 2019) for each enzyme, and resulting sequences were checked in NCBI's Conserved Domains Database (CDD; Lu et al. 2020), an online tool for fast identification of conserved domains in protein sequences. CDD was also used on the separation of sequences belonging to fused proteins. In those cases, each conserved domain was put separately into the phylogenetic tree of its specific enzyme – e.g.: the heterokonts' fusion of ATPS and APSK was separated and is partially present in the ATPS and APSK trees.

Final masked alignments were used to generate a neighbor-joining (NJ) tree to serve as initial topology for a Randomized Axelerated Maximum Likelihood (RAxML). The maximum likelihood tree, that with the highest probability of showing the correct topology, was achieved by running RAxML with 1000 non-parametric bootstraps in the IQ Tree Software (Nguyen et al. 2015). Based on its Bayesian selection criteria, the software suggested an evolution model after testing approximately 500 models for each list of sequences (Kalyaanamoorthy et al. 2017).

### 3.3. Results and Discussion

#### 3.3.1. Sequences targeting: sulfate reduction is predicted in chloroplast in algae

The predicted cellular localization for each eukaryotic photosynthetic group is summed up in Table 1 (see Supplemental Table 1 for detailed prediction results of all retrieved sequences of eukaryotic phototrophs). The localization of the primary (reductive) sulfate metabolism steps appeared to be similar amongst photosynthetic groups: sulfate reduction enzymes, ATPS, APSR and SiR, were mainly predicted within plastids while cysteine biosynthesis (SAT and OAS-TL) was suggested to happen as well in other cell compartments where proteins are synthesized. Some differences in this trend were observed but were usually associated to an unreliable prediction – see reliability class (RC) in Supplemental Table 1 –, like the case of mitochondrial predictions for green algal SiR and red algal ATPS and SiR. Further, mitochondrial APSR prediction in green algae, despite showing a high RC according to the software used, was not validated *in vivo*: for instance, APSR of the green alga *C. reinhardtii* was immunolocalized exclusively within the plastids (Patron et al. 2008), and not in the mitochondrion as predicted from sequence targeting software. APSK, the enzyme involved in the secondary (sulfation) sulfate metabolism, was predicted to occur on chloroplasts, mitochondria and cytosol of plants and green and red algae. In red lineage algae, various clades – e.g.: diatoms – possess the APSK domain solely fused to ATPS and pyrophosphatase. This complex is predicted to exist only in the cytosol.

These results, hence, are partially coherent with what is assumed for algae, mostly based on observations in plants. Most of the differences from previous assumptions observed among the *in silico* predictions presented here do not agree with common knowledge and some were already experimented *in vivo* or *in vitro*. With respect to the sulfation pathway, however, there is not enough information on algae to sustain or refute the idea of APSK existing in the cytosol, chloroplast and mitochondrion (Table 1). In plants, though, APSK seems to exist only in the cytosol and chloroplasts (Koprivova and Kopriva 2016), contrarily to the predicted *in silico*. The prediction of APSK exclusively in cytosol of red lineage algae is an interesting feature that may suggest the physical separation of reduction and sulfation – in plastids and cytosol, respectively – in this group (Prioretti et al. 2014; see more information in Chapter 4).

For red lineage species APSR, SiR and OAS-TL, results did not allow to infer a most common localization, and are labeled “variable” on Table 1. This can be due to multiple reasons. Localizations’ predictions of sequences belonging to red lineage algae might reflect the diversity of the group with a highly heterogenous predictions among species. We thus cannot exclude that species-specific differences in the sublocalization of enzymes exists. However, the research on several red lineage species is still lacunouous, and wrong prediction can presently be due to incorrect annotations in the coding sequence starting methionine, which lead to an annotated protein sequence N-terminus lacking the signal peptide. An example of the thorough investigation of a non-annotated pre sequence in *P. triornutum*’s ATPS sequence is given in the following chapter. Also, Secondary endosymbionts, due e.g. to the different number of membranes surrounding the chroloplast because of their evolutive history, require specific softwares for protein localization predictions, which have recently started to developed (Bruce 2001, Patron and Waller 2007).

**Table 1:** Number of sequences per species and their predicted cellular localization. Data is an approximation of the the analyses of all retrieved sequences (see Supplemental Table 1 for all results).

<b>Enzyme</b>	<b>General description (sequences per species; localization)</b>			
	<b>Plants</b>	<b>Green algae</b>	<b>Red algae</b>	<b>Red lineage</b>
<b>ATPS</b>	chloroplast	chloroplast / mitochondria	cytosol / mitochondria	cytosol / chloroplast
<b>APK</b>	chloroplast / cytosol / mitochondria	chloroplast / cytosol / mitochondria	chloroplast / cytosol / mitochondria	cytosol
<b>APR</b>	chloroplast	mitochondria	chloroplast	variable
<b>SiR</b>	chloroplast	chloroplast / mitochondria	chloroplast / mitochondria	variable
<b>SAT</b>	chloroplast / cytosol / mitochondria	chloroplast / cytosol / mitochondria	chloroplast / cytosol / mitochondria	chloroplast / cytosol / mitochondria
<b>OAS-TL</b>	chloroplast / cytosol / mitochondria	chloroplast / cytosol / mitochondria	chloroplast / cytosol / mitochondria	variable

### 3.3.2. *Phylogenetic analyses*

#### 3.3.2.1. *ATPS phylogenetic analysis reveals functional clusters*

The general distribution of taxa in the ATPS tree was intriguing and showed a high degree of divergence among sequences (Figure 9). Isoforms encoded by species belonging to well-defined groups were frequently not monophyletic. In the analyses performed in this thesis, this was particularly observed in the two distantly related isoforms found in red algae and red lineage, both groupings were well-supported (>96 maximum likelihood bootstraps; identified with stars in Figure 9 B). From the two red algae isoforms, one was closely related to Archea and  $\beta$ -cyanobacteria, whereas the other was related to plants and to the sulfurylase domain of the red lineage kinase-sulfurylase-pyrophosphatase fusion. Instead, the other red lineage isoform, the mono-functional ATPS, was closer to green algae and  $\alpha$ -cyanobacteria. Plants and green algae's isoforms, on the other hand, were independently monophyletic, albeit completely unrelated. Patron et al. (2008) have noticed that the cyanobacterial origin of this enzyme is unlikely amongst algae. The authors also found evidence for eukaryote to prokaryote gene transfer and two reversal cellular targeting of host- and endosymbiont-originated proteins.

In the ATPS tree, sequences from  $\alpha$ - and  $\beta$ -cyanobacteria were clustered separately. One of the different characteristics between these types of cyanobacteria is the susceptibility of their ATPSes to redox regulation. The so-called  $\alpha$ -cyanobacteria contain redox-sensitive ATPS and are mostly marine, possessing Rubisco 1A and  $\alpha$ -carboxysomes; whereas ATPS non-sensitive to redox regulation exists in  $\beta$ -cyanobacteria, containing Rubisco 1B and  $\beta$ -carboxysomes (Prioretti et al. 2016). Interestingly, it suggests that the mode of regulation of ATPS may have been selected by the kind of environment where aquatic phototrophs thrived: (i) the oceanic-dominant cyanobacteria from the genus *Prochlorococcus* and *Synechococcus*, possess a redox regulated ATPS; and (ii) the mostly coastal and freshwater  $\beta$ -cyanobacteria possess an ATPS non-sensitive to redox regulation (Prioretti et al. 2014). If this separation occurred before the single event of chloroplast acquisition, then several independent lateral gene transfers occurred for the distribution of ATPS to other photosynthetic clades, given the distant relation between green algae and plants, and red algae and red lineage algae. Or, ATPS do have a cyanobacterial origin, but enzymes evolved convergently according to the characteristics of the environment where its possessors lived, resulting on a substantial

difference even among cyanobacteria. With the information currently at hand, the multiple and complex origins of ATPS can be only hypothesized.

ATPSes diversified susceptibility to redox regulation has been confirmed by *in silico* analyses and *in vitro* biochemical experiments (Prioretti et al. 2014, 2016, Rosenwasser et al. 2014; see Chapter 4). The tree could thus be divided in one monophyletic group of redox sensitive ATPSes, containing green algae,  $\alpha$ -cyanobacteria and red lineage monofunctional ATPS sequences, whereas all other sequences would be contained in a second group of non-sensitive to redox regulation ATPSes.



A

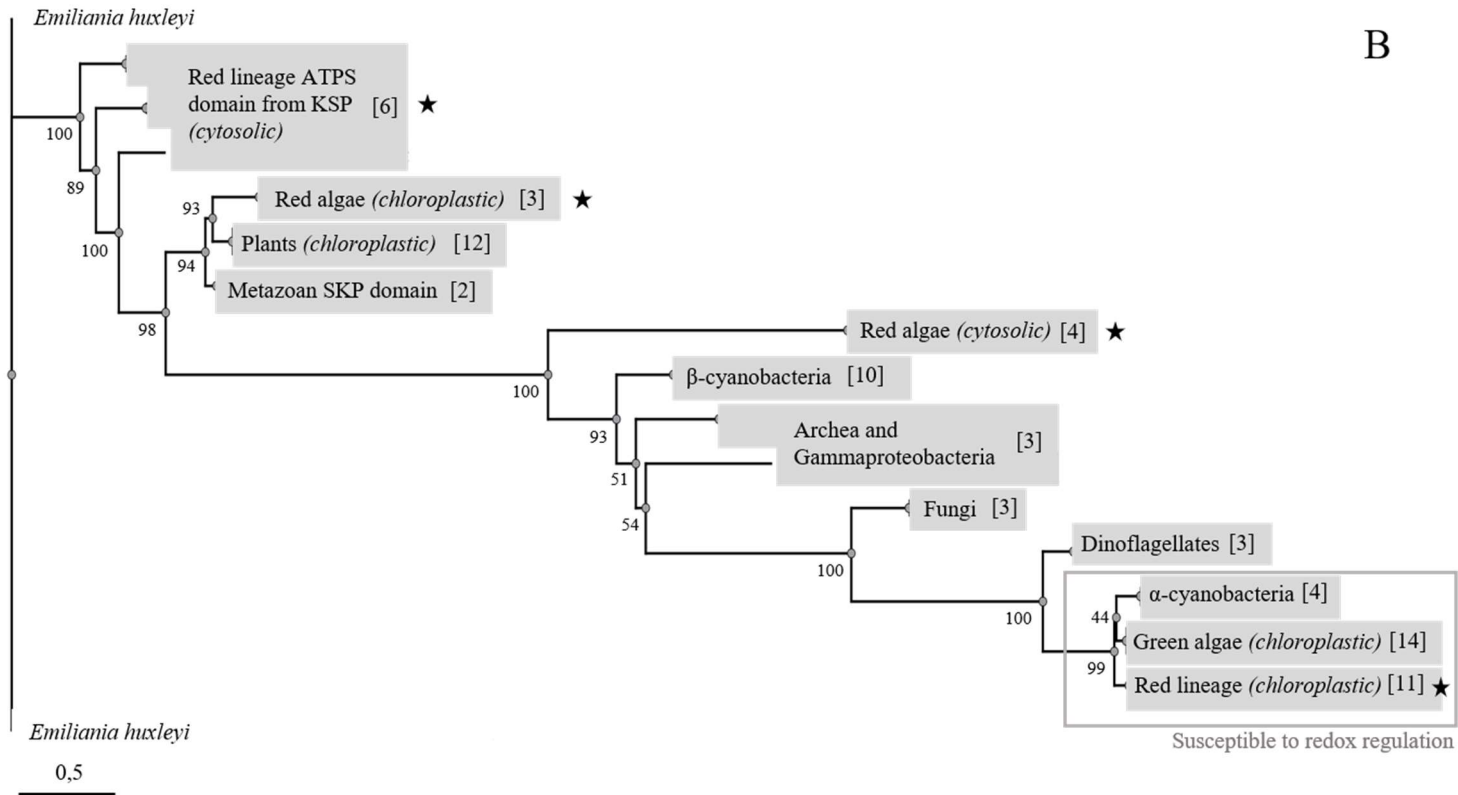
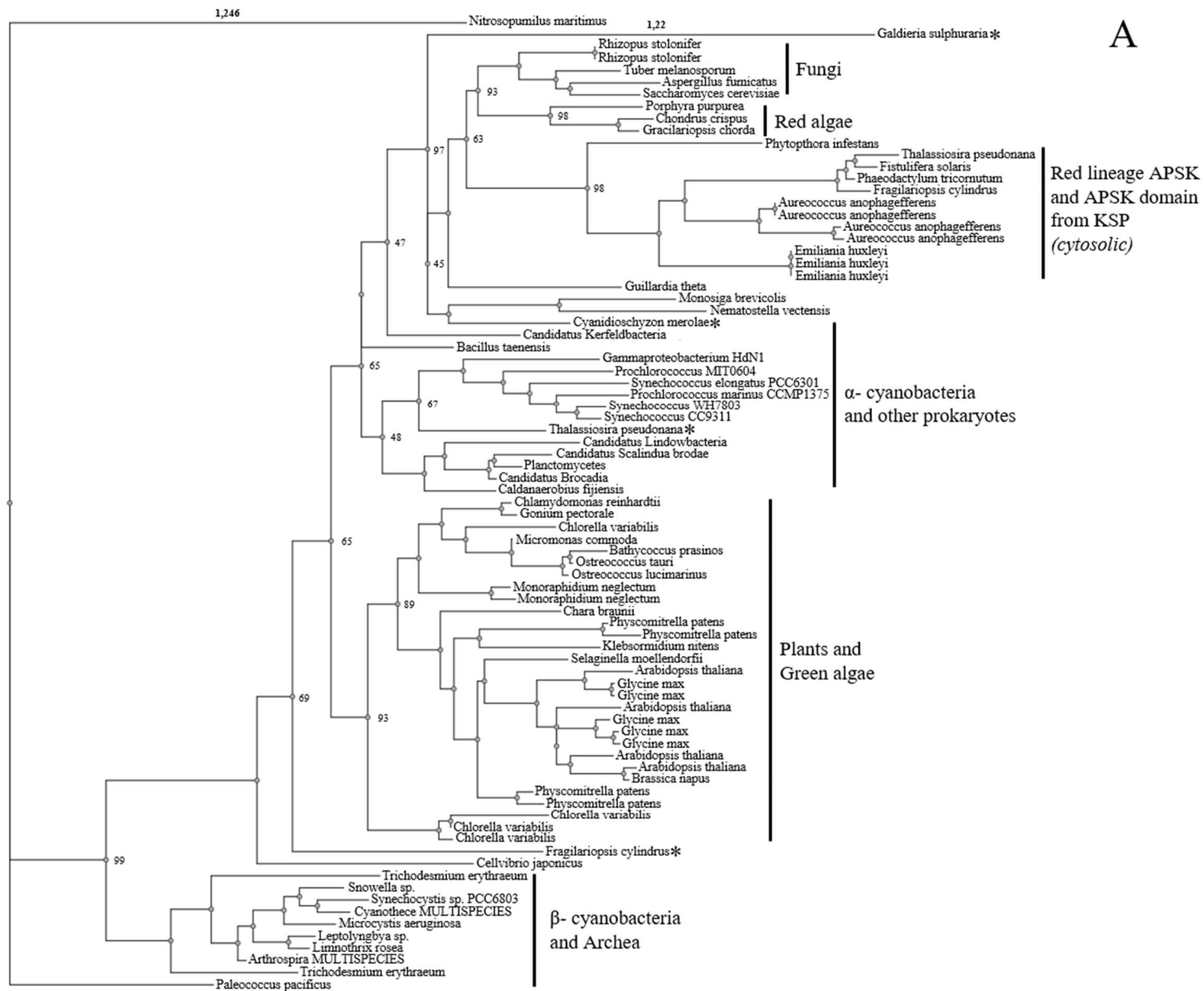


**Figure 9:** Maximum likelihood phylogenetic tree of ATPS with (A) all taxa or (B) collapsed branches. Although taxon *Emiliania huxleyi* is drawn at root, this tree is unrooted. Numbers at nodes are ultrafast bootstrap support (%). Branches' lengths are proportional to distance as showed in the scale bar. Groups are identified and, when there is evidence for enzyme localization, it is described between parenthesis. Gray rectangle highlights taxa with known susceptibility to redox regulation. Stars (in B) indicate noteworthy branches mentioned in text. Numbers in brackets (in B) show the number of sequences in each collapsed branch.

### 3.3.2.2. APSK and APSR: the fate of APS is differently defined among algal groups

The phylogenetic tree of APSK (Figure 10) resulted on a mostly monophyletic grouping of the well-defined photosynthetic groups, except for the cyanobacteria. Like in the ATPS tree,  $\alpha$ - and  $\beta$ -cyanobacteria were distantly grouped. Also, the monofunctional APSK sequences from the extremophile red algae *Cyanodioschyzon merolae* and *Galdieria sulphuraria* were located outside of the well-supported red algal cluster (98 maximum likelihood bootstraps). Instead, they first branched together with the metazoan APSK domain of a fused PAPS synthetase, whereas the latter formed a sister group with the ‘red algae/red lineage/fungi/metazoan’ clade (asterisks in Figure 10 A). This clade, containing all red-plastid algae, formed a sister group with  $\alpha$ -cyanobacteria, albeit relatively uncertain (65 maximum likelihood bootstraps). Interestingly, in contrast to what was observed in the ATPS tree, plants APSK are more closely related to  $\beta$  - cyanobacteria whereas red lineage APSK are closer to  $\alpha$  -cyanobacteria. Ravilious et al. (2012) showed that, in plants, redox regulation of APSK is an important part of the pathway’s regulation and sulfur partitioning.

Several red secondary endosymbionts presented the kinase domain of the fused KSP protein as the only APSK. Generally, they all grouped together at the same clade of their monofunctional APSK, when present. The only exceptions were observed in the diatoms *Thalassiosira pseudonana* and *Fragilariopsis cylindrus*, whose monofunctional APSKs were very distant from the red lineage cluster (asterisks in Figure 10 A). These cases, however, were not highly supported (<69 maximum likelihood bootstraps). The intracellular separation of APSK and APSR – the two enzymes that compete for the same substrate, APS – may be another important characteristic regarding sulfur partitioning, at least in those species that contains only the fused APSK (see next Chapter). The clade containing green-plastid organisms, on the other hand, was entirely monophyletic and well supported (93 maximum likelihood bootstraps). In the APSK tree, this group was closely related to the  $\beta$ -cyanobacteria.



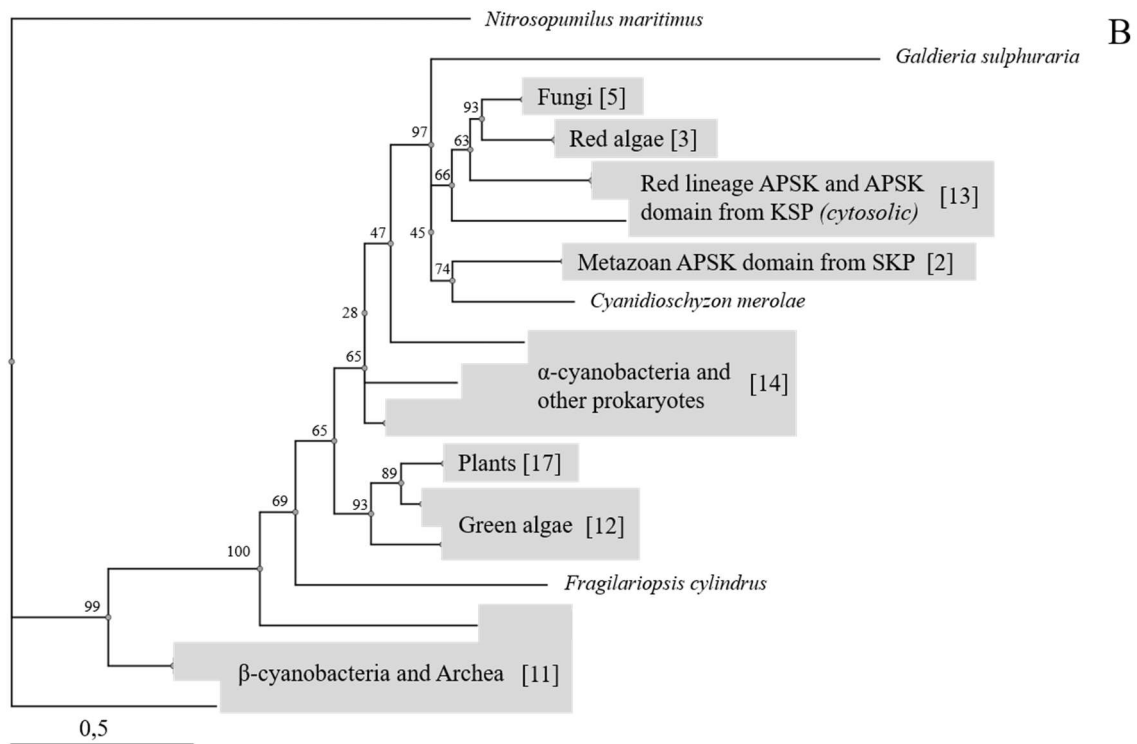


**Figure 10:** Maximum likelihood phylogenetic tree of APSK with (A) all taxa or (B) collapsed branches. Although taxon *Nitrosopumilus maritimus* is drawn at root, this tree is unrooted. Numbers at nodes are ultrafast bootstrap support (%). Branches' lengths are proportional to distance as showed in the scale bar. Groups are identified and, when there is evidence for enzyme localization, it is described between parenthesis. Asterisks (in A) indicate noteworthy sequences, which are mentioned in text. Numbers in brackets (in B) show the number of sequences in each collapsed branch.

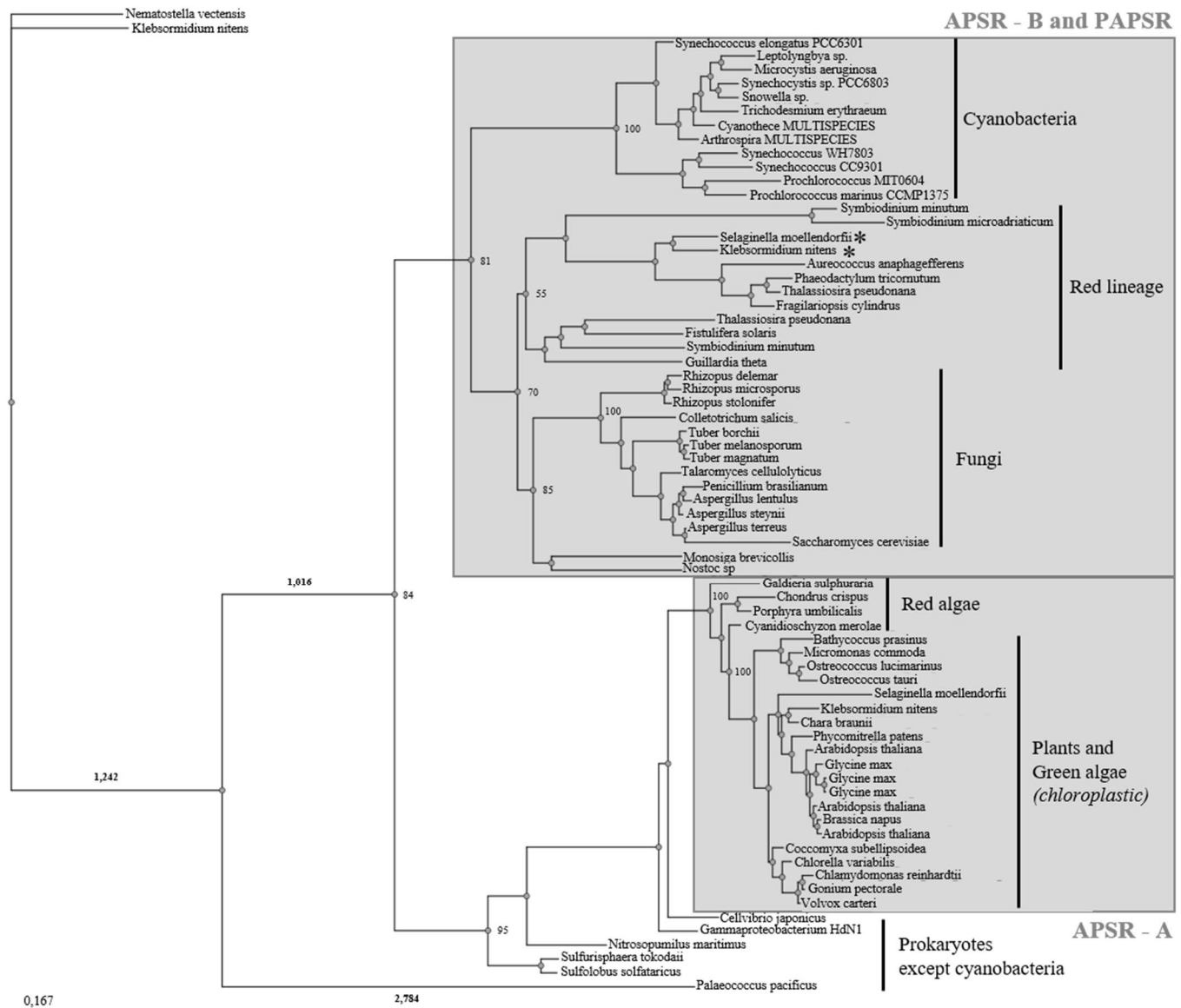
The separation between the Fe-S binding (APSR A) and the non-Fe-S binding enzymes (APSR B and PAPSR) was well defined among the clades of the APSR phylogenetic tree (highlighted in Figure 11). Plants and primary-plastid algae could be found in the same clade closely related to prokaryotes that are not cyanobacteria, forming a well-supported APSR A clade (100 maximum likelihood bootstraps). The less supported group of APSR B and PAPSR (81 maximum likelihood bootstraps) contained cyanobacteria, red lineage algae and fungi sequences as sister groups.

Although most well-defined photosynthetic groups were grouped together, red algae were very distantly related to their descendants, the red lineage algae. Also, the charophyte *Klebsormidium nitens* and the lycophyte *Selaginella moellendorffii* presented one sequence each that grouped outside the cluster containing APSR A from plants and/or green algae (asterisks in Figure 11 A). This branch was well-supported (99 maximum

likelihood bootstraps) within the red lineage algae clade, forming sister groups with dinoflagellates and diatoms.

In plants, for example, APSK and APSR compete for APS within the chloroplast, and the partitioning of sulfur to reduction or sulfation is driven by the differential redox regulation of those enzymes (Ravilious et al. 2012). In the past, a similar control mechanism was assumed to be conserved among all photosynthetic organisms but, recently, other possibilities have been hypothesized based on *in vitro* experiments (Giordano and Raven 2014, Prioretti et al. 2016). If the phylogenetic relationships shown here (Figure 9, Figure 10 and Figure 11) are a reliable proxy for enzymatic modes of regulation like that of ATPS (Prioretti et al. 2014), then they strongly suggest that the regulation of sulfur assimilation and partitioning is diverse in different groups of algae (see Chapter 4 for more details on sulfur partitioning in diatoms).

A



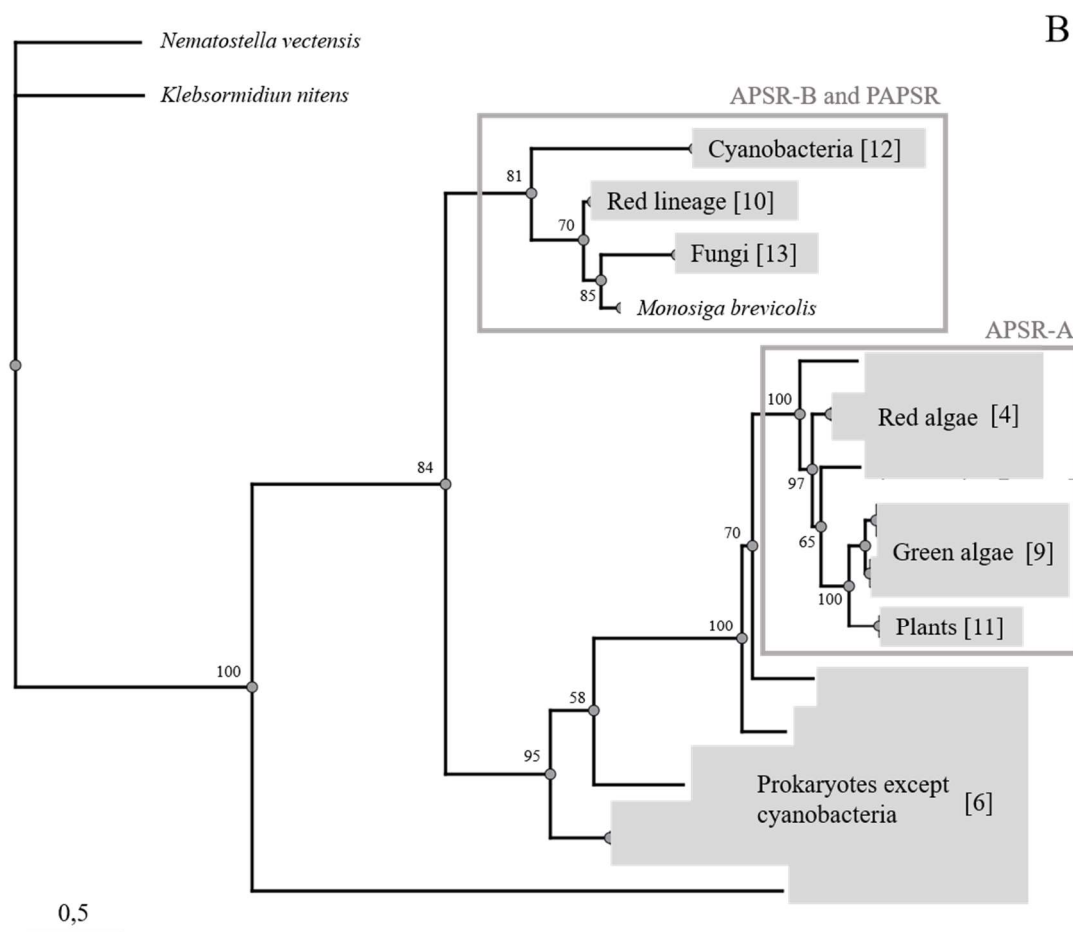


**Figure 11:** Maximum likelihood phylogenetic tree of APSR with (A) all taxa or (B) collapsed branches. Although taxon *Nematostella vectensis* is drawn at root, this tree is unrooted. Numbers at nodes are ultrafast bootstrap support (%). Branches' lengths are proportional to distance as showed in the scale bar. Groups are identified and, when there is evidence for enzyme localization, it is described between parenthesis. Gray rectangle highlights taxa with different types of enzymes – APSR A or B, and PAPSIR. Asterisks (in A) indicate noteworthy sequences, which are mentioned in text. Numbers in brackets (in B) show the number of sequences in each collapsed branch.

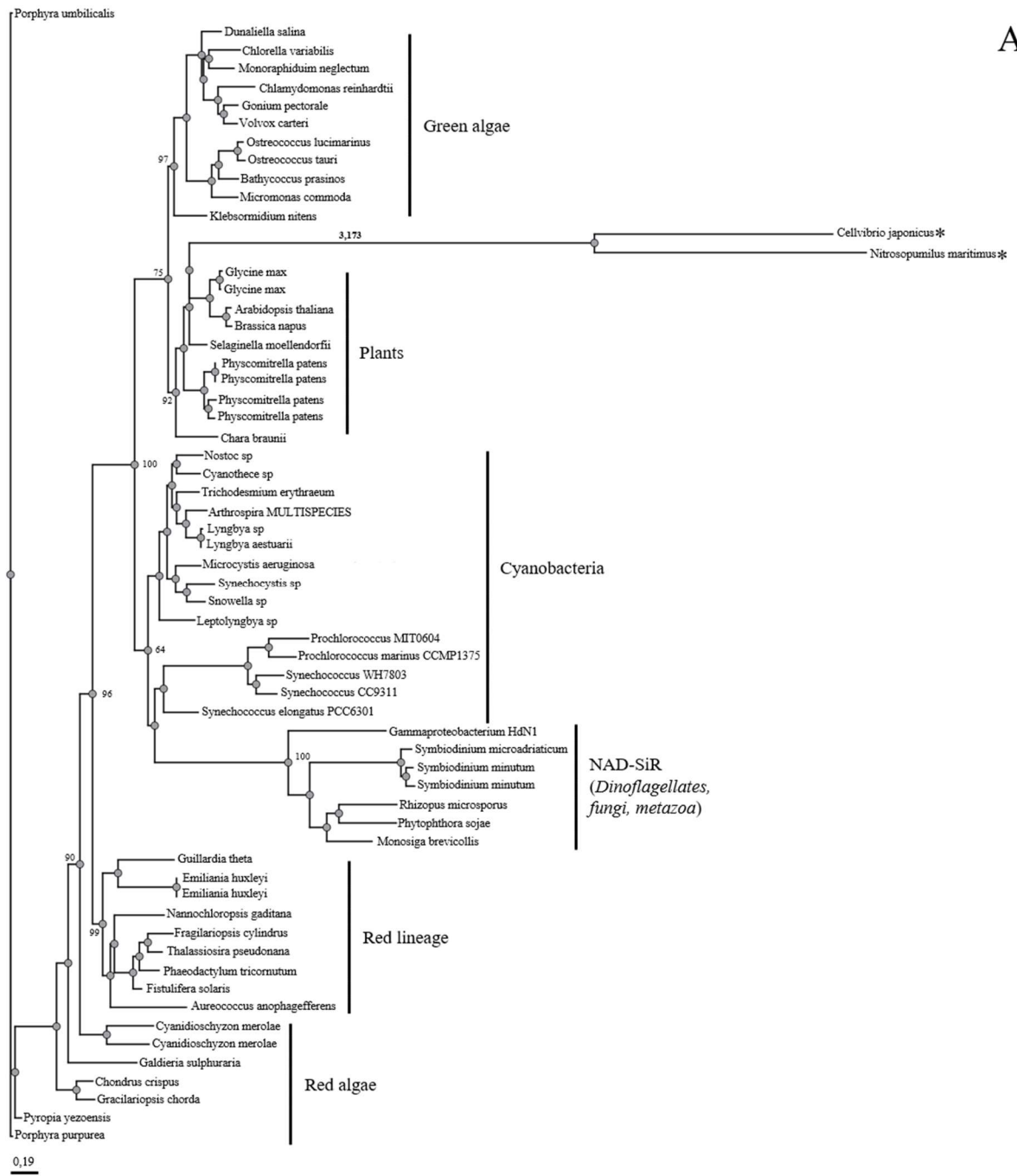
### 3.3.2.3. SiR shows a conventional distribution of taxa

SiR sequences' search resulted on a wider distribution Fd-SiR among photosynthetic organisms as compared to NAD-SiR. The two types of enzyme were clearly separated in the SiR tree (100 maximum likelihood bootstraps), except for two Archea sequences (asterisks in Figure 12 A) that were identified as NAD-SiR and branched together with plants. The only group of algae that grouped within the NAD-SiR cluster was the peculiar clade of dinoflagellates (Figure 12). Within the much bigger cluster of Fd-SiR sequences, a conventional separation of well-defined photosynthetic

groups could be observed (>75 maximum likelihood bootstraps): plants and green algae were monophyletic and closely related, as also were the red algae and their descendants red lineage algae.

According to the scientific consensus, all plastids can be traced back to one endosymbiotic event in which a cyanobacterium was taken up by a eukaryotic cell, followed by the reduction of the endosymbiont to an organelle, the primary plastid. Some groups of algae, like diatoms and haptophytes, possess secondary plastids originated from a secondary endosymbiotic event: the uptake of a eukaryotic alga containing primary plastids into a heterotrophic host cell (Gentil et al. 2017). Again, the alga was subsequently reduced to an organelle, the secondary plastid. In this sense, one may think that it is also possible to trace plastidic proteins back to a cyanobacterial origin. Results like the ones found in the SiR tree, where well-defined groups are clearly separated and relationships are as according to common knowledge of photosynthesis evolution, suggest a one-way vertical inheritance of the referred enzyme. Such observation contrasts with unconventional relationships, particularly evident in the analysis of ATPS, which suggest the occurrence of independent evolutive events and horizontal transfer(s) (Patron et al. 2008). SiR is a highly active and nearly constitutive enzyme that consumes sulfite, a toxic intermediate metabolite (Giordano and Raven 2014). This critical physiological role is possibly one reason for which SiR was not as diversified as the other enzymes involved in sulfate assimilation.

A



B

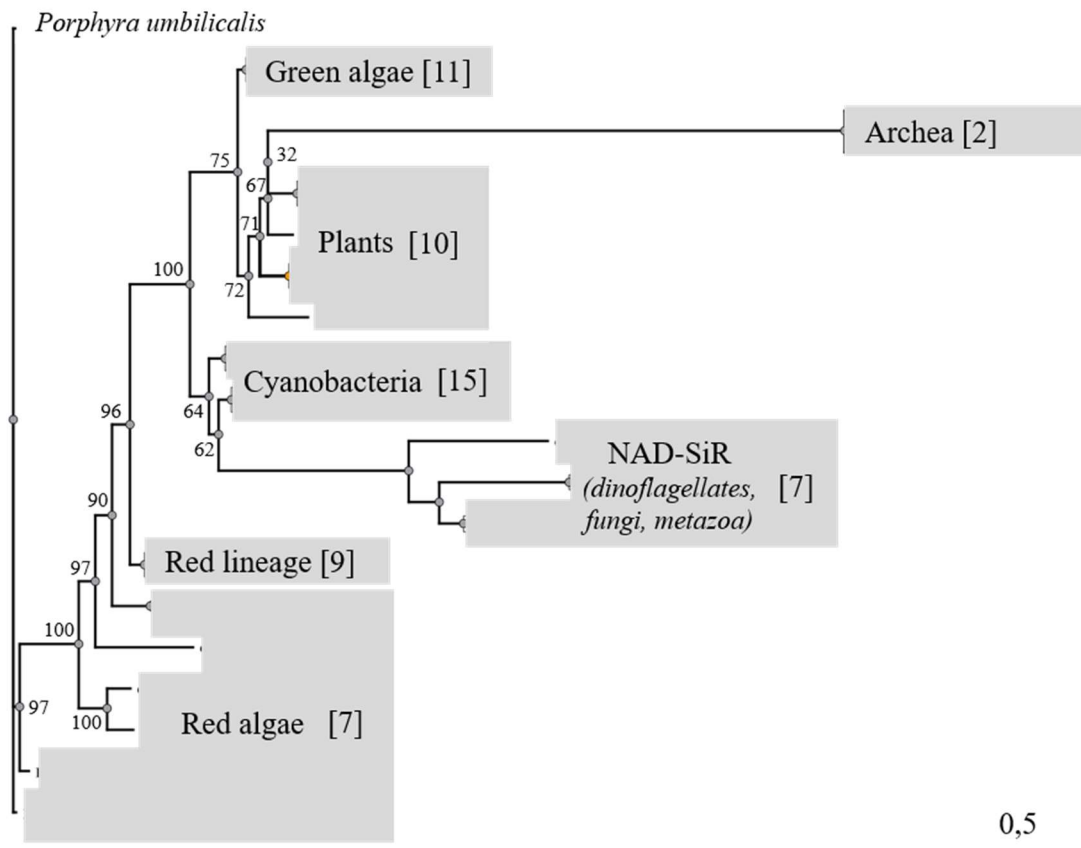


**Figure 12:** Maximum likelihood phylogenetic tree of SiR with (A) all taxa or (B) collapsed branches. Although taxon *Porphyra umbilicalis* is drawn at root, this tree is unrooted. Numbers at nodes are ultrafast bootstrap support (%). Branches' lengths are proportional to distance as showed in the scale bar. Asterisks (in A) indicate noteworthy sequences, which are mentioned in text. Numbers in brackets (in B) show the number of sequences in each collapsed branch.

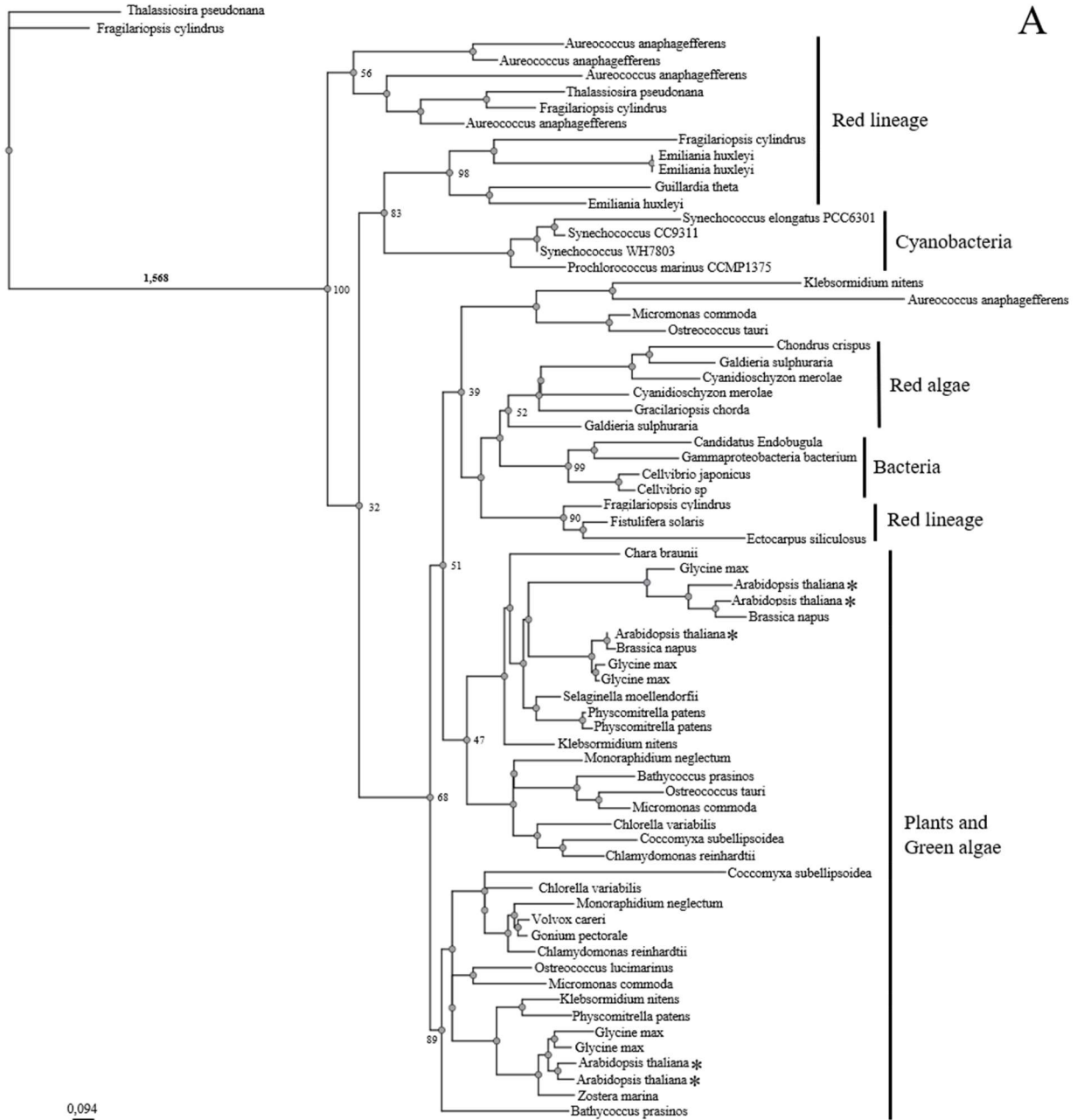
#### 3.3.2.4. Serine Acetyl Transferase

Within the SAT phylogenetic tree, isoforms belonging to the same taxa were frequently distant from each other. This happened several times in plants, green algae, and secondary red algae (Figure 13). Plants and green algae branched into two different clades, one well supported and the other poorly supported (89 and 47 maximum likelihood bootstraps respectively). According to the information available in the model plant *Arabidopsis thaliana* – the most studied organism in this list –, the first branch was related to a cytosolic isoform (*Serat3*) whereas the second contained its plastidic isoform (*Serat1*; Howarth et al. 2003, Watanabe et al. 2008; reference sequences from *A. thaliana* are signed with an asterisk in Figure 13 A). It is also suggested that different SAT isoforms might have different feedback regulation by substrates in *A. thaliana* (Hell and

Leustek 2005) Similarly, red lineage algae branched into three different clades, one of them relatively uncertain (56 maximum likelihood bootstraps) whereas the other were well supported (>90 maximum likelihood bootstraps). Whereas the first was closer to cyanobacteria, the last two were closely related to other prokaryotes.

Although it is an important step to better understand algal sulfur metabolism, the strictly *in silico* approach carried out in this chapter clearly brings analytical limitations. In the case of SAT, finally, analysis may be complicated by functional plasticity, but by a higher compartmentalization and number of isoforms. Given the common knowledge that cysteine biosynthesis occurs in several cell compartments and that at least two of these compartments have an – primary, secondary and tertiary – endosymbiotic origin, the complexity of host-endosymbiont relations increases tremendously. Using less sequences in a narrower approach, Bromke et al. (2013) investigated the phylogenetic relationships of cysteine synthesis using sequences from *T. pseudonana* as a reference and found evidence of a red algae origin of one SAT isoform

A



0,094

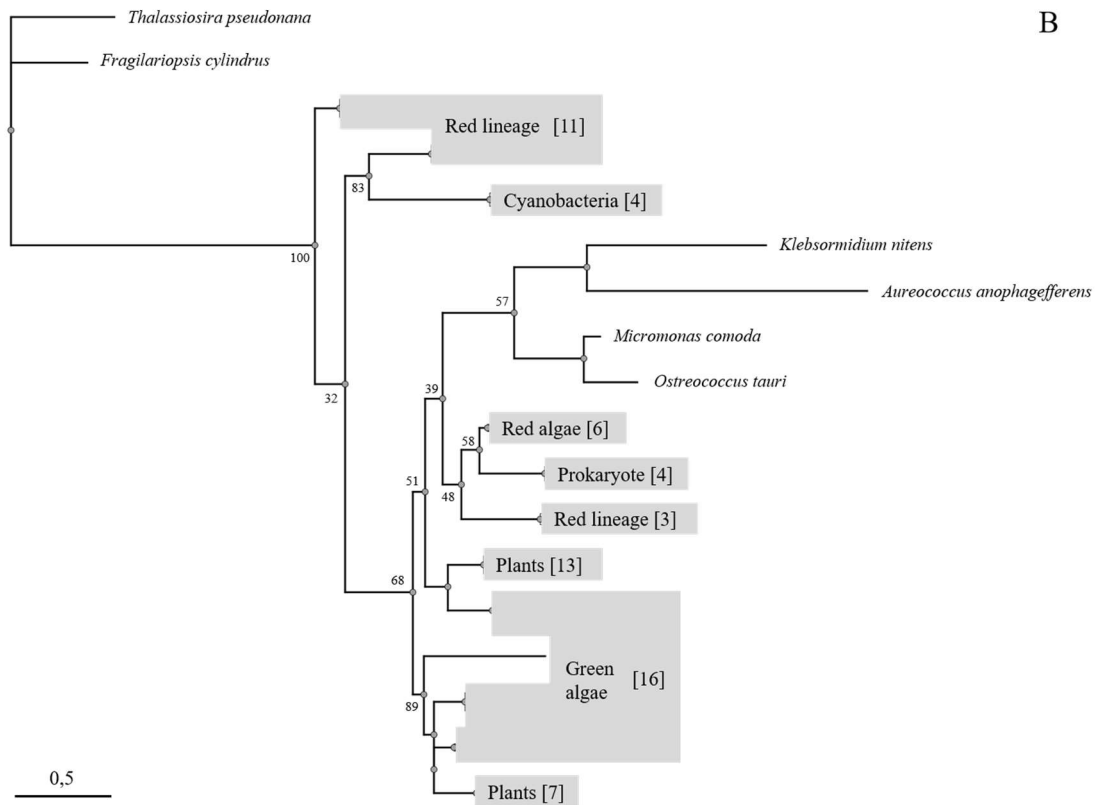


**Figure 13:** Maximum likelihood phylogenetic tree of SAT with (A) all taxa or (B) collapsed branches. Although taxon *Thalassiosira pseudonana* is drawn at root, this tree is unrooted. Numbers at nodes are ultrafast bootstrap support (%). Branches' lengths are proportional to distance as showed in the scale bar. Asterisks (in A) indicate noteworthy sequences, which are mentioned in text. Numbers in brackets (in B) show the number of sequences in each collapsed branch.

OAS-TLs A and B known in bacteria – also called CysK and CysM, respectively – grouped separately and divided the OAS-TL tree in two clusters more closely related to each of the forms of bacterial enzyme (identified in Figure 14 B). Although all photosynthetic eukaryotes contained OAS-TL-like sequences belonging to each of these clusters, this does not necessarily mean that both OAS-TL types are widespread along algae groups. Within the most studied photosynthetic system regarding OAS-TLs, *A. thaliana*, all the sequences that are known to function as OAS-TL *in vivo* were assembled closer to the bacterial CysK cluster (asterisks in Figure 14 A). Whereas only one OAS-TL-like sequence from *A. thaliana* was positioned closer to the bacterial CysM cluster. Due to the functional plasticity of OAS-TL, it is not possible to conclude if an OAS-TL-like sequence really acts in cysteine synthesis just by sequence similarity. Even in *in vitro* assays, overexpressed OAS-TL-like proteins from *A. thaliana* presented OAS-TL and  $\beta$ -cyanoalanine synthase (CAS) activities (Jost et al. 2000). Additionally, a few sequences

of green algae, red lineage algae, charophytes and lycophytes assumed an intermediate position as related to the primary division of the CysK and CysM clusters. This happened in four branches, one of them highly uncertain (9 maximum likelihood bootstraps) and the other three well supported (100 maximum likelihood bootstraps).

The well-known groups of green- and red-plastid algae and fungi were generally monophyletic in each of their aforementioned assemblages. In the cluster closer to CysM, one OAS-TL-like sequence from the aplastidic heterokont *Phytophthora sojae* was positioned in a sister group from that of chloroplastic heterokonts together with the choanoflagellate *Monosiga brevicolis* (asterisks in Figure 14 A). Interestingly, in the same cluster, all other sequences from the genus *Phytophthora* were strongly grouped together (100 maximum likelihood bootstraps). Also, in the other cluster, *P. sojae* was outside of the plastid-containing heterokonts clade. In this cluster, however, it was the only representant of the genus.

The pyridoxal-phosphate dependent superfamily is a highly heterogeneous protein family, and it is likely that some sequences used in this thesis does not act like true OAS-TLs within cells. This could explain the duplicity of monophyletic assemblages and the branches that are unrelated to the known bacterial CysK and CysM on FIGURE.



B

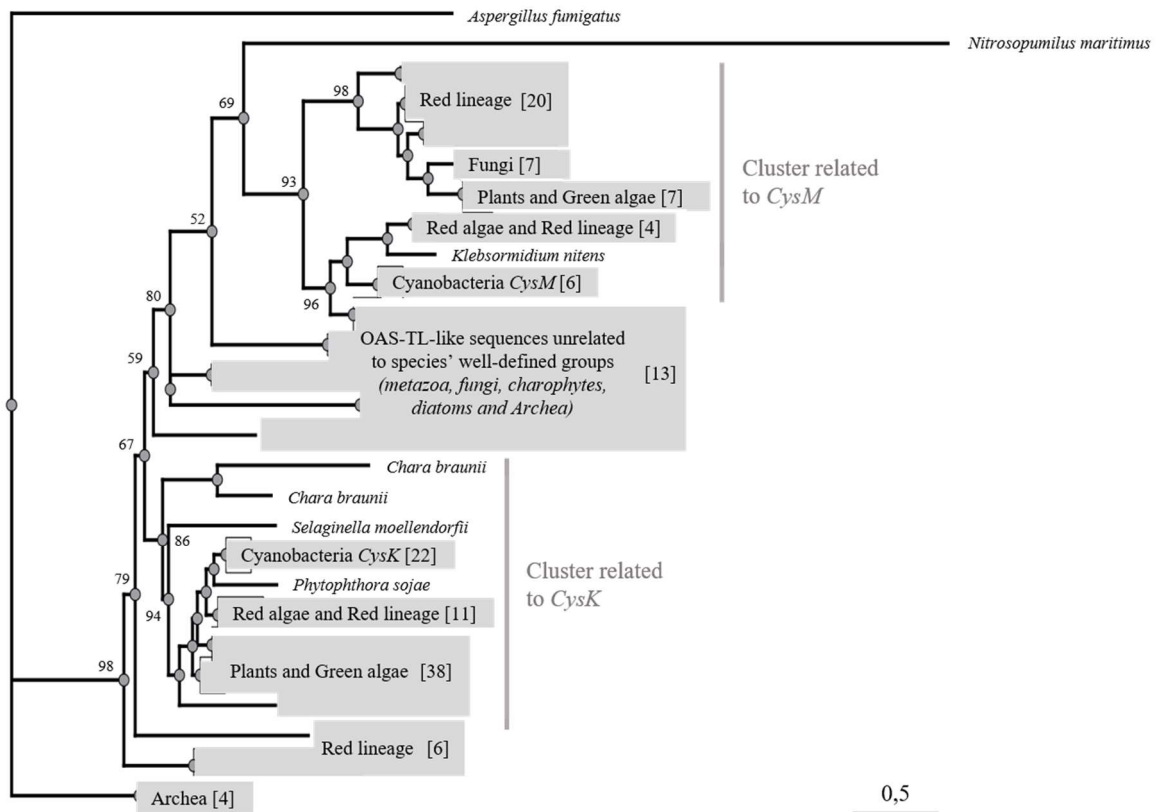


**Figure 14:** Maximum likelihood phylogenetic tree of OAS-TL with (A) all taxa or (B) collapsed branches. Although taxon *Aspergillus fumigatus* is drawn at root, this tree is unrooted. Numbers at nodes are ultrafast bootstrap support (%). Branches' lengths are proportional to distance as showed in the scale bar. Asterisks (in A) indicate noteworthy sequences, which are mentioned in text. Numbers in brackets (in B) show the number of sequences in each collapsed branch.

### 3.4. Concluding remarks

Relying mostly in observations made in plants, it is frequently assumed that sulfate assimilation is confined in plastids and functionally similar among all photosynthetic eukaryotes (the only known exception is the mitochondrial sulfate reduction in *Euglena gracilis*, there is no evidence to believe it is a more general trend). The broad *in silico* analysis presented here shows that, although this is a fair assumption regarding the pathways' intracellular localization, it is not true for its functionality. The relationships of the core enzymes involved in sulfate assimilation suggest that sulfur metabolism is rather diverse among phototrophs. Whereas few hypotheses have been proved by the rare biochemical experiments conducted in taxa that are not plants or the model green alga *C. reinhardtii*, many other ideas are still lacking biochemical experimentation. For instance, it is not clear whether there is a link between this metabolic diversity and the Sulfate Facilitation Hypothesis (SFH), a central issue in this thesis (see Chapter 5).

ATPS presents very peculiar phylogenetic relationships that contrast with most other investigated enzymes. The peculiar separation of redox sensitive and non-sensitive forms of ATPS, together with the diversified predicted localization of APSK strongly suggests that these reactions harbor the modes of sulfate assimilation's regulation. A combination of redox regulation and/or cellular localization of those enzymes appears to coordinate sulfur assimilation and partitioning in photosynthetic organisms. the regulation of the pathway resides on the combination of characteristics of the first steps of sulfate assimilation (i.e. ATPS, APSK and APSR).

### 3.5. Supplemental material – Chapter 3

**Supplemental Table 1:** Predicted localization of retrieved sequences further used for phylogenetic analysis. Plants, green and red algae sequences' localizations were predicted using TargetP 1.1 (Emanuelsson et al. 2007). Red lineage sequences' localizations were predicted using the heterokont subcellular localization targeting method (HECTAR; Gschloessl et al. 2008). RC (Reliability Class) is a 1-to-5 measure of how confident TargetP is in each prediction, based on the difference between the highest and the second highest output predictive scores (1 = very reliable prediction; 5 = not reliable prediction).

	Enzyme Sequences retrieved	Sequence ID*	Predicted localization	RC (TargetP)
<b>ATP Sulfurylase</b>				
<b>Plants</b>	Glycine_max_ATPS2	XP_006593708.1	chloroplast	2
	Glycine_max_ATPS1(PLASTID)	XP_003556071.1	chloroplast	3
	Glycine_max_ATPS3	NP_001235668.2	chloroplast	3
	Physcomitrella_patens_ATPS1(PLASTID-LIKE)	XP_024358180.1	chloroplast	1
	Physcomitrella_patens_ATPS2(PLASTID-LIKE)	XP_024363096.1	chloroplast	1
	Selaginella_moellendorffii_ATPS	XP_002976030.2	-	3
	Arabidopsis_thaliana_APS2	NP_564099.1	chloroplast	2
	Arabidopsis_thaliana_APS1	NP_188929.1	chloroplast	1
	Arabidopsis_thaliana_APS3	NP_193204.1	chloroplast	1
	Arabidopsis_thaliana_APS4	NP_199191.1	chloroplast	2
	Brassica_napus_ATPS_chloroplastic	XP_022576010.1	chloroplast	1
	Brassica_napus_ATPS	XP_013641918.1	chloroplast	2
<b>Green algae</b>	Ostreococcus_lucimarinus_CCE9901_ATPS	XP_001420064.1	-	4
	Ostreococcus_tauri_ATPS	XP_022839735.1	-	5
	Volvox_carteri_ATPS	XP_002950333.1	mitochondrion	3
	Coccomyxa_subellipsoidea_ATPS	XP_005645981.1	-	4
	Tetraabaena_socialis_ATPS	PNH10001.1	mitochondrion	3
	Bathycoccus_prasinos_ATPS	XP_007510313.1	chloroplast	5
	Gonium_pectorale_ATPS	KXZ43014.1	chloroplast	3
	Tetraselmis_suecica_ATPS	<i>See Prioretti et al., 2014</i>	chloroplast	1
	Chlorella_variabilis_ATPS1	XP_005849203.1	chloroplast	1
	Chlorella_variabilis_ATPS2	XP_005848036.1	mitochondrion	2
	Monoraphidium_neglectum_ATPS	XP_013893869.1	chloroplast	5
	Micromonas_commoda_ATPS	XP_002504659.1	-	4
	Chlamydomonas_reinhardtii_ATS2	JGI133924	mitochondrion	1
Chlamydomonas_reinhardtii_ATS1	JGI196910	-	4	
<b>Red algae</b>	Chondrus_crispus_ATPS1	XP_005713611.1	mitochondrion	4
	Chondrus_crispus_ATPS2	XP_005716520.1	-	2
	Cyanidioschyzon_merolae_ATPS1	XP_005538770.1	mitochondrion	4
	Cyanidioschyzon_merolae_ATPS2	XP_005539160.1	-	5
	Galdieria_sulphuraria_ATPS	XP_005708627.1	-	5
	Porphyra_purpurea	AAP97122.1	-	5
	Gracilariopsis_chorda	PXF48074.1	-	2
<b>Red lineage</b>	Fragilariopsis_cylindrus_ATPS	OEU15974.1	other localisation	
	Fragilariopsis_cylindrus_KSP_ATPSdomain	OEU22662.1	other localisation	
	Fistulifera_solaris_ATPS	GAX18652.1	chloroplast	
	Phaeodactylum_tricornutum_ATPS	JGI42282	other localisation	
	Phaeodactylum_tricornutum_SKP_ATPS_domain	JGI19901	other localisation	
	Thalassiosira_pseudonana_ATPS	JGI1326	other localisation	
	Thalassiosira_pseudonana_SPK_ATPS_domain	JGI269714	other localisation	
	Amphydinium_carterae_ATPS	<i>See Prioretti et al., 2014</i>	signal peptide	
	Amphydinium_carterae_APR-ATPS	<i>See Prioretti et al., 2014</i>	other localisation	
	Amphydinium_klebsii_ATPS	<i>See Prioretti et al., 2014</i>	signal peptide	
	Amphydinium_klebsii_APR-ATPSdomain	<i>See Prioretti et al., 2014</i>	other localisation	
	Symbiodinium_microadriaticum_ATPS	OLP82460.1	signal peptide	
	Emiliana_huxleyi_ATPS1	JGIEmihul_415495	signal peptide	
	Emiliana_huxleyi_ATPS2	JGIEmihul_459734	signal peptide	

Emiliana_huxleyi_ATPSdomain1	JGIEmihul_452787	other localisation
Emiliana_huxleyi_ATPSdomain2	JGIEmihul_467682	other localisation
Aureococcus_anophagefferens_KSP_ATPSdomain	XP_009042144.1	other localisation
Aureococcus_anophagefferens_ATPS1	XP_009035156.1	chloroplast
Aureococcus_anophagefferens_SPK_ATPSdomain	XP_009040631.1	other localisation
Nannochloropsis_gaditana_CCMP526	XP_005855174.1	chloroplast
Guillardia_theta_CCMP2712	XP_005841894.1	other localisation
Phytophthora_sojae_ATPSdomain	XP_009527256.1	other localisation
Ectocarpus_siliculosus_ATPS	CBN77774.1	chloroplast
Chrysochromulina_sp_CCMP291_ATPS	KOO28507.1	chloroplast

### APS Kinase

<b>Plants</b>	Selaginella_moellendorffii_APSK	EFJ23052.1	-	3
	Arabidopsis_thaliana_APK	NP_179082.1	chloroplast	3
	Arabidopsis_thaliana_APK3	NP_001319463.1	-	4
	Arabidopsis_thaliana_AKN2	NP_195704.1	chloroplast	4
	Arabidopsis_thaliana_APK4	NP_569050.1	chloroplast	3
	Glycine_max_APSK_X1	XP_006579943.1	mitochondrion	3
	Glycine_max_APSK2	NP_001237036.2	-	3
	Glycine_max_APSK3	XP_003554016.1	-	5
	Glycine_max_APSK_Uncat	NP_001241077.1	secreted	2
	Glycine_max_APSK3_2	XP_006598976.1	-	4
	Physcomitrella_patens_APSK1	XP_024362795.1	-	3
	Physcomitrella_patens_APSK2	XP_024364762.1	mitochondrion	5
	Physcomitrella_patens_APSK3	XP_024368620.1	-	3
	Physcomitrella_patens_APSK4	XP_024386689.1	-	5
	Brassica_napus	XP_013656564.1	chloroplast	5
	<b>Green algae</b>	Monoraphidium_neglectum_1APSK	XP_013893041.1	-
Monoraphidium_neglectum_2APSK		XP_013900589.1	chloroplast	2
Micromonas_commoda_APSK_chloroplast		XP_002507043.1	mitochondrion	3
Chlamydomonas_reinhardtii_APK1		JGI184419	mitochondrion	4
Chlorella_variabilis_APSK1		XP_005843477.1	chloroplast	5
Chlorella_variabilis_APSK2		XP_005842851.1	mitochondrion	2
Chlorella_variabilis_APSK3		XP_005843476.1	chloroplast	2
Gonium_pectorale		KXZ55601.1	-	2
Ostreococcus_lucimarinus_CCE9901		XP_001419808.1	-	3
Ostreococcus_tauri		OUS48844.1	mitochondrion	2
Bathycoccus_prasinos		XP_007510755.1	-	5
Coccomyxa_subellipsoidea_C-169	XP_005650798.1	-	3	
<b>Red algae</b>	Cyanidioschyzon_merolae_APSK	XP_005535232.1	chloroplast	5
	Chondrus_crispus_APSK	XP_005717980.1	-	2
	Galdieria_sulphuraria_APSK	XP_005704785.1	mitochondrion	1
	Gracilariopsis_chorda	PXF42298.1	-	4
	Porphyra_purpurea	AAP97123.1	-	3
<b>Red lineage</b>	Phytophthora_infestans_APSKdomain	ABY65330.1	other localisation	
	Phaeodactylum_tricornutum_SKP_APSK_domain	JGI19901	other localisation	
	Thalassiosira_pseudonana_ASK1	JGI35055	other localisation	
	Thalassiosira_pseudonana_SKP_APSK_domain	JGI269714	other localisation	
	Fragilariopsis_cylindrus_APSK	OEU12388.1	other localisation	
	Fragilariopsis_cylindrus_SPK_APSKdomain	OEU22662.1	other localisation	
	Fistulifera_solaris	GAX17053.1	signal anchor	
	Emiliana_huxleyi_SKP_APSK_domain1	JGIEmihul_452787	other localisation	
	Emiliana_huxleyi_KSP_APSK_domain2	JGIEmihul_467682	other localisation	
	Aureococcus_anophagefferens_APSK1	XP_009032708.1	other localisation	
	Aureococcus_anophagefferens_APSK2	XP_009034160.1	other localisation	
Aureococcus_anophagefferens_1SKP_APSKdomain	XP_009042144.1	other localisation		
Aureococcus_anophagefferens_2SKP_APSKdomain	XP_009040631.1	other localisation		
Guillardia_theta_APSK	XP_005839420.1	other localisation		

### APS Reductase

<b>Plants</b>	Selaginella_moellendorffii_APSR	EFJ32876.1	chloroplast	1
	Selaginella_moellendorffii_PAPSR	XP_002961179.1	chloroplast	2
	Arabidopsis_thaliana_APR2	NP_176409.1	chloroplast	1
	Arabidopsis_thaliana_APR1	NP_192370.1	chloroplast	1
	Arabidopsis_thaliana_APR3	NP_193930.1	chloroplast	1
	Glycine_max_APSR3	NP_001235612.1	chloroplast	1

	Glycine_max_APSR2	XP_003529636.1	chloroplast	1
	Glycine_max_APSR1	NP_001347343.1	chloroplast	1
	Physcomitrella_patens_APSR	XP_024373952.1	chloroplast	3
	Brassica_napus	XP_013641464.1	chloroplast	1
<b>Green algae</b>	Micromonas_commoda_APSR	XP_002505765.1	-	1
	Chlamydomonas_reinhardtii_MET16	JGI131444	mitochondrion	1
	Chlorella_variabilis_APSR	XP_005843278.1	-	4
	Gonium_pectorale	KXZ47493.1	mitochondrion	1
	Volvox_carteri_f_nagariensis	XP_002947921.1	mitochondrion	3
	Bathycoccus_prasinus_APSR	XP_007513487.1	chloroplast	1
	Ostreococcus_lucimarinus_APSR	XP_001422646.1	mitochondrion	3
	Ostreococcus_tauri_APSR	OUS45812.1	mitochondrion	3
<b>Red algae</b>	Cyanidioschyzon_merolae_APSR	XP_005539193.1	chloroplast	3
	Chondrus_crispus_PAPSR	XP_005713885.1	chloroplast	3
	Galdieria_sulphuraria_APSR	XP_005708366.1	chloroplast	5
<b>Red lineage</b>	Fragilariopsis_cylindrus_PAPSR	OEU10673.1	chloroplast	
	Phaeodactylum_tricornutum_PAPSR	JGI25956	chloroplast	
	Thalassiosira_pseudonana_PAPSR1	JGI35690	other localisation	
	Thalassiosira_pseudonana_PAPSR2	JGI24887	chloroplast	
	Aureococcus_anophagefferens_PAPSR	XP_009035983.1	other localisation	

### Sulfite Reductase

<b>Plants</b>	Arabidopsis_thaliana_SIR(ferredoxin)	NP_196079.1	chloroplast	2
	Glycine_max_SIR1(ferredoxin)	XP_003540209.1	chloroplast	1
	Glycine_mas_SIR2(ferredoxin)	NP_001347225.1	chloroplast	1
	Brassica_napus	XP_013648151.1	chloroplast	1
	Physcomitrella_patens_SIR1(ferredoxin)	XP_024368477.1	chloroplast	2
	Physcomitrella_patens_SIR2(ferredoxin)	XP_024368477.1	chloroplast	2
	Physcomitrella_patens_SIR3(ferredoxin)	XP_024371608.1	-	4
	Physcomitrella_patens_SIR4(ferredoxin)	XP_024373516.1	chloroplast	5
	Selaginella_moellendorffii_SIR	EFJ33435.1	chloroplast	5
<b>Green algae</b>	Chlamydomonas_reinhardtii_SIR1(ferredoxin)	JGI206154	mitochondrion	4
	Chlamydomonas_reinhardtii_SIR3(NADPH)	JGI188119	mitochondrion	3
	Monoraphidium_neglectum_NADPH_SIR	XP_013906706.1	mitochondrion	5
	Monoraphidium_neglectum1_ferredoxin_SIR	XP_013903342.1	-	1
	Monoraphidium_neglectum2_ferredoxin_SIR	XP_013903020.1	mitochondrion	2
	Micromonas_commoda_ferredoxin_SIR	XP_002504905.1	chloroplast	1
	Chlorella_variabilis_SIR(ferredoxin)	XP_005846743.1	chloroplast	2
	Chlorella_variabilis_SIR(NADPH)	XP_005849295.1	mitochondrion	2
	Volvox_carteri_f_nagariensis	XP_002948803.1	mitochondrion	4
	Gonium_pectorale	KXZ50217.1	mitochondrion	3
	Coccomyxa_subellipsoidea_C-169	XP_005649394.1	chloroplast	4
	Ostreococcus_lucimarinus_CCE9901	XP_001420730.1	chloroplast	4
	Bathycoccus_prasinos	XP_007508559.1	chloroplast	1
Ostreococcus_tauri	OUS43157.1	chloroplast	3	
<b>Red algae</b>	Cyanidioschyzon_merolae_SIR1(ferredoxin)	XP_005535840.1	mitochondrion	3
	Cyanidioschyzon_merolae_SIR2(ferredoxin)	XP_005534858.1	chloroplast	4
	Cyanidioschyzon_merolae_SIR(NADPH)	XP_005538651.1	mitochondrion	4
	Chondrus_crispus_SIR(NADPH)	XP_005711057.1	secreted	4
	Chondrus_crispus_SIR(ferredoxin)	XP_005714495.1	chloroplast	4
	Galdieria_sulphuraria_SIR(NADPH)	XP_005709228.1	secreted	2
	Galdieria_sulphuraria_SIR(ferredoxin)	XP_005706287.1	mitochondrion	3
	Gracilariopsis_chorda	PXF47635.1	chloroplast	5
	Porphyra_purpurea	AAP97125.1	-	4
<b>Red lineage</b>	Phytophthora_sojae1_SIR(NADPH)	XP_009516220.1	other localisation	
	Phytophthora_sojae2_SIR(NADPH)	XP_009516225.1	other localisation	
	Phaeodactylum_tricornutum_SIR(ferredoxin)	JGI24374	signal peptide	
	Thalassiosira_pseudonana_SIR(ferredoxin)	JGI270365	other localisation	
	Fistulifera_solaris	GAX15574.1	chloroplast	
	Fragilariopsis_cylindrus_SIR(ferredoxin)	OEU12781.1	other localisation	
	Symbiodinium_microadriaticum_[NADPH]	OLP88546.1	other localisation	
	Emiliana_huxleyi_SIR3(ferredoxin)	JGIEmihu1_104042	other localisation	
Emiliana_huxleyi_SIR2(ferredoxin)	JGIEmihu1_454897	signal peptide		

Emiliana_huxleyi_SIR1(ferredoxin)	JGIEmihul_470997	signal peptide
Guillardia_theta_SIR	XP_005828960.1	signal peptide
Nannochloropsis_gaditana	EWM24004.1	other localisation
Aureococcus_anophagefferens_SIR(ferredoxin)	XP_009035079.1	signal peptide

### Serine Acetyl Transferase

<b>Plants</b>	Arabidopsis_thaliana_SERAT2	NP_175988.1	-	2	
	Arabidopsis_thaliana_ATSERAT3	NP_565421.1	-	2	
	Arabidopsis_thaliana_SERAT2;2	NP_187918.1	chloroplast	5	
	Arabidopsis_thaliana_SERAT3	NP_195289.3	chloroplast	4	
	Arabidopsis_thaliana_SERAT1	NP_200487.1	-	3	
	Glycine_max_SAT1(PLASTID)	XP_003551487.1	mitochondrion	5	
	Glycine_max_SAT2_X3	XP_003538905.1	mitochondrion	4	
	Glycine_max_SAT2_X2	XP_003519846.3	-	4	
	Glycine_max_SAT5	XP_003528805.2	-	1	
	Glycine_max_SAT4	NP_001235640.2	-	1	
	Brassica_napus_chloroplastic_SAT	XP_013649422.1	-	2	
	Brassica_napus_SAT	XP_013667010.1	-	3	
	Physcomitrella_patens_SAT2_X1	XP_024357770.1	mitochondrion	4	
	Physcomitrella_patens_SAT5-like	XP_024362956.1	chloroplast	1	
	Physcomitrella_patens_SAT_5like	XP_024364111.1	chloroplast	5	
	Physcomitrella_patens_SAT	XP_024383195.1	chloroplast	2	
	Selaginella_moellendorffii_SAT	XP_024535154.1	-	3	
	Zostera_marina_SAT	KMZ76347.1	-	2	
	<b>Green algae</b>	Chlamydomonas_reinhardtii_SAT2	JGI205984	chloroplast	4
		Chlamydomonas_reinhardtii_SAT1	JGI205985	chloroplast	2
Monoraphidium_neglectum1_SAT		XP_013894964.1	mitochondrion	5	
Monoraphidium_neglectum2_SAT		XP_013903946.1	-	2	
Micromonas_commoda1_SAT		XP_002509226.1	-	2	
Micromonas_commoda2_SAT		XP_002502676.1	-	4	
Micromonas_commoda3_SAT		XP_002503605.1	chloroplast	2	
Chlorella_variabilis_SAT1		XP_005844216.1	mitochondrion	5	
Chlorella_variabilis_SAT2		XP_005847380.1	mitochondrion	5	
Volvox_carteri_f_nagariensis		XP_002952755.1	mitochondrion	3	
Gonium_pectorale		KXZ51000.1	-	2	
Ostreococcus_lucimarinus_CCE9901		XP_001421904.1	-	2	
Bathycoccus_prasinus_SAT1		XP_007512855.1	-	4	
Bathycoccus_prasinus_SAT2		XP_007508962.1	chloroplast	3	
Coccomyxa_subellipsoidea_SAT1		XP_005650036.1	-	4	
Coccomyxa_subellipsoidea_SAT2		XP_005652016.1	secreted	3	
Ostreococcus_tauri_SAT1		XP_022839524.1	mitochondrion	2	
Ostreococcus_tauri_SAT2	XP_003082052.1	mitochondrion	5		
<b>Red algae</b>	Cyanidioschyzon_merolae_SAT1	XP_005535017.1	mitochondrion	4	
	Cyanidioschyzon_merolae_SAT2	XP_005536437.1	chloroplast	5	
	Galdieria_sulphuraria_SAT1	XP_005704685.1	chloroplast	4	
	Galdieria_sulphuraria_SAT2	XP_005704099.1	-	2	
	Chondrus_crispus_SAT	XP_005711151.1	chloroplast	4	
<b>Red lineage</b>	Fistulifera_solaris	GAX27875.1	signal peptide		
	Phaeodactylum_tricornutum_SAT	JGI46665	signal peptide		
	Thalassiosira_pseudonana_SAT1	JGI16842	other localisation		
	Thalassiosira_pseudonana_SAT	JGI270332	chloroplast		
	Thalassiosira_pseudonana_SAT2	JGI31984	other localisation		
	Fragilariopsis_cylindrus_SAT1	OEU14194.1	other localisation		
	Fragilariopsis_cylindrus_SAT2	OEU17487.1	other localisation		
	Fragilariopsis_cylindrus_SAT3	OEU08851.1	other localisation		
	Fragilariopsis_cylindrus_SAT4	OEU13395.1	other localisation		
	Emiliana_huxleyi_SAT1	JGIEmihul_234967	mitochondrion		
	Emiliana_huxleyi_SAT2	JGIEmihul_248485	mitochondrion		
	Emiliana_huxleyi_SAT3	JGIEmihul_55024	other localisation		
	Emiliana_huxleyi_SAT4	JGIEmihul_55103	other localisation		
	Emiliana_huxleyi_SAT5	JGIEmihul_55105	other localisation		
	Aureococcus_anophagefferens_SAT1	XP_009033693.1	signal peptide		
	Aureococcus_anophagefferens_SAT2	XP_009033990.1	other localisation		
	Aureococcus_anophagefferens_SAT3	XP_009043396.1	chloroplast		
Aureococcus_anophagefferens_SAT4	XP_009035984.1	other localisation			
Aureococcus_anophagefferens_SAT5	XP_009037810.1	other localisation			

Aureococcus_anophagefferens_SAT6	XP_009037504.1	other localisation
Gracilariopsis_chorda	PXF46113.1	mitochondrion
Ectocarpus_siliculosus_SAT	CBJ32520.1	other localisation
Guillardia_theta_SAT	XP_005823295.1	other localisation

### O-Acetyl Serine Thiol Lyase

<b>Plants</b>	Arabidopsis_thaliana_OASTL1	NP_175984.1	secreted 4
	Arabidopsis_thaliana_OASB	NP_001189745.1	chloroplast 1
	Arabidopsis_thaliana_CysD1	NP_001325893.1	- 1
	Arabidopsis_thaliana_OASA2	NP_001326025.1	- 2
	Arabidopsis_thaliana_OASC	NP_191535.2	chloroplast 3
	Arabidopsis_thaliana_CysC1	NP_191703.1	mitochondrion 2
	Arabidopsis_thaliana_OASA1	NP_001190732.1	- 2
	Arabidopsis_thaliana_CysD2	NP_001031956.1	- 1
	Arabidopsis_thaliana_DES1	NP_001330587.1	- 1
	Glycine_max_OAS-TL1	NP_001238392.2	- 2
	Glycine_max_OAS-TL2	NP_001238411.2	- 1
	Glycine_max_OAS-TL6	NP_001238426.2	- 2
	Glycine_max_OAS-TL3	NP_001235117.2	chloroplast 5
	Glycine_max_OAS-TL4	NP_001235131.2	chloroplast 1
	Glycine_max_OAS-TL7	NP_001235267.2	- 2
	Physcomitrella_patens_OASTL1	XP_024360091.1	chloroplast 2
	Physcomitrella_patens_OASTL2	XP_024376683.1	secreted 5
	Physcomitrella_patens_OASTL3	XP_024401665.1	chloroplast 3
	Physcomitrella_patens_OASTL4	XP_024402951.1	chloroplast 3
	Selaginella_moellendorffii_OASTL	EFJ18842.1	- 3
	Brassica_napus_OASTL	XP_022559423.1	- 1
<b>Green algae</b>	Monoraphidium_neglectum1_OASTL	XP_013895923.1	mitochondrion 2
	Monoraphidium_neglectum2_ZincOASTL	XP_013905530.1	- 4
	Micromonas_commoda_ZincOASTL	XP_002499947.1	chloroplast 5
	Micromonas_commoda_OASTL	XP_002499779.1	- 4
	Chlamydomonas_reinhardtii_OASTL1	JGI175651	chloroplast 2
	Chlamydomonas_reinhardtii_OASTL4	JGI189320	mitochondrion 2
	Chlamydomonas_reinhardtii_OASTL2	JGI196485	secreted 4
	Chlamydomonas_reinhardtii_OASTL3	JGI196886	mitochondrion 2
	Chlorella_variabilis_OASTL1	XP_005848464.1	- 2
	Chlorella_variabilis_OASTL2	XP_005851130.1	- 4
	Chlorella_variabilis_OASTL3	XP_005843662.1	- 3
	Chlorella_variabilis_OASTL4	XP_005847962.1	- 5
	Chlorella_variabilis_OASTL5	XP_005843968.1	- 5
	Chlorella_variabilis_OASTL6	XP_005850314.1	- 4
	Volvox_carteri_f_nagariensis	XP_002948674.1	chloroplast 5
	Coccomyxa_subellipsoidea_C-169	XP_005649760.1	- 3
	Gonium_pectorale	KXZ50203.1	- 3
	Tetraabaena_socialis	PNH06523.1	secreted 5
	Ostreococcus_tauri	OUS46697.1	mitochondrion 3
	Ostreococcus_tauri	XP_003082455.2	chloroplast 2
	Bathycoccus_prasinus_OASTL	XP_007514623.1	- 2
Bathycoccus_prasinus_CYSSYNTH	XP_007512946.1	- 4	
Ostreococcus_lucimarinus_OASTL1	XP_001420867.1	- 3	
Ostreococcus_lucimarinus_2OASTL	XP_001421219.1	- 3	
<b>Red algae</b>	Cyanidioschyzon_merolae_OASTL1	XP_005536023.1	chloroplast 5
	Cyanidioschyzon_merolae_OASTL2	XP_005539314.1	chloroplast 2
	Chondrus_crispus_OASTL1	XP_005714916.1	- 4
	Chondrus_crispus_OASTL2	XP_005719404.1	- 2
	Galdieria_sulphuraria_OASTL	XP_005706612.1	mitochondrion 5
<b>Red lineage</b>	Phaeodactylum_tricornutum_CysK	JGI54915	other localisation
	Phaeodactylum_tricornutum_CysK(2)	JGI542	other localisation
	Thalassiosira_pseudonana_OASTL	JGI270338	chloroplast
	Thalassiosira_pseudonana_OASTL1	JGI38294	other localisation
	Thalassiosira_pseudonana_OASTL2 Bromke_2013	JGI31829	other localisation
	Thalassiosira_pseudonana_OASTL3 Bromke_2013	JGI1247	other localisation
	Thalassiosira_pseudonana_OASTL4 Bromke_2013	JGI267987	other localisation
	Thalassiosira_pseudonana_OASTL5 Bromke_2013	JGI264585	signal peptide
	Fragilariopsis_cylindrus_OASTL1	OEU17518.1	other localisation
	Fragilariopsis_cylindrus_OASTL2	OEU22832.1	other localisation

Fragilariopsis_cylindrus_OASTL3	OEU18536.1	chloroplast
Fragilariopsis_cylindrus_OASTL4	OEU07594.1	other localisation
Aureococcus_anophagefferens_1OASTL	XP_009039736.1	other localisation
Aureococcus_anophagefferens_2OASTL	XP_009040394.1	signal peptide
Aureococcus_anophagefferens_3OASTL	XP_009040394.1	other localisation
Aureococcus_anophagefferens_4OASTL	XP_009039224.1	other localisation
Emiliana_huxleyi_OASTL1	JGIEmihu1_42684	other localisation
Emiliana_huxleyi_OASTL2	JGIEmihu1_435967	other localisation
Emiliana_huxleyi_OASTL3	JGIEmihu1_440100	other localisation
Emiliana_huxleyi_OASTL4	JGIEmihu1_445218	other localisation
Emiliana_huxleyi_OASTL5	JGIEmihu1_445667	other localisation
Emiliana_huxleyi_OASTL6	JGIEmihu1_460677	other localisation
Emiliana_huxleyi_OASTL7	JGIEmihu1_74893	signal peptide
Chrysochromulina_sp_CysSynt	KOO26973.1	signal peptide
Ectocarpus_siliculosus_CysSynt	CBJ33850.1	other localisation
Ectocarpus_siliculosus_Cysteine_synthase	CBJ25649.1	signal peptide
Phytophthora_infestans_cysteine_synthase_putative	XP_002999267.1	signal peptide
Phytophthora_parasitica_CysSynt	XP_008892344.1	other localisation
Phytophthora_parasitica	ETL95873.1	other localisation
Phytophthora_cactorum_Cysteine_synthase2	RAW33481.1	signal peptide
Phytophthora_sojae1_OASTL	XP_009518901.1	other localisation
Phytophthora_sojae2_OASTL	XP_009534564.1	other localisation
Phytophthora_sojae3_OASTL	XP_009530251.1	mitochondrion
Fistulifera_solaris	GAX26691.1	other localisation
Nannochloropsis_gaditana	EWM29059.1	signal peptide
Guillardia_theta_OASTL	XP_005822180.1	other localisation

The outputs “-” and “other localization” mean the same for TargetP and HECTAR, respectively. It means that no expected targeting regions were found within the inputted sequence. In those cases, nuclear and/or cytosolic localization may be discussed if applies.

\* Sequence IDs are mostly NCBI accession numbers or, when identified, JGI protein IDs. The few times when sequences were not yet available in public databases, the reference is identified.

## 4. CHARACTERIZATION OF ATPS FROM *P. TRICORNUTUM*

### 4.1. Introduction

It seems that the peculiarities found on the sulfate reduction and assimilation among algae can be largely attributed to ATPS heterogeneity (Patron et al. 2008; Chapter 3). It is arguably the most phylogenetically diverse among the enzymes involved in sulfur metabolism. Multiple origins, fusions and targeting have been reported (Patron et al. 2008, Bradley et al. 2009, Bromke et al. 2013). More recently, the description of a huge diversity also in the ATPS's susceptibility to redox regulation (Rosenwasser et al. 2014, Prioretti and Giordano 2016) created a new horizon of experiments and hypotheses to investigate this singular enzyme. Although sequences analyses, and *in vitro* experiments paved a solid understanding of ATPS's redox regulation so far, the physiological mechanisms that drive it are still unclear.

*Phaeodactylum tricornutum* (Bohlin, 1898) is a genome-sequenced pennate diatom (Bowler et al. 2008; see more information in Chapter 5) belonging to the group of organisms whose ATPS is redox regulated and, conveniently, possessing a small number of ATPS isoforms (two; see Chapter 3). When in cultivation, *P. tricornutum* grows consistently and responds very well to genetic transformations, which make it a model system for diatoms (Zaslavskaja et al. 2000, Miyahara et al. 2013, Zhang and Hu 2014, Karas et al. 2015). For these reasons, *P. tricornutum* is used in this chapter to investigate the allocation, function and mechanism for the *in vivo* redox regulation of ATPS.

The enzymes' cellular allocations are here studied via green fluorescent protein (GFP)-fusion targeting. GFPs are naturally occurring proteins, existing in a variety of cnidarians coupled with other chemiluminescent proteins to control *in vivo* luminescence. Its ability to generate a highly visible internal fluorophore is tremendously valuable and rendered it as a well-established marker of gene expression and protein targeting in intact cells and organisms. The most successful and numerous class of GFP applications has been as a genetic fusion partner to host proteins to monitor their localization and fate, as it was used in this study. The gene encoding a GFP is fused in-frame with the gene encoding the endogenous protein of interest and the resulting chimera expressed in the cell or organism of interest. The ideal result is a fusion protein that maintains the normal functions and localizations of the host protein but is now fluorescent (Tsien 1998).

Reverse genetics techniques are historically important tools to study genes and/or proteins functions. Due to the diplontic life cycle and lack of sexual reproduction of *P. tricornutum* in culture, some well-known methods of genetic manipulation like random mutagenesis and crossing are not available. However, two very powerful tools for site-directed genome editing were recently developed: the Transcription Activator-Like Effector Nuclease (TALEN; Christian et al. 2010, Li et al. 2011) and the Clustered Regularly Interspaced Short Palindromic Repeats (CRISPR/Cas9; Cong et al. 2013). Whereas both systems are very efficient, the first has been regularly and successfully used in *P. tricornutum* (Serif et al. 2017) and is used in this chapter. TALEs are a class of naturally occurring DNA binding proteins first described in the plant pathogen *Xanthomonas* sp. used to modulate gene expression in host plants and facilitate bacterial infection. The central region of the protein contains tandem repeats of 34 amino acid sequences, named monomers, that are important for DNA recognition and binding (Figure 15 A). The sequence of each monomer is highly conserved, only differing in the 12<sup>th</sup> and 13<sup>th</sup> amino acid residues – termed Repeat Variable Diresidues (RVDs) –, which determine the nucleotide binding specificity of each TALE (Sanjana et al. 2011; Figure 15 B). Thus, each monomer targets one nucleotide and the linear sequence of monomers in a TALE specifies a target DNA sequence in the 5' - 3' orientation. In this sense, the programmable nature of TALEs allows scientists to introduce directed mutagenic events in target organisms. For instance, TALEs can be appropriately assembled with effector domains such as transcription factors (TALE-TF) or nucleases (TALEN) to achieve a wide array of experimental goals.

TALENs are constructed by fusing a C-terminal truncation of the TALE DNA binding domain with a non-specific FokI endonuclease catalytic domain. In this procedure, two TALENs target a pair of binding sites in opposite DNA strands separated by 14-20 bp –space for FokI dimerization and activity (Figure 15 C). When FokI dimerizes, it performs a double-strand break (DSB) in the region between the TALEN binding sites. Cell mechanisms of DSB's repair generally results in insertions and/or deletions that may render the gene no longer functional, creating a gene knock out.

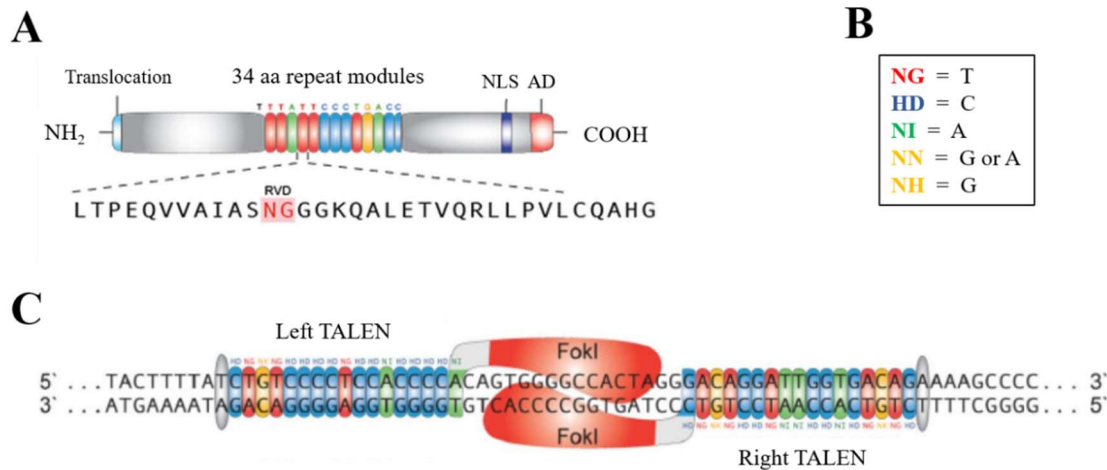


**Figure 15:** Schematic representation of (A) a TALE, highlighting the amino acid sequence of one tandem repeat module and the RVD within it; (B) RVDs' specificity to each nucleotide; and (C) a pair of TALENs binding the DNA strand. Modified from Sanjana et al. (2011).

The studies of regulation by the changes in redox state of thiol groups (S-S ↔ 2SH) were initially carried out in the context of photosynthesis. The influence of light/dark on activity of chloroplast enzymes was then thoroughly investigated, as well as the effects of a wide range of photosynthetic inhibitors (Buchanan 1980). Later, a number of mechanistic systems were described – e.g.: ferredoxin / thioredoxin; NADP / thioredoxin; glutathione / glutaredoxin – and, today, redox regulation embraces virtually every type of living organism (Buchanan and Balmer 2005). Along with other modes of regulation, these systems enable the cells to minimize the so-called futile cycling and maximize the use of available energy resources. Finally, in this chapter the activity of *P. tricornutum*'s ATPS is assessed as a function of light and, if affected, the signal transduction that led to the enzymatic regulation was investigated via the use of the photosynthesis inhibitor 3-(3',4'-dichlorophenyl)-1,1'-dimethyl urea (DCMU). It was hypothesized that similarly to nitrate reductase (Giordano et al. 2005a), the first step in the pathway of nitrate reduction, also the first step in the reduction of sulfate is modulated through the sensing of the redox state of the plastoquinone (PQ) pool.

## 4.2. Material and Methods

### 4.2.1. Diatom cells culture conditions for GFP fusion and knockouts

*Phaeodactylum tricornerutum* (UTEX 646 University of Texas Culture Collection, Austin, USA) wildtype cells were grown axenically in modified liquid f/2 medium supplemented with half-concentrated artificial sea salts (16,6 g·L<sup>-1</sup> Tropic Marin™, Wartemberg) and 0,09 μmol·L<sup>-1</sup> MnCl<sub>2</sub> (Guillard 1975). Cells were cultured at a constant temperature of 20 ± 1°C, illuminated with 40 μmol photons·m<sup>-2</sup>·s<sup>-1</sup> under a 16:8h (light:dark) photoperiod while constantly shaking at 100 rpm.

### 4.2.2. In silico retrieval of putative signal- and transit peptides

ATP Sulfurylase sequences from *P. tricornerutum* (Supplemental Figure 1) were retrieved from the Joint Genome Institute (JGI) sequencing project of this diatom (<http://genome.jgi-psf.org/Phatr2/Phatr2.home.html>) (Bowler et al. 2008). Sequences were evaluated for the presence of signal- and transit peptides with the aid of the web application of heterokont subcellular localization targeting method (HECTAR; Gschloessl et al. 2008). Pre-sequences were manually checked and cut sites were predicted using the online tool SignalP 4.0 (Petersen et al. 2011). Also, DNA sequences of the two alleles of the ATP-S and KSP genes were determined by aligning the individual sequence reads in the whole genome shotgun sequencing (WGS) database (NCBI).

### 4.2.3. Protein localization

#### 4.2.3.1. Construction of GFP-fusion vectors

Full length sequences of ATP Sulfurylase including the putative signal- and transit peptides but excluding the stop codon (Supplemental Figure 1) were amplified from *P. tricornerutum* genomic DNA and inserted in-frame via Kspal (HpaI) into the GFP-fusion vector pPhaT1-Kspal-GFP (Supplemental Figure 2). This vector was previously derived from the standard *P. tricornerutum* transformation vector (GenBank AF219942) (Zaslavskaja et al. 2000). Vector was equipped with enhanced GFP (eGFP; λ<sub>excitation</sub> ~ 488nm; λ<sub>emission</sub> ~ 508nm) sequence allowing the expression of C-terminally tagged fusion proteins, and a phleomycin D1-resistance cassette for mutant selection (Supplemental Figure 2). One step digestion-ligation was made in a mixture containing enzyme buffer; vector (2 ng·μL<sup>-1</sup>); insert (10 ng·μL<sup>-1</sup>; vector:insert = 1:5); DTT (1 mmol·L<sup>-1</sup>); ATP (10

mmol·L<sup>-1</sup>); restriction enzyme (Kspal 10 units); DNA T4-Ligase (5 Units); in a total volume of 20 µL. Final mixture was incubated overnight at 16°C, followed by addition of restriction enzyme (Kspal 10 Units) and incubation for 30 minutes at 37°C for final digestion. Reactions were deactivated for 20 minutes at 80°C and final plasmids were transformed into electrocompetent *Escherischia coli* cells via electroporation (Bio-Rad Micropulser) in 0,2 mm gap cuvettes. Obtained *E. coli* transformant colonies were screened via PCR and vector sequence were verified by Sanger sequencing (Microsynth Seqlab, Göttingen, Germany). In the correct constructs, ATP-Sulfurylase was C-terminally fused to eGFP.

#### 4.2.3.2. Nuclear bombardment of GFP-fusion vectors

Cells of *P. tricornutum* cultivated as described in Section 4.2.1 were genetically transformed using a Bio-Rad Biolistic PDS-1000/He Particle Delivery System (Bio-Rad, Hercules, CA, USA) fitted with 1350 psi rupture disks (Apt et al. 1996). One hundred µL of a concentrated cell suspension (~10<sup>9</sup> cells·mL<sup>-1</sup>) were placed in the center of a solid modified f/2 plate without antibiotic and bombarded with a mixture containing 3 mg of tungsten particles (M10 size, BioRad, Hercules, CA) impregnated with 5 µg of plasmid DNA (vector); CaCl<sub>2</sub> (125 µmols); and spermidine (2 µmols) (see Kroth 2007). For further selection and cultivation of *P. tricornutum* transformants, cells were transferred to solid modified f/2 (half-concentrated sea salts) plates containing 75 µg·mL<sup>-1</sup> of Zeocin™. Solid medium contained 1,5 % bacto-agar.

#### 4.2.3.3. Characterization of GFP mutants by epifluorescence microscopy

Analyses of transformed cell lines were conducted using an epifluorescence microscope Olympus BX51 (Olympus Europe, Hamburg, Germany) in combination with a Zeiss AxioCam MRm digital camera system (Carls Zeiss, Jena, Germany). Chlorophyll autofluorescence and green GFP fluorescence of the transformants have been dissected using the mirror unit U-MWSG2 (Olympus) and the filter set 41020 (Chroma Technology Corp, Rockingham, VT, USA), respectively. Multichannel fluorescence pictures were taken and assembled with the Axio Vision 40' V.4.6.3.0 Documentation software (Carl Zeiss; Jena, Germany).

Additional images were acquired on a confocal laser scanning microscope LSM 510 META (Carl Zeiss MicroImaging GmbH, Göttingen, Germany) using a Plan-

Neofluar 40 x 1.3 Oil DIC objective. GFP and chlorophyll fluorescence were excited at 488 nm, filtered with a beam splitter (HFT 488/543), and detected by two different photomultipliers with a bandpass filter (BP 505-530) for GFP fluorescence and a low pass filter (LP 650) for chlorophyll autofluorescence.

#### 4.2.4. Transcription activator-like effector nucleases (TALEN) mediated gene knockouts

##### 4.2.4.1. Choosing targeting sequences

Possible target sites for *P. tricornutum*'s monofunctional ATP-S (JGI Protein ID 42282) and KSP (JGI Protein ID 19901) were generated in the TAL Effector Nucleotide Targeter 2.0 (Doyle et al. 2012) using a fixed repeat array length of 19 RVDs per TALEN (20 in total), a spacer length of 15 to 22 bp between each TALEN, and the *P. tricornutum*'s genome reference sequence (ID GCF\_000150955.2) to predict possible off-target effects. An appropriate target site should be in an exon region, inside or upstream the first functional domain, and have no predicted off- targets. This way, the likelihood to obtain protein's loss of function in mutants is increased.

After screening the results, the best candidates had their cutting efficiency estimated in SAPTA (Scoring Algorithm to Predict TALEN Activity; Lin et al. 2014). Interpretation of the last results considered that composite score should be higher than 30 – which is achieved when both right and left TALEN single strand annealing activities are around 10% –, and the scores of each individual TALEN of a pair should be similar (Lin et al. 2014). Following these recommendations, the best two pairs of TALENs were chosen in order to perform two independent knock out attempts for each gene (Table 2).

**Table 2:** Cut site (number of amino acids from sequence start), sequences and scores (individual and composite) of chosen pairs of TALENs for independent knockout attempts of both tested isoforms of *P. tricornutum* ATP Sulfurylase.

Enzyme	Cut site		TALEN sequence	Individual score	Composite score
ATP-S	165	Left	T-AGTGCGCTCGCCATGGCCA	26,46	40,77
		Right	T-CAAGTCGACGAGCGTCTCG	14,42	
	583	Left	T-CCCGGGACACTCATGGTTCG	18,69	39,36
		Right	T-GACCTTGCCGCCCATGTAG	18,20	
KSP	132	Left	T-CTTGATCAACGACATTGAT	24,72	45,13
		Right	T-GAGGCCAGCCTTCCCCAA	25,61	
	533	Left	T-CATCCCTACATTCAACACA	18,57	39,93
		Right	T-TCTCCGCCAATCAAGTAGT	19,58	

#### 4.2.4.2. Assembly of TALEN plasmids

TALEN plasmids were assembled according to Sanjana et al. (2011) considering all modifications given in Serif et al. (2017). First, a TALE monomer library was built containing monomers with all possible RVDs and constructed in a way that will occupy a specific position when assembled as hexamers. The monomers were then digested and ligated via a Golden Gate type reaction into hexamers, amplified via PCR and purified. Lastly, three hexamers plus the plasmid containing the backbone of the vector – as well as the first and the last RVDs, the nuclease domain, and antibiotic resistance cassette – were digested and ligated in a second Golden Gate type reaction. The resulting plasmids were sequenced (Microsynth SeqLab, Germany) to verify correct assembly and order of the 20 TALE monomers.

#### 4.2.4.3. Nuclear bombardment of TALEN plasmids

Nuclear transformation of *P. tricornutum* cells was performed as described in Section 4.2.3.2. In this case, however, a pair of TALENs needed to be integrated for the correct dimerization of FokI and effectiveness of the technique. Thus, a bi-vector system was transformed simultaneously by impregnating tungsten particles with 1,25 µg of each plasmid. Selective growth was carried out as described earlier, but simultaneous integration of both plasmids was selected by the addition of 75 µg·mL<sup>-1</sup> of Zeocin<sup>TM</sup> and 150 µg·mL<sup>-1</sup> of nourseothricin to solid f/2 medium to select only cells harboring both vectors.

#### 4.2.4.4. Screening transformant colonies

After transformation cells from colonies grown in selective medium were inoculated in modified liquid f/2 medium and cultivated as described in Section 4.2.1. Then, cell pellets corresponding to 25 mL of cultures in exponential growth phase (3 - 6 x 10<sup>6</sup> cells·mL<sup>-1</sup>) were used to extract genomic DNA using the nexttec<sup>TM</sup> 1 step DNA isolation from tissues and cells kit (Biozym, Hessisch Oldendorf, Germany). Genomic DNAs of cultures to be screened were then amplified on an allele-specific PCR. This PCR uses the allelic polymorphisms determined earlier to amplify each allele individually, allowing thus to differentiate mono- and bi-allelic mutants. For that, primers were designed flanking the predicted TALEN cut positions, and such primers possess allele-specific differences in the 3' terminal base, highly discriminated by certain DNA

polymerases without proofreading activity (Supplemental Table 2). Therefore, allele-specific PCR for screening was performed using SNP Pol DNA Polymerase (Genaxxon, Germany) according to the manufacturer's instructions. PCR products were separated by electrophoresis in 1% agarose gel and differential migration would indicate different fragments' length, due to the insertions/deletions caused by the TALEN cut.

#### **4.2.5. *In vivo redox regulation of ATPS***

##### *4.2.5.1. Culture conditions*

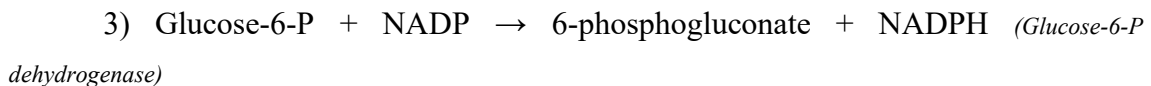
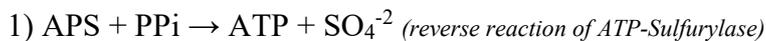
The diatom *Phaeodactylum tricornutum* (UTEX 646, Austin, USA) was batch cultured photo-autotrophically in 250 mL sterile Erlenmeyer flasks containing 125 mL of AMCONA medium (Fanesi et al. 2014; detailed recipe in the following chapter). Cultures were maintained in a growth chamber (Termaks AS<sup>®</sup>, Norway) at  $20 \pm 2^\circ\text{C}$ , exposed to lateral illumination of  $100 \mu\text{mol photons}\cdot\text{m}^{-2}\cdot\text{s}^{-1}$  measured with a quanta-meter (LI-250 Light Meter; LI-COR Inc.) on the outer surface of the vessels and provided by fluorescent lamps (OSRAM<sup>®</sup> Cool White) under a 12:12h (light:dark) photoperiod. Cell growth was followed by daily counts and, for ATPS activity assays, cells were always harvested from late exponential growth phase.

##### *4.2.5.2. Measurement of ATPS activity*

For enzymes' extraction, cells were collected by centrifugation at  $4000\cdot\text{g}$  for 10 minutes at  $4^\circ\text{C}$  and washed twice with an iso-osmotic solution of NaCl ( $0,5 \text{ mol}\cdot\text{L}^{-1}$ ) to remove residual salts that could interfere in the assays. The final pellet was resuspended in  $800 \mu\text{L}$  of an extraction medium containing  $50 \text{ mmol}\cdot\text{L}^{-1}$  Tris-HCl (pH 8),  $1 \text{ mmol}\cdot\text{L}^{-1}$  EDTA,  $10 \text{ mmol}\cdot\text{L}^{-1}$   $\text{MgCl}_2$  (Giordano et al. 2000) where cell lysis was performed by nitrogen decompression, using a cell disruption bomb (4639 Cell Disruption Vessel; Parr Instrument Company, Molin, IL, USA) at the pressure of 2000 psi ( $\sim 137 \text{ bar}$ ). After decompression, cell lysis was confirmed under an optical microscope (Leitz, HM-LUX 3). The slurry was collected into a  $1,5 \text{ mL}$  plastic tube to which Triton X-100 (0,1% v/v) and glycerol (10% v/v) were added to a final volume of 1 mL and vigorously mixed. After incubation on ice for protein solubilization (10-15 minutes), the final slurry was centrifuged for 15 minutes at  $13000\cdot\text{g}$  at  $4^\circ\text{C}$  and the supernatant – i.e.: protein crude extract – was immediately used for spectrophotometric enzymatic assay. Protein

concentration on crude extract was determined using Peterson's method (Peterson 1977; more details on the method in the following chapter) modified in a way that extraction medium was added to calibration curves' mixtures in the same volume as crude extract aliquots for measurement in samples.

ATP-S activity was measured on crude extract spectrophotometrically at 25°C, using a Beckman DU 640 Spectrophotometer (Beckman Coulter), according to Burnell (1984). The reaction mixture contained: APS (1 mmol·L<sup>-1</sup>), PPi (1 mmol·L<sup>-1</sup>), MgCl<sub>2</sub> (5 mmol·L<sup>-1</sup>), glucose (5 mmol·L<sup>-1</sup>), NADP (300 μmol·L<sup>-1</sup>), hexokinase and glucose-6-P dehydrogenase from baker's yeast (5 units, H8629 Sigma-Aldrich), Tris-HCl pH 8 (50 mmol·L<sup>-1</sup>), with (for *in vitro* redox regulation tests) or without (for *in vivo* redox regulation tests) the addition of reduced dithiothreitol (DTT<sub>red</sub>; 10 mmol·L<sup>-1</sup>). The volume of crude extract added to the assay mixture was 40 μL for a final volume of 500 μL. The final reaction mixture was made to induce the coupling of the reverse reaction of ATP-S with the reactions catalyzed by hexokinase and glucose-6-P dehydrogenase, resulting in an adenosine 5'-phosphosulfate (APS)-dependent reduction of NADP<sup>+</sup> to NADPH, as follows:



The rate of NADPH production was measured as the change of absorbance at 340 nm and recorded for 10 minutes. The values of absorbance were converted to enzyme activity using the Lambert-Beer law:

$$\text{ATP-S activity } (\mu\text{mol} \cdot \text{min}^{-1} \cdot \text{mL}^{-1}) = [\Delta\text{Abs}_{340\text{nm}} \div (\epsilon_{\text{NADH}} \cdot d)] \cdot \text{dilution factor}$$

Where  $\Delta\text{Abs}_{340\text{nm}}$  is the measured variation of absorbance of NADPH at 340 nm per minute (min<sup>-1</sup>);  $\epsilon_{\text{NADH}}$  is the extinction coefficient of NADH at 340 nm (=6,22 mM<sup>-1</sup>·cm<sup>-1</sup>); d is the optical path length (=1 cm); and the dilution factor of the sample on the final reaction mixture is calculated by dividing the volume of final reaction mixture (=500 μL) by the volume of crude extract added (=40 μL). Finally, the specific activity of ATP-Sulfurylase was normalized by amount of proteins by dividing the result as described (expressed in μmol·min<sup>-1</sup>·mL<sup>-1</sup>) by the concentration of proteins (in mg·mL<sup>-1</sup>) in each sample. All enzymatic assays were performed in at least three biological replicates and

blanks were made with the exact same mixture where the substrate (APS) was substituted by milli-Q water.

The influence of photosynthesis on the *in vivo* redox regulation of *P. tricornutum*'s ATP Sulfurylase was assessed by measuring its activity after cells from the same culture were sequentially exposed to dark, light and to the addition of 3-(3'4'-dichlorophenyl)-1,1'-dimethyl urea (DCMU) in culture medium (final concentration 5  $\mu$ M). Activity assays were performed as previously described and DCMU (1 mM stock solution) was dissolved in dimethyl sulfoxide (DMSO). Control experiments showed that the concentration used was effective during the entire course of experiments (24h), and that DMSO alone did not affect photosynthesis and/or enzyme activity of *P. tricornutum* cells. For measurements in dark, cells were harvested after 12h in darkness; light measurements were performed in cells harvested after at least 2h of light exposure; and further measurements were carried out after 1, 3, 6 and 24h of DCMU addition. Cell harvesting and subsequent steps for activity assays were performed as described except that for dark measurements all steps were carried out in semi-darkness, and that after the addition of DCMU cultures were permanently illuminated.

### 4.3. Results

The diatom *P. tricornutum* encodes two isoforms of putative ATP Sulfurylases termed from now on as ATPS (JGI Protein ID 42282) and KSP (JGI Protein ID 19901). The first consists on a monofunctional enzyme, while the latter is a longer isoform that consists on a monogenic fusion of an APS Kinase, ATP Sulfurylase and a Pyrophosphatase domains, which is known to be found exclusively in heterokonts (Bradley et al. 2009). Both isoforms share 25,83% sequence identity, with ATP-S core domains being 31,34% conserved.

#### 4.3.1. ATP Sulfurylases' localization

ESTs suggested the existence of a pre-sequence upstream the annotated ATPS sequence in *P. tricornutum*'s genome project, as well as an intron region (Figure 16 A). The translation of the whole new sequence resulted on a clear predictable bipartite signal- and transit peptide and an equally clear ASAF motif, known to target proteins to the chloroplast stroma (Kilian and Kroth 2005; Figure 16). No pre-sequences were found on the KSP sequence.

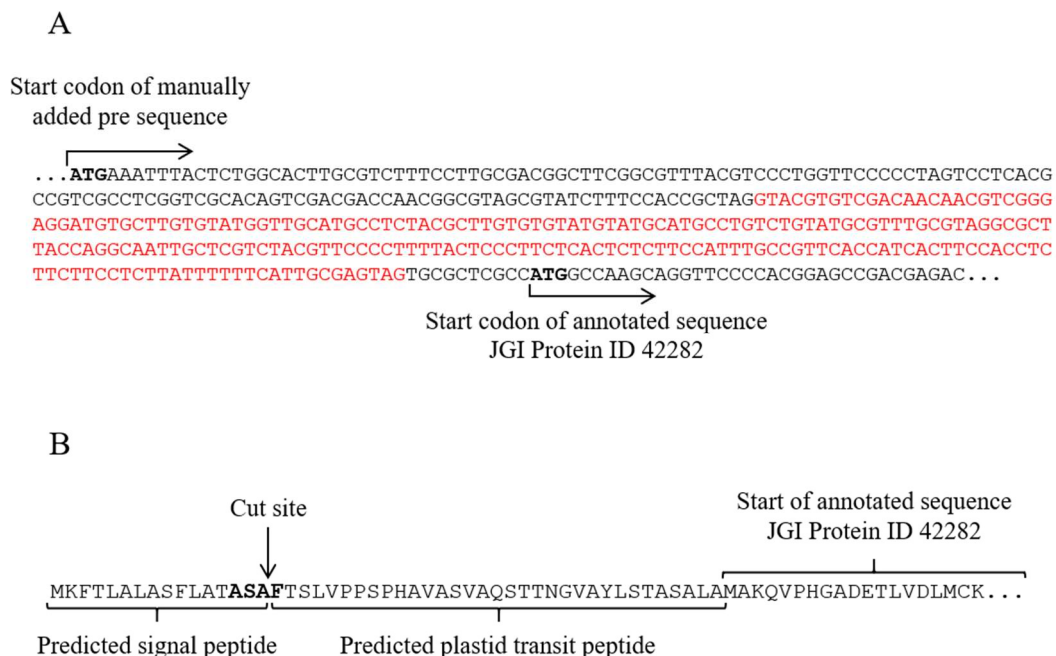


**Figure 16:** Characterization of a non-annotated pre-sequence of ATPS in *P. tricornutum* (JGI Protein ID 42282). (A) The nucleotide sequence is located in chromosome 21 (487621-488019), intron is showed in red and start codons are highlighted in bold; and (B) Amino acid sequence with predicted signal-, transit peptides and cut site, ASAF motif is highlighted in bold.

The full-length sequence of both the manually modified sequence of the monofunctional ATPS and the KSP sequence were cloned into the *P. tricornutum* transformation vector pPhaT1 containing the eGFP sequence, yielding plasmids with the eGFP fusion that were transformed biolistically into *P. tricornutum* cells. Expression of the ATPS-eGFP construct showed that green GFP fluorescence was congruent with the red chlorophyll fluorescence from the plastids, indicating that ATPS is localized in the chloroplasts (Figure 17). Although green fluorescence was clearly associated to the plastids, it was unevenly distributed throughout their area. Thus, making it difficult to make further assumptions on specific localization within the chloroplast. On the other hand, the expression of the KSP-eGFP resulted on a much weaker and inconsistent GFP signal. Although results were far from conclusive, they suggested that KSP was localized outside of the chloroplast (Figure 18).

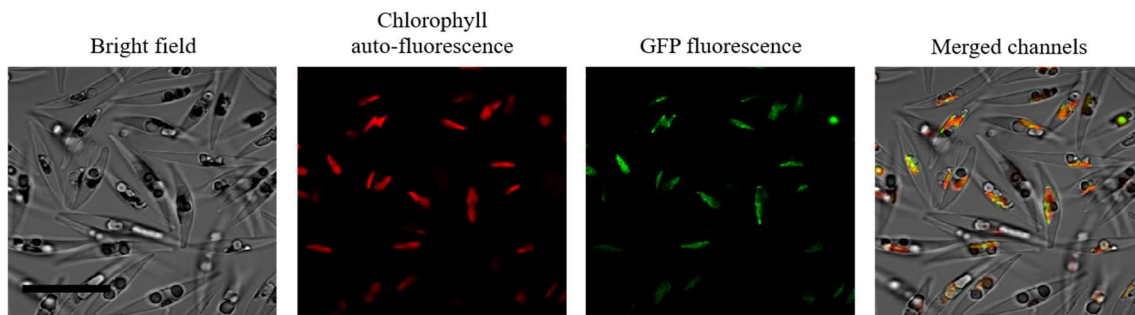


**Figure 17:** Confocal photomicrographs showing the localization of the ATPS:GFP fusion expressed in *Phaeodactylum tricornutum*. Scale bar represents 10  $\mu\text{m}$ .

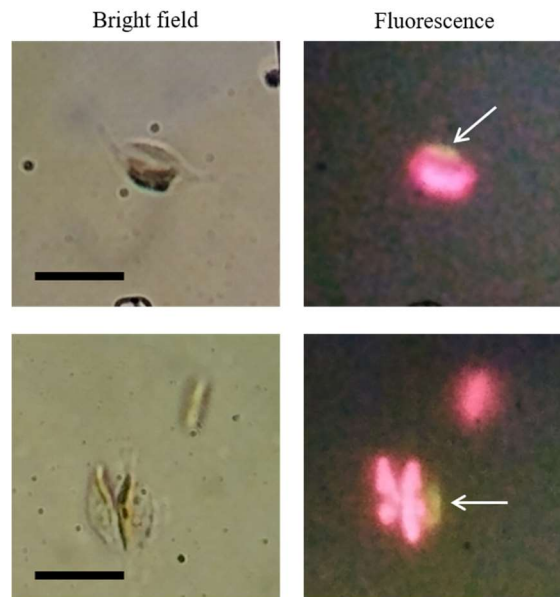


**Figure 18:** Photomicrographs showing the KSP:GFP fusion expressed in *P. tricornutum*. Arrows point to the GFP fluorescence. Note that the cells' shapes are considerably different from Figure 17 and that the green fluorescence was not consistently observed in all cells in culture. Scale bars represent 10  $\mu$ m.

#### 4.3.2. *ATP Sulfurylase knockouts*

Various attempts of biolistic transformation of *P. tricornutum* cells with the TALEN constructs designed for ATP-S knockouts resulted in no transformant colonies. On the other hand, 25 transformant colonies thrived from the biolistic bombardment of *P. tricornutum* with the KSP TALEN constructs. Surprisingly, however, the amplification via allele specific PCR showed no size shifts in the fragment of interest – i.e.: the TALEN cut site (Figure 19). This could mean that cell repair mechanisms successfully repaired the double-strand break caused by the TALEN, or that DNA constructs were integrated in a way that antibiotic resistance was correctly expressed whereas the TALEN was not. In both cases, functional knockout would not have happened. Therefore, there was no motivation for further screening steps, such as sequencing, on those transformant colonies.

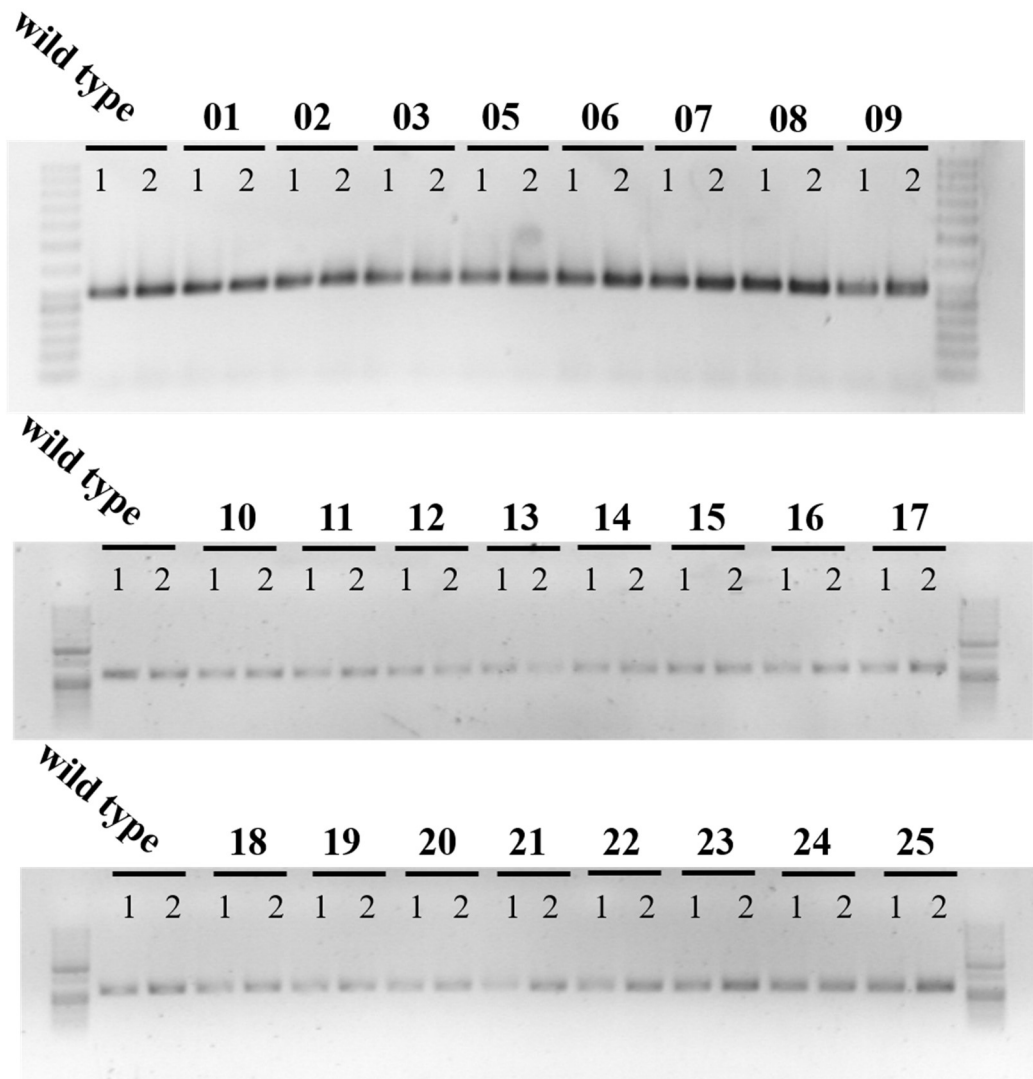


**Figure 19:** Electrophoresis gel of allele specific amplification products from genomic DNA of all colonies resulting from the transformation of *P. tricorutum* cells with the KSP TALEN plasmids. In this screening step, size shifts would indicate insertions/deletions caused by small errors in the cell repair mechanism, that could result in functional knockout and, hence, motivate further screening steps. Text and numbers in bold, above the gel wells, identify the colonies; numbers below identify the two different alleles.

### 4.3.3. Redox regulation of *P.tricornutum* ATP Sulfurylase

ATP Sulfurylase activity from *P. tricornutum* cell extracts was significantly affected by the addition of DTT<sub>red</sub> on the reaction medium (Figure 20). Introduction of the reducing agent resulted on a 34% increase of ATP Sulfurylase activity, indicating that the enzyme is redox-regulated, thus encouraging further investigation on physiological mechanisms that might be involved in redox-based regulation of enzyme activity, such as photosynthesis.

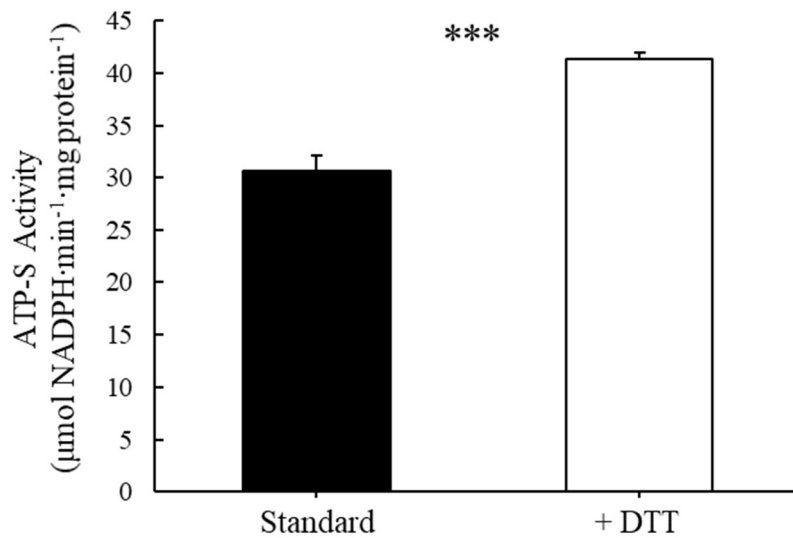


**Figure 20:** ATP Sulfurylase activity of *P. tricornutum* cell extracts in the absence (black bar) or presence (white bar) of the reducing agent DTT<sub>red</sub>. Data are the means of at least three biological replicates ( $n \geq 3$ ) and error bars show standard deviation. Asterisks indicate significant differences (\*\*\*) =  $p < 0,001$

Interestingly, although the exposure to light influenced enzymatic activity, the addition of the photosynthetic inhibitor DCMU to the reaction medium did not (Figure 21). After 12h in darkness, cells showed ATP Sulfurylase activity approximately 60% lower than cells harvested from the same cultures after illumination for at least 2h. Then, DCMU was added to the same culture flasks, illumination was kept constant, and activity measurements were carried out at regular time intervals. ATP Sulfurylase activity values were essentially the same during the entire monitoring period after the addition of DCMU (24h), which in turn, were not different from activity of cells exposed to light. This suggests that although ATP Sulfurylase is an enzyme that can be redox regulated, its *in vivo* regulation is not strictly dependent on the photosynthetic electron transport chain.

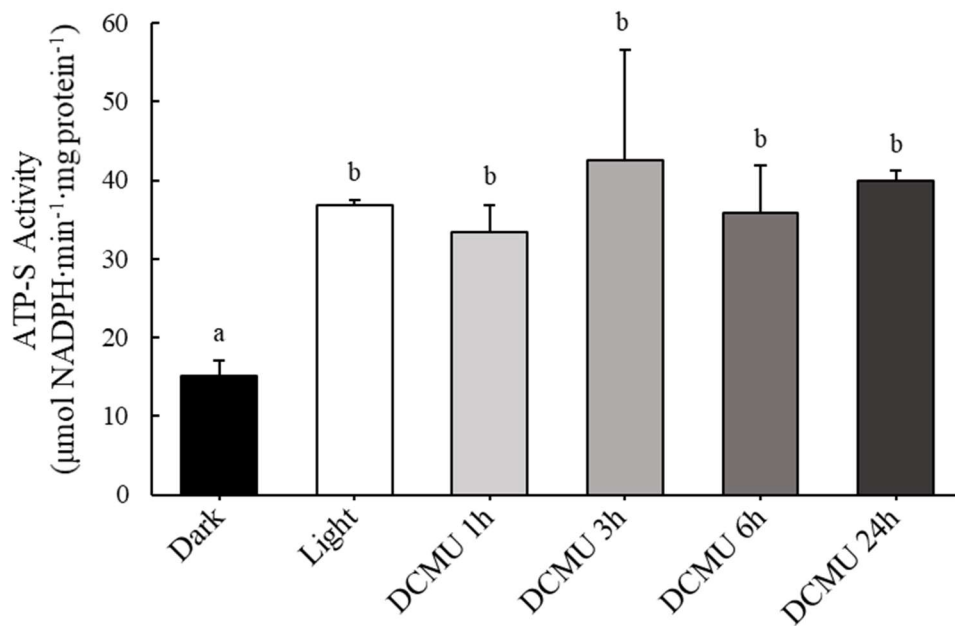


**Figure 21:** ATP Sulfurylase activity of *P. tricornutum* cell extracts from the same cultures exposed to dark (black bar), light (white bar), or DCMU in the presence of light for 1, 3, 6 and 24h (bars in grayscale). Data are means of three biological replicates (n=3) and error bars show standard deviation. Different letters over bars indicate statistically significant differences ( $p < 0,05$ ).

## 4.4. Discussion

### 4.4.1. ATP Sulfurylase function and localization in diatoms

As most diatoms, *P. tricornutum* possesses two isoforms of ATPS (see Chapter 3). One is a monofunctional enzyme expected – and confirmed here – to be localized in the chloroplasts as part of the primary sulfate metabolism; whereas the other is part of a bigger fused protein containing also a kinase and a pyrophosphatase domain, perhaps functioning efficiently as a PAPS synthetase (Bradley et al. 2009, Prioretti et al. 2014). There are weak evidences, based on sequence analysis, that in *T. pseudonana* these isoforms are inversely allocated (Bromke et al. 2013). In this thesis, there is evidence to suggest that the reduction and sulfation reactions are physically separated in diatoms by the different allocation of the enzymes involved, and the partitioning is driven by the redox regulation of the reductive pathway (Figure 22). For this suggestion, a single species stands for the entire division of diatoms, a gross oversimplification. Nonetheless, it provides a starting point for further appreciation on algal sulfur metabolism.

Based on this thesis' results and research, there are at least four evidences that reinforce the hypothesis illustrated in Figure 22. First, there is no monofunctional APK present in *P. tricornutum*'s genome, only that within the KSP multi-protein – this is not true for *T. pseudonana* and *F. cylindrus*, both contain one sequence for a monofunctional APK likely to be cytosolic (see Chapter 3). It is highly probable that the KSP functions as an efficient PAPS synthetase for sulfation in heterokonts (Bradley et al. 2009). Secondly, Patron et al. (2008) and Kopriva et al. (2007) observed an uneven distribution of APR and SiR within the chloroplasts of the green alga *C. reinhardtii* and the moss *P. patens* respectively. Based on these uneven and congruent distribution, the authors suggested that the enzymes of sulfate activation and reduction may form a multi-enzyme complex. The same so-called “spotty pattern” of localization within plastids was observed here for ATPS, the enzyme responsible for sulfate activation (Figure 17). Another relevant piece of information is that in plants the partitioning of sulfur to primary or secondary metabolism seems to be controlled by redox regulation, but in a different way. At least in *A. thaliana*, APK and APR co-exist inside the chloroplasts and compete for their mutual substrate, APS. According to Ravilious et al. (2012), the redox state affects both enzymes, but in opposite ways – while one is stimulated, the other is inhibited. The authors suggest that this feature, unique to plants, evolved after the bifurcation of plant

lineage. Hence, different modes of regulating sulfate partitioning might have evolved convergently in other lineages, like diatoms. Finally, the unsuccessful knockout attempts carried out in this thesis may suggest that both enzymes are essential for *P. tricornutum*'s life. Indeed, the metabolism suggested in Figure 22 implies on a one-way non-redundant path for reduction and sulfation. In that scenario, a malfunction in any of the tested enzymes would severely affect the metabolic route, possibly being lethal.

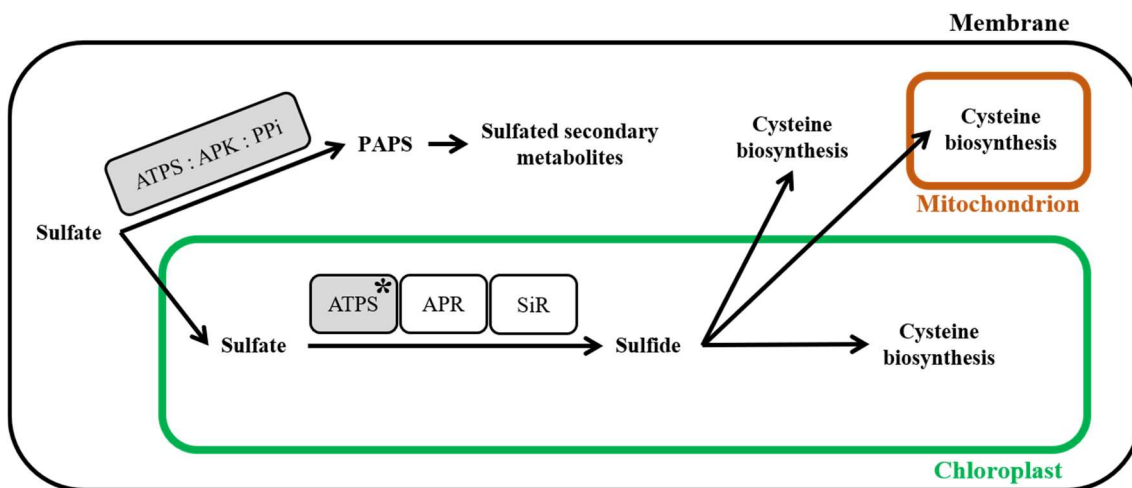


**Figure 22:** Schematic representation of the suggested sulfate metabolism in diatoms, with emphasis on the partitioning into reduction or sulfation. Tested enzymes are highlighted in gray, and the asterisk indicates the redox-sensitive enzyme.

#### 4.4.2. *In vivo* redox regulation of ATP Sulfurylase

Light exercises a major regulatory role in chloroplasts. Such regulations might be associated to the thioredoxin system, changes in stromal pH,  $Mg^{+2}$  concentration, or other consequences of the functioning of the photosynthetic electron transport chain. These signals, likewise, are transduced to enzymatic inhibition / stimulation via a number of possible mediators (Buchanan 1980, Buchanan and Balmer 2005). In this chapter, the activity of ATPS from *P. tricornutum*'s cells extracts was stimulated by both the exposure to light and to a non-physiological reducing agent (Figure 20 and Figure 21) It should be noted that the ATPS:KSP ratio in crude extracts is not known, as well as whether the sulfurylase domain of KSP is able to perform its activity in the conditions of the assays. Based on these results, one can assume that the plastidic and redox-sensitive ATPS is stimulated by the reducing power generated by photosynthesis, however the signal transduction mechanism involved remains poorly understood.

DCMU is an herbicide that blocks the non-cyclic electron transport at the plastoquinone (PQ) binding site of quinone B (Q<sub>B</sub>), thus impeding the reduction of the PQ pool (Trebst 1974). The redox state of the PQ pool seems to be a physiological proxy for the general photochemical performance, and regulate the activity and/or expression of pivotal proteins, such as the LHCB1 (Escoubas et al. 1995), D1 (Trebish and Danon 2001) and even the cytosolic nitrate reductase of *C. reinhardtii* (Giordano et al. 2005a). Interestingly, the addition of DCMU on *P. tricornutum* did not affect ATPS activity, suggesting that the redox state of the PQ pool is not the mediator of ATPS's regulation.

## 4.5. Supplemental material – Chapter 4

**Supplemental Table 2:** List of primers used in this study and their function.

Primers		
Name	Sequence (5'-3')	Function
atps_fwd	ATGAAATTTACTCTGGCACT	Amplification of JGI 42282 from gDNA
atps_rev	CATATTGTCTCGTAGAACCT	
atps_scr	GACTGTGCGACCGAGGCGAC	Screening for correct JGI 42282 inserts
ksp_fwd	AAGGGCGCCACGCTCTGGAT	Amplification of JGI 19901 from gDNA
ksp_rev	CGTTCCCCTACACCCCGGAC	
ksp_scr	GAATCCCAAATCACGGTTGA	Screening for correct JGI 19901 inserts
v36_seqUP	GCTTCAATTTGCTGGATGT	Screening primers of vector pPhaT1-KspAI-GFP
v36_seqREV	TTAAGGAAGGATAGAGACT	
atps_all1_f1	AGGATGTGCTTGTGTATGC <b>ATGCA</b>	Screening of JGI 42282 TALEN transformants via allele specific PCR.
atps_all2_f1	AGGA <b>AG</b> TGCTTGTGTATG <b>ATTGCG</b>	
atps_all1_f2	AATTGCTCGTCTACGTTCCCCT <b>TT</b>	
arps_all2_f2	AATTGCTCGTCTACGTTCCCCT <b>TG</b>	
atps_all1_r1	TCGTT <b>CATGAATCCCGTCAAAGGA</b>	
atps_all2_r1	CGTT <b>CATGAATCCCGTCAAAGGC</b>	
atps_all1_r2	CATGATGAGTTCGACGTCG <b>CAC</b>	
atps_all2_r2	CATGATGAGTTCGACGTCG <b>CAG</b>	
ksp_all1_f1	TGGTCGGGGCGCCCAA <b>ACTA</b>	Screening of JGI 19901 TALEN transformants via allele specific PCR.
ksp_all2_f1	TGGTCGGGGCGCCCAA <b>ACTC</b>	
ksp_all1_f2	AGTGCAGGGTTTCCAACAG <b>G</b>	
ksp_all2_f2	AGTGCAGGGTTTCCAACAG <b>A</b>	
ksp_all1_r1	TCGTGGATCCGGATCATCC <b>G</b>	
ksp_all2_r1	TCGTGGATCCGGATCATCC <b>T</b>	
ksp_all1_r2	TATCTCCGAGGCCCGGCG <b>AC</b>	
ksp_all2_r2	TATCTCCGAGGCCCGGCG <b>AT</b>	

Primers used for fragment amplification from *P. tricornutum* gDNA were designed with the aid of primer BLAST (Ye et al. 2012). Interallelic nucleotide polymorphisms used in the screening of TALEN transformants are indicated by bold nucleotides in the sequences.

>ATP-S (JGI Protein ID 42282)

ATGGCCAAGCAGGTTCCCCACGGAGCCGACGAGACGCTCGTCTGACTTGATGTGCAAGACGGACGAGGAAAAGAACGCC  
GCCATCGCCAAGGCTACCGTCTGAACTAGAGGCCCTCGGACCGTCTGACGCTCGAAGTCAATCATGAACGCCGGA  
TTCTCTCCTTTGACGGGATTCATGAACGAAGAAGAGTACCAATCGGTCGTCGAGAATATGGCGCTGCCGGACGGTACC  
GTTTTTCGGACTGCCCGTCGTTTTGATACCGACGACGAAAATCTGCAACCCGGCACCACCATTCTGCTCAAGCAGGGC  
GACCGGCCATTGCCACCGTCTGAGCTCACGGACAAGTTACGCCCCGACAAGCCCTGGAATGTCTCAAATGCTACGGA  
ACCTCACAGATCGAGCATCCCGGGACACTCATGGTCGCCACCGAGCGTGGTCTTACTACATGGGCGGCAAGGTCACC  
GGCCTCAACCTACCCGTGCGCGAATTCCTGTCGCAAGACGCCCCAGGAAGTCAGGGCCGGACTCCCCGACGACAAGGAC  
GTGGTGGCCTTTCAGTGGCGCAACCCCGTCCACCGCGCGCACTACGAACTCTTACCCGCGCTCTCGACGATGCCCTC  
GTGAGCGAAGGCGGTATCGTGTGGTGCACCCGACCTGCGGGCCACACAGGCCGACGACATTTCTGGTGAAGTCCGT  
TACAAGACCTACGAAGTGTCAAGGAAGAAACCGCCAATCCCGGGTGCAGTGGGAGTACCTGCCGTAATCGATGCAC  
ATGGCCGGACCCCGGAAGCATTTCAGCACATGATCATCCGCAAGAAGTTGGTTGCACGCACTTTATCATTTGGACGC  
GACATGGCCGGGAGCAAGAGCTCCGTCACCTGGTACGACTTTTACGGAGCTACGACGCCAGGAATGCGCCGAGAAG  
TATTCGGCACAGCTCGGCGTGACACCCGTGCCAGTCTCAACCTCGTGTACACGGAAGAAGAAGGCTACACCACCGCC  
GACTATGCCGACGAAAAGGGCTACACACCAAGAAGTTGTCCGGTACCAAGTTCCGTCAAATGCTACGTGGGGGCGAC  
GACATTCGGAATGGTTCGCCTTTAAGAGCGTCTGAAGTTCTACGAGACAATATGTAA

>KSP (JGI Protein ID 19901)

ATGACGGGATGTTCCGGTGC GGCAAAACCACCATTGCCACCGCACTCGAAGATCAACTCGTCAAGAGTTACGGGAAA  
CACGTCACCGTCTGGACGGGATAAACCCTCCGCACCGGACTCAACCGTGATTTGGGATTTCTCGAAGCCGATCGCGCC  
GAGTCGGTCCGACGGACCCGGGAACTCGCCACACTCTTTGCCGACGCGGGTGTCTGACGCTCGTCCGACTCATCTCG  
CCCTACCGCAAGGATCGCGACGCCGTACGCAACGTCACGTCGACCAAGGCATTCCCTTTTACGAAGTATTCCTCGAC  
GTGCCCGTGGATGAACCTCAAAAACGCGATCCCAAGGGACAGTACGCTCGTGTGAGTCCGGAGAAGTCAAACACTTT  
ACCTGCATCGACGACCCCTATGATGAACCCCTGCAACCAGAAATTACCCTCAAAAACGACGAACTCACCATTGAACAG  
TCGGTGCAGATTCTCTTTTCGACGACTCGAACGAGACGGAATTCTGGTGGGGCGCCAAACTTAGTCCGCCGGTCTG  
CCCAACCCGACGGGGACGCTTTGGTGGACTTGCACGTTCCCGACGAATCCAAAGAAGCCCGTCCGCGCGAGGCGGCG  
ACCCTCCCCAAGGTCTTGATCAACGACATTGATCTCAACTGGTTGCAAACCATTTGGGGAAGGCTGGGCCTCACCGCTC  
CGAGTTTCATGCGCGAAGGCACACTGTTGAAACCCGCACTTTAATTCGATCCTCACGGATCCCTTCAACCTCACG  
GGCAACCCCTGCGACTGGAACCCGCACTGAACTTTGATCACTTTTCCGCCATCCGGCCCCAACCGCGTCTCCATG  
CCATTCCCATCACCCCTCTCTGTACATCTTTTACCAAGGACCTCATTGACGCTCGTCCCACAACCGCGTCCGCTTTG  
GTGACACAAATGGGACACACCGTGGCCATTCTACGCGATCCCGAAGTCTACGCCAACCGCAAGGAAGAAATCGTGACG  
CGTATGTACGGTGTCTGGATCCGGATCATCCCTACATTCAACACATTTATCGGGGCGGCGACTACTTGATTTGGCGGA  
GAAATCGAAGTGTGATCGCATCCGCTACAATGACGGCTCGACAGTGGCGCAAAAACAGCGACGGAGCTCGTGCAA  
GAGTTCAGAGCAAAGGGGCGACACGGTGTACGCCTTCCAAACGCGTAACCCGACCCACGCGGGTACCGGTACCTG  
ATGCGTTCGCCGGTGAAGACCTGCGTCTCAGGGTACCAGAAACCCGTCCTGTGGTTGAGTCCCTGGGCGGTGG  
ACCAAGGCGACGACGTCGCGTCTGATGTGCGGTCAAACAGCACGCAAGTCTGCAAGCGGGCACCCCATCCC  
GGTGGCCTCGATCCGGAATCCACCGTCATGGCTATTTGGCCGCTCCCATGGTCTACGCCGGACCCACCGAAGTCCAG  
TTCCACGCCAAGTACGGCGCTCCGCGGGAGCCTCGTACTTTGTGGTGGCGCGATCCCGCGGAATGAAAGGATCG  
CCCAACCGGTGGCGCACCCGGACGATGACCTCTACGACGGTAACACGGAGCTTACGTTCTGCAGAACTCGCCGGGC  
CTCGGAGATATGAAGATGCTGAGCTTTGTCAAAGTCAATGTACGACACCACGACAATATTTATGAAGATTCCGGACGAA  
GCGCGGTGGCGGACTTTATCAGTATTTCCGGCAGTAAAATGCGACTGTTGGCCCGGAACGGGGCCACCCCTGCAGT  
CCCACCAATATTCGACGGATCTGGTCAAGCCAACTGCTCCCGAGCGGATTCATGGTACCGGACGGTTGGAATCAA  
GTGGTGCATACTACCGGAATATTGATGATGTGCAACGCTGGACGCGTGGAGTCAACCTCGCGTAGATCCCCCACG  
GCACCGCGCACACGATCAAGGCCAGTTTGGTTCCCGATCCTTCCACCTGACTAGTACAGAATACGAATCCTTCTGG  
CACGACATTCCTTGAGTCCATCGGGCAATCCGAAACCGTAGTCAACATGGTACGGAATTTCCATGTATTGCACG  
GCCAAAATGGAGATTCAAAGATGCTGTCCAACAGTCCCATTTGCTCAGGACACCAACAGCGACGGTTCCGCCGCTCAC  
TACAGCTACGGTACGCCCTTTTCAACTATGGTCTCATTCACAAACATGGGAAGATCCCAACCTAAAATCTGCGCAA  
GGGTACGGTGGGACAACGATCCGCTCGACGTTATCGAATTGGGGTCTGCGCCCTTGCAATGGGTGGACTAACGCCG  
TGTCGGGTGTTGGGATCGTTTGGAGCTATTGACGAAGGCCGAAACGGACCACAAGATTCTGTGCAATTGCCGTGGACGAC  
AAAGACGCCAACCAATCCATTCTTGAAGATTTGGAGCGTGTCAAGCCGGTCACTTGGACAAGCTCCGGGATTTG  
TTGAAGCGGTACAAGACGAGCGAGGGCAAAGCGGAAAACAATTTGGCGTCTGAAACGCCGCGCACCGCGATGGAAGCC  
GTAGGCGTCATTCAAGAAACGCACGGACGCTGGCGATCATTGTGGTAAGGATGGAACGACAGTCTATTCTCTTTCG  
AGCAAGACGCCGGTTTTCTGGCTCAGCAGTCCGGGGTGTAGGGGAACGTAA

**Supplemental Figure 1:** Nucleotide sequences of the two isoforms of ATP Sulfurylase of *P. tricornutum*, ATP-S (JGI Protein ID 42282) and KSP (JGI Protein ID 19901).

## >pPhaT1-KspAI-GFP

GGGCTGCAGGACGAATGGAGGATTATCACCGCAAAAATGAACTTCGAAAAAACTTTTCGAGCGACCATGGAAAAGGA  
GGATCAGATTCAGATTACAACAGTGGATTGCTCTGGTAGCAAATATCTTCTGCTAGATTGGCTCATGGTCGGTTTTGG  
ACGTTTCGAAGCTCACCGTCAAAAGAAAACAAAAGAGAAGAAATGACGTCTTCGTGACGTAGAATCTACGACTGTACTCGG  
ATCTGGGAAATGAATTGACTCACGGTCTTCTTCGAGTCTGTACAGGCCCTTGGTCCGAACCCCCACACGATTTTTG  
CACCAAAGATTTGCTTCAATTTGCTGGATGTTTTGACTGCAAGATCAGCTGGCCTAGCAAGAGTGTCTGTTGCTTC  
GTCGGGAATCCCTACGAATTCAGTTCGACAAAATTTGCTGCCGTTTCGAGAATTCGATCGTC**GTAAACGGAGTGA**  
**GCAAGGGCGAGGAGCTGTTACCGGGGTGGTGCCATCTGGTTCGAGCTGGACGGCGACGTAACCGGCCACAAGTTCA**  
**GCGTGTCCCGCGAGGGCGAGGGCGATGCCACCTACGGCAAGCTGACCTGAAGTTTATCTGCACCACCGGCAAGCTGC**  
**CCGTGCCCTGGCCACCCCTCGTGACCACCCCTGACCTACGGCTGCAGTGCCTCAGCCGCTACCCCGACCACATGAAGC**  
**AGCACGACTTCTTCAAGTCCGCCATGCCGAAGGCTACGTCCAGGAGCGCACCATCTTCTTCAAGGACGACGGCAACT**  
**ACAAGACCCGCGCGAGGTGAAGTTGAGGGCGACACCCCTGGTGAACCGCATCGAGCTGAAGGGCATCGACTTCAAGG**  
**AGGACGGCAACATCTGGGGACAAGCTGGAGTACAACATAACAGCCACAACGTCTATATCATGGCCGACAAGCAGA**  
**AGAACGGCATCAAGGTGAACTTCAAGATCCGCCACAACATCGAGGACGGCAGCGTGCAGCTCGCCGACCCTACCAGC**  
**AGAACACCCCATCGGCGACGGCCCGTGTCTGCTGCCGCAACCACTACCTGAGCACCCAGTCCGCCCTGAGCAAAG**  
**ACCCCAAGCAAGCGGATCACATGGTCTGCTGACCTGCGGCTGACCGCCGCGGGGATCACTTCGGCATGACGAA**  
**TGTACAAGTAAAGCGATCATCGACTAATTCGAGCTCGGTACCCGGGATCCTTAGAGTCGACCTGCAGGCATGCAAG**  
CTTCAGAAGCGTGTATCGAACTCAACCAGGACGTGCGGCACAAAATGGGCATCCTTGTCTCATGGTGCACGAACAG  
TTGGGAGTCTATCCTTCCCTTAAAAATTTAATTTTTCATTAGTTGCAGTCACTCCGCTTTGGTTTTCACAGTCAGGAAT  
AACACTAGCTCGTCTTACCATGGATGCCAATCTCGCCTATTCATGGTGTATAAAAGTTCAACATCCAAAGCTAGAAC  
TTTTTGGAAAAGAGAAAGAAATATCCGAATATGGGCACGGCGTCCGCTATTGTTGGAGTGGACTAGCAGAAAGTGAAGG  
CACAGGATGAGTTTTCTCGAGACATACCTTACGGCTGCTTACTGTACAGTCAACTGACAGTAATCGTTGATCCG  
GAGAGATTCAAAATTTCAATCTGTTTGGACCTGGATAAAGACAAAAGAGCGACATCCTGACATGAACCCGTAACAGCA  
AATCCTGGTTGAACACGTATCCTTTTGGGGGCTCCGCTACGACGCTCGCTCCAGCTGGGGCTTCTTACTATACACA  
GCGCGCATATTTACGGTTCAGATGTCAAGATGGCCAAGTTGACCAGTCCGCTTCCGGTGTCCACCGCGCGCAGC  
TCGCCGGAGCGGTGAGTTCGGACCGACCGGCTCGGGTTCCTCCGGGACTTCGTGGAGGACGACTTCGCCGTTGTGG  
TCCGGGACGACGTGACCTGTTTCATCAGCGCGTCCAGGACAGGTGGTGCAGCAACACCTGGCCTGGGTGTGGG  
TGCGCGGCTGGACGAGTGTACGCCGAGTGGTGGAGGTCGTGTCCACGAACTTCCGGGACGCCTCCGGGCCGGCCA  
TGACCGAGTCCGGCAGCGCGGTGGGGCGGGAGTTCGCCCTGCGCGACCGCGCCGCACTGCGTGCATTCGTGG  
CCGAGGAGCAGGACTGAACCTTCCCTTAAAAATTTAATTTTTCATTAGTTGCAGTCACTCCGCTTTGGTTTTCACAGTCAG  
GAATAACACTAGCTCGTCTTACCATGGATGCCAATCTCGCCTATTTCATGGTGTATAAAAGTTCAACATCCAAAGCTA  
GAACTTTTGGAAAAGAGAAAGAAATATCCGAATAGGGCACGGCGTCCGCTATTGTTGGAGTGGACTAGCAGAAAGTGAAG  
AAGGCACAGGATGAGTTTTCTCGAGGCCGCTCCCTATAGTGAGTCTGATTAATTTTCGATAAGCCAGGTTAACTGC  
ATTAATGAATCGGCCAACCGCGGGGAGAGGCGGTTTGGCTATTGGGCGCTCTTCCGCTTCTCGCTCACTGACTCGC  
TGCCTCGGTGCTTCCGCTGCGGCGAGCGGTATCAGTCACTCAAAGGCGGTAATACGGTTATCCAGAGTACAGGGG  
ATAACGCAGGAAAGAACATGTGAGCAAAAGGCCAGCAAAAGGCCAGGAACCTGAAAAGGCCGCGGTGCTGCGCTTTT  
TCCATAGGCTCCGCCCCCTGACGAGCATCAAAAAATCGACGCTCAAGTCAGAGGTGGCGAAAACCCGACAGGACTAT  
AAAGATACCAGGCGTTTCCCTTGAAGCTCCCTCGTGCCTCTCCTGTTCCGACCCTGCCGCTTACCGGATACCTGT  
CCGCTTTTCTCCCTTCCGGAAGCGTGGCGCTTCTCAATGCTCAGCTGTAGGTATCTCAGTTCGGTGTAGGTGCTTC  
GCTCCAAGCTGGGCTGTGTGCAGAACCCCGTTCAGCCGACCGCTGCGCTTATCCGGTAACTATCGTCTTGAGT  
CCAACCCGTAAGACACGACTTATCGCCACTGGCAGCAGCCACTGGTAACAGGATTAGCAGAGCGAGGTATGTAGGCG  
GTGCTACAGAGTTCTTGAAGTGGTGGCTAACTACGGCTACACTAGAAGGACAGTATTTGGTATCTGCGCTCTGTGA  
AGCCAGTTACTTTCGAAAAGAGTTGGTAGCTCTTGATCCGGCAAAACAAACCACCGCTGGTAGCGGTGGTTTTTTT  
TTTTGCAAGCAGCAGATTACGCGCAGAAAAAAGGATCTCAAGAAGATCCTTTGATCTTTTCTACGGGGTCTGACGCTC  
AGTGGAACGAAAACACTCACGTTAAGGGATTTTGGTTCATGAGATATCAAAAAGGATCTTACCTAGATCCTTTTAAAT  
AAAAATGAAGTTTTTAAATCAATCTAAAGTATATATGAGTAACTTGGTCTGACAGTTACCAATGCTTAATCAGTGAGG  
CACCTATCTCAGCGATCTGTCTATTTTCGTTTCATCCATAGTTGCTGACTCCCCGTCGTGTAGATAACTACGATACGGG  
AGGGCTTACCATCTGGCCCCAGTGTGCAATGATACCCGCGACACCAGCTCACCGGCTCCAGATTTATCAGCAATAA  
ACCAGCCAGCCGGAAGGGCGAGCGCAGAGTGGTCTGCAACTTTTATCCGCTCCATCCAGTCTATTAATTTGTTGCC  
GGGAAGCTAGAGTAAGTAGTTTCGCCAGTTAATAGTTTGGCGCAACGTTGTTGCCATTGCTACAGGCATCGTGGTGTAC  
GCTCGTCTGTTGGTATGGCTTCATTCAGCTCCGCTTCCCAACGATCAAGGCGAGTTACATGATCCCCATGTTGTGCA  
AAAAAGCGTTAGCTCCTTCGGTCTCCGATCGTTGTGAGAAAGTGGCCGAGTGTATCACTCATGGTTATGG  
CAGCACTGCATAATTTCTTACTGTGATGCCATCCGTAAGATGCTTTTTCTGTGACTGGTGTGACTCAACCAAGTCAT  
TCTGAGAATAGTGTATGCGGCGACCGAGTTGCTCTTGGCCGGCTCAATACGGGATAATACCGGCCACATAGCAGAA  
CTTTAAAGTGTCTCATCTTGGAAAACGTTCTTCCGGGCGAAAACCTCTCAAGGATCTTACCCTGTTGAGATCCAGTT  
CGATGTAACCCACTCGTGCACCCCACTGATCTTACGATCTTTACTTTTACCAGCGTTTTCTGGGTGAGCAAAAACAG  
GAAGGCAAAATGCGCAAAAAAGGGAATAAGGGCGACACGGAAATGTTGAATACTCATACTCTTCTTTTTTCAATATT  
ATTGAAGCATTTATCAGGGTTATTGTCTCATGAGCGGATACATATTTGAATGTATTTAGAAAAATAACAAATAGGGG  
TTCCGCGCACATTTCCCGAAAAGTGCCACCTGACGTCTAAGAAACCATTAATATCATGACATTAACCTATAAAAAATA  
GGCGTATCACGAGGCCCTTTCGTCTCGCGCGTTTCGGTGTGACGGTGAACCTCTGACACATGCAGCTCCCGGAGA  
CGGTACAGCTTGTCTGTAAGCGGATGCCGGGAGCAGACAAGCCGTCAGGGCGGTGAGCGGGTGTGGCGGGTGTGTC  
GGGGTGGCTTAACTATCGGCATCAGAGCAGATTGTACTGAGAGTGCACCATATGGACATATGTCTGTAGAACCGG  
GCTACAATTAATACATAACCTTATGTATCATACATACAGATTTAGGTGACACTATAGAACCAGATCCCC

**Supplemental Figure 2:** Nucleotide sequence of the GFP-fusion vector pPhaT1-KspAI-GFP. KspAI restriction site is indicated in bold red, and GFP domain in bold green.

## 5. SULFATE LIMITATION IN MARINE MICROALGAE

### 5.1. Introduction

Over the past billion years, the structure and composition of marine phytoplankton has experienced two major shifts. In the first, green algae joined cyanobacteria to compose the most prominent primary producers in late Proterozoic oceans. This episode appears to be associated with the emergence of nitrate in seawater as a consequence of the Neoproterozoic oxygenation, giving advantage to eukaryotic microalgae over nitrogen-fixer cyanobacteria (Knoll et al. 2007). The second shift consists in the raise to dominance of chlorophyll *a + c* containing microalgae – essentially but not exclusively diatoms, dinoflagellates and coccolithophorids –, replacing the green algae and, to some extent, cyanobacteria from the late Paleozoic Era until today's oceans (Knoll et al. 2007, Ratti et al. 2011). Unlike the first example, the drivers that led to this event are not clear.

There are at least three classes of hypothesis to explain a case as such: (i) first, it may be that evolutionary changes and the emergence of novel groups in the phytoplankton community naturally led to changes in phytoplankton composition rather than environmental drivers. In fact, diatoms and dinoflagellates show biological adaptations that favor their abundance in oceans (Delwiche 2007, Bowler et al. 2008). However, the abovementioned events are not chronologically coincident with the evolutionary origins of the emerging phytoplankton groups, suggesting the influence of external factors (Falkowski et al. 2004, Knoll et al. 2007). (ii) Alternatively, Vermeij (1977) suggested that the escalating predation during the Mesozoic Era drove remarkable changes in marine mollusks. Likewise, in a microscopic point of view, phytoplankton changes may have been driven by zooplankton predation pressure, selecting diatoms, dinoflagellates and coccolithophorids “armored” with frustules, thecae and coccoliths respectively (Ratti et al. 2013). The zooplanktonic fossil record is, however, too poor to substantiate such idea and one can only infer about planktonic predation pressure in ancient eras (Falkowski et al. 2004). (iii) Finally, seawater chemistry changed through time. Such variations may have favored different microalgae taxa successively. It has been proposed, for example, that the decrease in iron availability in seawater provided an advantage to chlorophyll *a + c* microalgae, due to the lower requirement of their plastids for iron when compared to green algae (Quigg et al. 2003). These hypotheses are not mutually exclusive, but all aspect may have contributed to phytoplankton changes during the history of Earth.

Within the third class of ideas, the Sulfate Facilitation Hypothesis (SFH) takes advantage of the remarkable increase of sulfate concentration in seawater that occurred simultaneously to the domination of chlorophyll *a + c* microalgae, to argue that the sulfate availability was the main – or one of the mains – driver of this event. Geological and stratigraphic coincidences favoring the SFH are clear (see Section 2 ; Ratti et al. 2011 and references therein). In freshwater environments where sulfate availability did not show the same increment and range typically from 10 to 500  $\mu\text{mol}\cdot\text{L}^{-1}$  – 2-3 orders of magnitude lower than those found in today’s oceans –, primary production is still dominated by chlorophyll *a + b* algae (Norici et al. 2005; Giordano et al. 2005). Finally, the fact that algal species belonging to the red lineage generally present lower molar C:S ratios when compared to cyanobacteria and green algae (Ho et al. 2003, Norici et al. 2005) indicates a lower efficiency of sulfur usage, and represents another argument in favor of the SFH.

Although the empirical evidences are sound, ten years after the first proposal of the SFH by Ratti et al. (2011) the biochemical information is still limited to very few species of microalgae. In sum, the available information clearly show that red lineage microalgae are more susceptible to growth limitation by sulfur – i.e.: growth is impaired in much higher concentrations of sulfate – when compared to green lineage species (Ratti et al. 2011, Prioretti and Giordano 2016). Due to the absence of studies on red algae (chlorophyll *a + phycobilins*), it is impossible to suggest whether the sensitivity to sulfur observed in red secondary-plastids algae is inherited via their red plastid origin. *In silico* sequences analyses of the core sulfate assimilation enzymes (see Chapter 3) showed a remarkable heterogeneity amongst photosynthetic organisms, contradicting the conserved sulfate assimilation metabolism once believed in (Patron et al. 2008, Prioretti et al. 2014). The enzymatic machinery of sulfate assimilation from red and green lineage microalgae exposed to different concentrations of sulfate did not show clear differences though (Prioretti and Giordano 2016). Hence, it is still obscure whether the mechanistic reasons for the different sensitivity to sulfur deficiency between red and green lineage algae relies in actual differences in sulfur metabolism.

There are two leading studies that addressed attention specifically to the biochemical basis of the SFH. Ratti et al. (2011) and Prioretti and Giordano (2016) similarly exposed microalgae belonging to different groups (cyanobacteria, green algae, diatoms, dinoflagellates and coccolithophorids) to various concentrations of sulfate in culture medium (from 30 to 1  $\text{mmol}\cdot\text{L}^{-1}$ ), and assessed a number of biochemical and physiological parameters. In those cases, the lower growth rate in response to the decrease

of sulfate in the medium ( $<10 \text{ mmol}\cdot\text{L}^{-1}$ ) showed that the red lineage species were exposed to limiting concentrations of sulfur. On the other hand, the cyanobacteria and green algae were not, given that their growth rate was essentially the same in all treatments. Thus, analyses were always performed in cyanobacteria and green algae exposed to optimal concentrations of sulfate, a situation where reallocation of resources is not supposed to be necessary (Raven and Johnston 1991). It should be noted that it was not the aim of the referred authors to find growth-limiting concentrations of sulfate for each microalgal group. Those pioneer studies paved a biochemical way to investigate the SFH. But, on the other hand, in those experiments the authors could not assess and compare the responses of microalgae to sulfur limitation, raising the question whether these responses would be different among taxa.

In light of the initial answers and the new horizon of questions generated by the previous studies, this thesis investigates if the responses of different groups of marine microalgae to sulfur limitation are diverse. To do that, the green alga *Tetraselmis suecica*, the red alga *Porphyridium purpureum*, the diatom *Phaeodactylum tricornerutum* and the dinoflagellate *Amphidinium carterae* were exposed to growth-limiting concentrations of sulfate in culture medium in order to investigate the physiological and biochemical strategies of each species under sulfur limitation. Such single species are neither authentic representatives of the ancient phytoplankton community, nor representatives of entire divisions of microalgae. However, generalizations are crucial starting points for hypothesis-driven studies, and most of those algae – except *T. suecica* – represent new knowledge for the topic. Available information will be summarized at the end of this chapter, and results will be discussed mostly with respect to the SFH.

## 5.2. Material and Methods

### 5.2.1. Culture conditions

The prasinophyte *Tetraselmis suecica* (CCAP 66/4, Scotland, UK), the rhodophyte *Porphyridium purpureum* (CCAP 1380/3, Scotland, UK), the diatom *Phaeodactylum tricornutum* (UTEX 646, Austin, USA) and the dinoflagellate *Amphidinium carterae* (CCAP 1102/3, Scotland, UK) were batch cultured photoautotrophically in 250 mL sterile Erlenmeyer flasks containing 125 mL of AMCONA medium (Fanesi et al. 2014) modified in order to use sodium sulfate ( $\text{Na}_2\text{SO}_4$ ) as the only source of sulfur (Table 3). Sulfate standard concentration in the medium was 25 mM  $\text{Na}_2\text{SO}_4$  (named S replete condition) and it was gradually decreased in order to achieve growth limiting concentrations for each microalga (named S limited condition). Cultures were maintained in a growth chamber (Termaks AS<sup>®</sup>, Norway) at  $20 \pm 2^\circ\text{C}$ , exposed to lateral illumination of  $100 \mu\text{mol photons}\cdot\text{m}^{-2}\cdot\text{s}^{-1}$  measured with a quanta-meter (LI-250 Light Meter; LI-COR Inc.) on the outer surface of the vessels and provided by fluorescent lamps (OSRAM<sup>®</sup> Cool White) under a 12:12h (light:dark) photoperiod. The initial cell density varied mildly among species (see Section 2.5.3) in order to optimize growth and avoid the occurrence of a ‘lag phase’, and inoculums were taken from a previous culture during exponential growth. All analyses were performed in cells harvested from late exponential growth phase, and all cultures were acclimated to the diverse conditions for at least four generations before any analysis. During experimental growths, flasks were manually shaken at least five times a day.

**Table 3:** Recipe of AMCONA medium (Fanesi et al. 2014) as used in this study.

<b>Salt</b>	<b>Final Concentration in medium</b>
NaCl	363 mmol·L <sup>-1</sup>
Na <sub>2</sub> SO <sub>4</sub>	25 mmol – 100 nmol·L <sup>-1</sup>
KCl	8,04 mmol·L <sup>-1</sup>
NaHCO <sub>3</sub>	2,07 mmol·L <sup>-1</sup>
KBr	725 µmol·L <sup>-1</sup>
H <sub>3</sub> BO <sub>3</sub>	372 µmol·L <sup>-1</sup>
NaF	65,7 µmol·L <sup>-1</sup>
MgCl <sub>2</sub> · 6H <sub>2</sub> O	41,2 mmol·L <sup>-1</sup>
CaCl <sub>2</sub> · 2H <sub>2</sub> O	9,14 mmol·L <sup>-1</sup>
SrCl <sub>2</sub> · 6H <sub>2</sub> O	82,0 µmol·L <sup>-1</sup>
NaNO <sub>3</sub>	549 µmol·L <sup>-1</sup>
NaH <sub>2</sub> PO <sub>4</sub> · H <sub>2</sub> O	21,0 µmol·L <sup>-1</sup>
Na <sub>2</sub> SiO <sub>3</sub> · 9H <sub>2</sub> O	205 µmol·L <sup>-1</sup>
CuCl <sub>2</sub> · 2H <sub>2</sub> O	40,0 nmol·L <sup>-1</sup>
TRIS-HCl, pH 8,05	10,0 mmol·L <sup>-1</sup>
<b>Metal Stock I</b>	<b>Stock Concentration (1 mL·L<sup>-1</sup>)</b>
FeCl <sub>3</sub> · 6H <sub>2</sub> O	6,56 mmol·L <sup>-1</sup>
Na <sub>2</sub> EDTA · 2H <sub>2</sub> O	6,56 mmol·L <sup>-1</sup>
<b>Metal Stock II</b>	<b>Stock Concentration (1 mL·L<sup>-1</sup>)</b>
ZnCl <sub>2</sub>	254 µmol·L <sup>-1</sup>
CoCl <sub>2</sub> · 6H <sub>2</sub> O	5,69 µmol·L <sup>-1</sup>
MnCl <sub>2</sub> · 4H <sub>2</sub> O	2,42 mmol·L <sup>-1</sup>
Na <sub>2</sub> MoO <sub>4</sub> · 2H <sub>2</sub> O	6,10 µmol·L <sup>-1</sup>
Na <sub>2</sub> SeO <sub>3</sub>	1,00 µmol·L <sup>-1</sup>
NiCl <sub>2</sub> · 6H <sub>2</sub> O	6,30 µmol·L <sup>-1</sup>
Na <sub>2</sub> EDTA · 2H <sub>2</sub> O	8,29 mmol·L <sup>-1</sup>
<b>Vitamin Stock</b>	<b>Stock Concentration (1 mL·L<sup>-1</sup>)</b>
Thiamine-HCl	297 µmol·L <sup>-1</sup>
Biotin	4,09 µmol·L <sup>-1</sup>
B <sub>12</sub>	1,47 µmol·L <sup>-1</sup>

### 5.2.2. Cell density and volume determination

Cell growth was followed by daily counts using either an automatic cell counter CASY® TT (Innovatis AG, Reutlingen, Germany) or by direct optical microscopy (Leitz, HM-LUX 3) cell counting with the aid of a Bürker hemocytometer (Paul Marienfeld GmbH & Co., Germany). Samples were harvested at regular intervals (“time of inoculation”  $\pm$  2h) and flasks were vigorously shaken before sampling. Comparison of cell density determinations of the same sample using both methods showed very similar values, and differences were always below 10%. Cell volume determinations, on the other hand, were only performed in the automatic cell counter.

#### 5.2.2.1. Bürker hemocytometer

A hemocytometer consists of a thick microscope slide with a grid of perpendicular lines etched in the center. On a Bürker hemocytometer, the grid has nine large squares (1 mm<sup>2</sup> each) delimited by triple lines and divided by double lines (0,05 mm apart) into 16 grouped squares of 0,20 mm sides (Figure 23).

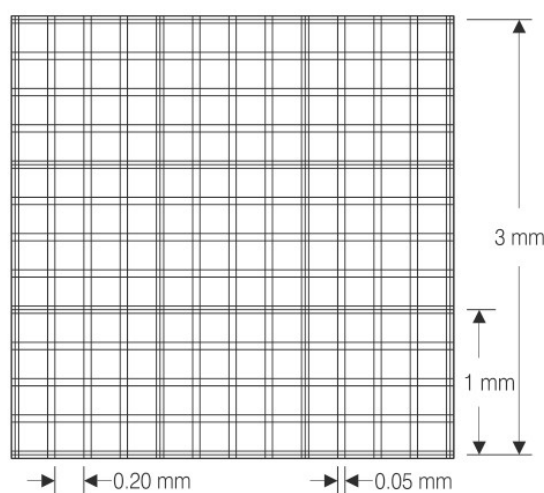


**Figure 23:** Representation and dimensions of a Bürker hemocytometer’s grid.

When coupled with the proper cover glass and filled with 15-20  $\mu$ L of cell suspension, the chamber depth is 0,1 mm. Hence, on the Bürker chamber, one large square corresponds to 0,1 mm<sup>3</sup> or 0,1  $\mu$ L (= 1 mm x 1 mm x 0,1 mm), and cell density expressed in cells·mL<sup>-1</sup> can be calculated as follows:

$$\text{Cell density (cells}\cdot\text{mL}^{-1}\text{)} = \frac{\text{Total cells counted} \times \text{Dilution factor} \times 10^4}{\text{Number of large squares counted}}$$

In this study, a minimum of 100 cells per sample were counted as described for statistical significance. When possible, counts were repeated up to four times in distinct areas of the same grid. The whole counting process was made at least twice (i.e.: two grids) for each sample.

#### 5.2.2.2. *CASY® TT Automatic cell counter*

The CASY® TT automatic cell counter uses electric field to estimate both number and volume of viable cells. For that, 100 µL aliquots of cultures were diluted in 10 mL of an electrolyte solution specifically developed for that instrument (CASY® ton; Innovatis AG, Reutlingen, Germany) and the resulting solution, applied to the equipment's routine. Cells were pumped through a 60 or 150 µm capillary at a constant flow rate while two platinum electrodes applied a pulsed low voltage field of 1 MHz. Each cell causes a perturbation on the previously known electrolyte background electrical resistance and, at last, the resulting number of cells is the total number of conductivity fluctuation events corrected by the instrument for the initial dilution of the sample. Furthermore, the volume of electrolyte displaced by cells during their passage is used to determine cellular volume. Dead cells, with damaged membrane or partially empty, exert a lower resistance to the current and can therefore be discriminated from viable cells. All determinations performed in the automatic cell counter were made in three biological and three instrumental replicates.

#### 5.2.3. *Determination of specific growth rate*

Cultures were set to an initial cell density of about  $7,5 \times 10^4$  cells·mL<sup>-1</sup> for *Tetraselmis suecica* and *Phaeodactylum tricornerutum* and  $10^5$  cells·mL<sup>-1</sup> for *Porphyridium purpureum* and *Amphidinium klebsii*, then growth was followed daily as previously described. The specific growth rate ( $\mu$ ) was determined from the angular coefficient ( $\alpha$ ) of the linear regression of the logarithm of the cell density values during exponential growth (Monod 1949). Determination of specific growth rate was carried out in, at least, three biological replicates.

#### 5.2.4. Extraction and quantification of pigments

To determine chlorophylls and carotenoids content, cells were harvested by centrifugation and resuspended in methanol 100% for *T. suecica*, *P. purpureum* and *A. klebsii*, and in a mixture of methanol:tetrahydrofuran (80:20; v/v) for *P. tricornutum* (Norici et al. 2011). Centrifuge configuration varied mildly among species depending on cellular characteristics (5-10 minutes at 2000-4000·g), in order to achieve pellet integrity. Pigments' extraction occurred overnight at -20°C in the dark, and the resulting slurry was further centrifuged at 13.000·g for 3-5 min to separate the pigments' extract from the colorless pellet. Concentrations were determined spectrophotometrically with a Beckman DU 640 Spectrophotometer (Beckman Coulter), as follows:

(i) Chlorophylls *a* (absorbance at 665 nm) and *b* (absorbance at 652 nm) present in the Chlorophyceae *T. suecica* (Ritchie 2006):

$$\text{Chl } a \text{ (}\mu\text{g}\cdot\text{mL}^{-1}\text{)} = 16,5169\cdot\text{Abs}_{665\text{nm}} - 8,0962\cdot\text{Abs}_{652\text{nm}}$$

$$\text{Chl } b \text{ (}\mu\text{g}\cdot\text{mL}^{-1}\text{)} = 27,4405\cdot\text{Abs}_{652\text{nm}} - 12,1688\cdot\text{Abs}_{665\text{nm}}$$

(ii) Chlorophyll *a* (absorbance at 665 nm) from the Rhodophyceae *P. purpureum* (Ritchie 2006):

$$\text{Chl } a \text{ (}\mu\text{g}\cdot\text{mL}^{-1}\text{)} = 12,9447\cdot\text{Abs}_{665\text{nm}}$$

(iii) Chlorophylls *a* (absorbance at 665 nm) and *c* ( $C_1+C_2$ ; absorbance at 632 nm) in the Bacillariophyceae *P. tricornutum* (Wellburn 1994, Ritchie 2006):

$$\text{Chl } a \text{ (}\mu\text{g}\cdot\text{mL}^{-1}\text{)} = 13,2654\cdot\text{Abs}_{665\text{nm}} - 2,6839\cdot\text{Abs}_{632\text{nm}}$$

$$\text{Chl } c \text{ (}\mu\text{g}\cdot\text{mL}^{-1}\text{)} = 28,8191\cdot\text{Abs}_{632\text{nm}} - 6,0138\cdot\text{Abs}_{665\text{nm}}$$

(iv) Chlorophylls *a* (absorbance at 665 nm) and *c* ( $C_2$ ; absorbance at 632 nm) present in the Dinophyceae *A. klebsii* (Ritchie 2006):

$$\text{Chl } a \text{ (}\mu\text{g}\cdot\text{mL}^{-1}\text{)} = 13,6849\cdot\text{Abs}_{665\text{nm}} - 3,4551\cdot\text{Abs}_{632\text{nm}}$$

$$\text{Chl } c \text{ (}\mu\text{g}\cdot\text{mL}^{-1}\text{)} = 32,9371\cdot\text{Abs}_{632\text{nm}} - 7,0140\cdot\text{Abs}_{665\text{nm}}$$

The water-soluble phycobiliproteins present in the harvested cells of the red alga *P. purpureum* were extracted with a freshly prepared solution of 50 mmol·L<sup>-1</sup> sodium phosphate buffer; pH 6,7; ionic strength 0,1 (Ruan et al. 2018). Once on such extraction medium, cell lysis was performed by nitrogen decompression at the pressure of 2000 psi, on a cell disruption bomb (4639 Cell Disruption Vessel; Parr Instrument Company, Molin, IL, USA) and pigment extraction occurred overnight at 4°C in the dark. Cell breakage was checked on an optical microscope (Leitz, HM-LUX 3) and the resulting slurry was further centrifuged at 13.000·g for 3-5 min to separate the pigments' extract from the colorless pellet. Concentrations were determined spectrophotometrically with a Beckman DU 640 Spectrophotometer (Beckman Coulter) using the following equations (Bennet and Bogorad 1973):

$$PC \text{ (mg} \cdot \text{mL}^{-1}\text{)} = \frac{Abs_{615nm} - 0,474 \cdot Abs_{652nm}}{5,34}$$

$$APC \text{ (mg} \cdot \text{mL}^{-1}\text{)} = \frac{Abs_{652nm} - 0,280 \cdot Abs_{615nm}}{5,09}$$

$$PE \text{ (mg} \cdot \text{mL}^{-1}\text{)} = \frac{Abs_{562nm} - 2,41 \cdot PC - 0,849 \cdot APC}{9,62}$$

#### **5.2.5. Extraction and quantification of proteins**

Total proteins contents were determined using an optimization of Lowry's method described by Peterson (1977). Cells were harvested by centrifugation, resuspended in 500 µL of a solution containing 1% (v/v) Sodium Dodecyl Sulfate (SDS) and 0,1 mol·L<sup>-1</sup> sodium hydroxide (NaOH) and vigorously shaken for about one minute. The detergent power of SDS in the presence of NaOH facilitates membrane disruption and the solubilization of membrane proteins. Then, 500 µL of a mixture called Reagent A (Table 4) were added and let sit for 10 minutes at room temperature. The aim of this step is to allow the copper present in Reagent A to bind the proteins in an alkaline environment. Subsequently, 250 µL of Reagent B (Table 4) were added and immediately mixed thoroughly. Reagent B consists on a dilution of the Folin & Cicalteu's phenol reagent (Sigma-Aldrich) in water. The lateral chains of some aminoacids are able to reduce the Folin & Cicalteu's phenol reagent in the presence of copper (+II), producing a compound with maximum absorbance at 750 nm (Chou and Goldstein 1960). The final mixture –

sample + Reagent A + Reagent B – was incubated at room temperature for 30 minutes before measurements in a Beckman DU 640 Spectrophotometer (Beckman Coulter). The absorbance values were converted to protein concentration with the aid of a wide range calibration curve constructed with known quantities of bovine serum albumin (BSA).

**Table 4:** Reagents used for the determination of total proteins according to Peterson (1977).

<b>Reagent A</b>	
H <sub>2</sub> O milli-Q	25% (v/v)
SDS 10% (m/v)	25% (v/v)
NaOH 0,8 mol·L <sup>-1</sup>	25% (v/v)
CTC Reagent	25% (v/v)
<b>CTC Reagent</b>	
CuSO <sub>4</sub> · 5H <sub>2</sub> O	0,1% (m/v)
Na-K tartrate	0,2% (m/v)
Na <sub>2</sub> CO <sub>3</sub>	10% (m/v)
<b>Reagent B</b>	
H <sub>2</sub> O milli-Q	83,3% (v/v)
Folin & Cicalteu's phenol reagent	16,7% (v/v)

### **5.2.6. Macromolecular pools size – Fourier Transform Infra-Red (FTIR) Spectroscopy**

A Tensor 27 FTIR Spectrometer (Bruker Optics, Ettlingen, Germany) was used to assess variations on the main organic pools – proteins, lipids and carbohydrates – of whole cell samples of each microalga and experimental condition. FTIR Spectroscopy uses Mid Infrared Radiation (MIR), in the wavenumber range of 4000-400 cm<sup>-1</sup> to identify molecules – or functional groups within molecules – based on different chemical bonds' vibrations. The number of vibrational modes of a functional group depends on whether it is linear or non-linear and the number of atoms that compose it. Hence, different functional groups of a molecule are subjected to a specific type of vibrational motion and emit a specific amount of energy.

A Michelson's interferometer is used to determine the intensity of the signal as a function of position. The interferometer consists on a set of three thoroughly positioned mirrors, one of them movable. A broad band Infrared (IR) radiation is emitted and directed to a collimating mirror that align all radiations and makes them parallel. The

collimated radiation then reaches a beam splitter which allows 50% of the radiation to pass to a fixed mirror whereas the remaining 50% is redirected to a mirror that moves. The beams are subjected to a round-trip to the mirror and back to the beam splitter, where they are recombined and finally directed through the sample to the detector (Figure 24). If the mirrors are equidistant from the beam splitter, the radiation reflected by the two mirrors travel the same distance before reaching the detector, but if the moving mirror moves away, one of the light beams travels an additional distance, causing a retardation. At the detector, the intensity of the signal is measured as a function of the displacement of the moving mirror and gives an output called interferogram. The Fourier transform is a mathematical operation that allows to convert a function of intensity versus displacement to a function of intensity versus wavenumbers. After this mathematical transformation, thus, an interferogram can be corrected to a transmission/absorption spectrum.

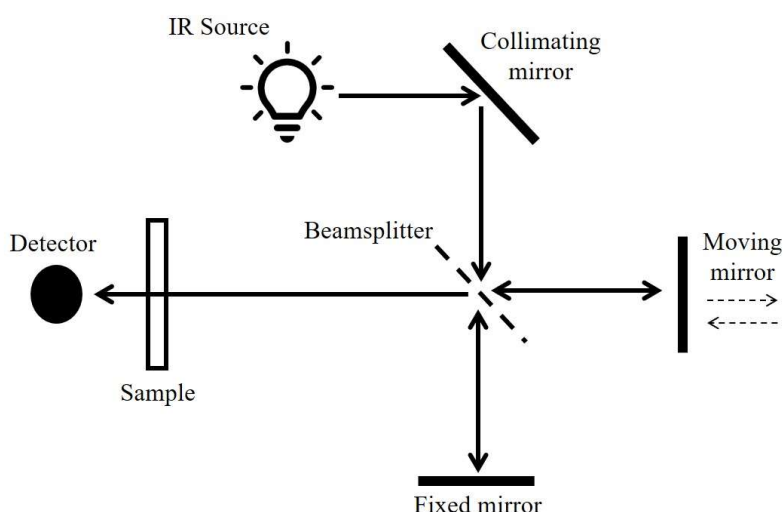


**Figure 24:** Schematic view of a Michelson's interferometer.

#### 5.2.6.1. Semi quantification of lipids and carbohydrates

For FTIR spectroscopy analysis, cells were harvested by centrifugation and washed twice with a 0,5 mol·L<sup>-1</sup> ammonium formate solution, isosmotic to the growth medium. The washing step removes residual salts and molecules that may have been released to the medium (Zhu and Lee 1997). Ammonium formate is used for such washing because, in heat, is degraded to the gaseous carbon dioxide (CO<sub>2</sub>) and ammonia (NH<sub>3</sub>) that are then released to the air. The final pellets were resuspended on adequate volume of isosmotic ammonium formate, from which 50 μL were transferred to a silicon window

subsequentially dried in oven at 80°C overnight. To act as a blank, a 50 µL drop of the ammonium formate solution alone was deposited on a silicon window and exposed to the exact same routine. To each species and treatment, analyses were carried out in three biological and, at least, two instrumental replicates depending on the amount of available biomass.

Acquisition and analysis of spectra were made on the OPUS 6.5 Software (Bruker Optics GmbH, Ettlingen, Germany). Each peak of a spectrum was attributed to a specific macromolecular pool (Table 5) according to Giordano et al. (2001). Although the silica peak (~1075 cm<sup>-1</sup>) of the diatom *P. tricornutum* may obscure carbohydrate-related peaks (~1200-900 cm<sup>-1</sup>), Palmucci et al. (2011) observed that the ~1050 cm<sup>-1</sup> peak is strongly correlated to the carbohydrate quantification by the phenol-sulfuric method (Dubois et al. 1951) even for diatoms, and that was used in this study. In order to identify more accurately the position, width and height of each peak a second derivative function was calculated for each spectrum where well-defined valleys were considered reliable peaks in the original spectrum. Finally, integrals of peaks areas were calculated using a “curve fitting” tool on the OPUS 6.5 Software.

**Table 5:** Peaks assignment (Giordano et al. 2001, Palmucci et al. 2011).

Wavenumber (cm <sup>-1</sup> )	Ligation	Assignment
~1740	C=O of ester functional groups	Lipids
~1650	C=O of amides	Proteins
~1075	Si-O of silicate frustules	Silica frustules of diatoms
~1050	C-O-C of polysaccharides	Carbohydrates

Since this analysis does not allow an absolute quantification of the macromolecular pools, the semi-quantification of lipids and carbohydrates was calculated by correlating the pool size obtained from the FTIR spectroscopy with that of a reference pool, measured independently through a quantitative method – in this case, proteins (see Section 5.2.5). The semi-quantification of lipids and carbohydrates was, then, calculated as follows (Palmucci et al. 2011):

$$\text{Concentration}_{\text{pool}} = \frac{\text{Absorbance}_{\text{pool}}}{\text{Absorbance}_{\text{proteins}}} \times \text{Concentration}_{\text{proteins}} \times \frac{\epsilon_{\text{proteins}}}{\epsilon_{\text{pool}}}$$

Where “pool” stands for the macromolecular pool to be semi-quantified based on the FTIR absorbance and absolute quantification of proteins; and  $\epsilon$  is the extinction

coefficient. Given the difficulty of determining the molar absorptivity coefficient of unknown mixture of macromolecules, “ $\epsilon_{\text{proteins}} / \epsilon_{\text{pool}}$ ” was not determined and was considered as a constant of unknown value (Palmucci et al. 2011).

### ***5.2.7. Elemental composition – Total X-ray Reflection Fluorescence (TXRF)***

The cellular concentrations of phosphorus (P), sulfur (S), potassium (K), calcium (Ca), iron (Fe), manganese (Mn), copper (Cu) and zinc (Zn) were determined by total X-ray reflection fluorescence (TXRF) spectrometry using a S2 PICOFOX Spectrometer (Bruker AXS Microanalysis GmbH, Berlin, Germany). This method is based on the ionization induced by X-ray ( $\sim 0,01\text{-}10$  nm wavelength) on the electron shell of elements. When ionized, an atom may pass to an excited state by transferring one or more electrons to higher orbitals. To refill the electronic gap, an electron from a higher energy level is forced to descend, releasing a quantity of energy equal to the difference of energy between the orbitals involved, under the form of a photon (fluorescence). The wavelength of the emitted radiation is characteristic for each atom and its intensity is proportional to the element concentration in the sample. In the particular case of the S2 PICOFOX Spectrometer, the instrument is built in a way that the X-ray beam reaches the sample in an angle that maximizes total reflection away from the detector, whereas the detector is positioned in a way to maximize the detection of fluorescence exclusively. This technique allows to assess the elemental composition of a complex system like a cell with a high level of accuracy. In order to obtain an absolute quantification, it is necessary to add an internal standard to the sample. In this study, gallium (Ga) was used as standard since it is not present in algal cells.

#### *5.2.7.1. Quantification of elemental cell quotas*

For the TXRF spectrometry analysis, cells were harvested by centrifugation and washed twice with a  $0,5 \text{ mol}\cdot\text{L}^{-1}$  ammonium formate solution, isosmotic to the growth medium. The final pellet was resuspended in 1 mL of milli-Q water to which 5  $\mu\text{L}$  of a gallium solution ( $1 \text{ g}\cdot\text{L}^{-1}$ ) was added (final concentration  $5 \mu\text{g}\cdot\text{mL}^{-1}$ ). The concentration of each element in the samples was calculated with respect to the signal obtained from gallium. From the resulting cell suspension, an aliquot of 10  $\mu\text{L}$  was deposited in the center of a quartz sample carrier and dried at  $60^\circ\text{C}$  until dryness was detected by naked eye (three to five minutes). The sample carrier was then inserted in the S2 PICOFOX

Spectrometer to go through the routine of acquisition and analysis of spectra on the software SPECTRA 5.3 (Bruker AXS Microanalysis GmbH, Berlin, Germany). Each sample was measured for 1000 seconds and each treatment was measured in, at least, three biological replicates. Before analysis, the spectroscopic detection of the instrument was verified and, if necessary, corrected through a “Gain Correction” function using a standard mono-element (Arsenic, As).

#### ***5.2.8. Elemental composition – Elemental combustion analysis***

Carbon (C) and nitrogen (N) cell quotas were determined using an elemental combustion analyzer 4010 (Costech Analytical Technologies Inc.). The instrument can be divided into (i) a combustion system, responsible for sampling, combustion and pneumatics; (ii) a detector system, responsible for separating and measuring combustion products; and (iii) a data handling system, which is a EAS32 software package (Costech Analytical Technologies Inc.) for instrument control, data acquisition and report generation.

Samples were dropped in the combustion reactor, which is a quartz column filled with reduced copper wires and tungsten trioxide ( $\text{WO}_3$ ) kept at constant temperature of  $980^\circ\text{C}$ . Upon combustion in the presence of a saturating oxygen flow ( $30\text{ mL}\cdot\text{min}^{-1}$ ) and an oxidant catalyst ( $\text{WO}_3$ ), biomass is fully converted to  $\text{CO}_2$ ,  $\text{H}_2\text{O}$ ,  $\text{N}_2$  and  $\text{SO}_2$ . The gases are then carried by an inert gas (He) flow ( $100\text{ mL}\cdot\text{min}^{-1}$ ) through a column filled with magnesium perchlorate that holds the water. Excess oxygen, not used for combustion, is absorbed by the high-performance copper wires. The gases flow through a gas chromatographic separation column which is kept at constant temperature ( $\pm 0,1^\circ\text{C}$ ). As they pass through the column, the gases are separated and detected sequentially by the thermal conductivity detector, that generates an electrical signal proportional to the amount of element in the sample. The EAS software (Costech Analytical Technologies Inc.) compares the elemental peak to a known standard material and generates a report for each element on a weight basis. Standard curves were generated using known quantities of sulfanilamide.

##### ***5.2.8.1. Sample preparation***

Cells were harvested by centrifugation and washed twice with a  $0,5\text{ mol}\cdot\text{L}^{-1}$  ammonium formate solution, isosmotic to the growth medium. The final pellet was dried

at 70°C until constant weight was reached. Dry biomass (0,4-2 mg) was then transferred to tin capsules to which was also added a small amount of vanadium pentoxide ( $V_2O_5$ ) in order to facilitate complete combustion.

### **5.2.9. Photosynthetic parameters – Pulse Amplitude Modulated (PAM) fluorometry**

The *in vivo* variable fluorescence of photosystem II (PSII) chlorophyll *a* ( $P_{680}$ ) was assessed using a Dual-PAM 100 fluorometer (Heinz Walz GmbH, Effeltrich, Germany). This fluorometer is able to separate the effect of the actinic light that drives photosynthesis and the low intensity modulated measuring light that is used to probe the state of the photosynthetic apparatus via the measured fluorescence intensity. Only fluorescence changes induced by the modulated measuring light is registered by the instrument and, thus, it serves as a reliable proxy to indirectly assess all other energy quenching mechanisms. This way the low intensity measuring light can be used to measure both the minimal (induced by the measuring light itself) and maximal (induced by a strong light pulse) fluorescence values (Schreiber et al. 1986).

#### **5.2.9.1. Principles of fluorescence measurements**

Each quantum of light absorbed by a molecule of chlorophyll rises an electron from the ground state to an excited state. Upon de-excitation, a small proportion of the excitation energy is dissipated as red fluorescence (~750 nm). The evaluative characteristic of chlorophyll fluorescence arises from the fact that it is complementary to alternative pathways of de-excitation which are primarily photochemistry and heat dissipation (Maxwell and Johnson 2000). Therefore, changes in fluorescence yield reflect changes in photochemical efficiency and/or heat dissipation.

In the dark-acclimated state (i.e.: when Quinone A ( $Q_A$ ) pool is fully oxidized, and all PSII reaction centers are able to perform photosynthesis), samples are exposed to a modulated measuring light with an intensity too low to induce electron transport through PSII (photochemistry) but high enough to elicit a minimum value for chlorophyll fluorescence, named  $F_0$ . Application of a high intensity saturating pulse to dark adapted samples induces a maximum value of fluorescence by “closing” all PSII reaction centers. At this point, the maximal possible value for fluorescence ( $F_m$ ) is recorded. The difference between  $F_0$  and  $F_m$  is the variable fluorescence ( $F_v$ ) and correspond to the ability of PSII to perform photosynthesis, assuming no other quenching mechanisms. It has been shown

theoretically and empirically that  $F_v/F_m$  is a robust indicator of the maximum quantum yield of PSII photochemistry (Misra et al. 2012). If an actinic light sufficiently strong to induce photosynthesis is applied, a rapid rise in fluorescence will be subsequently quenched by photochemical and non-photochemical events until it reaches a steady state level of fluorescence in light. Fluorescence emitted in a light-acclimated state is then termed  $F'$  – sometimes referred as  $F_s'$ , if in steady state (Baker 2008). The application of a saturating pulse under actinic illumination transiently closes all the reaction centers and provides a value of maximal fluorescence in the light adapted state, termed  $F_m'$ . Note that this is less than the dark adapted  $F_m$  value due to the contribution of non-photochemical mechanisms of quenching. The difference between  $F_m'$  and  $F'$  is termed  $F_q'$  (Murchie and Lawson 2013). Based on those measurements in dark- and light-adapted samples, the following parameters can be calculated:

(i) PSII operating efficiency ( $\Phi_{PSII}$ ): the quantum efficiency of PSII electron transport in the light.

$$\Phi_{PSII} = (F_m' - F') / F_m'$$

(ii) Photochemical quenching: estimates the fraction of PSII reaction centers with oxidized  $Q_A$ , or available to perform photosynthesis. Its calculation can be based on the puddle model ( $q_P$ ), considering that each reaction center has its own antenna complex and excitation can only reach a single reaction center; or on the lake model ( $q_L$ ), which considers that the energy captured by the antenna system can reach multiple reaction centers. In this work, results are preferentially shown as the latter.

$$q_P = (F_m' - F') / (F_m' - F_0')$$

$$q_L = (F_q' / F_v') / (F_0' / F')$$

(iii) Coefficient of non-photochemical quenching ( $q_N$ ) and Non-Photochemical Quenching (NPQ): both indicate the proportion of excitation energy dissipated as heat, consisting of three components: energy dependent quenching ( $q_E$ ); photoinhibitory quenching ( $q_I$ ); and state-transition quenching ( $q_T$ ). Whereas the first ( $q_N$ ) is based on total energy available, the latter (NPQ) is calculated based on excitation energy used on photochemistry. In this work, results are preferentially shown as the latter.

$$q_N = (F_m - F_m') / (F_m - F_0')$$

$$\text{NPQ} = (F_m / F_m') - 1$$

### 5.2.9.2. Fluorescence measurements

Cells were harvested by centrifugation and resuspended in 2 mL of fresh AMCONA medium, with Na<sub>2</sub>SO<sub>4</sub> concentrations according to each treatment. Final cell concentration varied mildly among species in order to maximize fluorescence signal and minimize background fluctuations (3x10<sup>6</sup> cells·mL<sup>-1</sup> for *T. suecica*; 10<sup>7</sup> cells·mL<sup>-1</sup> for *P. purpureum*, *P. tricornutum* and *A. carterae*). Samples were then dark acclimated for 15 minutes at room temperature and placed into the sample holder of Dual-PAM-100 under continuous stirring to be exposed to a customized routine. First, a weak measuring light (17 μmol photons·m<sup>-2</sup>·s<sup>-1</sup>) was applied, followed by a saturating pulse of light (10000 μmol photons·m<sup>-2</sup>·s<sup>-1</sup>) to measure F<sub>v</sub>/F<sub>m</sub> of dark-adapted cells, then actinic illumination was incremented in 20 steps of 60 seconds each (from 0 to 1955 μmol photons·m<sup>-2</sup>·s<sup>-1</sup>) followed by 5 minutes in the dark. At the end of each light-incrementing step, as well as after 1 and 5 minutes of darkness, a saturating pulse of light was applied allowing the determination of photosynthetic parameters as described in Section 5.2.9.1. The gradually increasing illumination routine (also termed Light Curve – LC) provides a reliable assessment of photosynthetic performance as a function of irradiance, whereas the subsequent 5 minutes in darkness allows to assess the potential of cells' photosynthetic apparatus to “relax” after light exposure (Ralph and Gademann 2005). To quantitatively compare LCs, they were fitted with the model proposed by (Platt et al. 1980):

$$\text{rETR} = \text{rETR}_{\text{max}} \cdot (1 - e^{(-\alpha \cdot I / \text{rETR}_{\text{max}})})$$

Where rETR is the photosynthetic rate, rETR<sub>max</sub> is the maximum photosynthetic rate, I is the irradiance, and α is the angular coefficient of the initial linear response of the curve. From those parameters, it was calculated the light intensity at which the onset of light saturation occurs, named E<sub>k</sub>:

$$E_k = \text{rETR}_{\text{max}} / \alpha$$

All fluorescence measurements were performed in at least three biological replicates.

### **5.2.10. ATP Sulfurylase activity**

Sample preparation and enzymatic activity assays of ATPS in microalgal cells was determined as described in Section 4.2.5.2, except that, here, standard conditions were used without the addition of DTT, DCMU or any reagent other than those described in Burnell (1984). In contrast to the described in Chapter 4, light regimes were the same before measurements, which were always performed approximately two hours after cultivation light turned on (photoperiod 12:12h).

### **5.2.11. Statistical analysis**

#### *5.2.11.1. Univariate analyses*

All data are shown as the means and standard deviation ( $\pm$ SD) of three to six ( $3 \leq n \leq 6$ ) independent biological replicates. Results were analyzed using Statistica 8.0 data analysis software system (StatSoft Inc. 2007). Student's T test was used to compare differences between values of the two distinct treatments (S sufficient and S starved), and one-way analysis of variance (ANOVA) followed by Fisher's least significant difference (LSD) multiple comparison *post-hoc* test was used when other variable levels were present (e.g.: various sulfate concentrations). All statistical analyses were performed with a significance level of  $\alpha=0,05$ .

#### *5.2.11.2. Multivariate analyses*

To compare treatments based on multiple results (e.g.: elemental composition), Principal Component Analysis (PCA) was carried out using PAST version 2.17c (Hammer et al. 2001) and calculated based on a correlation matrix. In order to perform the analysis, data from three biologically independent replicates were standardized (z-score) and normality was checked via Shapiro-Wilk test.

## 5.3. Results

### 5.3.1. Growth-limiting concentrations of sulfate

All experimental species were exposed to different concentrations of Na<sub>2</sub>SO<sub>4</sub> in the culture medium until growth limitation was achieved. Figure 25 depicts specific growth rate ( $\mu$ ), final cell yield and average cell volume determined for each sulfate concentration tested.

Each species, already in S replete conditions, was characterized by specific growth parameters. In the growth conditions employed, the green alga *Tetraselmis suecica* showed the highest growth rate, whereas the lowest ones were observed in the dinoflagellate *A. carterae*. Final cell yield was the highest in the diatom *Phaeodactylum tricorutum* and again the lowest in *A. carterae*. When growth limitation was achieved, generally the final cell yields also decreased along with the growth rates, except for that of *A. carterae*, that remained unaltered.

Growth-limiting concentrations of sulfate varied broadly among species. In *T. suecica* and *P. tricorutum*, the final cell yield was affected simultaneously with the growth rate, but at markedly different concentrations (100 nM and 10  $\mu$ M respectively). In *P. purpureum*, final cell yield observed at 10  $\mu$ M Na<sub>2</sub>SO<sub>4</sub> was significantly lower than the value observed at 25 mM while growth rate was lower than the control value at 100 nM. The final cell yield of *A. carterae* was not significantly affected.

Based on these results, cultures' conditions named "S replete" and "S limited" were chosen for each microalga to design experiments assessing biochemical and physiological parameters as a function of sulfur availability. For all species, S replete treatments were performed at 25 mM Na<sub>2</sub>SO<sub>4</sub>. S limited treatments, on the other hand, varied according to the species cultivated: 100 nM Na<sub>2</sub>SO<sub>4</sub> for *T. suecica* and *P. purpureum*; 1  $\mu$ M Na<sub>2</sub>SO<sub>4</sub> for *P. tricorutum*; and 1 mM Na<sub>2</sub>SO<sub>4</sub> for *A. carterae*.

Noteworthy, in all species the average cell volumes were higher in S limited conditions as compared to cells grown in the respective S replete ones (Figure 25).

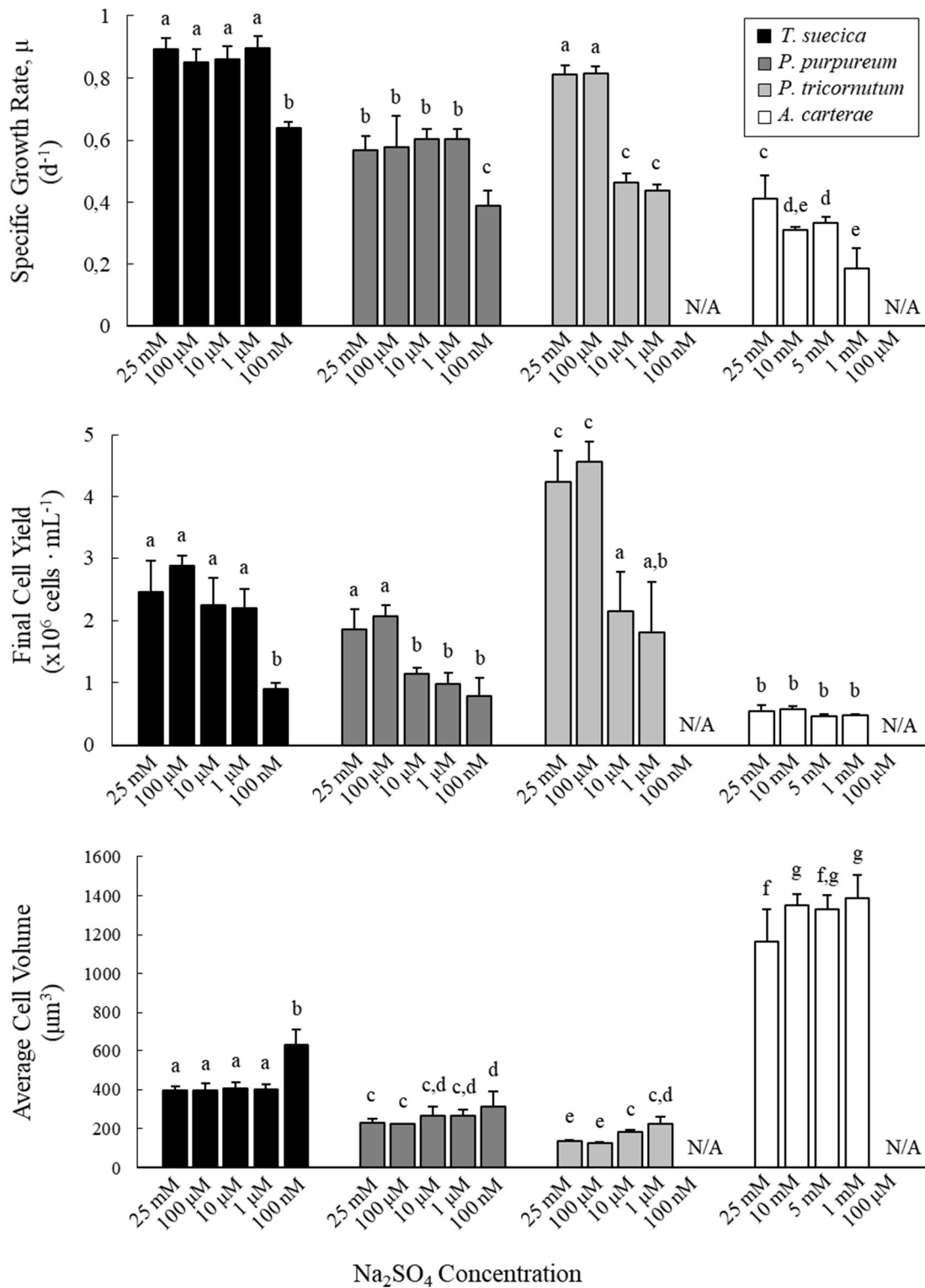


**Figure 25:** Specific growth rate, final cell yield and average cell volume of *Tetraselmis suecica* (black bars), *Porphyridium purpureum* (dark gray bars), *Phaeodactylum tricorntutum* (light gray bars) and *Amphidinium carterae* (white bars) as a function of sulfur concentration in AMCONA medium. Data are means of 3 to 9 biological replicates ( $3 \leq n \leq 9$ ) and error bars show standard deviation. Different letters over bars illustrates significant differences ( $p < 0.05$ ) and N/A means not applied (no growth).

### 5.3.2. Growth, pigments and sulfate limitation

Growth curves of the four microalgae batch-grown photoautotrophically in AMCONA medium (Fanesi et al. 2014) modified as described for S replete and S limited treatments are presented in Figure 26.

A detailed inspection of the growth curves of the four selected species in S limited conditions evidenced a lag phase in all growth curves, except for that of *P. tricornutum*. It was particularly pronounced in *P. purpureum* and *A. carterae*, consisting on a smaller number of cells per mL on the first day than that inoculated in the beginning of cultivations.

Exponential growth generally lasted about 5 to 7 days of cultivation and, in most cases, its duration was not or little affected by sulfate availability. The exception was observed in the S limited cultivation of the dinoflagellate *A. carterae*, where exponential growth – slower than S replete – was maintained during the whole monitored period (11 days). After growing exponentially, cultures went through a deacceleration phase until stationary growth phase was reached, and net cell number remained stable. In *T. suecica* and *A. carterae*, sulfate availability affected the time cells spent to reach stationary growth phase. In the green alga, S limited treatments showed a more abrupt deacceleration and net growth was stopped about three days before S replete treatments. On the contrary, the dinoflagellate's S limited growth did not reach stationary phase during the 11 days of growth monitoring.

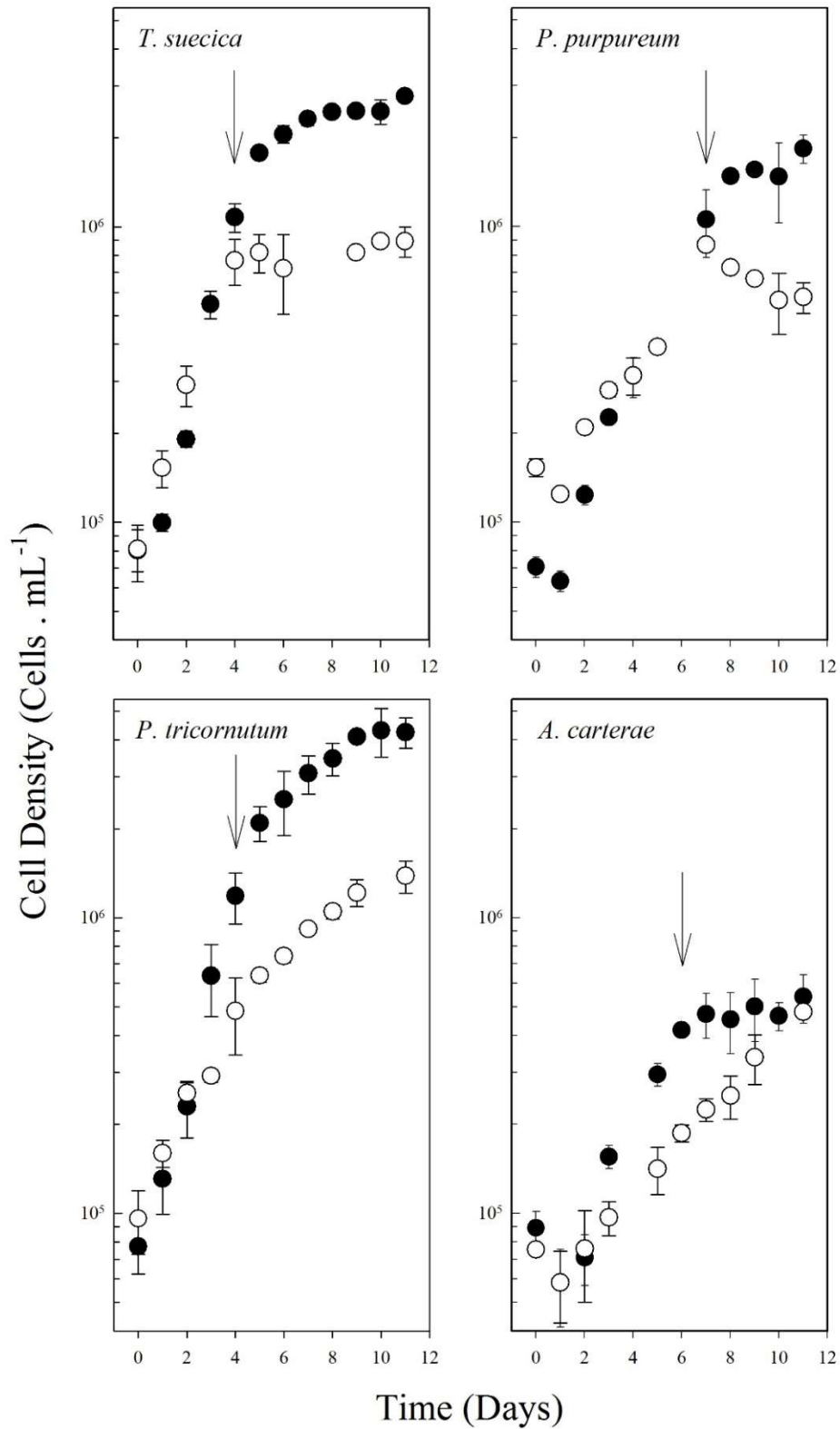


**Figure 26:** Photoautotrophic batch growth of *T. suecica*, *P. purpureum*, *P. tricornutum* and *A. carterae* at 20±2°C under irradiance of 100 μmol photons·m<sup>-2</sup>·s<sup>-1</sup> in S replete (black circles) and S limited (white circles) AMCONA medium. Each growth curve shows the means of three to nine independent experiments (3≤n≤9), and bars show standard deviation. The arrows indicate the sampling days for biomass analyses.

Numerical comparison of growth parameters (Table 6) showed that specific growth rate decreased about 30% in S limited treatments of *T. suecica* and *P. purpureum* and about 50% for *P. tricornutum* and *A. carterae* when compared to S replete ones. Furthermore, upon sulfur limitation, final cell yield decreased circa 60% for all species, except for that of the dinoflagellate *A. carterae*, which did not vary significantly. All tested cells increased their volumes during sulfur limitation. The biggest among the experimental cells, *A. carterae*, presented the lowest increase (ca. 10%), while *P. tricornutum*, the smallest and the only pennate-shaped tested cell, presented the highest increase in volume (ca. 70%). Cellular dry weight of *P. purpureum* was the only one affected by S limitation, being 50% higher when compared to the S replete one.

Finally, whereas chlorophyll *a* per cell never differed between S replete and S limited treatments, the amount of the main accessory pigments (i.e.: chlorophyll *b* in green algae; phycobilins in red algae; and chlorophyll *c* in diatoms and dinoflagellates) increased upon sulfate limitation in most microalgae, with the exception of *A. carterae*. Hence, except for the case of the dinoflagellate, the chlorophyll *a* : accessory pigments ratio varied significantly as a function of sulfate availability. Given that cell volume significantly changed in most cases, pigments were calculated also on a volume basis (Supplemental Table 3). In this case, contrarily, chlorophyll *a* per biovolume decreased significantly in all S limited treatments, except for that of *A. carterae*. Whereas among accessory pigments, only chlorophyll *b* of *T. suecica* was significantly affected and was significantly lower on S limited cells.

**Table 6:** Specific growth rate, final cell yield, average cell volume and pigments content of the four studied microalgae grown at 20±2°C under irradiance of 100  $\mu\text{mol photons}\cdot\text{m}^{-2}\cdot\text{s}^{-1}$ . Except for the final cell yield, which was calculated in early stationary phase, all parameters were determined during exponential growth phase. Data are the means of three to nine independent experiments ( $3\leq n\leq 9$ )  $\pm$  standard deviation. Asterisks in the species name indicate significant differences between S replete and S limited treatments ( $p<0,05$ ).

Parameter	Microalgae	Treatments	
		S replete	S limited
Specific Growth Rate, $\mu$ ( $\text{d}^{-1}$ )	<i>T. suecica</i> *	0,894 $\pm$ 0,035	0,640 $\pm$ 0,018
	<i>P. purpureum</i> *	0,570 $\pm$ 0,045	0,389 $\pm$ 0,051
	<i>P. tricornutum</i> *	0,811 $\pm$ 0,031	0,439 $\pm$ 0,020
	<i>A. carterae</i> *	0,389 $\pm$ 0,092	0,185 $\pm$ 0,069
Final Cell Yield ( $\times 10^6$ cells $\cdot\text{mL}^{-1}$ )	<i>T. suecica</i> *	2,451 $\pm$ 0,505	0,893 $\pm$ 0,105
	<i>P. purpureum</i> *	1,849 $\pm$ 0,334	0,781 $\pm$ 0,294
	<i>P. tricornutum</i> *	4,235 $\pm$ 0,511	1,809 $\pm$ 0,529
	<i>A. carterae</i>	0,629 $\pm$ 0,048	0,516 $\pm$ 0,064
Average Cell Volume ( $\mu\text{m}^3$ )	<i>T. suecica</i> *	396,1 $\pm$ 22,22	629,5 $\pm$ 82,64
	<i>P. purpureum</i> *	228,6 $\pm$ 23,79	311,8 $\pm$ 79,42
	<i>P. tricornutum</i> *	134,7 $\pm$ 5,590	226,8 $\pm$ 33,16
	<i>A. carterae</i>	1165 $\pm$ 162,9	1385 $\pm$ 118,9
Dry Weight ( $\text{pg}\cdot\text{cell}^{-1}$ )	<i>T. suecica</i>	278,7 $\pm$ 131,9	372,8 $\pm$ 142,6
	<i>P. purpureum</i> *	90,04 $\pm$ 29,72	137,8 $\pm$ 16,03
	<i>P. tricornutum</i>	93,81 $\pm$ 26,93	112,0 $\pm$ 44,43
	<i>A. Carterae</i>	563,5 $\pm$ 116,8	462,9 $\pm$ 87,61
Chlorophyll <i>a</i> ( $\text{pg}\cdot\text{cell}^{-1}$ )	<i>T. suecica</i>	2,031 $\pm$ 0,075	1,785 $\pm$ 0,167
	<i>P. purpureum</i>	0,499 $\pm$ 0,067	0,385 $\pm$ 0,105
	<i>P. tricornutum</i>	0,303 $\pm$ 0,037	0,284 $\pm$ 0,015
	<i>A. carterae</i>	1,588 $\pm$ 0,114	1,693 $\pm$ 0,045
Chlorophyll <i>b</i> ( $\text{pg}\cdot\text{cell}^{-1}$ )	<i>T. suecica</i> *	0,935 $\pm$ 0,087	0,669 $\pm$ 0,076
Chlorophyll <i>c</i> ( $\text{pg}\cdot\text{cell}^{-1}$ )	<i>P. tricornutum</i> *	0,044 $\pm$ 0,008	0,084 $\pm$ 0,012
	<i>A. carterae</i>	0,572 $\pm$ 0,053	0,657 $\pm$ 0,057
Phycobiliproteins ( $\text{pg}\cdot\text{cell}^{-1}$ )	<i>P. purpureum</i> *	2,380 $\pm$ 0,226	3,538 $\pm$ 0,448

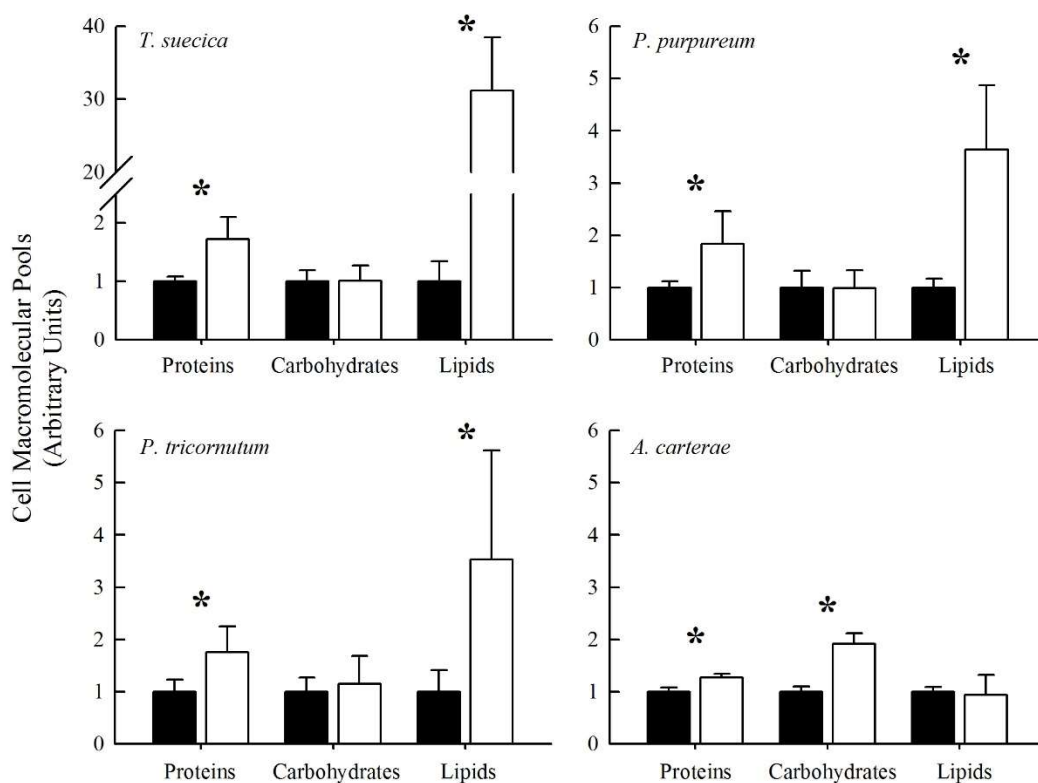
### 5.3.3. Macromolecular pools

Table 7 and Figure 27 showed that in all cases, proteins per cell were higher in the S limited treatment in comparison to those in the S replete one. The most pronounced increase (around 80%) was observed in the diatom *P. tricornutum*, whereas the lowest (around 30%) was that of the dinoflagellate *A. carterae*. When proteins were calculated on a volume basis, they were not significantly different, neither between treatments nor between species, except in the case of *A. carterae* (Supplemental Table 3). FTIR analyses allowed to analyze the relative amount of the main macromolecular pools: proteins, carbohydrates and lipids. Whilst the carbohydrate : protein ratio was lower in sulfur limited cultures of *T. suecica* and *P. purpureum*, it did not change in *P. tricornutum* cells and, conversely, it was higher in cells of *A. carterae*. All S limited cells showed an increase of the the lipid : protein ratio, except for the dinoflagellate's ones, which remained unaltered. Finally, the lipid : carbohydrates ratio was affected in all species. However, whereas it was higher in S limited treatments of *T. suecica*, *P. purpureum* and *P. tricornutum*, as compared to the values in S replete cultures, it was lower in *A. carterae* (Table 7).

The ratios of macromolecular pools obtained by FTIR (Table 7) were used to semi-quantify the carbohydrate and lipid pools based on the absolute amount of proteins (Figure 27). The lipids' pools of S limited cultures of *T. suecica*, *P. purpureum* and *P. tricornutum* was substantially higher when compared to that of S replete cultures. The only exception was found in *A. carterae* cells, where lipids' pool size was not affected by sulfur concentration. On the other hand, the carbohydrates' pool of the dinoflagellate was the only one affected and significantly increased by sulfur availability when compared to the other species.

**Table 7:** Absolute measured values of proteins per cell, and ratios of macromolecular pools (proteins, lipids and carbohydrates) of S replete and S limited treatments of *Tetraselmis suecica*, *Porphyridium purpureum*, *Phaeodactylum tricorutum* and *Amphidinium carterae*. The data are means of 3 to 6 independent experiments ( $3 \leq n \leq 6$ )  $\pm$  standard deviation. Asterisks represent significant differences of the given macromolecular pool or ratio between treatments of the same species ( $p < 0,05$ )

Species	Proteins (pg·cell <sup>-1</sup> )		Carbohydrates / Proteins		Lipids / Proteins		Lipids / Carbohydrates	
	S replete	S limited	S replete	S limited	S replete	S limited	S replete	S limited
<i>Tetraselmis suecica</i>	54,40 $\pm$ 4,308	93,66 $\pm$ 20,76*	0,731 $\pm$ 0,125	0,427 $\pm$ 0,054*	0,021 $\pm$ 0,007	0,379 $\pm$ 0,030*	0,029 $\pm$ 0,004	0,893 $\pm$ 0,052*
<i>Porphyridium purpureum</i>	32,95 $\pm$ 3,839	60,51 $\pm$ 20,42*	1,212 $\pm$ 0,355	0,655 $\pm$ 0,019*	0,074 $\pm$ 0,009	0,147 $\pm$ 0,004*	0,167 $\pm$ 0,077	0,381 $\pm$ 0,019*
<i>Phaeodactylum tricorutum</i>	21,64 $\pm$ 4,949	38,13 $\pm$ 10,64*	0,601 $\pm$ 0,087	0,638 $\pm$ 0,238	0,185 $\pm$ 0,062	0,370 $\pm$ 0,193*	0,324 $\pm$ 0,118	0,561 $\pm$ 0,103*
<i>Amphidinium carterae</i>	66,90 $\pm$ 4,592	93,42 $\pm$ 10,44*	0,700 $\pm$ 0,036	1,054 $\pm$ 0,090*	0,095 $\pm$ 0,004	0,070 $\pm$ 0,028	0,364 $\pm$ 0,013	0,065 $\pm$ 0,009*



**Figure 27:** Semi-quantification of macromolecular pools of the four studied microalgae grown in S replete (black bars) and S limited (white bars) modified AMCONA medium. The pools' size is expressed relatively to the values found in S replete conditions, that was set to 1. Asterisks above bars indicates significant differences between S replete and S limited treatments ( $p < 0,05$ ).

#### 5.3.4. Elemental composition

Elemental cell quotas varied amongst different species. When S replete and S limited treatments were compared, however, differences within the same species were not so evident and less common (Figure 28). Whereas in *T. suecica*, elemental composition expressed as  $\text{pg}\cdot\text{cell}^{-1}$  was poorly affected by sulfur availability, nitrogen quota was significantly higher in all other tested species grown in S limited regime. Carbon was also significantly higher in S limited cells of *P. purpureum* and *A. carterae*. In the latter species, also iron cell quota increased in S limited cells. Finally, in all species the sulfur cell quota showed a tendency to decrease in S limited conditions, although only in the dinoflagellate *A. carterae* the difference was statistically significant from the S replete treatment.

Given that cell volume changed as a function of sulfate limitation, the elemental cell quotas were calculated also on a biovolume basis (Supplemental Table 3). Calculated that way, the sulfur cell quotas of all tested species were significantly lower in S limited conditions as compared to S replete ones. Also, the number of significantly different values of elements' cell quotas between treatments was higher when calculations were made based on cell volume.

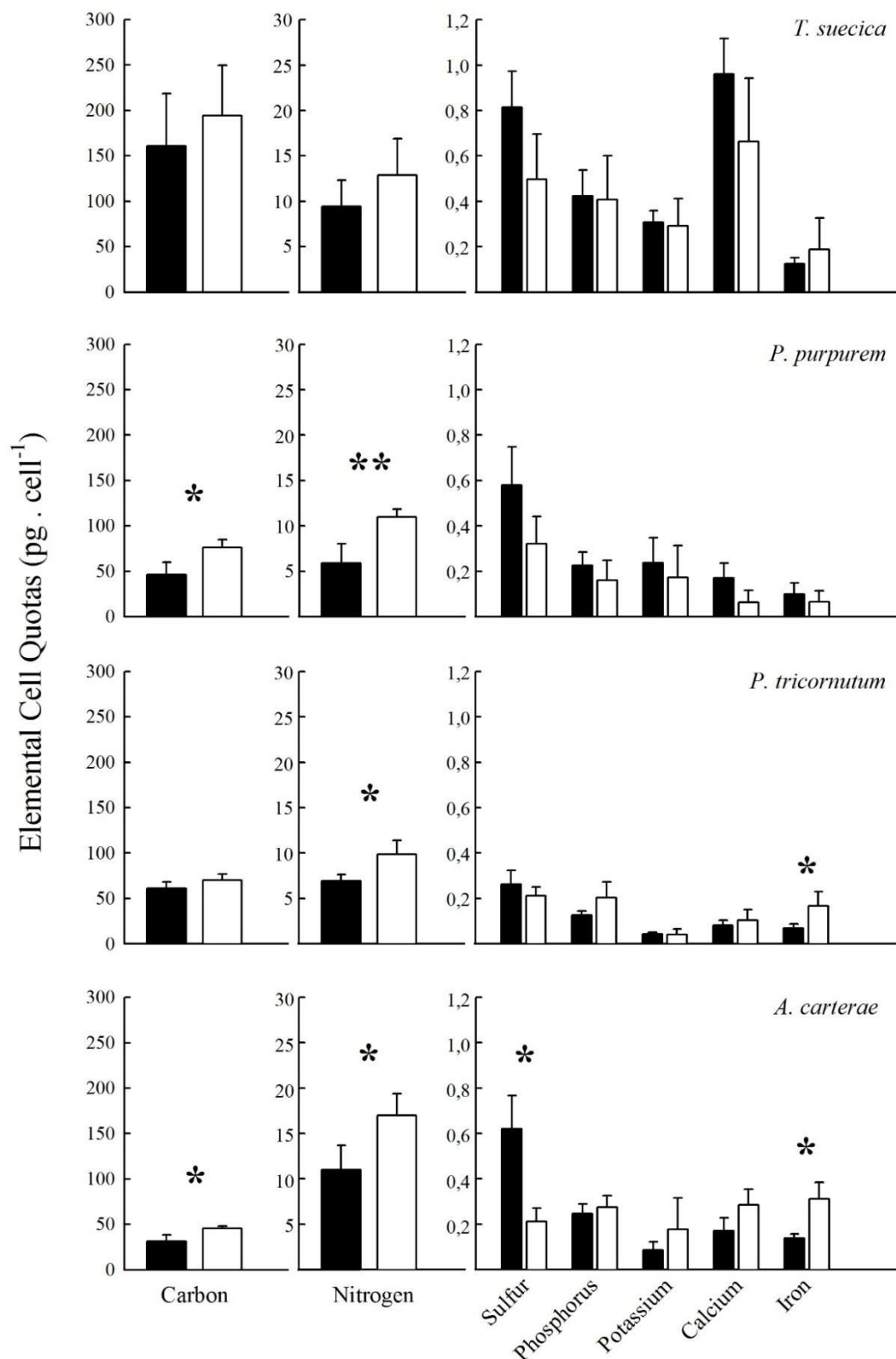


**Figure 28:** Elemental cell quotas of the four experimental microalgae grown in S replete (black bars) and S limited (white bars) modified AMCONA medium at 20±2°C under 100 μmol photons·m<sup>-2</sup>·s<sup>-1</sup>. The data are the means of at least three biological replicates (n≥3) and error bars show standard deviation. Asterisks indicate significant differences between treatments (\* = p<0,05; \*\* = p<0,01).

The ratios between elements, with emphasis on sulfur – C:N, C:S, N:S, S:P, S:K, S:Ca, S:Fe – are shown in Table 8 and contribute to the assessment on species-specific elemental fluctuations. This way, the values obtained are independent of the calculation basis (i.e. per cell or biovolume) and complement the overall investigation of elemental balance. In this sense, elemental ratios relative to S varied substantially among the four experimental species and also separated them in groups – namely, the ones whose growth was limited in lower concentrations of S and the ones limited in greater concentrations of S (Table 8). C:S and N:S ratios significantly changed upon S limitation in all four species, while the other ratios relative to S changed only in *P. tricornutum* and *A. carterae*. Only in the diatom the C:N, ratio changed between S replete and S limited treatments.

A Principal Component Analysis (PCA) was performed using the percentage values of the main macroelements – C, N, S and P – of all experimental algae (Table 8; Figure 29). PCA explained nearly 90% of the variations present in the dataset, with Principal Component (PC) 1 accounting for 56,65% and PC2, for 32,75%. The biplot graph allows to see on a two-dimensional space the correlation between each biological replicate (score plot) and each elemental content vector (loading plot). The main loadings that were represented on PC1 (X-axis) were nitrogen, sulfur and phosphorus, whereas on PC2 (Y-axis) carbon was the main loading factor. Species were well separated in the scores plot. The scores plot clearly differentiated S replete and S limited treatments of *T. suecica* and *P. purpureum*, but not those of *P. tricornutum* and *A. carterae*. Furthermore, whereas S replete replicates' scores of *T. suecica* and *P. purpureum* were distant from each other and from the other species' scores, their S limited scores got closer to each other and to the other species' scores, especially that of *P. tricornutum*.

**Table 8:** Elemental cell quotas and ratios of *T. suecica*, *P. purpureum*, *P. tricorutum* and *A. carterae* grown in S replete and S limited modified AMCONA medium at 20±2°C under 100 μmol photons·m<sup>-2</sup>·s<sup>-1</sup>. The data are the means of at least three biological replicates (n≥3) ± standard deviation. Asterisks indicate significant differences between treatments of the referred element for the same species.

Elemental cell quotas and ratios	Microalgae							
	<i>T. suecica</i>		<i>P. purpureum</i>		<i>P. tricorutum</i>		<i>A. carterae</i>	
	S replete	S limited	S replete	S limited	S replete	S limited	S replete	S limited
<b>Carbon (%)</b>	68,72±8,37	59,00±1,09*	51,71±1,51	55,49±0,43	59,32±2,37	54,83±2,47	51,66±0,29	50,11±1,87
<b>Nitrogen (%)</b>	4,07±0,17	3,90±0,18	6,51±0,21	8,00±0,62*	6,57±0,07	7,64±0,20*	18,22±0,93	18,59±1,16
<b>Sulfur (%)</b>	0,32±0,09	0,13±0,03*	0,65±0,02	0,23±0,07*	0,29±0,06	0,16±0,01*	0,72±0,23	0,15±0,04*
<b>Phosphorus (%)</b>	0,16±0,03	0,11±0,02	0,25±0,04	0,11±0,05*	0,14±0,02	0,16±0,04	0,29±0,10	0,20±0,04*
<b>C:N</b>	17,00±1,20	15,22±0,60	7,97±0,47	6,97±0,48	9,03±0,39	7,19±0,45*	2,84±0,13	2,71±0,28
<b>C:S</b>	193,24±34,88	408,58±67,00*	79,88±1,21	253,01±66,76*	236,88±29,71	334,97±32,73*	50,34±0,36	264,86±18,26*
<b>N:S</b>	11,44±1,68	26,90±3,52*	10,06±0,65	36,30±8,93*	26,80±3,08	46,59±2,24*	17,75±0,71	103,92±5,17*
<b>S:P</b>	1,96±0,24	1,28±0,55	2,60±0,42	2,19±0,66	1,84±0,46	1,16±0,36*	2,51±0,35	0,76±0,09*
<b>S:K</b>	2,64±0,18	1,75±0,72	1,83±0,24	1,51±0,09	5,52±2,16	7,76±4,17	8,04±2,44	1,53±0,73*
<b>S:Ca</b>	0,85±0,08	0,78±0,31	3,49±0,54	4,19±0,47	2,83±0,60	2,53±1,04	3,75±1,06	0,75±0,15*
<b>S:Fe</b>	6,54±0,25	3,31±2,23	6,30±1,56	3,92±0,21	3,50±1,48	1,48±0,61*	4,44±0,61	0,68±0,03*

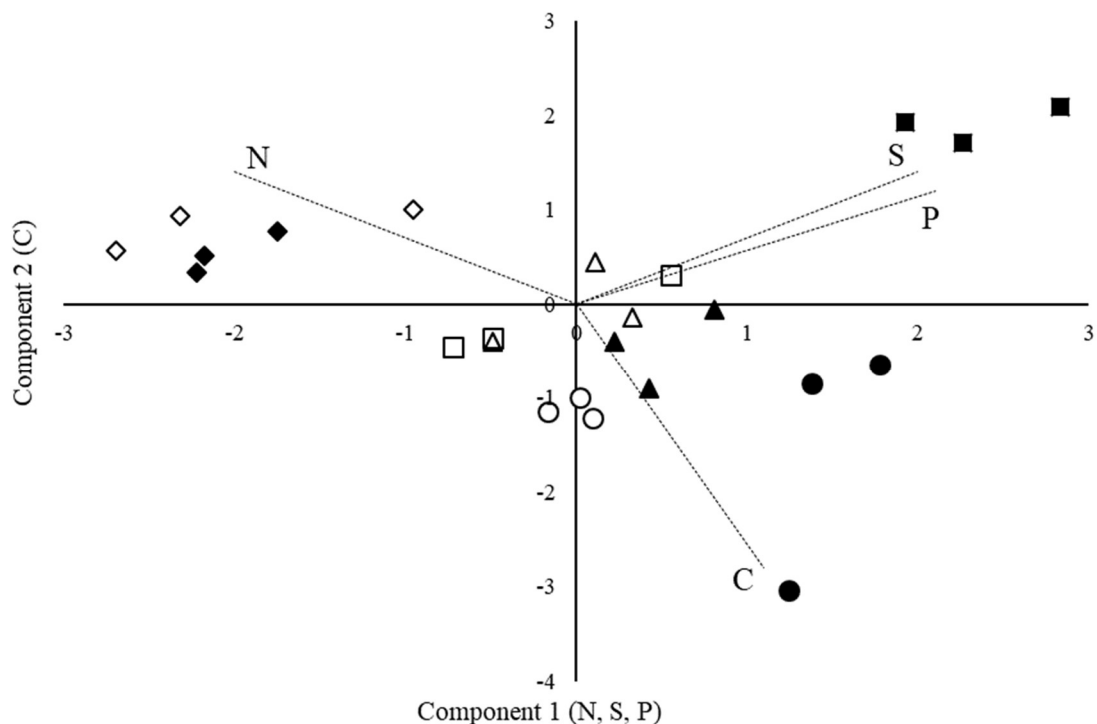


**Figure 29:** Principal Component Analysis (PCA) of standardized percentage of carbon (C), nitrogen (N), sulfur (S) and phosphorus (P) (loading plots are represented as dashed lines) on the biomass of *T. suecica* (circles), *P. purpureum* (squares), *P. tricorutum* (triangles) and *A. carterae* (diamonds) cultivated on S replete (filled symbols) and S limited (open symbols) modified AMCONA medium.

### 5.3.5. Photosynthetic parameters

Cells from S replete and S limited culture conditions were also characterized for their photosynthetic capacity by analyzing *in vivo* their response to increasing illumination in light curve experiments (Figure 30, Figure 31, Figure 32, Figure 33 and Table 9). Maximum photosynthetic efficiency ( $F_v/F_m$ ) was diversified among species grown in S replete conditions and was the highest in *T. suecica* and lowest in S limited *A. carterae*. Looking at the effects of sulfate limitation, only the diatom and the dinoflagellate resulted in significantly different  $F_v/F_m$  between S replete and S limited growth (Table 9). Amongst the parameters calculated via the curve fitting of relative electron transport rate (rETR) – namely, the angular coefficient of the linear portion of the curve ( $\alpha$ ); maximum electron transport rate (rETR<sub>max</sub>); and the onset of light saturation ( $E_k$ ) –, none was significantly altered as a function of S concentration (Figure 30; Table 9).

Other parameters obtained during the light curves followed by five minutes recovery in darkness – namely, photosystem II quantum yield ( $\Phi_{PSII}$ ); photochemical

quenching (qL); and non-photochemical quenching (NPQ) – were very similar in *T. suecica* regardless of sulfate concentration during growth. In the other species, however, mild fluctuations were observed especially on quenching values. Photochemical quenching of the red alga *P. purpureum* was lower in S limited treatments when compared to S replete, whereas, on the contrary, *P. tricornutum* and *A. carterae* presented higher photochemical quenching in S limited treatments. After five minutes of relaxation, potential for photochemical quenching was recovered in all species and treatments except for S replete culture of the dinoflagellate (Figure 32).

During the gradual increment in light intensity, non-photochemical quenching mechanisms of *P. tricornutum* and *A. carterae* were activated more slowly in S limited treatments when compared to S replete ones. Nevertheless, final values were virtually the same. Contrarily to their activation, deactivation of non-photochemical quenching mechanisms in *P. tricornutum* was faster in S limited treatments. Again, final values after five minutes of darkness were the same. That was not the case only for *P. purpureum*, where non-photochemical quenching values after darkness was still considerably higher than in the beginning of measurements. As a matter of fact, on the S limited treatments of the red alga, NPQ values continued to increase after one minute of darkness (Figure 33). It is noteworthy that non-photochemical quenching values of *P. purpureum* were substantially lower than the ones found on the other species, especially that of the green algae, which showed the highest values of NPQ.

**Table 9:** Photosynthetic efficiency ( $F_v/F_m$ ) and rapid light curve's parameters ( $\alpha$ ,  $rETR_{max}$ ,  $E_k$ ) of the four studied microalgae grown in S replete and S limited modified AMCONA medium at  $20\pm 2^\circ\text{C}$  under irradiance of  $100 \mu\text{mol photons}\cdot\text{m}^{-2}\cdot\text{s}^{-1}$ . All parameters were determined during exponential growth phase. Data are the means of three to six independent experiments ( $3\leq n\leq 6$ )  $\pm$  standard deviation. Asterisks in the species name indicates significant differences between treatments ( $p<0,05$ ).

Parameter	Microalgae	Treatments	
		S replete	S limited
<b>F<sub>v</sub>/F<sub>m</sub></b>	<i>T. suecica</i>	0,743 $\pm$ 0,008	0,746 $\pm$ 0,018
	<i>P. purpureum</i>	0,380 $\pm$ 0,043	0,425 $\pm$ 0,040
	<i>P. tricornutum</i> *	0,563 $\pm$ 0,008	0,470 $\pm$ 0,041
	<i>A. carterae</i> *	0,330 $\pm$ 0,028	0,214 $\pm$ 0,081
<b><math>\alpha</math></b>	<i>T. suecica</i>	0,366 $\pm$ 0,004	0,388 $\pm$ 0,028
	<i>P. purpureum</i>	0,244 $\pm$ 0,037	0,249 $\pm$ 0,020
	<i>P. tricornutum</i>	0,248 $\pm$ 0,009	0,242 $\pm$ 0,035
	<i>A. carterae</i>	0,152 $\pm$ 0,012	0,140 $\pm$ 0,033
<b>rETR max</b> (a.u.)	<i>T. suecica</i>	129,6 $\pm$ 3,768	133,5 $\pm$ 5,750
	<i>P. purpureum</i>	69,28 $\pm$ 14,28	67,15 $\pm$ 9,213
	<i>P. tricornutum</i>	137,6 $\pm$ 8,746	133,1 $\pm$ 2,665
	<i>A. carterae</i>	60,17 $\pm$ 4,626	59,80 $\pm$ 2,352
<b>E<sub>k</sub></b> ( $\mu\text{mol photons}\cdot\text{m}^{-2}\cdot\text{s}^{-1}$ )	<i>T. suecica</i>	448,8 $\pm$ 7,584	385,5 $\pm$ 48,95
	<i>P. purpureum</i>	374,6 $\pm$ 34,04	372,8 $\pm$ 30,09
	<i>P. tricornutum</i>	554,5 $\pm$ 30,49	557,5 $\pm$ 76,68
	<i>A. carterae</i>	396,6 $\pm$ 43,26	381,6 $\pm$ 6,532

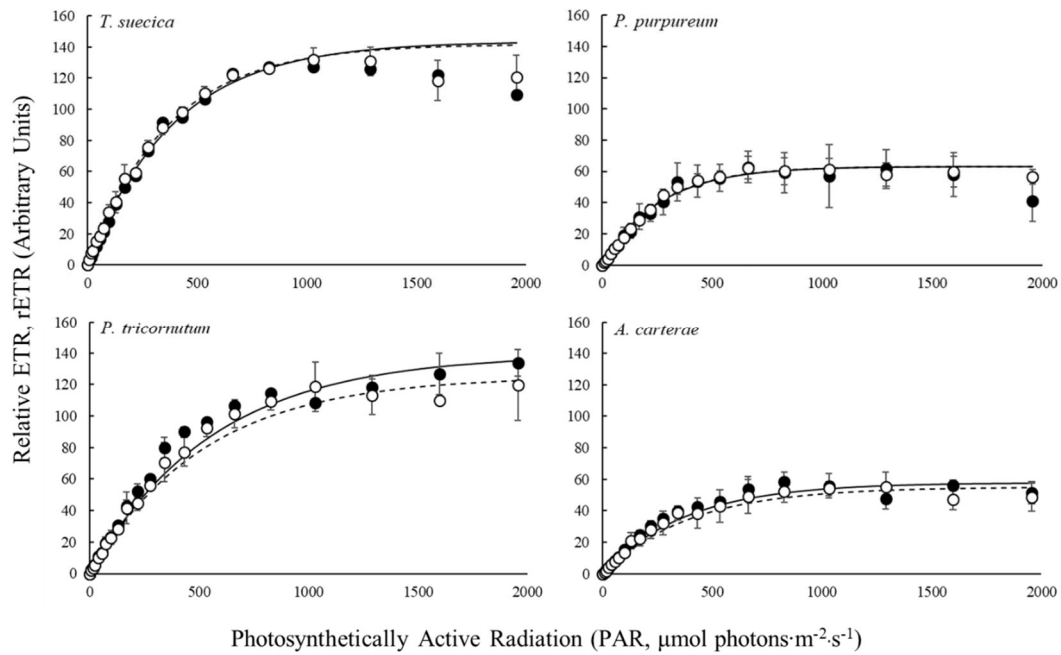


**Figure 30:** Light curves (LC) of the four studied microalgae grown in S replete (black circles) and S limited (white circles) modified AMCONA medium at  $20\pm 2^\circ\text{C}$  under irradiance of  $100 \mu\text{mol photons}\cdot\text{m}^{-2}\cdot\text{s}^{-1}$ . Regression curves of S replete (continuous line) and S limited (dashed line) treatments are also plotted and error bars show standard deviation of at least three biologically independent experiments ( $n\geq 3$ ).

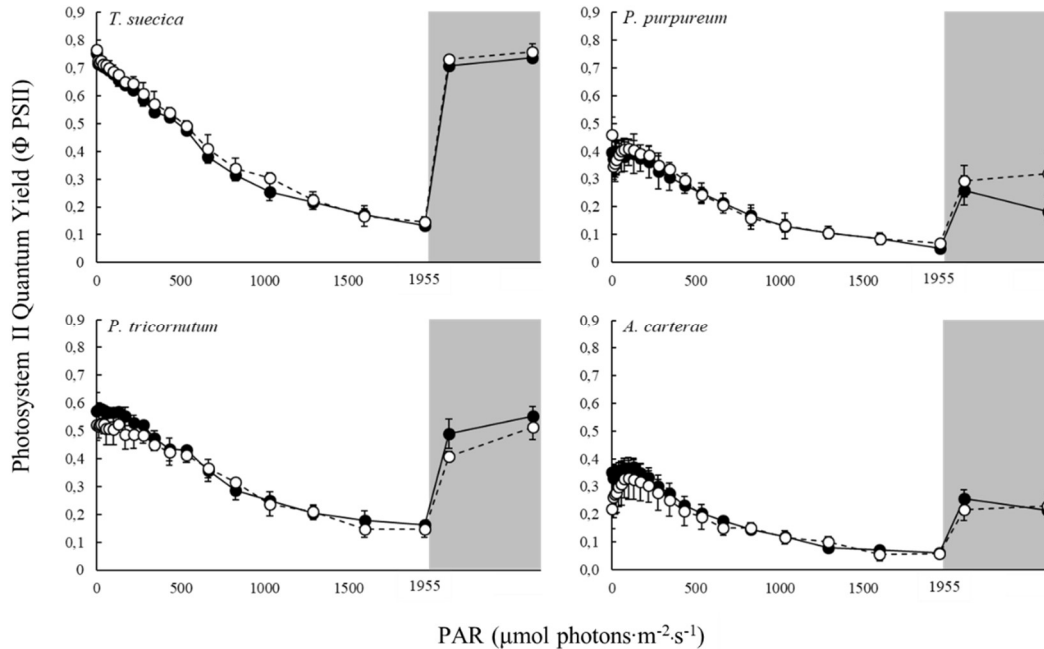


**Figure 31:** Photosystem II quantum yield ( $\Phi_{\text{PSII}}$ ) of the four studied microalgae grown in S replete (black circles; continuous line) and S limited (white circles; dashed line) modified AMCONA medium at  $20\pm 2^\circ\text{C}$  under irradiance of  $100 \mu\text{mol photons}\cdot\text{m}^{-2}\cdot\text{s}^{-1}$ . Twenty steps (one minute each) of increasing PAR were followed by five minutes of recovery in darkness (gray area). Data are the means of at least three biological replicates ( $n\geq 3$ ) and error bars show standard deviation.

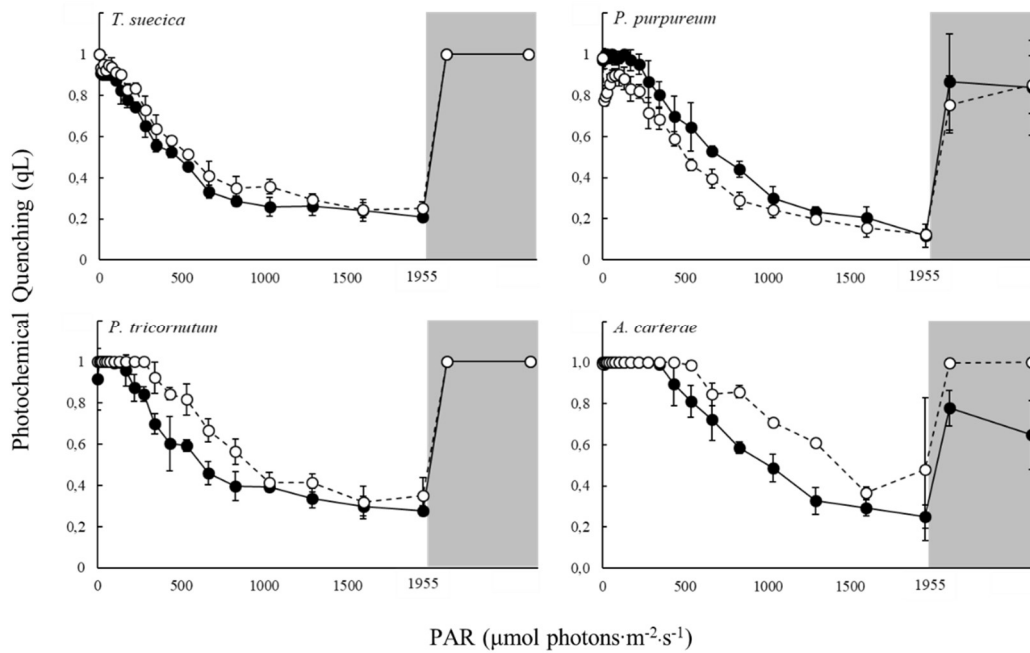


**Figure 32:** Photochemical quenching (qL) of the four studied microalgae grown in S replete (black circles; continuous line) and S limited (white circles; dashed line) modified AMCONA medium at  $20\pm 2^\circ\text{C}$  under irradiance of  $100 \mu\text{mol photons}\cdot\text{m}^{-2}\cdot\text{s}^{-1}$ . Twenty steps (one minute each) of increasing PAR were followed by five minutes of recovery in darkness (gray area). Data are the means of at least three biological replicates ( $n\geq 3$ ) and error bars show standard deviation.

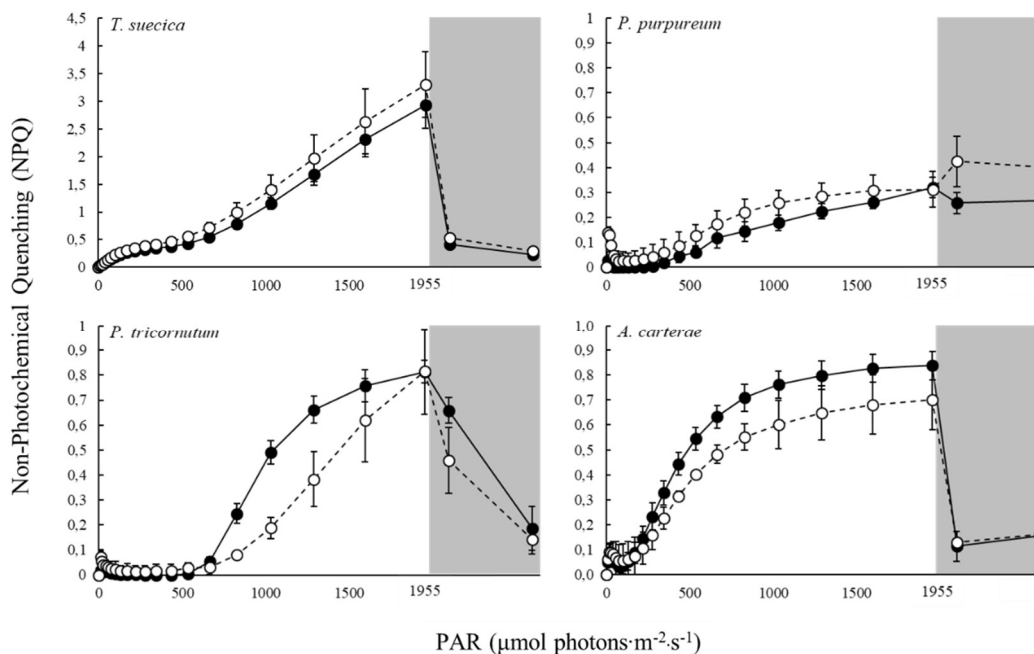


**Figure 33:** Non-photochemical quenching (NPQ) of the four studied microalgae grown in S replete (black circles; continuous line) and S limited (white circles; dashed line) modified AMCONA medium at  $20\pm 2^\circ\text{C}$  under irradiance of  $100 \mu\text{mol photons}\cdot\text{m}^{-2}\cdot\text{s}^{-1}$ . Twenty steps (one minute each) of increasing PAR were followed by five minutes of recovery in darkness (gray area). Data are the means of at least three biological replicates ( $n\geq 3$ ) and error bars show standard deviation.

### 5.3.6. *ATP Sulfurylase activity*

ATP-S activity of each species was presented on a cell basis as well as on a protein basis (Figure 34). In both cases, higher and similar values of ATP-S activity were found in the green alga *T. suecica* and the dinoflagellate *A. carterae* when compared to the activity of other species.

When ATP-S activity of S replete and S limited cultures was compared, activity of the green alga never significantly changed, regardless of the calculation basis. That was not the case of all other experimental microalgae, whose activities were affected in particular when expressed on a cell basis (Figure 34). Indeed, S limited cells of *P. purpurem* and *P. tricornutum* showed a significant increase of ATPS activity. Red-plastid algae were the only ones whose ATPS activity was somehow affected by sulfate concentration available in the growth medium.

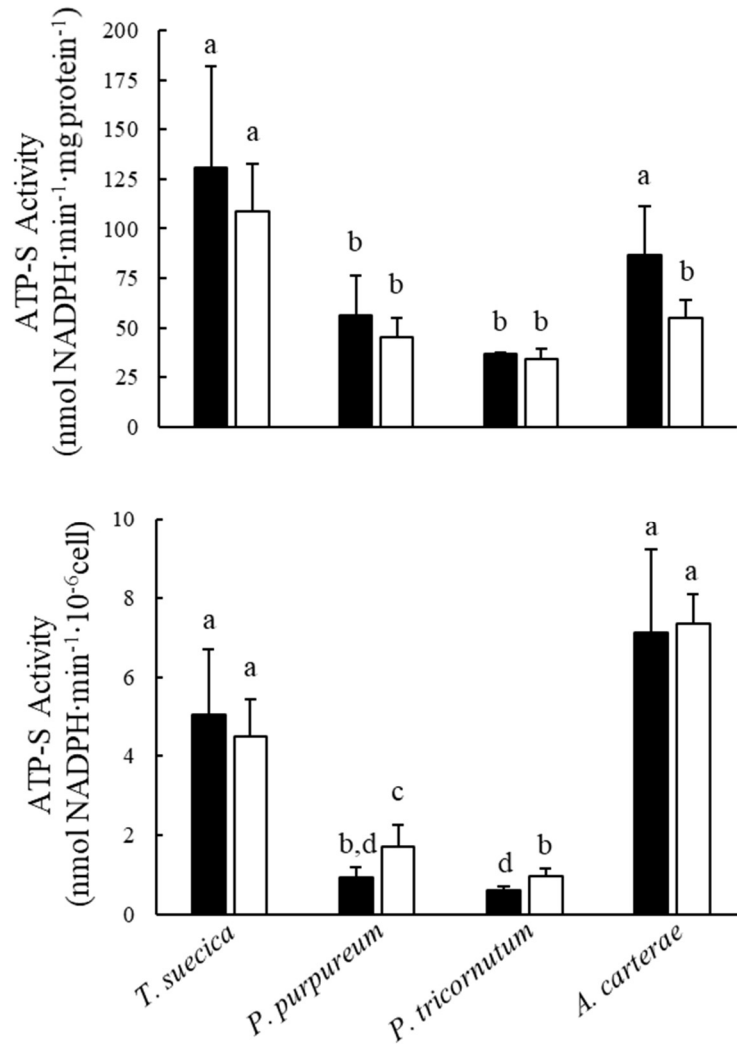


**Figure 34:** ATP Sulfurylase activity of the four studied microalgae grown in S replete (black bars) and S limited (white bars) modified AMCONA medium at  $20 \pm 2^\circ\text{C}$  under irradiance of  $100 \mu\text{mol photons}\cdot\text{m}^{-2}\cdot\text{s}^{-1}$ . Enzyme activity was calculated on protein (upper graph) and cell basis (lower graph). Data are the means of at least three independent biological replicates and error bars show standard deviation. Different letters above the bars represent statistical differences ( $p < 0,05$ ).

## 5.4. Discussion

### 5.4.1. Marine algae of different phylogeny are characterized by a different sulfate limiting concentration

A general and somewhat ideal definition of limitation states that an organism is limited when it is not growing as fast as it is theoretically able to (Gibson 1971). In accordance to Liebig's law of the minimum (Liebig 1841), microalgae growth is determined by the nutrient that happens to be in limiting supply; any moderate increase or decrease in the supply of other components will have little or no effect on the rate of growth. In this chapter, growth limitation of four microalgal species was achieved by decreasing the sulfur availability in growth medium. The sensitivity of each microalga to sulfur availability varied dramatically: the higher the sulfate concentration that limits growth, the more sensitive is considered the microalga. The diatom *P. tricornutum* and the dinoflagellate *A. carterae* had their growth limited when exposed to concentrations of sulfate respectively 1000- and 10000-fold higher than that which limited the growth of the green and red alga, and thus are substantially more sensitive to sulfate limitation (Figure 25). Although some cautions must be taken in generalizations, the sensitivity to sulfate limitation seems to separate microalgae into primary – little or non-sensitive to sulfur concentration on growth medium – and secondary endosymbionts – sensitive to sulfur concentration on growth medium.

Phytoplankton sensitivity to sulfate availability is a crucial characteristic that supports the so-called Sulfate Facilitation Hypothesis (SFH; Ratti et al. 2011). In fact, the hypothesis states that the raise to dominance of chlorophyll *a + c* microalgae over green lineage algae that happened about 250 million years ago was primarily driven by the increase of sulfate in seawater observed in the same period. From reported results, species showing lower C:S ratios, generally observed in red-plastid algae, have a higher sensitivity to sulfur limitation due to a lower usage efficiency (Norici et al. 2005, Ratti et al. 2011, Prioretti and Giordano 2016). However, unlike most diatoms and other red lineage algae (Ho et al. 2003), *P. tricornutum* presented a high C:S ratio, comparable to that of green algae and cyanobacteria (Table 8 and Table 10), while being, as other diatoms, more sensitive to sulfur limitation than the red alga *P. purpureum* characterized by a substantially lower C:S ratio. This indicates that correlating the sensitivity to sulfur limitation with the C:S ratio of a species (and even a group) may be an amiss assumption

and other physiological mechanisms may be involved in such response (Ratti et al. 2013, Giordano et al. 2018). Moreover, given the different growth limiting concentrations of sulfur observed in *P. tricornutum* and *A. carterae* as compared to the one in *P. purpureum*, sensitivity to sulfur does not appear to be an inherited characteristic from the primary red plastid, but rather, to be a result of the extremely complicated process of secondary endosymbiosis (McFadden 2014). Therefore, the mechanistic reasons that lead to a higher sensitivity of chlorophyll *a + c* algae to sulfur limitation are still unclear. Previous studies could not address a specific physiological link to the differences of sensitivity found among taxa but, still, did not fully explore cellular responses under nutrient limitation (Ratti et al. 2011, Prioretti and Giordano 2016). Equally unclear are the responses to this limitation and whether different groups of microalgae will respond differently, even if limiting conditions consist in very different concentrations. These topics are discussed in the following Section.

**Table 10:** Approximate growth-limiting concentrations of sulfur and C:S ratios of marine microalgae found in literature.

Species	Sulfate limiting concentration	Culture medium	C:S ratio in S replete conditions*	References
<i>Synechococcus</i> sp.	-	AMCONA	150 - 450	Prioretti and Giordano (2016); Ratti <i>et al.</i> (2011)
<i>Dunaliella salina</i>	6 $\mu\text{mol}\cdot\text{L}^{-1}$	<i>Recipe in Ref.</i>	-	Giordano <i>et al.</i> (2000)
<i>Tetraselmis suecica</i>	< 1 $\mu\text{mol}\cdot\text{L}^{-1}$	AMCONA	150 - 200	Prioretti and Giordano (2016); this thesis
<i>Porphyridium purpureum</i> <sup>†</sup>	< 1 $\mu\text{mol}\cdot\text{L}^{-1}$	AMCONA	80	This thesis
<i>Thalassiosira pseudonana</i>	5 $\text{mmol}\cdot\text{L}^{-1}$	AMCONA	30	Prioretti and Giordano (2016)
<i>Thalassiosira weissflogii</i>	5 $\text{mmol}\cdot\text{L}^{-1}$	modified AMCONA	40	Ratti <i>et al.</i> (2011)
<i>Phaeodactylum tricornutum</i> <sup>†</sup>	< 100 $\mu\text{mol}\cdot\text{L}^{-1}$	AMCONA	230	This thesis
<i>Amphydinium klebsii</i>	5 $\text{mmol}\cdot\text{L}^{-1}$	AMCONA	120	Prioretti and Giordano (2016)
<i>Amphydinium carterae</i> <sup>†</sup>	10 $\text{mmol}\cdot\text{L}^{-1}$	AMCONA	50	This thesis
<i>Protoceratium reticulatum</i>	1 $\text{mmol}\cdot\text{L}^{-1}$	modified AMCONA	70	Ratti <i>et al.</i> (2011)
<i>Emiliana huxleyi</i>	5 $\text{mmol}\cdot\text{L}^{-1}$	ESAW; AMCONA	60	Bochenek <i>et al.</i> (2013); Ratti <i>et al.</i> (2011)
<i>Nannochloropsis gaditana</i> <sup>i</sup>	30 $\mu\text{mol}\cdot\text{L}^{-1}$	Nutribloom plus	15	Fernandes <i>et al.</i> (2020)
<i>Rhodomonas salina</i> <sup>i</sup>	30 $\mu\text{mol}\cdot\text{L}^{-1}$	Nutribloom plus	50	Fernandes <i>et al.</i> (2020)
<i>Isochrysis</i> sp. <sup>i</sup>	30 $\mu\text{mol}\cdot\text{L}^{-1}$	Nutribloom plus	15	Fernandes <i>et al.</i> (2020)

\* C:S ratios in this table are ranges or approximations.

<sup>†</sup> New taxa added to knowledge by this thesis. Note that *P. purpureum* is the first red alga analyzed in this perspective.

<sup>i</sup> Growth-limiting concentrations of sulfur may be higher. Finding the onset of limitation was not the aim of the authors.

#### 5.4.2. *Physiological responses to sulfate limitation*

Responses to changes in nutrient availability are primarily mediated by the biochemical machinery, which operates to maintain a sufficient rate of the component whose supply decreased and to maintain its acquisition and assimilation rates in balance with other resources (Droop 1973, Behrenfeld et al. 2008). When these processes fail, imbalances in the allocation of energy and elements to the cell pools may occur, and cell composition is then rearranged (Raven and Johnston 1991). In this chapter, many similar traits characterized S limited cells. Generally, sulfate limited cultures presented higher cell volume, a response possibly related to growth rate (Banse 1976). Also, protein pool size increased upon sulfate limitation, as well as carbon storage pools – also relatable to slower growing cells (Shuter 1979) – which are not the same for all microalgae. Whereas green, red algae, and diatoms store carbon as lipids (Kurpan Nogueira et al. 2015), dinoflagellates preferentially store carbon as carbohydrates (Hitchcock 1983). Interestingly, protein pools were only significantly higher in S limited treatments when calculated on a per cell basis. On a per volume basis (see Supplemental Table 3), protein pools were always essentially the same, regardless of sulfate concentration, indicating that the raise in cell volume might be a strategy to maintain the protein quotas. Similar results were found by Prioretti and Giordano (2016) growing a cyanobacteria, a green alga, a diatom and a dinoflagellate in low sulfate, but still in the mM range, indicating that such responses may not be specific to sulfur limitation. Also, Giordano et al. (2000) observed a raise in free non-sulfated amino acid pools in sulfur limited *Dunaliella salina* cells. Considering that free amino acids serve as chromogenic groups for the method used for protein determination in this thesis (Chou and Goldstein 1960; see Section 5.2.5), it is not possible to discuss whether the observed results are due to the same phenomena.

Highly sensitive species – the diatom and the dinoflagellate – showed: (i) elemental ratios dramatically imbalanced upon sulfate limitation (whereas only C:S and N:S were affected in the green and red alga; Table 8 and Table 11); and (ii) photosynthetic efficiency was significantly lower in S limited treatments (Table 11). Regarding elemental composition, Prioretti and Giordano (2016) suggested that the micronutrients' usage efficiency may have played an important role on phytoplankton composition throughout history. In fact, the number and significance of elemental ratios that were imbalanced in S limited cells when compared to S replete ones were directly proportional

to the species' sensitivity to sulfur limitation (Table 11). Interestingly, although it is proposed that chlorophyll *a + c* microalgae requires less iron as compared to red and green algae (Quigg et al. 2003), iron cell quotas increased significantly in S limited cells of the diatom and the dinoflagellate (Figure 28), indicating an association between sulfur metabolism and iron requirement. Moreover, the bi-plot PCA graph (Figure 29) suggests that sulfate limitation leads *T. suecica* and *P. purpureum*'s biomasses to a macroelemental composition (C, N, P and S) similar to that observed on *P. tricornutum* and *A. carterae*'s, which are indifferent to sulfate availability. Consequently, the apparent homeostasis of the main macroelements in *P. tricornutum* and *A. carterae* plus the perturbation of other elements' cell quotas – as represented by iron – upon sulfate limitation, resulted on a more severe elemental imbalance in those species (Table 11).

**Table 11:** Comparison between elemental ratios of *T. suecica*, *P. purpureum*, *P. tricornutum* and *A. carterae* grown in S replete and S limited modified AMCONA medium. Asterisks indicate differences between treatments (\* =  $p < 0,05$ ; \*\* =  $p < 0,01$ ; \*\*\* =  $p < 0,001$ ).

Species	Elemental Ratios						
	C:N	C:S	N:S	S:P	S:K	S:Ca	S:Fe
<i>Tetraselmis suecica</i>		**	**				
<i>Porphyridium purpureum</i>		*	**				
<i>Phaeodactylum tricornutum</i>	**	*	***	*			*
<i>Amphidinium carterae</i>		**	**	**	*	**	***

The correlation between nutrients' balance and photosynthesis can be rather causal than independent (Falkowski and Raven 2007). Photosynthesis entails the use of sulfur in virtually every level of the process, from components of the electron transport chain – e.g.: Fe-S clusters – to carriers of the generated reducing power – e.g.: ferredoxin (Norici et al. 2005). However, variations in photosynthetic parameters were mild, if any, in the experimental species under sulfur limitation (see Section 5.3.5). The PSII maximum quantum yield ( $F_v/F_m$ ) decreased significantly only for the diatom *P. tricornutum* and the dinoflagellate *A. carterae*, coinciding with the high sensitivity to sulfur limitation observed by these algae (Table 9). Similarly, sulfur-starved rice (*Oryza sativa*) showed significant loss of photosynthetic efficiency (Lunde et al. 2008). In contrast, *T. pseudonana*, *P. reticulatum* and *E. huxleyi* did not show lower  $F_v/F_m$  when exposed to sulfur limiting conditions (Ratti et al. 2011), indicating that even though growth can be impaired by lower photosynthetic efficiency, it is not the driving force for

limitation in this case. Many causes can be addressed to the impairment of photosynthetic efficiency. In sulfur-starved rice, for example, Lunde et al. (2008) observed a pronounced decrease in the amount of Rubisco, which was not quantified in this thesis. Likewise, Giordano et al. (2000) observed a smaller amount of Rubisco in sulfur-limited *D. salina* but did not assess photosynthetic parameters. Varying pigments' composition may also imbalance the amount of energy reaching the reaction centers and impair photosynthetic efficiency. However, this is not compatible with the results, since all species – except the dinoflagellate – had significant differences in pigments contents and ratios, but not in  $F_v/F_m$ .

The ability to quench excessive energy may also affect photosynthetic efficiency and, indeed, both the diatom and the dinoflagellate showed a reduced NPQ in sulfur limited cells. This might be due to the importance of sulfated amino acids on the composition of the enzymes that regulate the xanthophyll cycle, a major NPQ process: violaxanthin / diadinoxanthin de-epoxidase contains 12 highly conserved cysteine residues (Simionato et al. 2015) and zeaxanthin / diatoxanthin epoxidase, 12 methionine residues (Coesel et al. 2008). In turn, NPQ of *T. suecica* was not affected by sulfate availability, suggesting that NPQ mechanisms of the green algae are less dependent on sulfur. In fact, it has been shown that light harvesting complex-stress related (LHCSR) proteins, which regulates NPQ, function differently in green algae and diatoms (Bailleul et al. 2010, Zhu and Green 2010, Lepetit et al. 2017) The red alga *P. purpureum*, on the other hand, showed the lowest and most divergent NPQ response between S replete and S limited treatments. Many red algae rely on phycobilisomes' mobility as main quenching mechanism (Kaňa et al. 2014). And, it has been shown in cyanobacteria that the lipid composition of photosynthetic membranes strongly influences the mobility of phycobilisomes (Sarcina et al. 2001), and that the balance of sulfo- and phospholipids in the cell membranes can vary widely upon nutrient limitation (Van Mooy et al. 2006). It is possible that the lipid composition of *P. purpureum*'s photosynthetic membranes was altered and, therefore, phycobilisome's diffusion and NPQ were impaired. In sum, the diversity of the photosynthetic apparatus and regulatory mechanisms in different algae (Niyogi and Truong 2013) might contribute to the diversified effects of sulfur limitation here presented.

ATP Sulfurylase is certainly intriguing in terms of phylogenetic origins (see Chapter 3), modes of regulation (Prioretti et al. 2016), fusions and locations (Bradley et al. 2009). In fact, the recent revelation of a remarkable heterogeneity of ATPSes in

microalgae by Prioretti et al. (2016) led to the suggestion that this enzyme could be the main regulatory step of the sulfate assimilatory pathway in these microorganisms. Such idea contrasts to what was previously believed based on vascular plants – that sulfate assimilation is mainly regulated via APR/APK – and was tested by Prioretti and Giordano (2016) by measuring ATPS activity of microalgae belonging to different taxa exposed to high (30 mM) and low (5 mM) concentrations of sulfate. The choice for ‘high’ and ‘low’ concentrations of sulfate was arbitrary and not limiting for every species, and the results showed no particular trends among algal groups. In this thesis, the response of ATPS activity to proven sulfur limitation was different when comparing microalgae containing green and red plastids in comparison with the S replete regime. Impacts of sulfur availability on ATPS activity, however, did not seem to explain the diverse sensitivity to sulfur availability observed among the red plastid species (Figure 25 and Figure 34). The two species whose ATPS activity responded similarly to sulfur limitation showed very different sensitivity to low concentrations of sulfur – i.e.: *P. purpureum* was more resistant, and *P. tricornutum* more sensitive. In turn, enzymatic activity of *A. carterae* as a function of sulfur concentration showed the unique behavior to decrease in S limited cells. Similar results were found by Prioretti and Giordano (2016) in another dinoflagellate belonging to the same genus, confirming the frequently observed divergence of dinoflagellates’ metabolism from that of other algae (Butterfield et al. 2013).

Amongst the tested parameters, the physiological responses of microalgae to sulfur limitation can be finally grouped into three categories. First, those generic responses, that were essentially the same in all species, like the impairment of growth, increase of cell volume (Table 6), and the changes in the main macromolecular pools (Table 7 and Figure 27). It is hard to assume whether those are specific responses to growth limitation by sulfate, or responses to growth limitation *per se* (Droop 1973, Banse 1976). Secondly, one measured parameter that behaved differently between green- and red-plastid algae: ATPS activity (Figure 34). Within the red-plastid algae, ATPSes of the red alga and the diatom behaved very similarly, indicating that this chloroplastic enzyme might have been transmitted to diatoms by the red algal ancestor. This assumption, however, contradicts most evidences based on sequence analysis and *in vitro* regulation tests (see Chapter 3; Patron et al. 2008, Prioretti et al. 2014, 2016) that suggest different origin and regulation for diatoms’ ATPS compared to the red algal one. At last, the elemental balance – especially microelemental – and photosynthetic efficiency that were

particularly affected in the secondary red endosymbionts: the diatom and dinoflagellate (Table 9; Table 11). Put in context, those physiological responses are in line with the SFH, which means that the growth of chlorophyll *a + c* microalgae is suppressed in low sulfate concentrations where green lineage microalgae thrives optimally.

## 5.5. Supplemental material – Chapter 5

**Supplemental Table 3:** Parameters calculated on a biovolume basis of the four experimental microalgae grown in S replete and S limited modified AMCONA medium. The data are the means of at least three biological replicates ( $n \geq 3$ )  $\pm$  standard deviation. Asterisks represent significant differences of the given parameter between treatments of the same species ( $p < 0,05$ ).

Parameters (mass <sup>†</sup> · $\mu\text{m}^{-3}$ )	Microalgae							
	<i>Tetraselmis suecica</i>		<i>Porphyridium purpureum</i>		<i>Phaeodactylum tricornerutum</i>		<i>Amphidinium carterae</i>	
	S replete	S limited	S replete	S limited	S replete	S limited	S replete	S limited
<b>Chlorophyll a</b>	5,13 $\pm$ 0,19	2,83 $\pm$ 0,26*	2,49 $\pm$ 0,43	1,29 $\pm$ 0,26*	2,25 $\pm$ 0,28	1,25 $\pm$ 0,06*	1,24 $\pm$ 0,08	1,23 $\pm$ 0,04
<b>Chlorophyll b</b>	2,36 $\pm$ 0,22	1,06 $\pm$ 0,12*	-	-	-	-	-	-
<b>Chlorophyll c</b>	-	-	-	-	0,33 $\pm$ 0,06	0,37 $\pm$ 0,05	0,45 $\pm$ 0,04	0,48 $\pm$ 0,02
<b>Phycobilliproteins</b>	-	-	10,41 $\pm$ 0,99	11,50 $\pm$ 1,08	-	-	-	-
<b>Proteins</b>	137,33 $\pm$ 10,88	165,85 $\pm$ 31,51	146,97 $\pm$ 27,24	190,71 $\pm$ 23,56	154,01 $\pm$ 44,92	177,31 $\pm$ 32,23	52,61 $\pm$ 3,61	68,18 $\pm$ 7,66*
<b>Carbon</b>	406,55 $\pm$ 146,15	418,78 $\pm$ 26,30	202,35 $\pm$ 60,25	249,75 $\pm$ 35,18	453,80 $\pm$ 53,08	330,59 $\pm$ 1,92*	24,39 $\pm$ 5,71	33,30 $\pm$ 2,73
<b>Nitrogen</b>	23,88 $\pm$ 7,21	24,14 $\pm$ 7,08	25,78 $\pm$ 9,36	36,19 $\pm$ 7,25	50,32 $\pm$ 6,28	46,15 $\pm$ 2,78	8,60 $\pm$ 2,09	12,41 $\pm$ 1,87
<b>Sulfur</b>	2058,14 $\pm$ 399,46	903,13 $\pm$ 411,99*	2339,87 $\pm$ 525,44	1017,49 $\pm$ 189,68*	1707,64 $\pm$ 282,74	1004,78 $\pm$ 209,31*	484,70 $\pm$ 115,15	154,13 $\pm$ 43,49*
<b>Phosphorus</b>	1070,10 $\pm$ 290,31	729,13 $\pm$ 336,50	911,40 $\pm$ 204,43	491,66 $\pm$ 166,53	896,74 $\pm$ 125,02	957,61 $\pm$ 299,22	192,12 $\pm$ 33,54	201,25 $\pm$ 34,44
<b>Potassium</b>	777,30 $\pm$ 128,79	522,93 $\pm$ 210,37	1269,42 $\pm$ 154,38	506,42 $\pm$ 341,99*	302,20 $\pm$ 78,14	190,96 $\pm$ 112,22	66,45 $\pm$ 31,03	72,50 $\pm$ 21,75
<b>Calcium</b>	2426,80 $\pm$ 394,44	1184,03 $\pm$ 491,36*	687,38 $\pm$ 219,12	248,58 $\pm$ 92,06*	580,07 $\pm$ 152,65	486,98 $\pm$ 205,68	134,75 $\pm$ 46,02	206,51 $\pm$ 46,08
<b>Iron</b>	315,98 $\pm$ 69,51	197,32 $\pm$ 17,54	395,58 $\pm$ 169,91	258,55 $\pm$ 54,22	499,76 $\pm$ 138,35	779,44 $\pm$ 268,65	108,32 $\pm$ 13,99	226,72 $\pm$ 55,06*
<b>Manganese</b>	5,78 $\pm$ 1,27	4,56 $\pm$ 1,78	14,32 $\pm$ 7,15	12,58 $\pm$ 5,34	6,16 $\pm$ 4,08	6,05 $\pm$ 3,71	0,97 $\pm$ 0,14	0,50 $\pm$ 0,12*
<b>Copper</b>	3,69 $\pm$ 0,73	2,73 $\pm$ 1,60	2,48 $\pm$ 1,55	0,90 $\pm$ 0,32	3,88 $\pm$ 2,35	7,38 $\pm$ 4,45	1,12 $\pm$ 0,17	1,10 $\pm$ 0,30
<b>Zinc</b>	25,28 $\pm$ 1,19	15,63 $\pm$ 5,90	48,97 $\pm$ 12,99	32,99 $\pm$ 10,65	28,42 $\pm$ 9,51	33,67 $\pm$ 12,38	6,07 $\pm$ 0,59	7,14 $\pm$ 0,94

<sup>†</sup> Pigments, proteins, C and N are represented in ng· $\mu\text{m}^{-3}$ . S, P, K, Ca, Fe, Mn, Cu and Zn are presented in fg· $\mu\text{m}^{-3}$ .

## 6. GROWTH OF *P. TRICORNUTUM* IN OTHER SOURCES OF SULFUR

### 6.1. Introduction

Assessment of growth under different sources of nutrients – in this case, sulfur – consists on an efficient tool to suggest and determine possible mechanisms of cellular transports and conversions. For example, in C4 plants, sulfate is reduced only in the bundle sheath cells and L-cysteine is then transported to leaves (Burgener et al. 1998). Also, the coccolithophorid *Hymenomonas carterae* was able to thrive in sulfate-free growth medium enriched with sulfite, thiosulfate and L-cysteine, but not with L-methionine (Vairavamurthy et al. 1985), suggesting either a specific amino acid transport, or a limited amino acidic conversion. However, the identity of an L-cysteine transporter in plants and algae is still obscure (Gigolashvili and Kopriva 2014). The utilization of different sources of sulfur in growth media can be used to recover and/or complement genetically engineered strains. In fact, the chemical complementation with sodium sulfide ( $\text{Na}_2\text{S}$ ) was able to recover the lethal or, at least, very compromising silencing of SiR in *Arabidopsis thaliana* (Khan et al. 2010). Likewise, growth of a sulfate-starved green alga *Parachlorella kessleri* was successfully complemented with L-cysteine (Yamazaki et al. 2018). By adding L-cysteine, the authors were also able to partially complement – as compared to the wild-type – the growth of *P. kessleri* mutants that showed limited growth in sulfate-replete conditions.

This section describes an ongoing study that investigates the responses of growth, physiology, and biochemical composition of the model diatom *P. tricornutum* in the presence of alternative sources of sulfur instead of sulfate in the growth medium. Such investigation is inserted in the context of attempting to recover possibly lethal ATPS knockout mutants shown in Chapter 4. ATPS catalyzes sulfate activation, the first committed step into both primary and secondary sulfate assimilation routes and, reasonably, its knockout could severely or completely impair algal growth. Providing other sources of sulfur, containing more reduced sulfur than sulfate, might diminish the need of the activation step catalyzed by ATP Sulfurylase and, hence, render acclimated cells capable of growing with little or no ATPS activity.

Hence, in this chapter,  $\text{Na}_2\text{SO}_4$  was substituted by L-cysteine and  $\text{Na}_2\text{S}$  as the only sources of sulfur in AMCONA medium. The downstream usage of the more reduced sulfur present in cysteine and sodium sulfide and the possibility to skip the requirement

of a sulfate activation step were assessed. Hitherto, the complementation of ATPS-knockout transformant cell lines was only hypothesized.

## 6.2. Material and Methods

Growth and physiological characteristics of the model diatom *P. tricornutum* were assessed in modified AMCONA medium (Fanesi et al. 2014) where Na<sub>2</sub>SO<sub>4</sub> was substituted by L-cysteine (final concentration 1 mmol·L<sup>-1</sup>; Yamazaki et al. 2018) and Na<sub>2</sub>S (final concentration 100 μmol·L<sup>-1</sup>; Khan et al. 2010) as the only sources of sulfur.

Culture conditions were the same as that described in Section 5.2.1, except the different sources of sulfur on culture medium as mentioned above. Biochemical and physiological parameters investigated were (i) growth rate, cell density and cell volume; (ii) pigments' contents; (iii) absolute proteins values and semi-quantification of lipids and carbohydrates pools; (iv) elemental composition with the exception of carbon and nitrogen measurements; (v) photosynthetic parameters; and (vi) ATP-S activity. All these measurements were made according to that described in Section 5.2 and were compared to results of Na<sub>2</sub>SO<sub>4</sub>-replete or -limited cultures, as shown in Chapter 5.

## 6.3. Results

### 6.3.1. Growth

All measured growth parameters of cultures enriched with L-cysteine and Na<sub>2</sub>S were similar to that observed on Na<sub>2</sub>SO<sub>4</sub> replete (25 mmol·L<sup>-1</sup>) cultures and different to that of Na<sub>2</sub>SO<sub>4</sub> limited (1 μmol·L<sup>-1</sup>) cultures. The results of Na<sub>2</sub>SO<sub>4</sub> replete and limited cultures are those previously showed and discussed in Chapter 5.

Photoautotrophic batch growth curves (12:12h photoperiod) at 20 ± 2°C of *P. tricornutum* cells illuminated with 100 μmol photons·m<sup>-2</sup>·s<sup>-1</sup> in AMCONA medium (Fanesi et al. 2014) enriched with different sources of sulfur and different concentrations of Na<sub>2</sub>SO<sub>4</sub> are showed in Figure 35. Exponential growth was maintained for about 5 days, followed by a smooth deacceleration, reaching stationary phase after around 8 days of cultivation. This behavior was not affected neither by sulfur source nor by its availability.

Specific growth rates, final cell yields, and average cell volumes during exponential phase were essentially the same ( $p > 0,05$ ) for cells enriched with replete Na<sub>2</sub>SO<sub>4</sub>, Na<sub>2</sub>S and L-cysteine (Figure 36). Growth rates and cell yields were about 83 and 117% higher than those observed in Na<sub>2</sub>SO<sub>4</sub> limited cultures, respectively; whereas, contrarily, cell volume significantly decreased (ca. 43%) in all replete cultures.

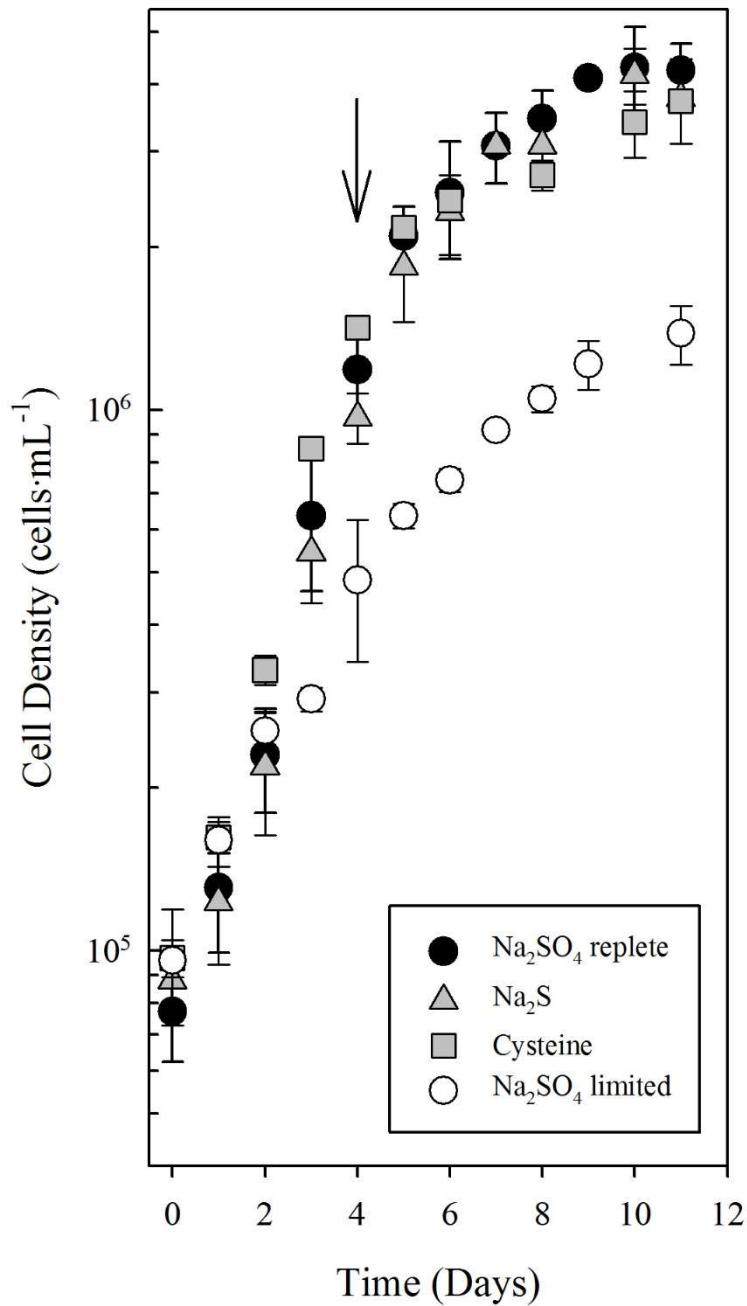


**Figure 35:** Photoautotrophic batch growth (12:12h photoperiod) of *P. tricorntutum* at  $20\pm 2^\circ\text{C}$  illuminated with  $100\ \mu\text{mol photons}\cdot\text{m}^{-2}\cdot\text{s}^{-1}$  in AMCONA medium enriched with  $25\ \text{mmol}\cdot\text{L}^{-1}$  (replete; black circles) or  $1\ \mu\text{mol}\cdot\text{L}^{-1}$  (limited; white circles)  $\text{Na}_2\text{SO}_4$ ;  $\text{Na}_2\text{S}$  (gray triangles); and L-cysteine (gray squares). Each growth curve shows the means of three to nine independent experiments ( $3\leq n\leq 9$ ), error bars show standard deviation. The arrows indicate the sampling day for biomass analyses.

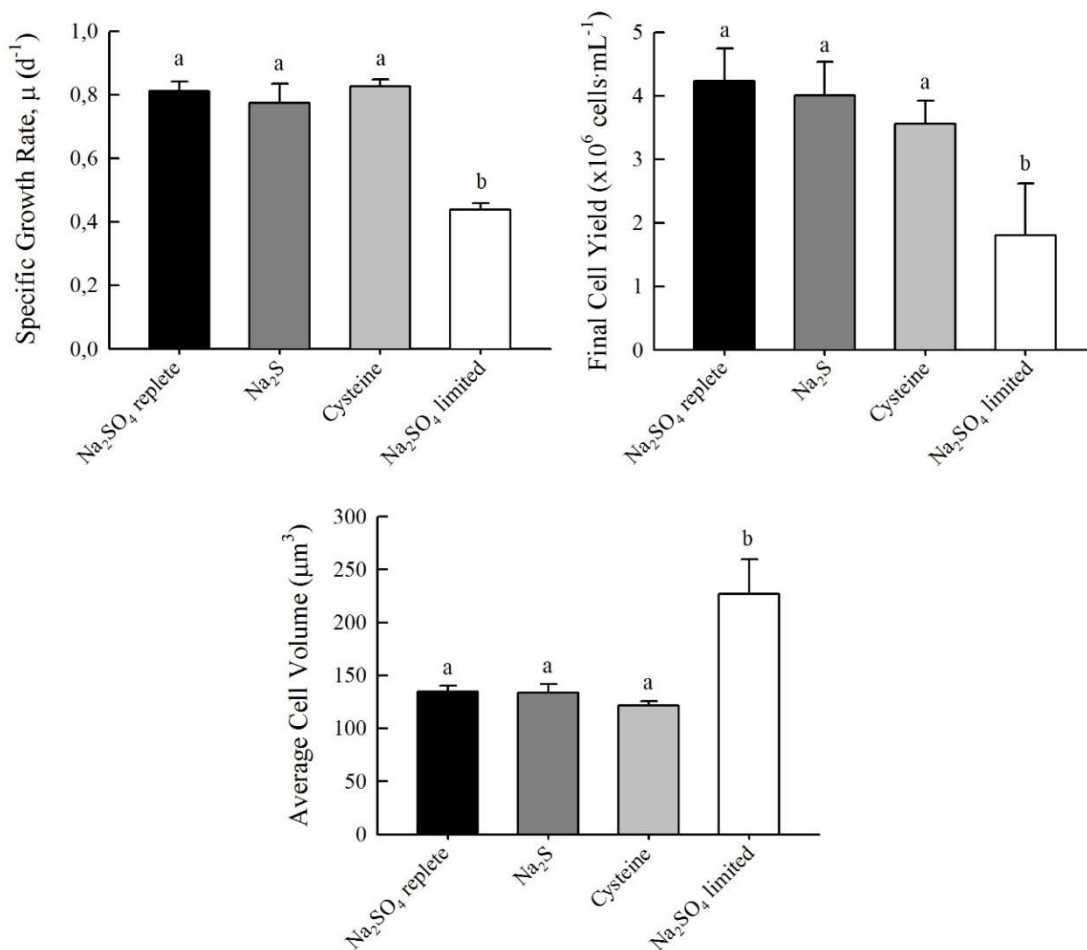


**Figure 36:** Specific growth rate, final cell yield and average cell volume of *P. tricornutum* grown at  $20 \pm 2^\circ C$  illuminated with  $100 \mu mol photons \cdot m^{-2} \cdot s^{-1}$  in AMCONA medium enriched with  $25 mmol \cdot L^{-1}$  (replete; black bars) or  $1 \mu mol \cdot L^{-1}$  (limited; white bars)  $Na_2SO_4$ ;  $Na_2S$  (dark gray bars); and L-cysteine (light gray bars). Data is shown as the means of three to nine independent experiments ( $3 \leq n \leq 9$ ), error bars show standard deviation. Different letters over bars represent statistically significant differences ( $p < 0,05$ ).

### 6.3.2. Macromolecular pools

In accordance to what was observed for growth, the biochemical composition of *P. tricornutum* cells grown with alternative sources of sulfur were very similar to that obtained when cells were grown in sulfate-rich medium (Figure 37). In fact, the absolute values of proteins calculated per cell and the semi-quantification of lipids based on protein content were the same for sulfate-,  $Na_2S$ - and cysteine-enriched AMCONA medium, only differing ( $p < 0,05$ ) from that observed on sulfate-limited growth. Furthermore, total chlorophylls ( $a + c$ ) content was always the same, regardless of S source or availability. On the other hand, the semi-quantification of carbohydrates per cell showed that not only

sulfate-limited cells results were significantly higher, but also the Na<sub>2</sub>S-enriched growth resulted in significantly lower amounts of sugars in cells when compared to sulfate-rich ones.

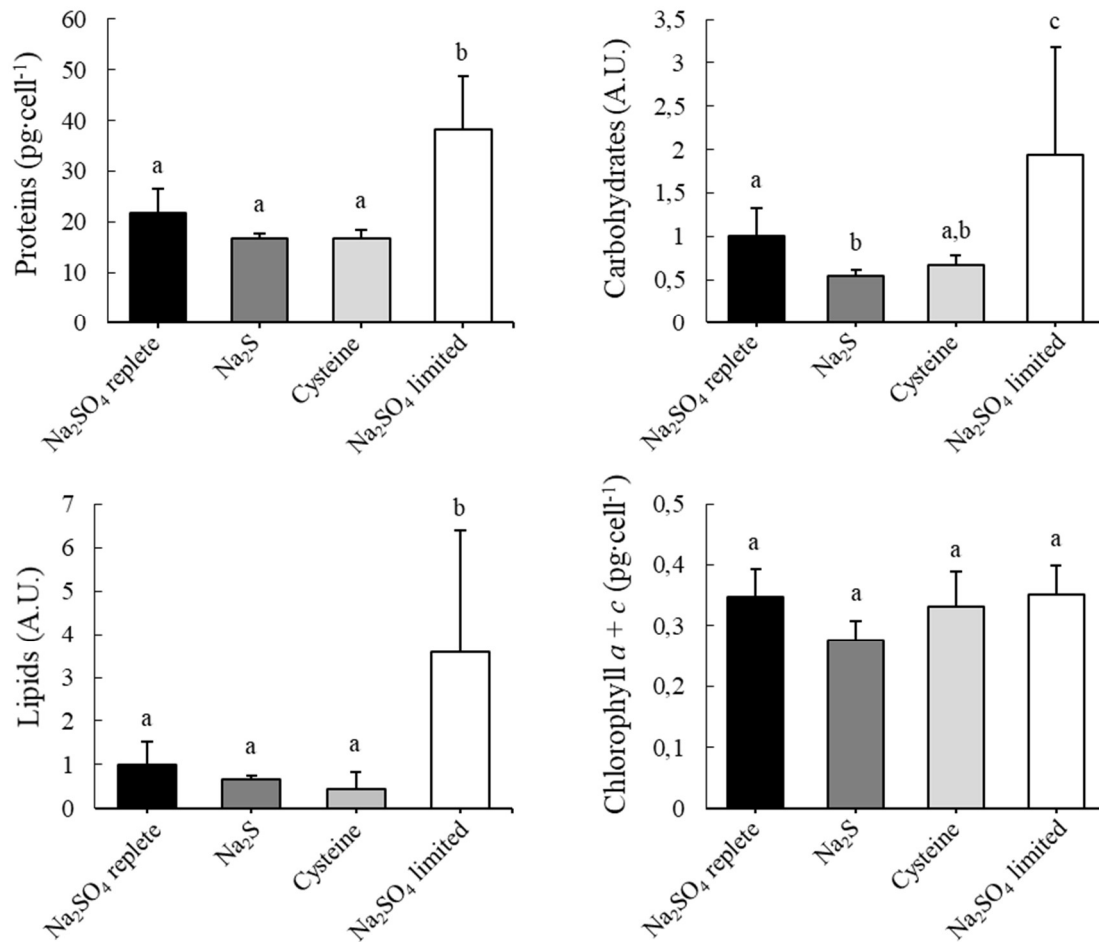


**Figure 37:** Proteins, carbohydrates, lipids and chlorophyll pools of *P. tricornutum* grown at 20±2°C illuminated with 100 μmol photons·m<sup>-2</sup>·s<sup>-1</sup> in AMCONA medium enriched with 25 mmol·L<sup>-1</sup> (replete; black bars) or 1 μmol·L<sup>-1</sup> (limited; white bars) Na<sub>2</sub>SO<sub>4</sub>; Na<sub>2</sub>S (dark gray bars); and L-cysteine (light gray bars). Arbitrary units (A.U.) used for carbohydrates and lipids were calculated based on the absolute measurements of proteins per cell and the macromolecular ratios obtained by FTIR, sulfate replete condition was set to 1 (see Section 5.2.6.1). Data is shown as the means of three to six independent experiments (3≤n≤6), error bars show standard deviation. Different letters over bars represent statistically significant differences (p<0,05).

### 6.3.3. Elemental composition

As previously discussed in Chapter 5, *P. tricornutum*'s elemental composition is substantially affected by sulfate availability. Although its impacts may be observed on elements' measurements per cell – e.g.: nitrogen and iron –, they are more pronounced when the elements' proportions as a function of sulfur are assessed. In general, when cells were grown in alternative sources of sulfur – Na<sub>2</sub>S and L-cysteine –, elemental cell quotas were very similar to those found in Na<sub>2</sub>SO<sub>4</sub>-replete cultures. The only exception was copper, whose values were essentially the same for Na<sub>2</sub>SO<sub>4</sub>-limited, Na<sub>2</sub>S- and cysteine-enriched cultures, and higher than those found in sulfate-replete cells (Figure 38).

Sulfur based elemental ratios (Figure 39) showed an apparent, yet statistically unsubstantiated, decrease of S:P, S:K, S:Ca and S:Mn in Na<sub>2</sub>S-enriched cultures when compared to all other treatments. Apart from that, few differences can be observed between the sulfate-replete cells and the ones enriched with alternative sources of S. The interesting exception is the S:Cu ratio, which resulted in lower values for Na<sub>2</sub>SO<sub>4</sub>-limited, Na<sub>2</sub>S- and cysteine-enriched cells when compared to Na<sub>2</sub>SO<sub>4</sub>-replete ones.

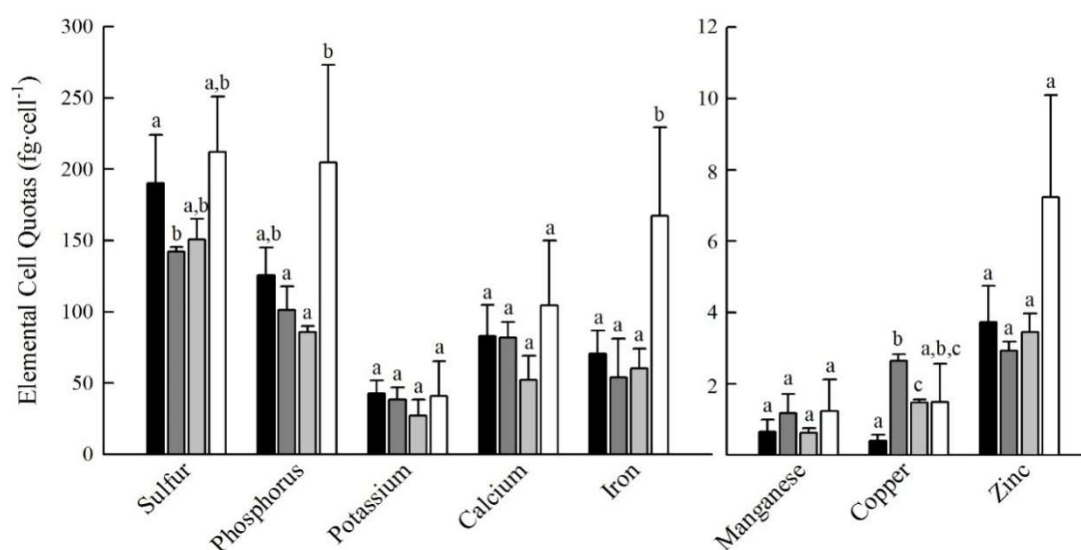


**Figure 38:** Elemental cell quotas of *P. tricornutum* grown in sulfate-replete (black bars), Na<sub>2</sub>S (dark gray bars), cysteine (light gray bars) and sulfate-limited (white bars) modified AMCONA medium at 20±2°C under 100 μmol photons·m<sup>-2</sup>·s<sup>-1</sup>. The data are the means of at least three biological replicates (n≥3) and error bars show standard deviation. Different letters over bars represent statistically significant differences for the same element cell quota between treatments.

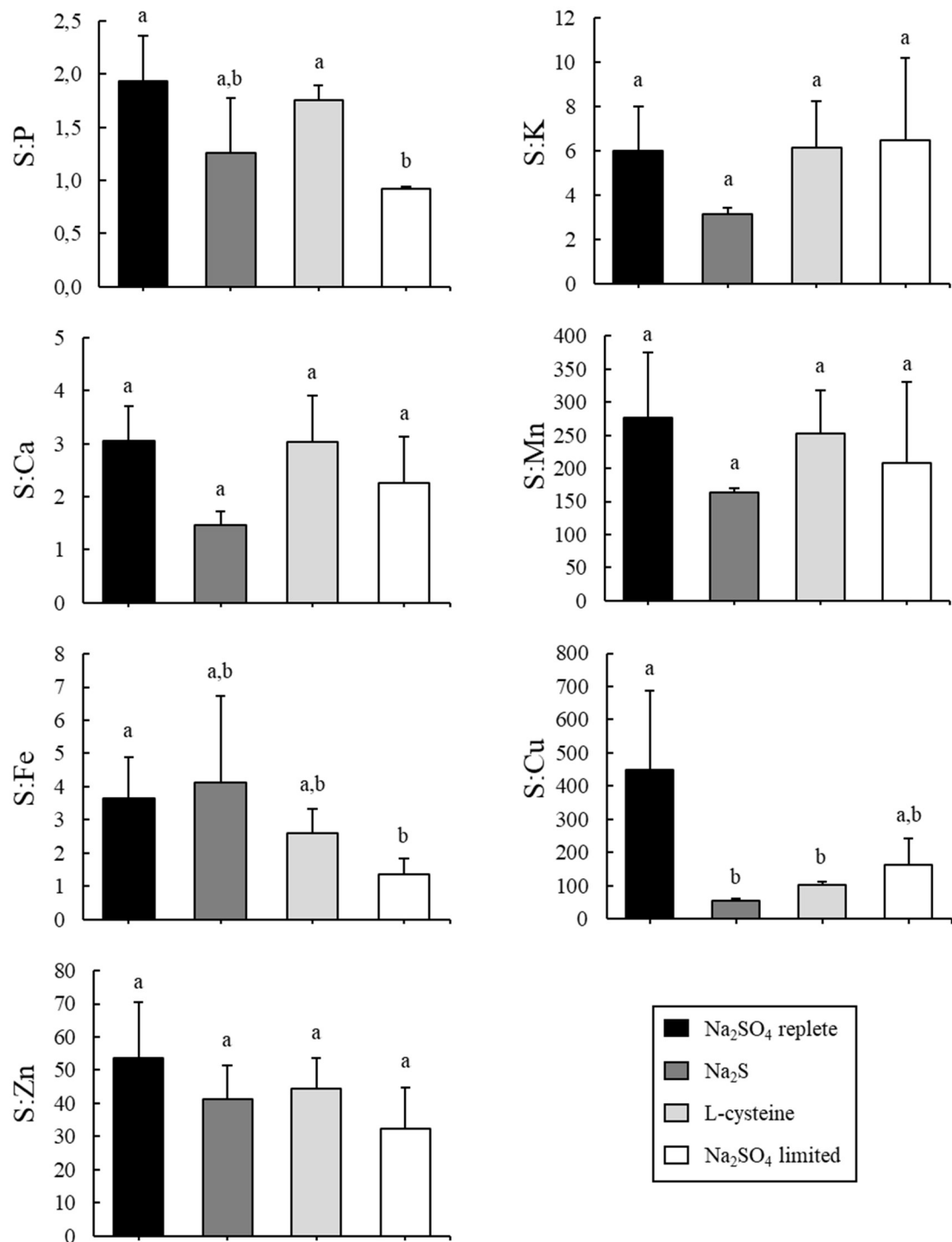


**Figure 39:** Elemental ratios of *P. tricorutum* grown in sulfate-replete (black bars), Na<sub>2</sub>S (dark gray bars), cysteine (light gray bars) and sulfate-limited (white bars) modified AMCONA medium at 20±2°C under 100 μmol photons·m<sup>-2</sup>·s<sup>-1</sup>. The data are the means of at least three biological replicates (n≥3) and error bars show standard deviation. Different letters above bars indicate statistically significant differences (p<0,05).

### 6.3.4. Photosynthetic parameters

As seen in Chapter 5, light curves (LC) of *P. tricornutum* were not affected by sulfate availability. However, significant differences were observed in LCs when cells were cultivated with other sources of sulfur. Interestingly, the most pronounced differences were found when Na<sub>2</sub>S-enriched cultures were compared to those supplied with L-cysteine (Figure 40). Whereas  $\alpha$  was the same in all treatments, in Na<sub>2</sub>S-enriched cells rETR<sub>max</sub> and E<sub>k</sub> were significantly lower when compared to all other conditions (Table 12). The same was true for the maximum PSII quantum efficiency (F<sub>v</sub>/F<sub>m</sub>), which was lower when cells were grown in Na<sub>2</sub>S, reaching similar values to those found in sulfate-depleted cultures. Contrarily, when *P. tricornutum* was grown in L-cysteine, F<sub>v</sub>/F<sub>m</sub> was significantly higher, even when compared to the standard sulfate-replete conditions (Table 12).

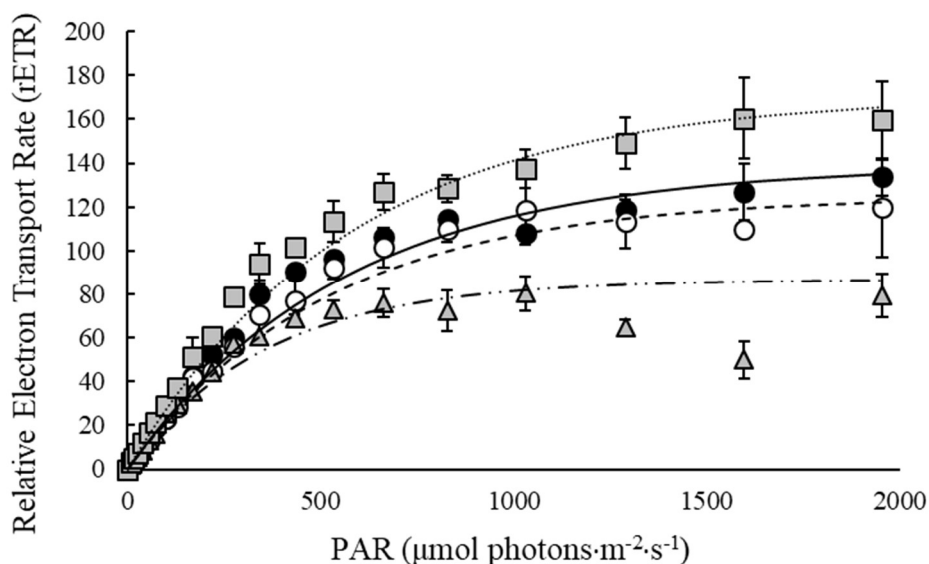


**Figure 40:** Relative electron transport rate as a function of light, and its fitted curve of *P. tricornutum* grown in sulfate replete (black circles; continuous line), sulfate limited (white circles; dashed line), Na<sub>2</sub>S- (gray triangles; dashed and dotted line), and L-Cysteine- (gray squares; dotted line) modified AMCONA medium at 20±2°C illuminated with 100  $\mu\text{mol photons}\cdot\text{m}^{-2}\cdot\text{s}^{-1}$ . Data are shown as the means of three to six independent replicates ( $3\leq n\leq 6$ ) and error bars show standard deviation.

**Table 12:** Photosynthetic efficiency ( $F_v/F_m$ ) and rapid light curve's parameters ( $\alpha$ ,  $rETR_{max}$ ,  $E_k$ ) of *P. tricornutum* grown in sulfate replete, sulfate limited,  $Na_2S$ , and L-cysteine enriched modified AMCONA medium at  $20\pm 2^\circ C$  under irradiance of  $100 \mu mol photons \cdot m^{-2} \cdot s^{-1}$ . All parameters were determined during exponential growth phase. Data are the means of three to six independent experiments ( $3 \leq n \leq 6$ )  $\pm$  standard deviation. Superscript letters on the same column represent statistically significant differences ( $p < 0,05$ ).

Treatments	Photosyntetic parameters			
	$F_v/F_m$	$\alpha$	$rETR_{max}$	$E_k$
<b>Na<sub>2</sub>SO<sub>4</sub> replete</b>	0,563 $\pm$ 0,008 <sup>a</sup>	0,248 $\pm$ 0,009 <sup>a</sup>	137,57 $\pm$ 8,75 <sup>a,c</sup>	554,54 $\pm$ 30,49 <sup>a</sup>
<b>Na<sub>2</sub>S</b>	0,469 $\pm$ 0,041 <sup>b</sup>	0,242 $\pm$ 0,021 <sup>a</sup>	82,37 $\pm$ 9,64 <sup>b</sup>	341,99 $\pm$ 56,39 <sup>b</sup>
<b>L-Cysteine</b>	0,676 $\pm$ 0,038 <sup>c</sup>	0,298 $\pm$ 0,016 <sup>a</sup>	163,80 $\pm$ 17,74 <sup>a</sup>	550,21 $\pm$ 62,13 <sup>a</sup>
<b>Na<sub>2</sub>SO<sub>4</sub> limited</b>	0,470 $\pm$ 0,041 <sup>b</sup>	0,242 $\pm$ 0,035 <sup>a</sup>	133,13 $\pm$ 2,66 <sup>c</sup>	557,47 $\pm$ 76,68 <sup>a</sup>

In the beginning of the routine that consisted on an increase of light followed by relaxation in the dark (Figure 41), cysteine-enriched cells presented a higher quantum efficiency of photosystem II ( $\Phi PSII$ ) when compared to all other conditions. During the 20 one-minute steps of light increment, however, this parameter decreased reaching essentially the same values for all treatments. Meanwhile, non-photochemical quenching mechanisms of cysteine-enriched cells reached the highest values among the observed, especially for NPQ. During the five minutes of relaxation in darkness, PSII quantum yield and photochemical quenching (qL) of  $Na_2S$ -enriched cells took longer to relax, given that values were lower than all other treatments after one minute of darkness. Nevertheless, after five minutes, the photosynthetic apparatus of cells exposed to all treatments returned to the initial relaxed state for every measured parameter.

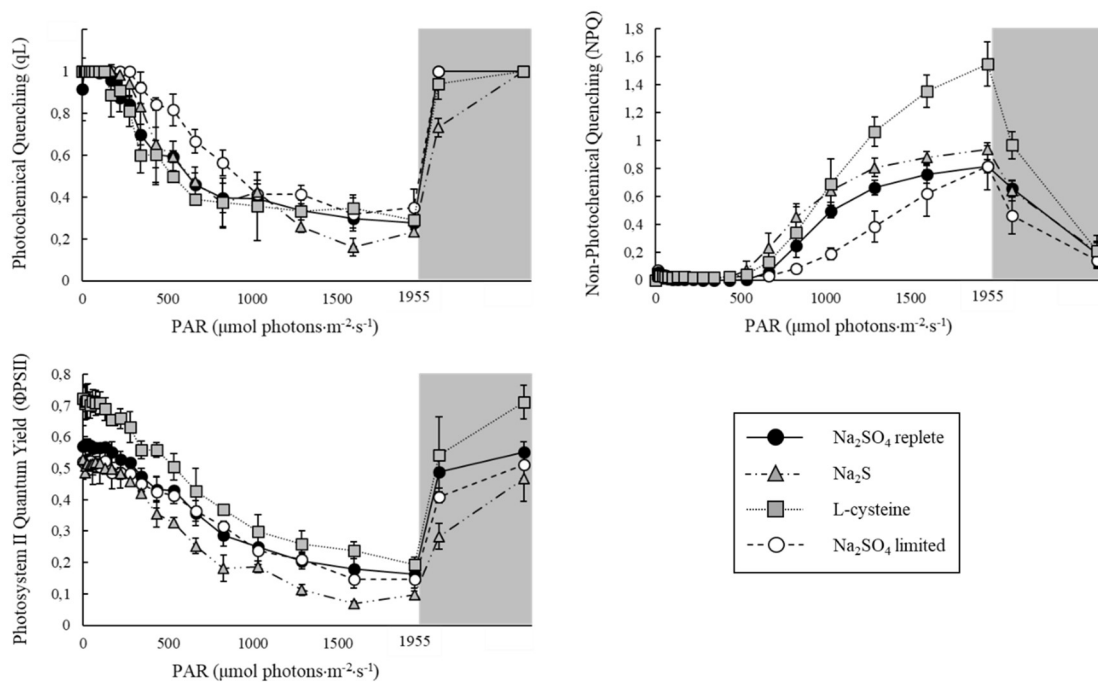


**Figure 41:** Photochemical (qL) and non-photochemical (NPQ) quenching, and photosystem II quantum yield ( $\Phi_{PSII}$ ) of *P. tricornutum* grown in sulfate replete (black circles; continuous line), sulfate limited (white circles; dashed line),  $\text{Na}_2\text{S}$ - (gray triangles; dashed and dotted line), and L-cysteine- (gray squares; dotted line) enriched modified AMCONA medium at  $20 \pm 2^\circ\text{C}$  under irradiance of  $100 \mu\text{mol photons}\cdot\text{m}^{-2}\cdot\text{s}^{-1}$ . Twenty steps (one minute each) of increasing PAR were followed by five minutes of recovery in darkness (gray area). Data are the means of three to six biological replicates ( $3 \leq n \leq 6$ ) and error bars show standard deviation.

### 6.3.5. ATP Sulfurylase activity

Activity of ATP Sulfurylase was not affected by the different tested sulfur sources in culture medium (Figure 42). As shown in Chapter 5, ATPS activity was comparatively higher in sulfate-limited cultures only when calculated on a per cell basis, due to variations on number and size of cells on those treatments. However, since there were no differences in cell number and/or size between the sulfate-replete cultures and the alternative sources of sulfur –  $\text{Na}_2\text{S}$  and L-cysteine –, enzyme activity was determined based on protein content of cell extracts. Differences per cell are expected to be the same when compared with  $\text{Na}_2\text{SO}_4$ -limited cells.

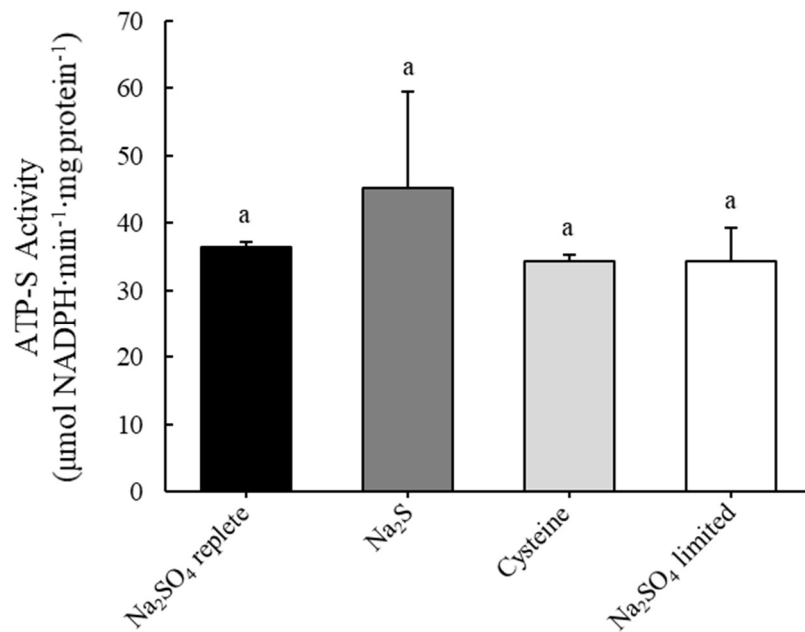


**Figure 42:** ATP Sulfurylase activity of *P. tricornutum* cell extracts cultivated in  $\text{Na}_2\text{SO}_4$ -replete (black bar);  $\text{Na}_2\text{S}$  (dark gray bar); L-cysteine (light gray bar) and  $\text{Na}_2\text{SO}_4$ -limited (white bar) AMCONA medium at  $20\pm 2^\circ\text{C}$  under irradiance of  $100 \mu\text{mol photons}\cdot\text{m}^{-2}\cdot\text{s}^{-1}$ . Data are the means of three to six biological replicates ( $3\leq n\leq 6$ ) and error bars show standard deviation. Different letters over bars indicate statistically significant differences ( $p < 0.05$ ).

## 6.4. Perspectives

The successful complementation of *P. tricornutum*'s growth with L-cysteine together with the higher copper cell quota achieved in these conditions (Figure 35, Figure 36 and Figure 38) may suggest, as proposed by Walsh et al. (2015), a Cys-Cu uptake system. The authors showed that cells take up more copper when cysteine is present, and it can increase the bioavailability of copper to Cu-limited cells of *E. huxleyi* and *T. pseudonana*. Furthermore, in this chapter *P. tricornutum* cells cultivated in sulfate-free growth medium complemented with sulfide also presented higher copper cell quotas as compared to control conditions, albeit not as high as those grown in cysteine (Figure 38). The existence of such transporter or any specific cysteine transporter, however, is unclear (Gigolashvili and Kopriva, 2014). Evidences from this thesis and from literature (Vairavamurthy et al. 1985; Burgener et al. 1998; Walsh et al. 2015; Yamazaki et al. 2018) foresee a fruitful investigation of microalgal transporters involved on sulfur metabolism.

The activity of ATPS, however, was not affected by the sulfur source or availability (Figure 42). Although this data suggests that the sulfate activation step is still required within cells, the ATPS activity assay protocol does not necessarily reflect the *in vivo* scenario (Burnell, 1984). In turn, it shows that the enzyme is still present and active in the protein extraction medium. As highlighted in the Introduction, this chapter reports a study associated to that presented in Chapter 4, as an attempt to recover possibly lethal ATPS-knockout transformant cells. In this sense, the results of growth, physiology and biochemical composition of *P. tricornutum* cells grown in sulfate-free medium complemented with L-cysteine and Na<sub>2</sub>S encourages a future attempt of recovering ATPS-knockout cell lines. Virtually every biochemical aspect that was compromised upon sulfate limitation reached essentially the same values as those of sulfate-replete medium.

## 7. CONCLUSIONS

Although the localization of the enzymatic machinery involved in sulfate assimilation in algae is consistent to what is assumed based on higher plants – specifically that sulfate assimilation happens primarily in the chloroplasts – the enzymes show a high degree of phylogenetic diversity. Results shown in Chapter 3 suggest that the study of some highly heterogenous and/or functionally plastic enzymes (e.g. SAT and OAS-TL) requires the addition of biochemical analyses to the strictly *in silico* investigation. As compared to the other enzymes analyzed, ATPS shows a remarkable heterogeneity, showing redox-sensitive and -insensitive forms of this enzyme and, hence, the potential for being a regulatory step of the pathway. Interestingly, results from Chapter 5 show that ATPS activity is sensitive to sulfur concentration only in some taxa, reinforcing its heterogeneity even amongst algae clades. Further studies are necessary for better understanding the regulation of sulfate assimilation in the various groups of phototrophs. For instance, in the case of *P. tricornutum*, activity of ATPS is regulated by light/dark exposure but, surprisingly, does not seem to be dependent on the redox state of the photosynthetic electron transport chain. The signal transduction might be carried out through other redox equivalents, capable of interacting with sources of reducing power other than photosynthesis, such as ferredoxin and/or glutaredoxin. Still regarding the model diatom, the localization of a redox-sensitive type of ATPS within the chloroplast and the prediction of a redox non-sensitive ATPS in the cytosol suggest a novel mode of regulation and sulfur partitioning. Although caution must be taken in generalizations, sequence similarity suggests that the mode of sulfur regulation and partitioning proposed in Chapter 4 is likely to be generally present in diatoms.

ATPS might be essential for survival, at least in diatoms, given that it was not possible to achieve ATPS-knockout colonies from *P. tricornutum* (Chapter 4). This model diatom, however, is capable of thriving optimally when culture medium is enriched with more reduced forms of sulfur ( $\text{Na}_2\text{S}$  and L-cysteine) instead of sulfate, a condition where sulfate activation – the reaction catalyzed by ATPS – could be unnecessary. Virtually all tested physiological parameters of  $\text{Na}_2\text{S}$ - and L-cysteine-enriched cells are successfully complemented to the same levels as to when sulfate is provided. Activity of ATPS in *P. tricornutum* was also essentially the same regardless of sulfur source, suggesting that the sulfate activation step is required. However, whilst the *in vitro* test proves that the enzyme is present and active in the protein extraction medium, it does not

necessarily mean that it is essential in live cells. These results encourage the attempt of the complementation of ATPS-knockout cell lines with Na<sub>2</sub>S or L-cysteine enriched culture media. This study, reported in Chapter 6, also encourages further investigation on microalgal transporters related to sulfur metabolism. In particular cysteine transporters, which are strongly suggested by indirect observations in literature, but not yet identified. In this thesis, results are indicative of a copper-cysteine transport system in red lineage algae, previously proposed by Walsh et al. (2015).

Growth of secondary endosymbionts evolved from red algae is limited in concentrations of sulfate much higher than those that limit growth of red and green primary endosymbionts. In a broad sense, this finding is a clear statement that the raise to dominance of marine red lineage algae during a period when sulfate concentration of seawater rapidly increased was not a mere coincidence, which corroborates with the Sulfate Facilitation Hypothesis. On the other hand, some aspects that were believed to physiologically explain the different sensitivity to sulfate among taxa seems to not necessarily apply, like the assumption that a lower C:S ratio would mean a higher sensitivity to sulfur starvation for example. According to results reported in Chapter 5, the metabolic link between algal physiology and their sensitivity to sulfate limitation appears to be the ability to maintain an elemental balance during such perturbation, given that the severity of elemental imbalance is directly proportional to the sensitivity to sulfur limitation. Together with the elemental cell composition, photosynthetic efficiency is a parameter hampered by sulfate limitation only in the more sensitive clades. Other investigated physiological traits, like the rearrangement of the main macromolecular pools and cell volume behaved very similarly when exposed to sulfur limitation and are likely to be a response to growth limitation *per se* instead of limitation by sulfur.

## 8. BIBLIOGRAPHY

- Andreae, M.O. 1986. The Ocean as a Source of Atmospheric Sulfur Compounds. *Role Air-Sea Exch. Geochemical Cycl.* 331–62.
- Apt, K.E., Kroth-Pancic, P.G. & Grossman, A.R. 1996. Stable nuclear transformation of the diatom *Phaeodactylum tricornutum*. *Mol. Gen. Genet.* 252:572–9.
- Archibald, J.M. 2009. The Puzzle of Plastid Evolution. *Curr. Biol.* 19:R81–8.
- Ayers, G.P. & Cainey, J.M. 2007. The CLAW hypothesis: A review of the major developments. *Environ. Chem.* 4:366–74.
- Bachvaroff, T.R., Gornik, S.G., Concepcion, G.T., Waller, R.F., Mendez, G.S., Lippmeier, J.C. & Delwiche, C.F. 2014. Dinoflagellate phylogeny revisited: Using ribosomal proteins to resolve deep branching dinoflagellate clades. *Mol. phylogeny Evol.* 70:314–22.
- Bailleul, B., Rogato, A., De Martino, A., Coesel, S., Cardol, P., Bowler, C., Falciatore, A. et al. 2010. An atypical member of the light-harvesting complex stress-related protein family modulates diatom responses to light. *Proc. Natl. Acad. Sci. U. S. A.* 107:18214–9.
- Baker, N.R. 2008. Chlorophyll fluorescence: A probe of photosynthesis in vivo. *Annu. Rev. Plant Biol.* 59:89–113.
- Banse, K. 1976. Rates of Growth, Respiration and Photosynthesis of Unicellular Algae As Related To Cell Size-a Review. *J. Phycol.* 12:135-140.
- Behrenfeld, M.J., Halsey, K.H. & Milligan, A.J. 2008. Evolved physiological responses of phytoplankton to their integrated growth environment. *Philos. Trans. R. Soc. B Biol. Sci.* 363:2687–703.
- Bennet, A. & Bogorad, L. 1973. Complementary chromatic adaptation in a filamentous blue-green alga. *J. Cell Biol.* 58:419–35.
- Bick, J.A., Dennis, J.J., Zylstra, G.J., Nowack, J. & Leustek, T. 2000. Identification of a new class of 5'-adenylylsulfate (APS) reductases from sulfate-assimilating bacteria. *J. Bacteriol.* 182:135–42.
- Birke, H., Müller, S.J., Rother, M., Zimmer, A.D., Hoernstein, S.N.W., Wesenberg, D., Wirtz, M. et al. 2012. The relevance of compartmentation for cysteine synthesis in phototrophic organisms. *Protoplasma.* 249:147–55.
- Bochenek, M., Etherington, G.J., Koprivova, A., Mugford, S.T., Bell, T.G., Malin, G. & Kopriva, S. 2013. Transcriptome analysis of the sulfate deficiency response in the

- marine microalga *Emiliana huxleyi*. *New Phytol.* 650–62.
- Bohrer, A.-S., Yoshimoto, N., Sekiguchi, A., Rykalski, N., Saito, K. & Takahashi, H. 2015. Alternative translational initiation of ATP sulfurylase underlying dual localization of sulfate assimilation pathways in plastids and cytosol in *Arabidopsis thaliana*. *Front. Plant Sci.* 5:1–10.
- Borowitzka, M.A. 2013. High-value products from microalgae-their development and commercialisation.
- Borowitzka, M.A., Beardall, J. & Raven, J. 2016. The physiology of microalgae. Springer. 673 pp.
- Bowler, C., Allen, A.E., Badger, J.H., Grimwood, J., Jabbari, K., Kuo, A., Maheswari, U. et al. 2008. The *Phaeodactylum* genome reveals the evolutionary history of diatom genomes. *Nature.* 456:239–44.
- Bradley, M.E., Rest, J.S., Li, W.H. & Schwartz, N.B. 2009. Sulfate activation enzymes: Phylogeny and association with pyrophosphatase. *J. Mol. Evol.* 68:1–13.
- Bromke, M.A., Hoefgen, R. & Hesse, H. 2013. Phylogenetic aspects of the sulfate assimilation genes from *Thalassiosira pseudonana*. *Amino Acids.* 44:1253–65.
- Bruce, B.D. 2001. The paradox of plastid transit peptides: Conservation of function despite divergence in primary structure. *Biochim. Biophys. Acta - Mol. Cell Res.* 1541:2–21.
- Brychkova, G., Grishkevich, V., Fluhr, R. & Sagi, M. 2013. An essential role for tomato sulfite oxidase and enzymes of the sulfite network in maintaining leaf sulfite homeostasis. *Plant Physiol.* 161:148–64.
- Buchanan, B.B. 1980. Role of Light in the Regulation of Chloroplast Enzymes. *Annu. Rev. Plant Physiol.* 31:341–74.
- Buchanan, B.B. & Balmer, Y. 2005. Redox regulation: A broadening horizon. *Annu. Rev. Plant Biol.* 56:187–220.
- Burgener, M., Suter, M., Jones, S. & Brunold, C. 1998. Cyst(e)ine Is the Transport Metabolite of Assimilated Sulfur from Bundle-Sheath to Mesophyll Cells in Maize Leaves. *Plant Physiol.* 116:1315–22.
- Burnell, J.N. 1984. Sulfate Assimilation in C<sub>4</sub> Plants. *Plant Physiol.* 75:873–5.
- Butterfield, E.R., Howe, C.J. & Nisbet, R.E.R. 2013. An analysis of dinoflagellate metabolism using EST data. *Protist.* 164:218–36.
- Charlson, R.J., Lovelock, J.E., Andreae, M.O. & Warren, S.G. 1987. Oceanic phytoplankton, atmospheric sulphur, cloud albedo and climate. *Nature.* 326:655–61.

- Chisti, Y. 2007. Biodiesel from microalgae. *Biotechnol. Adv.* 25:294–306.
- Chou, S.C. & Goldstein, A. 1960. Chromogenic groupings in the Lowry protein determination. *Biochem. J.* 75:109–15.
- Christian, M., Cermak, T., Doyle, E.L., Schmidt, C., Zhang, F., Hummel, A., Bogdanove, A.J. et al. 2010. Targeting DNA double-strand breaks with TAL effector nucleases. *Genetics.* 186:756–61.
- Coesel, S., Oborník, M., Varela, J., Falciatore, A. & Bowler, C. 2008. Evolutionary origins and functions of the carotenoid biosynthetic pathway in marine diatoms. *PLoS One.* 3.
- Cong, L., Ran, F.A., Cox, D., Lin, S., Barretto, R., Hsu, P.D., Wu, X. et al. 2013. Multiplex Genome Engineering Using CRISPR/Cas Systems. *Science* (New York, N.Y.). *Science.* 339:819–23.
- Crane, B.R., Siegel, L.M. & Getzoff, E.D. 1995. Sulfite reductase structure at 1.6 Å: Evolution and catalysis for reduction of inorganic anions. *Science.* 270:59–67.
- De Riso, V., Raniello, R., Maumus, F., Rogato, A., Bowler, C. & Falciatore, A. 2009. Gene silencing in the marine diatom *Phaeodactylum tricornutum*. *Nucleic Acids Res.* 37.
- Delwiche, C.F. 1999. Tracing the thread of plastid diversity through the tapestry of life. *Am. Nat.* 154.
- Delwiche, C.F. 2007. The Origin and Evolution of Dinoflagellates. Elsevier Inc. 191-205 pp.
- Doyle, E.L., Booher, N.J., Standage, D.S., Voytas, D.F., Brendel, V.P., Vandyk, J.K. & Bogdanove, A.J. 2012. TAL Effector-Nucleotide Targeter (TALE-NT) 2.0: Tools for TAL effector design and target prediction. *Nucleic Acids Res.* 40:117–22.
- Droop, M.R. 1973. Some Thoughts on Nutrient Limitation in Algae. *J. Phycol.* 9:264-272
- Dubois, M., Gilles, K., Hamilton, J.K., Rebers, P.A. & Smith, F. 1951. A colorimetric method for the determination of sugars. *Nature.* 168:167.
- El-Gebali, S., Mistry, J., Bateman, A., Eddy, S.R., Luciani, A., Potter, S.C., Qureshi, M. et al. 2019. The Pfam protein families database in 2019. *Nucleic Acids Res.* 47:D427–32.
- Emanuelsson, O., Brunak, S., von Heijne, G. & Nielsen, H. 2007. Locating proteins in the cell using TargetP, SignalP and related tools. *Nat. Protoc.* 2:953–71.
- Escoubas, J.-M., Lomas, M., LaRoche, J. & Falkowsky, P.G. 1995. Light Intensity Regulation of cab Gene Transcription is Signaled by the Redox State of the

- Plastoquinone Pool. *Proc. Natl. Acad. Sci.* 92:10237–41.
- Fábregas, J., Otero, A., Domínguez, A. & Patiño, M. 2001. Growth rate of the microalga *Tetraselmis suecica* changes the biochemical composition of *Artemia* species. *Mar. Biotechnol.* 3:256–63.
- Falkowski, P.G., Katz, M.E., Knoll, A.H., Quigg, A., Raven, J.A., Schofield, O. & Taylor, F.J.R. 2004. The evolution of modern eukaryotic phytoplankton. *Science* (80- ). 305:354–60.
- Falkowski, P.G. & Raven, J. 2007. Aquatic Photosynthesis. 2nd ed. Princeton University. 465 pp.
- Fanesi, A., Raven, J.A. & Giordano, M. 2014. Growth rate affects the responses of the green alga *Tetraselmis suecica* to external perturbations. *Plant, Cell Environ.* 37:512–9.
- Feldman-Salit, A., Wirtz, M., Hell, R. & Wade, R.C. 2009. A Mechanistic Model of the Cysteine Synthase Complex. *J. Mol. Biol.* 386:37–59.
- Field, C.B., Behrenfeld, M.J., Randerson, J.T., Falkowski, P., Field, C.B., Behrenfeld, M.J. & Randerson, J.T. 1998. Primary Production of the Biosphere : Integrating Terrestrial and Oceanic Components. *Science* (80). 281:237–40.
- Filutowicz, M., Wiater, A. & Hulanicka, D. 1982. Delayed inducibility of sulphite reductase in *cysM* mutants of *Salmonella typhimurium* under anaerobic conditions. *J. Gen. Microbiol.* 128:1791–4.
- Gao, Y., Schofield, O.M.E. & Leustek, T. 2000. Characterization of sulfate assimilation in marine algae focusing on the enzyme 5'-adenylylsulfate reductase. *Plant Physiol.* 123:1087–96.
- Gentil, J., Hempel, F., Moog, D., Zauner, S. & Maier, U.G. 2017. Origin of complex algae by secondary endosymbiosis: a journey through time. *Protoplasma.* 254:1835–43.
- Gibson, C.E. 1971. Nutrient Limitation. *Water Pollut. Control Fed.* 43:2436–40.
- Gigolashvili, T. & Kopriva, S. 2014. Transporters in plant sulfur metabolism. *Front. Plant Sci.* 5:1–16.
- Gill, B.C., Lyons, T.W. & Saltzman, M.R. 2007. Parallel, high-resolution carbon and sulfur isotope records of the evolving Paleozoic marine sulfur reservoir. *Palaeogeogr. Palaeoclimatol. Palaeoecol.* 256:156–73.
- Giordano, M., Chen, Y.B., Koblizek, M. & Falkowski, P.G. 2005a. Regulation of nitrate reductase in *Chlamydomonas reinhardtii* by the redox state of the plastoquinone pool. *Eur. J. Phycol.* 40:345–52.

- Giordano, M., Heraud, P., Beardall, J., Al, E.T., Kansiz, M., Heraud, P., Beardall, J. et al. 2001. Fourier transform infrared spectroscopy as a novel tool to investigate changes in intracellular macromolecular pools in the marine microalga *Chaetoceros muellerii* (Bacillariophyceae). *J. Phycol.* 37:271–9.
- Giordano, M., Norici, A. & Hell, R. 2005b. Sulfur and phytoplankton: Acquisition, metabolism and impact on the environment. *New Phytologist.* 166:371-382
- Giordano, M., Olivieri, C., Ratti, S., Norici, A., Raven, J.A. & Knoll, A.H. 2018. A tale of two eras: Phytoplankton composition influenced by oceanic paleochemistry. *Geobiology.* 498–506.
- Giordano, M., Pezzoni, V. & Hell, R. 2000. Strategies for the allocation of resources under sulfur limitation in the green alga *Dunaliella salina*. *Plant Physiol.* 124:857–64.
- Giordano, M. & Raven, J.A. 2014. Nitrogen and sulfur assimilation in plants and algae. *Aquat. Bot.*
- Gonzalez-Ballester, D. & Grossman, A.R. 2009. Sulfur: From Acquisition to Assimilation. *Chlamydomonas Sourceb. 3-Vol set.* 2:159–87.
- Gschloessl, B., Guerneur, Y. & Cock, J.M. 2008. HECTAR: A method to predict subcellular targeting in heterokonts. *BMC Bioinformatics.* 9:1–13.
- Guillard, R.R.L. 1975. Culture of Phytoplankton for Feeding Marine Invertebrates. In Smith, W. L. & Chanley, M. H. [Eds.] *Culture of Marine Invertebrate Animals*. Springer, pp. 29–60.
- Günel, S., Hardman, R., Kopriva, S. & Mueller, J.W. 2019. Sulfation pathways from red to green. *J. Biol. Chem.* 294:12293–312.
- Hammer, O., Harper, D.A.T. & Ryan, P.D. 2001. PAST: Paleontological statistics software package for education and data analysis. *Paleontol. Electron.* 4:1–9.
- Hanna, E., MacRae, I.J., Medina, D.C., Fisher, A.J. & Segel, I.H. 2002. ATP sulfurylase from the hyperthermophilic chemolithotroph *Aquifex aeolicus*. *Arch. Biochem. Biophys.* 406:275–88.
- Hell, R. 2002. Molecular physiology of plant sulfur metabolism. *Planta.* 202:138–40.
- Hell, R. & Leustek, T. 2005. Sulfur metabolism in plants and algae - A case study for an integrative scientific approach. *Photosynth. Res.* 86:297–8.
- Hitchcock, G.L. 1983. Photosynthate partitioning in cultured marine phytoplankton. I. Dinoflagellates. Variations in the biochemical composition of marine phytoplankton are regulated by the same environmental factors that control cell division. In marine

- diatoms , for exampl. 69:21–36.
- Ho, T.Y., Quigg, A., Finkel, Z. V., Milligan, A.J., Wyman, K., Falkowski, P.G. & Morel, F.M.M. 2003. The elemental composition of some marine phytoplankton. *J. Phycol.* 39:1145–59.
- Hodson, R.C., Schiff, J.A. & Mather, J.P. 1971. Studies of Sulfate Utilization by Algae. *Plant Physiol.* 47:306–11.
- Hofmann, E., Wrench, P.M., Sharples, F.P., Hiller, R.G., Welte, W. & Diederichs, K. 1996. Structural basis of light harvesting by carotenoids: Peridinin-chlorophyll-protein from *Amphidinium carterae*. *Science (80- )*. 272:1788–91.
- Hori, T., Norrm, R.E. & Chihara, M. 1986. Studies on the Ultrastructure and Taxonomy of the Genus *Tetraselmis* Subgenus *Parviselmis*. 123–35.
- Horita, J., Zimmermann, H. & Holland, H.D. 2002. Chemical evolution of seawater during the Phanerozoic: Implications from the record of marine evaporites. *Geochim. Cosmochim. Acta.* 66:3733–56.
- Howarth, J.R., Dominguez-Solís, J.R., Gutiérrez-Alcalá, G., Wray, J.L., Romero, L.C. & Gotor, C. 2003. The serine acetyltransferase gene family in *Arabidopsis thaliana* and the regulation of its expression by cadmium. *Plant Mol. Biol.* 51:589–98.
- Jobe, T.O., Zenzen, I., Rahimzadeh Karvansara, P. & Kopriva, S. 2019. Integration of sulfate assimilation with carbon and nitrogen metabolism in transition from C3 to C4 photosynthesis. *J. Exp. Bot.* 70:4211–21.
- Johnson, L.S., Eddy, S.R. & Portugaly, E. 2010. Hidden Markov model speed heuristic and iterative HMM search procedure. *BMC Bioinformatics.* 11.
- Jost, R., Berkowitz, O., Wirtz, M., Hopkins, L., Hawkesford, M.J. & Hell, R. 2000. Genomic and functional characterization of the *oas* gene family encoding O-acetylserine (thiol) lyases, enzymes catalyzing the final step in cysteine biosynthesis in *Arabidopsis thaliana*. *Gene.* 253:237–47.
- Kalyaanamoorthy, S., Minh, B.Q., Wong, T.K.F., Von Haeseler, A. & Jermin, L.S. 2017. ModelFinder: Fast model selection for accurate phylogenetic estimates. *Nat. Methods.* 14:587–9.
- Kaňa, R., Kotabová, E., Lukeš, M., Papáček, Š., Matonoha, C., Liu, L.N., Prášil, O. et al. 2014. Phycobilisome mobility and its role in the regulation of light harvesting in red algae. *Plant Physiol.* 165:1618–31.
- Kanehisa, M., Furumichi, M., Sato, Y., Ishiguro-Watanabe, M. & Tanabe, M. 2020. KEGG: integrating viruses and cellular organisms. *Nucleic Acids Res.* 1–7.

- Karas, B.J., Diner, R.E., Lefebvre, S.C., McQuaid, J., Phillips, A.P.R., Noddings, C.M., Brunson, J.K. et al. 2015. Designer diatom episomes delivered by bacterial conjugation. *Nat. Commun.* 6.
- Karsten, U., West, J.A., Zuccarello, G.C., Engbrodt, R., Yokoyama, A., Hara, Y. & Brodie, J. 2003. Low molecular weight carbohydrates of the bangiophycidae (Rhodophyta). *J. Phycol.* 39:584–9.
- Katoh, K., Rozewicki, J. & Yamada, K.D. 2018. MAFFT online service: Multiple sequence alignment, interactive sequence choice and visualization. *Brief. Bioinform.* 20:1160–6.
- Khan, M.S., Haas, F.H., Samami, A.A., Gholami, A.M., Bauer, A., Fellenberg, K., Reichelt, M. et al. 2010. Sulfite reductase defines a newly discovered bottleneck for assimilatory sulfate reduction and is essential for growth and development in *Arabidopsis thaliana*. *Plant Cell.* 22:1216–31.
- Kilian, O. & Kroth, P.G. 2005. Identification and characterization of a new conserved motif within the presequence of proteins targeted into complex diatom plastids. *Plant J.* 41:175–83.
- Knoll, A.H., Summons, R.E., Waldbauer, J.R. & Zumberge, J.E. 2007. The Geological Succession of Primary Producers in the Oceans. *Evol. Prim. Prod. Sea.* 133–63.
- Kobayashi, K. & Yoshimoto, A. 1982. Studies on yeast sulfite reductase. IV. Structure and steady-state kinetics. *Biochim. Biophys. Acta (BBA)/Protein Struct. Mol.* 705:348–56.
- Kooistra, W.H.C.F., Gersonde, R., Medlin, L.K. & Mann, D.G. 2007. The Origin and Evolution of the Diatoms. Their Adaptation to a Planktonic Existence. 207-249 pp.
- Kopriva, S., Büchert, T., Fritz, G., Suter, M., Benda, R., Schünemann, V., Koprivova, A. et al. 2002. The presence of an iron-sulfur cluster in adenosine 5'-phosphosulfate reductase separates organisms utilizing adenosine 5'-phosphosulfate and phosphoadenosine 5'-phosphosulfate for sulfate assimilation. *J. Biol. Chem.* 277:86–91.
- Kopriva, S., Fritzeimer, K., Wiedemann, G. & Reski, R. 2007. The putative moss 3'-phosphoadenosine-5'-phosphosulfate reductase is a novel form of adenosine-5'-phosphosulfate reductase without an iron-sulfur cluster. *J. Biol. Chem.* 282:22930–8.
- Koprivova, A. & Kopriva, S. 2016. Sulfation pathways in plants. *Chem. Biol. Interact.* 259:23–30.

- Koprivova, A., Melzer, M., Von Ballmoos, P., Mandel, T., Brunold, C. & Kopriva, S. 2001. Assimilatory sulfate reduction in C3, C3-C4, and C4 species of *Flaveria*. *Plant Physiol.* 127:543–50.
- Kredich, N.M. 1971. Regulation of L-Cysteine Biosynthesis in *Salmonella typhimurium*. *Biol. Chem.* 246:3474–84.
- Kroth, P.G. 2007. Genetic Transformation: A tool to study protein targeting in diatoms. In van der Giezen, M. [Ed.] *Protein Targeting Protocols*. 2nd ed. Humana Press, pp. 257–69.
- Kurpan Nogueira, D.P., Silva, A.F., Elia, O., Araújo Jo, Q.F. & Chaloub, R.M. 2015. Impact of temperature and light intensity on triacylglycerol accumulation in marine microalgae. *Biomass and Bioenergy*. 72:280-287
- Lalor, D.J., Schnyder, T., Saridakis, V., Pilloff, D.E., Dong, A., Tang, H., Leyh, T.S. et al. 2003. Structural and functional analysis of a truncated form of *Saccharomyces cerevisiae* ATP sulfurylase: C-terminal domain essential for oligomer formation but not for activity. *Protein Eng.* 16:1071–9.
- Lee, K.H., Jeong, H.J., Park, K., Kang, N.S., Yoo, Y. Du, Lee, M.J., Lee, J.W. et al. 2013. Morphology and molecular characterization of the epiphytic dinoflagellate *Amphidinium massartii*, isolated from the temperate waters off Jeju Island, Korea. *Algae*. 28:213–31.
- Lepetit, B., Gélina, G., Lepetit, M., Sturm, S., Vugrinec, S., Rogato, A., Kroth, P.G. et al. 2017. The diatom *Phaeodactylum tricornutum* adjusts nonphotochemical fluorescence quenching capacity in response to dynamic light via fine-tuned Lhcx and xanthophyll cycle pigment synthesis. *New Phytol.* 214:205–18.
- Leustek, T. 1996. Molecular genetics of sulfate assimilation in plants. 97:411–9.
- Li, T., Huang, S., Zhao, X., Wright, D.A., Carpenter, S., Spalding, M.H., Weeks, D.P. et al. 2011. Modularly assembled designer TAL effector nucleases for targeted gene knockout and gene replacement in eukaryotes. *Nucleic Acids Res.* 39:6315–25.
- Liebig, J. 1841. *Die organische chemie in ihrer unwendung auf agricultur und physiologie*. 1st ed. 372 pp.
- Lin, Y., Fine, E.J., Zheng, Z., Antico, C.J., Voit, R.A., Porteus, M.H., Cradick, T.J. et al. 2014. SAPTA: A new design tool for improving TALE nuclease activity. *Nucleic Acids Res.* 42:1–12.
- Lu, S., Wang, J., Chitsaz, F., Derbyshire, M.K., Geer, R.C., Gonzales, N.R., Gwadz, M. et al. 2020. CDD/SPARCLE: The conserved domain database in 2020. *Nucleic Acids*

- Res.* 48:D265–8.
- Lunde, C., Zygadlo, A., Simonsen, H.T., Nielsen, P.L., Blennow, A. & Haldrup, A. 2008. Sulfur starvation in rice: The effect on photosynthesis, carbohydrate metabolism, and oxidative stress protective pathways. *Physiol. Plant.* 134:508–21.
- Lunn, J.E., Droux, M., Martin, J. & Douce, R. 1990. Localization of ATP sulfurylase and O-acetylserine(thiol)lyase in spinach leaves. *Plant Physiol.* 94:1345–52.
- Lyle, S., Stanczak, J., Ng, K. & Schwartz, N.B. 1994. Rat Chondrosarcoma ATP Sulfurylase and Adenosine 5'-Phosphosulfate Kinase Reside on a Single Bifunctional Protein. *Biochemistry.* 33:5920–5.
- MacRae, I. & Segel, I.H. 1997. ATP sulfurylase from filamentous fungi: Which sulfonucleotide is the true allosteric effector? *Arch. Biochem. Biophys.* 337:17–26.
- MacRae, I.J., Segel, I.H. & Fisher, A.J. 2001. Crystal structure of ATP sulfurylase from *Penicillium chrysogenum*: Insights into the allosteric regulation of sulfate assimilation. *Biochemistry.* 40:6795–804.
- Maier, T.H.P. 2003. Semisynthetic production of unnatural l- $\alpha$ -amino acids by metabolic engineering of the cysteine-biosynthetic pathway. *Nat. Biotechnol.* 21:422–7.
- Malin, G. 1997. Sulphur, climate and the microbial maze. *Nature.* 387:857–9.
- Manton, I. & Parke, M. 1965. Observations on the fine structure of two species of *Platymonas* with special reference to flagellar scales and the mode of origin of the theca. *J. Mar. Biol. Assoc. United Kingdom.* 45:743–54.
- Martin, W., Baross, J., Kelley, D. & Russell, M.J. 2008. Hydrothermal vents and the origin of life. *Nat. Rev. Microbiol.* 6:805–14.
- Maxwell, K. & Johnson, G.N. 2000. Chlorophyll fluorescence - a practical guide. *J. Exp. Bot.* 51:659–68.
- McFadden, G.I. 2014. Origin and evolution of plastids and photosynthesis in eukaryotes. *Cold Spring Harb. Perspect. Biol.* 6:1–10.
- Melis, A. & Chen, H.C. 2005. Chloroplast sulfate transport in green algae - Genes, proteins and effects. *Photosynth. Res.* 86:299–307.
- Mera, R., Torres, E. & Abalde, J. 2016. Effects of sodium sulfate on the freshwater microalga *Chlamydomonas moewusii*: Implications for the optimization of algal culture media. *J. Phycol.* 52:75–88.
- Misra, A.N., Misra, M. & Singh, R. 2012. Chlorophyll Fluorescence in Plant Biology. *Biophysics (Oxf).*
- Miyahara, M., Aoi, M., Inoue-Kashino, N., Kashino, Y. & Ifuku, K. 2013. Highly

- efficient transformation of the diatom phaeodactylum tricornutum by multi-pulse electroporation. *Biosci. Biotechnol. Biochem.* 77:874–6.
- Monod, J. 1949. The Growth of Bacterial Cultures. *Annu. Rev. Microbiol.* 3:371–94.
- Mueller, J.W. & Shafqat, N. 2013. Adenosine-5'-phosphosulfate - A multifaceted modulator of bifunctional 3'-phospho-adenosine-5'-phosphosulfate synthases and related enzymes. *FEBS J.* 280:3050–7.
- Mugford, S.G., Matthewman, C.A., Hill, L. & Kopriva, S. 2010. Adenosine-5'-phosphosulfate kinase is essential for Arabidopsis viability. *FEBS Lett.*
- Mugford, S.G., Yoshimoto, N., Reichelt, M., Wirtz, M., Hill, L., Mugford, S.T., Nakazato, Y. et al. 2009. Disruption of Adenosine-5'-Phosphosulfate Kinase in Arabidopsis Reduces Levels of Sulfated Secondary Metabolites. *Plant Cell* 21:910–927.
- Murakoshi, I., Kaneko, M., Koide, C. & Ikegami, F. 1986. Enzymatic synthesis of the neuroexcitatory amino acid quisqualic acid by cysteine synthase. *Phytochemistry.* 25:2759–63.
- Murchie, E.H. & Lawson, T. 2013. Chlorophyll fluorescence analysis: A guide to good practice and understanding some new applications. *J. Exp. Bot.* 64:3983–98.
- Murillo, M. & Leustek, T. 1995. Adenosine-5'-triphosphate-sulfurylase from Arabidopsis thaliana and Escherichia coli are functionally equivalent but structurally and kinetically divergent: Nucleotide sequence of two adenosine-5'-triphosphate-sulfurylase cDNAs from Arabidopsis thaliana a. *Arch. Biochem. Biophys.* 323:195–204.
- Murray, S., Jørgensen, M.F., Daugbjerg, N. & Rhodes, L. 2004. Amphidinium revisited. II. Resolving species boundaries in the Amphidinium operculatum species complex (Dinophyceae), including the descriptions of Amphidinium trulla sp nov. and Amphidinium gibbosum. comb. nov. *J. Phycol.* 40:366–82.
- Nakayama, M., Akashi, T. & Hase, T. 2000. Plant sulfite reductase: Molecular structure, catalytic function and interaction with ferredoxin. *J. Inorg. Biochem.* 82:27–32.
- Nelson, W.A. & Ryan, K.G. 1988. Porphyridium purpureum (bory) drew et ross (porphyridiales, rhodophyceae)—first record of a marine unicellular red alga in New Zealand. *J. R. Soc. New Zeal.* 18:127–8.
- Ngo, D.H. & Kim, S.K. 2013. Sulfated polysaccharides as bioactive agents from marine algae. *Int. J. Biol. Macromol.* 62:70–5.
- Nguyen, L.T., Schmidt, H.A., Von Haeseler, A. & Minh, B.Q. 2015. IQ-TREE: A fast

- and effective stochastic algorithm for estimating maximum-likelihood phylogenies. *Mol. Biol. Evol.* 32:268–74.
- Niyogi, K.K. & Truong, T.B. 2013. Evolution of flexible non-photochemical quenching mechanisms that regulate light harvesting in oxygenic photosynthesis. *Curr. Opin. Plant Biol.* 16:307–14.
- Norici, A., Bazzoni, A.M., Pugnetti, A., Raven, J.A. & Giordano, M. 2011. Impact of irradiance on the C allocation in the coastal marine diatom *Skeletonema marinoi* Sarno and Zingone. *Plant, Cell Environ.* 34:1666–77.
- Norici, A., Hell, R. & Giordano, M. 2005. Sulfur and primary production in aquatic environments: An ecological perspective. *Photosynth. Res.* 86:409–17.
- Nozaki, T., Ali, V. & Tokoro, M. 2005. Sulfur-containing amino acid metabolism in parasitic protozoa. Elsevier Masson SAS. 1-99 pp.
- Palmucci, M., Ratti, S. & Giordano, M. 2011. Ecological and evolutionary implications of carbon allocation in marine phytoplankton as a function of nitrogen availability: A fourier transform infrared spectroscopy approach. *J. Phycol.* 47:313–23.
- Parey, K., Demmer, U., Warkentin, E., Wynen, A., Ermler, U. & Dahl, C. 2013. Structural, Biochemical and Genetic Characterization of Dissimilatory ATP Sulfurylase from *Allochromatium vinosum*. *PLoS One.* 8.
- Patron, N.J., Durnford, D.G. & Kopriva, S. 2008. Sulfate assimilation in eukaryotes: Fusions, relocations and lateral transfers. *BMC Evol. Biol.* 8:1–14.
- Patron, N.J. & Waller, R.F. 2007. Transit peptide diversity and divergence: A global analysis of plastid targeting signals. *BioEssays.* 29:1048–58.
- Pérez-Jiménez, J.R. & Kerkhof, L.J. 2005. Phylogeography of sulfate-reducing bacteria among disturbed sediments, disclosed by analysis of the dissimilatory sulfite reductase genes (*dsrAB*). *Appl. Environ. Microbiol.* 71:1004–11.
- Petersen, T.N., Brunak, S., Von Heijne, G. & Nielsen, H. 2011. SignalP 4.0: Discriminating signal peptides from transmembrane regions. *Nat. Methods.* 8:785–6.
- Peterson, G. 1977. A simplification of the protein assay method of Lowery et al. which is more generally applicable. *Anal. Biochem.* 356:246–56.
- Platt, T., Gallegos, C.L. & Harrison, W.G. 1980. Photoinhibition of Photosynthesis in Natural Assemblages of Marine Phytoplankton.
- Pomin, V.H. & Mourão, P.A.S. 2008. Structure, biology, evolution, and medical importance of sulfated fucans and galactans. *Glycobiology.* 18:1016–27.

- Pootakham, W., Gonzalez-Ballester, D. & Grossman, A.R. 2010. Identification and regulation of plasma membrane sulfate transporters in *Chlamydomonas*. *Plant Physiol.* 153:1653–68.
- Prioretti, L. & Giordano, M. 2016. Direct and indirect influence of sulfur availability on phytoplankton evolutionary trajectories. *J. Phycol.*
- Prioretti, L., Gontero, B., Hell, R. & Giordano, M. 2014. Diversity and regulation of ATP sulfurylase in photosynthetic organisms. *Front. Plant Sci.*
- Prioretti, L., Lebrun, R., Gontero, B. & Giordano, M. 2016. Redox regulation of ATP sulfurylase in microalgae. *Biochem. Biophys. Res. Commun.* 478:1555–62.
- Quigg, A., Irwin, A.J. & Finkel, Z. V. 2003. Evolutionary inheritance of elemental stoichiometry in phytoplankton. *Nature.* 425:526–34.
- Ralph, P.J. & Gademann, R. 2005. Rapid light curves: A powerful tool to assess photosynthetic activity. *Aquat. Bot.* 82:222–37.
- Ratti, S., Knoll, A.H. & Giordano, M. 2011. Did sulfate availability facilitate the evolutionary expansion of chlorophyll a+c phytoplankton in the oceans? *Geobiology.* 9:301-312.
- Ratti, S., Knoll, A.H. & Giordano, M. 2013. Grazers and Phytoplankton Growth in the Oceans: An Experimental and Evolutionary Perspective. *PLoS One.* 8.
- Raven, J.A. & Giordano, M. 2014. Algae. *Curr. Biol.* 24:590–5.
- Raven, J.A. & Johnston, A. 1991. Mechanisms of inorganic-carbon acquisition in marine phytoplankton and their implications for the use of other resources. *Limnol. Oceanogr.* 36:1701–14.
- Ravilious, G.E., Nguyen, A., Francois, J.A. & Jez, J.M. 2012. Structural basis and evolution of redox regulation in plant adenosine-5'-phosphosulfate kinase. *Proc. Natl. Acad. Sci.* 29:1138-1152
- Ravina, C.G., Barroso, C., Vega, J.M. & Gotor, C. 1999. Cysteine biosynthesis in *Chlamydomonas reinhardtii*. Molecular cloning and regulation of O-acetylserine(thiol)lyase. *Eur. J. Biochem.* 264:848–53.
- Ravina, C.G., Chang, C.I., Tsakraklides, G.P., McDermott, J.P., Vega, J.M., Leustek, T., Gotor, C. et al. 2002. The sac mutants of *Chlamydomonas reinhardtii* reveal transcriptional and posttranscriptional control of cysteine biosynthesis. *Plant Physiol.* 130:2076–84.
- Ritchie, R.J. 2006. Consistent sets of spectrophotometric chlorophyll equations for acetone, methanol and ethanol solvents. *Photosynth. Res.* 89:27–41.

- Rosenwasser, S., Graff van Creveld, S., Schatz, D., Malitsky, S., Tzfadia, O., Aharoni, A., Levin, Y. et al. 2014. Mapping the diatom redox-sensitive proteome provides insight into response to nitrogen stress in the marine environment. *Proc. Natl. Acad. Sci.* 111:2740–5.
- Ruan, Z., Prášil, O. & Giordano, M. 2018. The phycobilisomes of *Synechococcus* sp. are constructed to minimize nitrogen use in nitrogen-limited cells and to maximize energy capture in energy-limited cells. *Environ. Exp. Bot.* 150:152–60.
- Ruffet, M.L., Droux, M. & Douce, R. 1994. Purification and kinetic properties of serine acetyltransferase free of O-acetylserine(thiol)lyase from spinach chloroplasts. *Plant Physiol.* 104:597–604.
- San Pedro, A., González-López, C. V., Acién, F.G. & Molina-Grima, E. 2013. Marine microalgae selection and culture conditions optimization for biodiesel production. *Bioresour. Technol.* 134:353–61.
- Sanjana, N.E., Cong, L., Zhou, Y., Cunniff, M.M., Feng, G. & Zhang, F. 2011. A Transcriptor Activator-Like Effector (TALE) Toolbox for Genome Engineering. *Nat. Protoc.* 7:171–92.
- Sarcina, M., Tobin, M.J. & Mullineaux, C.W. 2001. Diffusion of phycobilisomes on the thylakoid membranes of the cyanobacterium *Synechococcus* 7942: Effects of phycobilisome size, temperature, and membrane lipid composition. *J. Biol. Chem.* 276:46830–4.
- Satishchandrans, C. & Markham, G.D. 1989. Adenosine-5'-phosphosulfate Kinase from. 264:15012–21.
- Schreiber, U., Schliwa, U. & Bilger, W. 1986. Continuous recording of photochemical and non-photochemical chlorophyll fluorescence quenching with a new type of modulation fluorometer. *Photosynth. Res.* 10:51–62.
- Schwenn, J.D. & Schriek, U. 1984. A new role for thioredoxin in assimilatory sulphate reduction. Activation of the adenylylsulphate kinase from the green alga *Chlamydomonas reinhardtii* CW 15. *FEBS Lett.* 170:76–80.
- Scott, J.L., Broadwater, S.T., Saunders, B.D., Thomas, J.P. & Gabrielson, P.W. 1992. Ultrastructure of Vegetative Organization and Cell Division in the Unicellular Red Alga *Dixoniella Grisea* Gen. Nov. (Rhodophyta) and a Consideration of the Genus *Rhodella*.
- Serif, M., Lepetit, B., Weißert, K., Kroth, P.G. & Rio Bartulos, C. 2017. A fast and reliable strategy to generate TALEN-mediated gene knockouts in the diatom

- Phaeodactylum tricornutum. *Algal Res.* 23:186–95.
- Shuter, B. 1979. A model of physiological adaptation in unicellular algae. *J. Theor. Biol.* 78:519–52.
- Simionato, D., Basso, S., Zaffagnini, M., Lana, T., Marzotto, F., Trost, P. & Morosinotto, T. 2015. Protein redox regulation in the thylakoid lumen: The importance of disulfide bonds for violaxanthin de-epoxidase. *FEBS Lett.* 589:919–23.
- Spiro, P.A., Jacob, I.J., Nniff, J.I. & Logan, R.A. 1992. Global Inventory of Sulfur Emissions With 1 °xl ø Resolution of the in- Procedure yentory is motivated by the to understand origin procedure for computing emissions sulfate of deposition visibility climate Charlson emission extent recovery of reduced gase. *J. geophy.* 97:6023–36.
- Sunda, W.G., Kieber, D. & Kiene, R.P. 2002. An antioxidant function of DMSP and DMS in marine algae oceanic dimethylsulfide (DMS) photolysis. *Nature.* 418:317–20.
- Taguchi, Y., Sugishima, M. & Fukuyama, K. 2004. Crystal Structure of A Novel Zinc-Binding ATP Sulfurylase from Thermus thermophilus HB8. *Biochemistry.* 43:4111–8.
- Takahashi, H., Buchner, P., Yoshimoto, N., Hawkesford, M.J. & Shiu, S.H. 2012. Evolutionary relationships and functional diversity of plant sulfate transporters. *Front. Plant Sci.* 2:1–9.
- Takahashi, H., Kopriva, S., Giordano, M., Saito, K. & Hell, R. 2011. Sulfur Assimilation in Photosynthetic Organisms: Molecular Functions and Regulations of Transporters and Assimilatory Enzymes. *Annu. Rev. Plant Biol.* 62:157–84.
- Thauer, R.K., Jungermann, K. & Decker, K. 1977. Energy conservation in chemotrophic anaerobic bacteria. *Bacteriol. Rev.* 41:100–80.
- Trebitsh, T. & Danon, A. 2001. Translation of chloroplast psbA mRNA is regulated by signals initiated by both photosystems II and I. *Proc. Natl. Acad. Sci. U. S. A.* 98:12289–94.
- Trebst, A. 1974. Energy Conservation in Photosynthetic Electron Transport of Chloroplasts. *Annu. Rev. Plant Physiol.* 25:423–58.
- Tsien, R.Y. 1998. The green fluorescent protein. *Annu. Rev. Biochem.* 67:509–44.
- Ueno, Y. 2018. Earth Science. Coping with low ocean sulfate. *Science.* 346:703–4.
- Vairavamurthy, A., Andreae, M.O. & Iverson, R.L. 1985. Biosynthesis of dimethylsulfide and dimethylpropiothetin by Hymenomonas carterae in relation to sulfur source and salinity variations. *Limnol. Oceanogr.* 30:59–70.

- Van Mooy, B.A.S., Rocap, G., Fredricks, H.F., Evans, C.T. & Devol, A.H. 2006. Sulfolipids dramatically decrease phosphorus demand by picocyanobacteria in oligotrophic marine environments. *Proc. Natl. Acad. Sci. U. S. A.* 103:8607–12.
- Vauclaire, P., Kopriva, S., Fell, D., Suter, M., Sticher, L., Von Ballmoos, P., Krähenbühl, U. et al. 2002. Flux control of sulphate assimilation in *Arabidopsis thaliana*: Adenosine 5'-phosphosulphate reductase is more susceptible than ATP sulphurylase to negative control by thiols. *Plant J.* 31:729–40.
- Vermeij, G.J. 1977. The Mesozoic Marine Revolution : Evidence from Snails , Predators and Grazers. *Paleobiology.* 3:245–58.
- Walsh, M.J., Goodnow, S.D., Vezeau, G.E., Richter, L. V. & Ahner, B.A. 2015. Cysteine Enhances Bioavailability of Copper to Marine Phytoplankton. *Environ. Sci. Technol.* 49:12145–52.
- Watanabe, M., Mochida, K., Kato, T., Tabata, S., Yoshimoto, N., Noji, M. & Saito, K. 2008. Comparative genomics and reverse genetics analysis reveal indispensable functions of the serine acetyltransferase gene family in *Arabidopsis*. *Plant Cell.* 20:2484–96.
- Wellburn, A.R. 1994. The Spectral Determination of Chlorophylls a and b, as well as Total Carotenoids, Using Various Solvents with Spectrophotometers of Different Resolution. *J. Plant Physiol.* 144:307–13.
- Wirtz, M., Droux, M. & Hell, R. 2004. O-acetylserine (thiol) lyase: An enigmatic enzyme of plant cysteine biosynthesis revisited in *Arabidopsis thaliana*. *J. Exp. Bot.* 55:1785–98.
- Yamaguchi, Y., Nakamura, T., Kusano, T. & Sano, H. 2000. Three *Arabidopsis* genes encoding proteins with differential activities for cysteine synthase and  $\beta$ -cyanoalanine synthase. *Plant Cell Physiol.* 41:465–76.
- Yamazaki, T., Konosu, E., Takeshita, T., Hirata, A., Ota, S., Kazama, Y., Abe, T. et al. 2018. Independent regulation of the lipid and starch synthesis pathways by sulfate metabolites in the green microalga *Parachlorella kessleri* under sulfur starvation conditions. *Algal Res.* 36:37–47.
- Ye, J., Coulouris, G., Zaretskaya, I., Cutcutache, I., Rozen, S. & Madden, T.L. 2012. Primer-BLAST: A tool to design target-specific primers for polymerase chain reaction. *BMC Bioinformatics.* 13.
- Yildiz, F.H., Davies, J.P. & Grossman, A.R. 1994. Characterization of sulfate transport in *Chlamydomonas reinhardtii* during sulfur-limited and sulfur-sufficient growth.

*Plant Physiol.* 104:981–7.

- Yoon, H.S., Müller, K.M., Sheath, R.G., Ott, F.D. & Bhattacharya, D. 2006. Defining the major lineages of red algae (Rhodophyta). *J. Phycol.* 42:482–92.
- Zaslavskaja, L.A., Casey Lippmeier, J., Kroth, P.G., Grossman, A.R. & Apt, K.E. 2000. Transformation of the diatom *Phaeodactylum tricornutum* (Bacillariophyceae) with a variety of selectable marker and reporter genes. *J. Phycol.* 36:379–86.
- Zhang, C. & Hu, H. 2014. High-efficiency nuclear transformation of the diatom *Phaeodactylum tricornutum* by electroporation. *Mar. Genomics.* 16:63–6.
- Zhao, F.J., Spiro, B., Poulton, P.R. & Mcgrath, S.P. 1998. Use of sulfur isotope ratios to determine anthropogenic sulfur signals in a grassland ecosystem. *Environ. Sci. Technol.* 32:2288–91.
- Zhu, C.J. & Lee, Y.K. 1997. Determination of biomass dry weight of marine microalgae. *J. Appl. Phycol.* 9:189–94.
- Zhu, S.H. & Green, B.R. 2010. Photoprotection in the diatom *Thalassiosira pseudonana*: Role of LI818-like proteins in response to high light stress. *Biochim. Biophys. Acta - Bioenerg.* 1797:1449–57.